(29) GCOE Event The 2ndGCOE International Symposium on "Weaving Science Web beyond Particle-Matter Hierarchy"

Date & Time: February 18, 2010 9:00 - 18:3, February 19, 2010 9:30-18:00 -

Place: Faculty of Science Aobayama Campus of Tohoku University

Invited Speakers:

Dr. Indranil Mazumdar (Tata Institute of Fundamental Research, India)
Prof. Philippe Marcq (PhysicoChimie Curie Institut Curie, France)
Prof. Young-Woo Son (Korea Institute for Advanced Study, Korea)
Dr.Jean Coupon (Institut d'Astrophysique de Paris, France)
Prof. Ryushi Goto (Osaka University, Japan)
Prof. Jenann Ismael (University of Arisona, USA and University of Sydney, Australia)
Prof. Jie Meng (Beihang University, China)
Prof. Huaizhe Xu (Beihang University , China)
Assistant Prof. Hojun IM (Hirosaki University)
M.S. Masahiro FUTAKI (The University of Tokyo)
Dr. Masahiko IGASHIRA (Osaka University)

Organizing Committee:

Prof. Hideo Kozono (Mathematics, Tohoku Univ.): Chairman
Assistant Prof. Katsuhiko Sato (Condensed Matter physics, Tohoku Univ.)
Assistant Prof. Yousuke Itoh (Astrophysics, Tohoku Univ.)
Assistant Prof. Yoshihiro Ueda (Mathematics, Tohoku Univ.)
Assistant Prof. Yuichi Nohara (Mathematics, Tohoku Univ.)
Assistant Prof. Masaki Asano (Particle Theory, Tohoku Univ.)
Assistant Prof. Yoshiyuki Onuki (Particle Experiment, Tohoku Univ.)
Assistant Prof. Takeshi Koike (Nuclear Experiment, Tohoku Univ.)
Assistant Prof. Hidekatsu Nemura (Nuclear Theory, Tohoku Univ.)
Assistant Prof. Jin Sung Park (Condensed Matter Physics, Tohoku Univ.)
Assistant Prof. Tatsuro Yuge (Condensed Matter Physics, Tohoku Univ.)
Assistant Prof. Tomohiro Yoshikawa (Astrophysics, Tohoku Univ.)
Assistant Prof. Shota Sato (Mathematics, Tohoku Univ.)
Assistant Prof. Yohei Matsuda (Nuclear Experiment, Tohoku Univ.)
Assistant Prof. Masafumi Kurachi (Particle Theory, Tohoku Univ.)
Dr. Masaru Yonehara (Philosophy, Tohoku Univ.)

Outline:

The aim of this Symposium is to explore new science frontiers through "Weaving Science Web beyond Particle-Matter hierarchy" among physics - astrophysics - mathematics - philosophy.

Number of participants:

Symposium:

Banquet:

Program:

February 18 Thursday

09:30 -	"Opening address"	**Kunio INOUE (GCOE program leader)**
Plenary Session		***Chairmen H. Tamura / T. Kawakatsu / Y. Hirayama***
09:30-10:20	"Halo World: The Story according to Faddeev, Efimov and Fano"	**I. MAZUMDAR** ***(Chairman H. Tamura)***
10:30-11:20	"Mechanics of Stress Fibers"	**P. MARCQ** ***(Chairman T. Kawakatsu)***
11:30-12:20	"Relativistic Dirac Electrons in Condensed Matters – Graphene and others"	**Y. W. SON** ***(Chairman Y. Hirayama)***
12:30-13:50	Lunch	
Parallel Session A - Particle/ Nuclear/ Astro-physics Group		***Chairman K. Hikasa***
13:50-14:20	"General WIMP search at International Linear Collider"	**M. ASANO**
14:30-15:00	"Primordial nucleosynthesis and recent topics in particle cosmology"	**K. KOHRI**
15:10-15:40	"Higgsless Models for the Electroweak Symmetry Breaking"	**M. KURACHI**
15:50-16:00	Coffee Break	
Parallel Session B – Condensed Matter Physics Group / Nuclear Physics		***Chairman R. Saito***
13:50-14:20	"Exciton effect of Raman resonance window of single wall carbon nanotubes"	**J. PARK**
14:30-15:00	"Properties of response function of nonequilibrium steady state"	**T. YUGE**
15:10-15:40	"Hyperon-nucleon interactions from lattice QCD"	**H.NEMURA**
15:50-16:00	Coffee Break	
Parallel Session C – Mathematics and Philosophy Group		***Chairman H. Kozono***
13:50-14:20	"Application of the anti-derivative method to the half space problem for damped wave equation with non-convexity"	**Y.UEDA**
14:30-15:00	"Toric degeneration of Gelfand-Cetlin systems"	**Y.NOHARA**
15:10-15:40	"Singular Backward Self-Similar Solutions of a Semilinear Parabolic Equation"	**S. SATO**
15:50-16:00	Coffee Break	
Special Session		***Chairman O. Hashimoto***
16:00-16:30	"Covariant density functional theory for Nuclear structure and application in astrophysics"	**J.Meng**
16:35-17:05	"Control of Magnetic Property and Magnetic Coupling Mechanism in ZnO based DMS"	**H.Xu**
Poster Session		
17:10-18:30	**80 Research assistants present their research.**	

February 19 Friday

Plenary Session *Chairmen K. Naoe / R. Miyaoka / T. Futamase*

09:30-10:20	"A Fresh Direction for Quantum Research: What Might Entanglement Be Telling Us?" **J.ISMAEL** *(Chairman K. Naoe)*
10:30-11:20	"Calabi-Yau structures and Einstein-Sasaki structures" **R. GOTO** *(Chairman R. Miyaoka)*
11:30-12:20	"Probing the large scale structure in the Universe with CFHTLS" **J. COUPON** *(Chairman T. Futamase)*
12:30-13:50	Lunch

Parallel Session A – Particle/ Nuclear/ Astro-physics Group *Chairmen H. Tamura / T. Futamase*

13:50-14:20	"Measurements of Cabibbo-Kobayashi-Maskawa unitary triangle angle phi3 at Belle experiment" **Y. ONUKI** *(Chairman H. Tamura)*
14:30-15:00	"Hypernuclear γ-ray spectroscopy at J-PARC" **T. KOIKE** *(Chairman H. Tamura)*
15:10-15:40	"Search for the alpha cluster condensed state in ^{16}0" **M. ITOH** *(Chairman H. Tamura)*
15:50-16:10	Coffee Break
16:10-16:40	"A dipole anisotropy of galaxy distribution: Does the CMB rest frame exist in the local universe?" **Y. ITOH** *(Chairman T. Futamase)*
16:50-17:20	"MOIRCS Deep Survey: Near-Infrared Observations of Galaxies at the Star-Forming Epoch of the Universe" **T. YOSHIKAWA** *(Chairman T. Futamase)*

Parallel Session B – Condensed Matter Physics Group *Chairmen Y. Kuramoto / T. Takahashi*

13:50-14:20	"From graphene to Z2 topological insulator" **K. IMURA** *(Chairman Y. Kuramoto)*
14:30-15:00	"Shear-induced phase separation of complex fluids" **K. SATO** *(Chairman Y. Kuramoto)*
15:10-15:40	"Ce 4f electronic structure of heavy-fermion systems across quantum critical point: a resonant angle-resolved photoemission study" **H. IM** *(Chairman Y. Kuramoto)*
15:50-16:10	Coffee Break
16:10-16:40	"Spin-resolved ultrahigh-resolution ARPES study of Rashba effect on semi-metal surface" **S. SOUMA** *(Chairman T. Takahashi)*
16:50-17:20	"Metal-contact effect on graphene" **R. NOUCHI** *(Chairman T. Takahashi)*

Parallel Session C – Mathematics and Philosophy Group *Chairmen T. Shioya / K. Naoe*

13:50-14:20	"Around Homological Mirror Symmetry" **M. FUTAKI** *(Chairman T. Shioya)*
14:30-15:00	"On the heat equation in a half space with a nonlinear boundary condition" **T. KAWAKAMI** *(Chairman T. Shioya)*
15:10-15:40	"An Approach to Experimental Philosophy of Mind" **M. IGASHIRA** *(Chairman K. Naoe)*
15:50-16:10	Coffee Break
16:10-16:40	"Utilitarianism and Rawls" **Masaru YONEHARA** *(Chairman K. Naoe)*

16:50-17:20	"Husserl and Disjunctivism: On the Theory of Perceptual Experience in Transcendental Phenomenology" **S. SATO** ***(Chairman K. Naoe)***
Collaborative Research Session A	***Chairman K. Inoue***
17:30-17:40	"Research Center for Electron Photon Science (Laboratory of Nuclear Science) Development of an electro-magnetic calorimter made up of ceramic Pr:LuAG scintillator" **T. ISHIKAWA**
17:40-17:50	"Study of geo neutrinos with KamLAND" **Y. SHIMIZU**
17:50-18:00	"Geometric Analysis on Einstein Equation" **S. YAMADA**
Collaborative Research Session B	***Chairman H. Yamamoto***
17:30-17:40	"Study of elementary particles, nuclei, and high pressure condensed matter in gravitational wave astronomy" **Y. ITOH**
17:45-17:55	"Development of Readout Board for FPCCD Detector" **Y. TAKUBO**
Collaborative Research Session C	***Chairman T. Ogawa***
17:30-18:40	"Theoretical formulation of morphology dynamics of membranes based on a combination of mathematical models and differential geometry" **K. SATO**
17:45-17:55	"The search for safety and certainty in foundations of mathematics from the logical and philosophical point of view" **K. YOKOYAMA**

Poster Presentations:

PO no.	Title / Name
1.	**Coherent control of excited states by multipulse photo excitation** Kenta Abe (Physics, D2, Tohoku Univ.)
2.	**de Haas –van Alphen effect studies in the Antiferro-Quadrupolar ordering systems: $Pr_{1-x}La_xPb_3$ and $U_{1-x}Th_xPd_3$** Toshiyuki Isshiki (Physics, D3, Tohoku Univ.)
3.	**Measurement of the Superparticle Mass Spectrum in the Long-Lived Stau Scenario at the LHC** Takumi Ito **(**Physics, D1, Tohoku University)
4.	**In situ NMR imaging of lithium- ion batteries during charge/discharge cycle** Yoshiki Iwai (Physics, D3, Tohoku University)
5.	**Crack propagation in largely deformed rubber sheet** Daiki Endo (Physics, D1, Tohoku University)
6.	**Optical response of photonic crystal with multi-layered structure** Rihei Endo (Physics, D2, Tohoku University)
7.	**Pseudo-spin Kondo effect in a capacitively-coupled parallel double quantum dot** Yuma OKAZAKI (Physics, D1, Tohoku University)
8.	**Spin and charge dynamics in a photo-excited double exchange system** Yu Kanamori (Physics, D2, Tohoku University)
9.	**Observation of ^{8}B Solar Neutrinos with KamLAND** Yoshiaki Kibe (Physics, D3, Tohoku University)
10.	**z~3 LYMAN BREAK GALAXY CLUSTER SURVEY IN SSA22 WITH VIMOS** Katsuki Kousai (Physics, D2, Tohoku University)
11.	**EELS and SXES studies of electronic structures of Al-TM alloys** Shogo Koshiya (Physics, D1, Tohoku University)
12.	**Comparison of membrane physical property changes between DMPC membrane and DMPE membrane induced by melittin** Atsuji Kodama (Physics, D3, Tohoku University)
13.	**Resonant x-ray scattering experiment on $Pr(Ru_{1-x}Rh_x)_4P_{12}$** Kotaro Saito (Physics, D1, Tohoku University)
14.	**Study of geo neutrinos with KamLAND** Yuri Shimizu (Physics, D3, Tohoku University)

15. **Pressure dependence of *B-T* phase diagram in heavy-fermion superconductor $CeRhSi_3$**
Tetsuya Sugawara (Physics, D2 Tohoku University)

16. **Neutral meson photoproduction with electromagnetic calorimeter complex FOREST**
Koutaku Suzuki (Physics, D3, Tohoku University)

17. **Micro-photoluminescence around spin phase transition of ν=2/3 fractional quantum Hall regime**
Jun-ichiro Hayakawa (Physics, D1, Tohoku University)

18. **Ionic conductivity of Trehalose-Water-Lithium iodide mixture in glass and supercooled liquid state**
Reiji Takekawa (Physics, D2, Tohoku University)

19. **Progress of the new DAQ system for wide-band solar neutrino observation with KamLAND**
Takemoto Yasuhiro (Physics, D1, Tohoku University)

20. **Double Chooz PMT preparation**
TABATA Hiroshi (Physics, D2, Tohoku University)

21. **Effects of lanthanoid ion on phosphate head groups in DMPC membrane and DMPC/DHPC mixtures.**
Kouya Tamatsukuri (Physics, D3, Tohoku University)

22. **Status of double beta decay experiment with KamLAND**
Azusa Terashima (Physics, D1, Tohoku University)

23. **Simulations on Dynamics of Wormlike Micellar System Using Particle-Field Hybrid Models**
Masatoshi Toda (Physics, D3, Tohoku University)

24. **Magneto-dielectric phenomena in charge ordered system with frustrated geometrical lattice**
Makoto Naka (Physics,D2, Tohoku University)

25. **Pi-mesonic decays of Λ hypernuclei**
Yoji Nakagawa (Physics, D1, Tohoku University)

26. **Axionic Mirage Mediation**
Shuntaro Nakamura (Physics, D3, Tohoku University)

27. **The Study of the Origin of Lyman alpha Emitters with Large Equivalent Widths**
Yuki Nakamura (Physics, D3, Tohoku University)

28. **Ultrafast broadband THz response of photo-induced metallic state in charge ordered**

insulator α-(BEDT-TTF $)_2I_3$
Hideki Nakaya (Physics, D3, Tohoku University)

29. **Ring-Exchange interaction in Orbital Degenerate System**
Joji Nasu (Physics, D2, Tohoku University)

30. **Shape Memory Effect Induced by Magnetic-Field Rotation in MnV_2O_4 Spinel Compound**
Yoichi Nii (Physics, D1, Tohoku University)

31. **The ω meson photoproduction on the nucleon in the threshold region**
Ryo HASHIMOTO (Physics, D3, Tohoku University)

32. **Prototype fast imaging detector for YN-scattering**
Ryotaro Honda (Physics, M1,Tohoku University)

33. **Ground state phase diagram of graphene in a high Landau level: A density matrix renormalization group study**
Tatsuya Higashi (Physics, D2, Tohoku University)

34. **Investigation of the n (γ,K^0) Λ reaction near the threshold**
K.Futatsukawa (Physics, D3, Tohoku University)

35. **Traffic flow of two lanes with a bottleneck**
Sho Furuhashi (Physics, D2, Tohoku University)

36. **Staggered Order with Kondo and Crystalline Field Singlets in f^2 System**
Shintaro Hoshino (Physics, D1,Tohoku University)

37. **Proton elastic scattering of ^9C at 290 MeV**
Yohei Matsuda (Physics, Assistant professor, Tohoku University)

38. **High Resolution and High Statistics Λ Hypernuclear Spectroscopy by the $(e,e'K^+)$ Reaction**
Akihiko Matsumura (Physics, D3, Tohoku University)

39. **External Gamma-ray Backgrounds of the KamLAND Detector**
Yukie Minekawa (Physics, D2, Tohoku University)

40. **Higgs Triplet Model**
Yusuke Motoki (Physics, D1, Tohoku University)

41. **Electron diffraction study of the low temperature phase of Hollandite-type oxide $K_2Cr_8O_{16}$**
Daisuke Morikawa (Physics, D1, Tohoku University)

42. **Light scattering by collective excitation of phonon in quantum paraelectrics**

Ryuta Takano (Physics, D1, Tohoku University)

43. **Formation of the Milky Way Based on the Analysis of Kinematics and Chemical Abundance of the Outer Halo Stars**
Miho Ishigaki (Astronomy, D3, Tohoku University)

44. **Searching for Luminous Core-Collapsed Supernovae in a High-z Proto-Cluster**
Nana Morimoto (Astronomy, D1, Tohoku University)

45. **A Study of Light Curves from Rapidly Rotating Neutron Stars**
Kazutoshi Numata (Astronomy, D3, Tohoku University)

46. **CMB Bispectrum from the Second-Order Cosmological Perturbations**
Daisuke Nitta (Astronomy, D3, Tohoku University)

47. **General Properties of Non-Radial Pulsations**
Aprilia (Astronomy, D3, Tohoku University)

48. **A Study on Mathematical Fuzzy Logic**
Ahmad Termimi Bin Ab Ghani (Mathematics, D1, Tohoku University)

49. **Some space-time integrability estimates of the solution for heat equations in two dimension**
Norisuke Ioku, (Mathematics, D2, Tohoku University)

50. **Well-posedness for Navier-Stokes equations in modulation spaces with negative derivative indices**
Tsukasa Iwabuchi (Mathematics, D2, Tohoku University)

51. **The soul conjecture for Riemannian orbifolds**
Naoki Oishi (Mathematics, D3, Tohoku University)

52. **A new approach to the existence of harmonic maps**
Toshiaki Omori (Mathematics, D2, Tohoku University)

53. **Stability of the interface of a Hele-Shaw flow with two injection points**
Michiaki Onodera (Mathematics, D3, Tohoku University)

54. **The Isomorphism between Motivic Cohomology and *K*-groups for Equi-Characteristic Regular Local Rings**
Yuki Kato (Mathematics, D3, Tohoku University)

55. **Bifurcations in semilinear elliptic equations on thin domains**
Toru Kan (Mathematics, D1, Tohoku University)

56. **On the curvature of the pseudo-volume form defining the carath_eodory measure hyperbolicity**
Shin Kikuta (Mathematics, D1, Tohoku University)

57. **Gödel's Incompleteness Theorem, Recursively Axiomatizable Theories, and Medvedev Degrees of Unsolvability**
Takayuki Kihara (Mathematics, D1, Tohoku University)

58. **Hypergeometric series on a *p*-adic field**
Kensaku Kinjo (Mathematics, D2, Tohoku Univercity)

59. **On Hasse principle of purely transcendental extension field in one variable**
Makoto Sakagaito (Mathematics, D3, Tohoku University)

60. **Large time behavior of solutions for system of nonlinear damped wave equations**
Hiroshi Takeda (Mathematics, D3, Tohoku University)

61. **Non-abelian generalization of Iwasawa theory**
Kazuaki Tajima (Mathematics, D1, Tohoku University)

62. **The quadratic subextension of the class field of a real quadratic field**
Toshihide Doi (Mathematics, D2, Tohoku University)

63. **Pattern formation by receptor-based models for regeneration experiments on Hydra**
Madoka Nakayama (Mathematics, D2, Tohoku University)

64. **The computational methods of canonical heights on elliptic curve**
Tadahisa Nara (Mathematics, D3, Tohoku University)

65. **Spatial branching process in random environment**
Nishimori Yasuhito (Mathematics, D1, Tohoku University)

66. **On a periodic decomposition of meromorphic functions**
Takanao Negishi (Mathematics, D2, Tohoku University)

67. **Difficulties of solving problems**
Kojiro Higuchi (Mathematics, D1, Tohoku University)

68. **Undecidability and weak theory of concatenation**
Yoshihiro Horihata (Mathematics, D2, Tohoku University)

69. **Davies' Conjecture for Pseudo-Schrödinger Operators and its Applications to Penalization Problem**
Masakuni Matsuura (Mathematics, D1, Tohoku University)

70. **Torsion points of Abelian varieties with values in infinite extension fields**
Yuken Miyasaka (Mathematics, D1, Tohoku University)

71. **Maximum principle for a biological model related to the motion of amoebae**
Harunori Monobe (Mathematics, D2, Tohoku University)

72. **Asymptotic behavior of solutions to the drift-diffusion equation in the whole spaces**
Masakazu Yamamoto (Mathematics, D3, Tohoku University)

73. **A study of the idea of systematic knowledge:**
    On the relation between nature and spirit in the organizational view of nature
    Fukuko Abe (Philosophy, D3, Tohoku University)

74. **Medical technology and surrogate decision-making**
    Haruka Hikasa (Philosophy, D3, Tohoku University)

75. **Hume's empiricism and the experimental method of reasoning**
    Hiromichi Sugawara (Philosophy, D1, Tohoku University)

76. **Epistemic deference and transmission of knowledge:**
    How should we (non-scientists) acquire warranted beliefs about scientific propositions?
    Mariko Nihei (Philosophy, D3, Tohoku University)

77. **The Finiteness of Human Beings and the Role of Technology**
    Ryozo Suzuki (Philosophy, D3, Tohoku University)

78. **What is ethically problematic in Biogenetics?**
    Takuma Obara (Philosophy, D3, Tohoku University)

79. **The ontological genesis of the theoretical attitude**
    Tetsurou Yamashita (Philosophy, D3, Tohoku University)

80. **Risk, uncertainty and the precautionary principle: How to deal with scientific uncertainty?**
    Yasuhiko Fujio (Philosophy, D3, Tohoku University)

81. **The mechanism of suppressed dynamical friction in a constant density core of dwarf galaxies**
    Shigeki Inoue (Astronomy, D2, Tohoku University)

Coherent control of excited states by multipulse photo excitation

Kenta Abe (Physics, D2, Tohoku Univ.)

1. Introduction

Ultrafast Energy Transfer in the primary process of the Light Harvesting Function

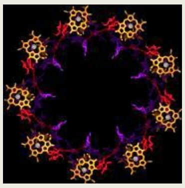

LH2 Complex. Red: Carotenoid, Gold, Purple: Bacteriochlorophyll

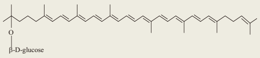

Rhodopin Glucoside

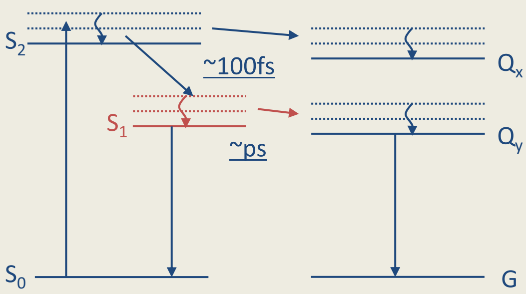

Ultrafast Energy Transfer from Carotenoid to Bacteriochlorophyll

Carotenoids play important rolls in the photosynthesis:

1. Provide absorbed light energy to Bacteriochlorophyll by ultrafast **highly-efficient** energy transfer.
2. Protect biological body from damage due to strong light.

2. Objective

Coherent Control of Vibrational Levels of Optically Forbidden S_1 State: Very Important Contribution to the Ultrafast Energy Transfer

P.J.Walla et al., J. Phys. Chem. A **106** (2002) 1909.
A.Wehling and P.J.Walla, J.Phys.Chem. B **109** (2005) 24510.

How to observe vibrations of an **optically forbidden** S_1 state?

1. Direct two-photon excitation.
2. Coherent control of S_1 after internal conversion from S_2 using multipulse excitation.

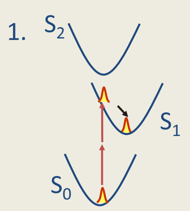

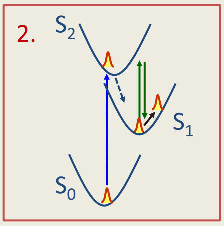

3. Sample

Nile Blue: Prototype System for Coherent Control of the Excited State

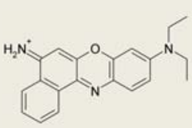

Nile Blue

Ring-breathing Mode:
Ground State 586cm^{-1} (56fs)
Excited State 568cm^{-1} (58fs)
A. C. Florean, et al., J. Phys. Chem. B **110**(2006)20023.

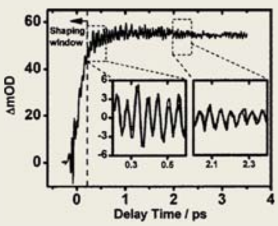

The strong vibrational mode of Nile Blue is observed by pump-probe spectroscopy.

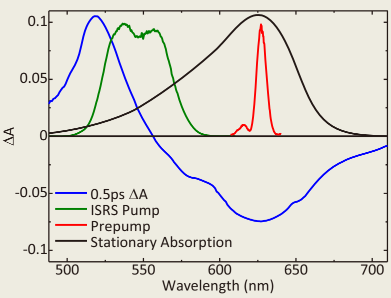

Nile Blue absorption and absorbance change spectra

4. Instruments

Two-Color Multipulse Excitation

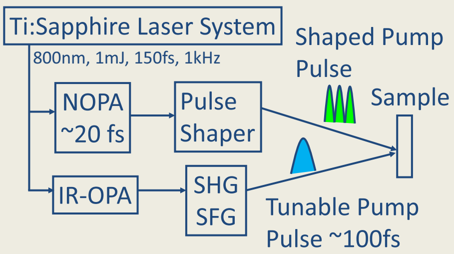

The tunable prepump (~100fs) generated by an infrared optical parametric amplifier (IR-OPA) was used to generate the excited state in the materials. The ultrashort transform-limit (TL) pulse (<20 fs) generated by a noncollinear OPA (NOPA) and its shaped pulse was used for the coherent control.

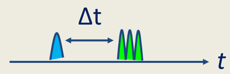

Δt is Widely Controllable.
Wavelength is Widely Tunable.

Pulse Shaper

A pulse shaper which consists of a spatial light modulator (SLM) with 800x600 pixels in a 4f arrangement modulated the TL pulse and generated the shaped pump pulse.

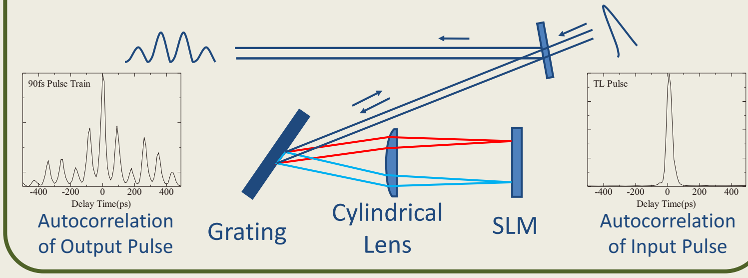

5. Results

1. Pulse Train Excitation with Several Spacing

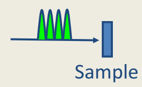

TL and 56 fs pulse train generate 56 fs vibration, while 90 fs pulse train generates 58 fs vibration with almost same amplitude.

Vibration in the excited state was generated by 90fs pulse train because of multipulse excitation effect.

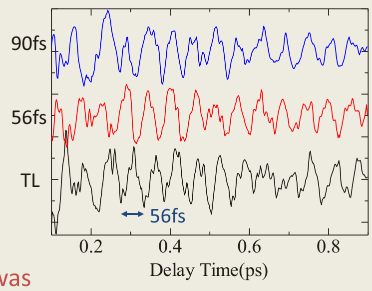

Coherent Vibration in Nile Blue

2. Two-Color Multipulse Excitation

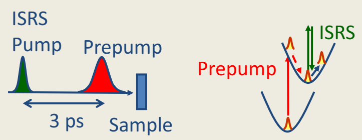

Lower frequency mode (58 fs mode) was observed with prepump.

Excited state was generated by prepump and it's coherent vibration was induced by ISRS pump.

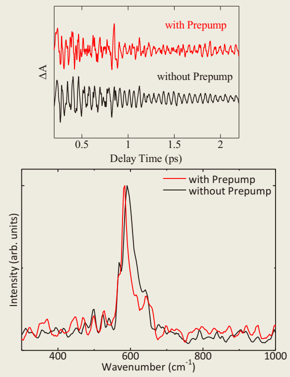

Fourier Transform of Signal

6. Summary

Multipulse Excitation can Successfully Induce the Coherent Vibration in the Excited States.

Next: Apply this Method to the Optically Forbidden S_1 State of Carotenoids.

Po.2

de-Haas -van Alphen effect studies in the Antiferro-Quadrupolar ordering systems: $Pr_{1-x}La_xPb_3$ and $U_{1-x}Th_xPd_3$

Department of Physics and CLTS, Tohoku Univ., IMR, Tohoku Univ.[A], NIMS[B]
T. Isshiki, T. Komatsubara, I. Satoh[A], H.S. Suzuki[B], N. Kimura, H. Aoki

Abstract

In the past decade, it is found that higher order multipoles (quadrupolar, octupolar, etc) play a key role in some rare earth and actinide systems. Although a great number of studies have been performed, the mechanism of multipolar ordering has not been clarified yet. We have focused on $Pr_{1-x}La_xPb_3$ which have nonmagnetic Γ_3 doublet in the crystalline electric field ground state and exhibits antiferro-quadrupolar(AFQ) ordering below 0.4K for x=0.00. In this system, a huge C/T value and the non-Fermi liquid behavior is observed, suggesting that the quadrupole moment hybridizes with the conduction electrons.

We have succeeded in observing the dHvA oscillations down to very low magnetic field on $Pr_{1-x}La_xPb_3$ and observing the change in the properties of conduction electrons together with that in the quadrupolar ordering. Moreover we study the dHvA effect on $5f^2$ localized system $U_{1-x}Th_xPd_3$ wchich exhibits AFQ orderings below 8T for x=0.00 to compare the results of $Pr_{1-x}La_xPb_3$ to those of $U_{1-x}Th_xPd_3$. Our results indicate that

(1) [redacted] come from the interaction between the quadrupole moments and the conduction electrons,
(2) The conduction electrons [redacted] the transition temperature of AFQ ordering in $Pr_{1-x}La_xPb_3$,
(3) There is [redacted] on x=0.03 for $Pr_{1-x}La_xPb_3$ and [redacted] for $U_{1-x}Th_xPd_3$ at which quadrupolar ordering is thought to disappear.

Introduction

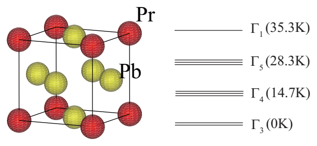

$PrPb_3$ has nonmagnetic Γ_3 doublet

Modulated quadrupolar phase

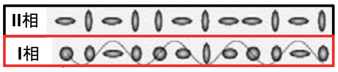

A huge C/T even at 50mK

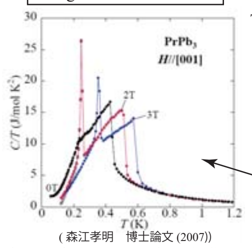

（森江孝明　博士論文 (2007)）

A huge C/T in AFQ-I phase indicates the existence of the heavy effective mass and corresponds to the structure of AFQ ordering.

Phase Diagram of $Pr_{1-x}La_xPb_3$

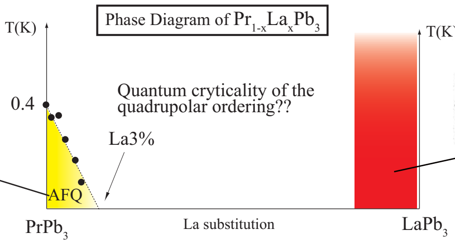

The conduction electrons hybridize with the quadrupole moment?

Non Fermi liquid behavior at low concentration range of Pr ion

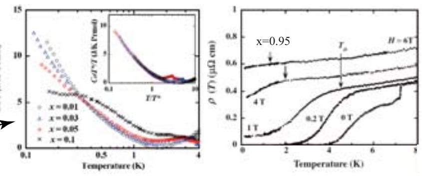

(Kawae et al., PRL 96 027210 (2006))　(Kawae et al., JPSJ 72 2141 (2003))

Quadrupolar Kondo effect is thought to be the origin of the non Fermi liquid.

dHvA effect study

$$M \propto A\sin\left(\frac{2\pi F}{H}+\phi\right)$$

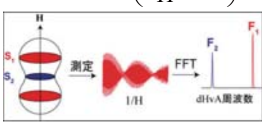

$$A \propto \frac{\lambda m^* T/B}{\sinh(\lambda m^* T/B)}\cdot\exp(-\lambda m^* T_D/B)$$

m*: effective mass (many-body effect)
T_D : dingle temperature (scattering rate)

[redacted]

Non Fermi liquid bihavior (x=0.97)

[redacted]

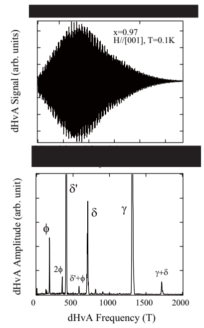

[redacted]

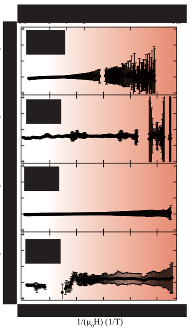

All of the Fermi surfaces are observed.
dHvA oscillations exist into the [redacted] with [redacted] in dHvA amplitude and effective mass.

[redacted] at very low magnetic field.

Results and Discussions

dHvA signal (x=0.00)

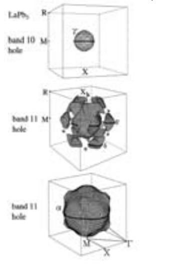

(Aoki et al. JPSJ 66 3988 (1997))

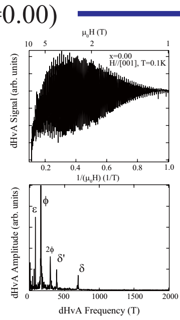

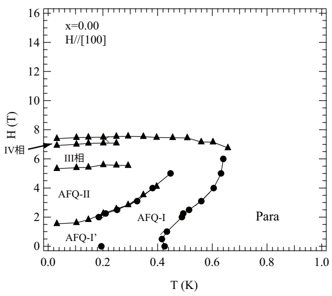

All of the Fermi surfaces are observed.
Especially φ branches, we have succeeded in observing the dHvA oscillations down to AFQ-I phase.

A huge C/T (x=0.00)

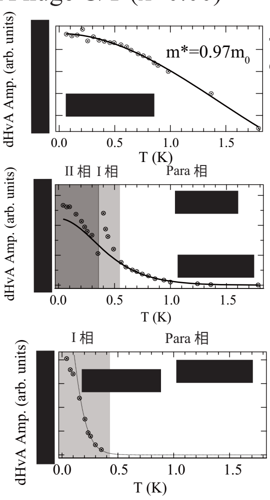

Temperature dependences of dHvA amplitude change with f electron state and correspond to the results of electric resistivity.

[redacted]

This means that the temperature dependence of dHvA amplitude in $PrPb_3$ is strongly affected by th change in scattering rate of conduction electrons rather than effective mass.

There is [redacted] strong mass enhancement even in AFQ-I phase.

Interaction between the quadrupole moment and the conduction electrons

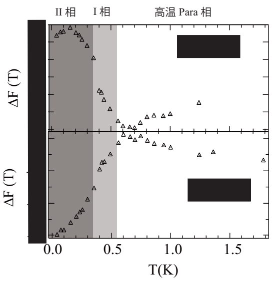

Temperature dependences of the dHvA frequences also change with f electron state and depend on Fermi surfaces.

Semiquantitative analysis

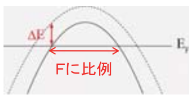

$$E=-\frac{\hbar^2k^2}{2m^*}\text{より、}$$

$$\Delta E=-\frac{1}{m^*/m_0}\frac{\hbar e}{m_0}\Delta F$$

6T	ΔE(meV)	λ
γ	-0.51	5.53
δ'	-0.27	1.94
φ	0.08	1.52

$m^*_{PrPb3}=\lambda m^*_{LaPb3}$

The ratio of λ corresponds to *p-f* mixing in $PrPb_3$

The shift of the energy band might come from the change of *p-f* mixing which depends on Fermi surfaces.

AFQ sturucture model

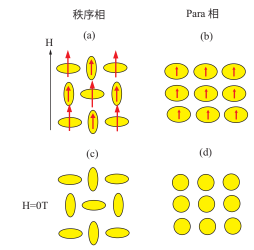

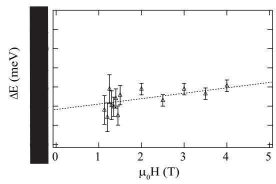

[redacted] the transition temperature of AFQ ordering in $PrPb_3$, indicating that the conduction electron might [redacted].

Quantum criticality of the quadrupolar ordering (x=0.03)

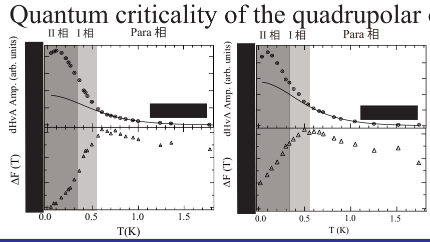

The small amount of La impurity [redacted]
This indicates that [redacted] order exists for x=0.03.

There might be [redacted] of quadrupolar ordering in $Pr_{1-x}La_xPb_3$ system.

Measurement of the Superparticle Mass Spectrum in the Long-Lived Stau Scenario at the LHC

Takumi Ito (Physics, D1)
Particle Theory and Cosmology Group
Tohoku University

Reference :
Tl. R. Kitano and T. Moroi, arXiv:0910.5853[hep-ph]

The 2nd GCOE International Symposium
2010.2.18.-19.

Introduction

Supersymmetry : A famous extension of the Standard Model

There are several reasons to consider SUSY seriously.

- Gauge coupling unification at the very high energy scale (GUT)
- Candidates of Dark Matter of the Universe
- Predicts a light higgs (prefered by EW precision measurements)
- Naturally solves gauge hierarchy problem

→ It will appear around TeV scale.

↔ in the energy range of the LHC experiments!

So, Question is

What is a signature of SUSY at the LHC?

Introduction

Signature of SUSY at the LHC...

→ It strongly depends on what the LSP is.

Popular candidates of LSP are:

- The lightest neutralino $\tilde{\chi}_1^0$ — Large missing p_T
- Gravitino $\tilde{\psi}_\mu$ — Weekly interacting (Gravity) → Long-lived NLSP which escapes from the detector → If NLSP is charged, we can observe its track
- ...

(LSP: Lightest SuperParticle)

Introduction

Long-lived stau scenario

- It is naturally realized when a model has a large tanβ (the ratio of two higgs' VEVs).
- Cosmological problems, which may be caused by the long-lived charged particle, can be avoided if there is weekly interacting LSP (i.e. gravitino).

A slow-moving charged track (= stau) informs us a production of superparticles in high energy experiments.

→ we can reduce Strandard Model backgrounds.

Further more, we can measure stau's momentum, velocity and energy as well as ones of SM particles.

→ All final state particles in the event are visible (except ν)

→ ***We have a opportunity to probe the SUSY in detail!***

Introduction

We discuss a determination of the superparticle masses at the LHC experiments in the model with the long-lived stau.

- Neutralinos
- Sleptons (selectron, smuon)
- Squarks

We perform a Monte Carlo analysis of sparticle production events at the LHC.
Our basic ideas and the simulated accuracies of the mass determinations are discussed in the following slides.

Monte Carlo Study; Model & Assumptions

GMSB [Dine,Nelson,Shirman(95)]
$\Lambda = 60\,\mathrm{TeV},\ M_{mess} = 900\,\mathrm{TeV},$
$N_5 = 3,\ \tan\beta = 35, \ldots$

$\tilde{g}$	1309
$\tilde{q}_L$	1230
$\tilde{q}_R$	1180
$\tilde{W}^0$	426
$\tilde{B}$	240
$\tilde{e}_R$	194
$\tilde{\mu}_R$	193
$\tilde{\tau}_1$	149

Reduced 1 GeV by hands

MSSM-LSP

masses are in GeV

Monte Carlo Analysis

Event Gen. by HERWIG6.510

Fast Detector Sim. by PGS4

67k events are generated (100 fb^{-1})

Asummptions

- Stau is stable in the detector.
- Stau with v < 0.9c can be identified. [Ambrosanio,Mele,Petrarca(01)]
- No SM backgrounds, if we find out at least one stau in the event.

Neutralino Masses

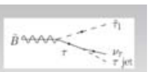

The lightest neutralino (bino) decay

bino → τ + stau

We consider hadronic decay mode of τ-lepton.

↔ Some part of the energy of τ is taken away by neutrino

$$M_{\tilde{B}} = \sqrt{(p_{\tilde{\tau}_1} + p_{\tau\text{-jet}} + p_{\nu_\tau})^2}$$
$$\geq \sqrt{(p_{\tilde{\tau}_1} + p_{\tau\text{-jet}})^2}$$

Endpoint ↕ bino mass

Event Selection

(1) At least one stau with 0.4c < v < 0.9c

(2) At least one τ-tagged object with p_T > 15 GeV

Neutralino Masses

To reduce BGs, we adopt a charge subtraction:

OS (τ stau) – SS (τ stau) = Signal

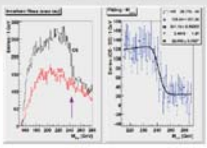

determined underlying
$M_{\tilde{B}}$ = 241.1 ↔ 239.5

Uncertainties
- Statistics ± 1 GeV
- Stau mass measurement [Ambrosanio et al.(01), Ellis et al.(06,07)] ± 100 MeV

→ Bino mass measurement : $\delta m_{\tilde{B}} \sim 1$ GeV

Neutralino Masses

Also, wino mass can be measured by using charge subtraction

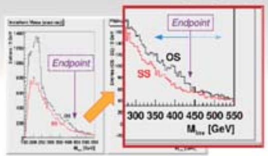

Neutralino Masses

Also, wino mass can be measured by using charge subtraction

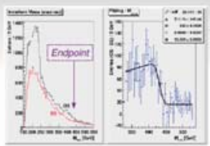

determined underlying
$M_{\tilde{W}^0}$ = 430.0 ↔ 425.9

Uncertainties
- Statistics ± 5 GeV
- Stau mass measurement ± 100 MeV

→ Wino mass measurement : $\delta m_{\tilde{W}^0} \sim 5$ GeV

Slepton Masses

2-step SUSY decay chain:

bino → $\ell^\pm$ + slepton$^\mp$,

slepton$^\pm$ → $\ell^\pm$ + τ + stau ; followed by τ → τ-jet + ν_τ

Collinear approximation; $p_\tau = r p_{\tau\text{-jet}}\ (r \geq 1)$

The value of r is determined by the condition:
$$m_{\tilde{B}}^2 = (p_{\tilde{\tau}_1} + p_{\ell'} + r p_{\tau\text{-jet}} + p_{\tilde{\tau}_1})^2$$

Then, $\longrightarrow M_{\tilde{\ell}} = \sqrt{(p_\ell + r p_{\tau\text{-jet}} + p_{\tilde{\tau}_1})^2}$

Event Selection

(1)(2) At least one pair of stau and τ-tagged jet (OS)

(3) At least one pair of leptons(SF,OS) with p_T > 15 GeV

Slepton Masses

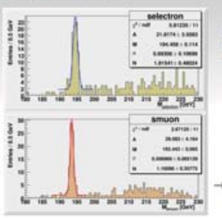

determined underlying
$M_{\tilde{e}}$ = 194.5 ↔ 194.4
$M_{\tilde{\mu}}$ = 193.4 ↔ 193.4

Uncertainties
- Statistics ± 100 MeV
- Stau mass measurement ± 100 MeV
- Bino mass measurement ± 1 GeV

→ Slepton masses:
$\delta m_{\tilde{e}} \sim \delta m_{\tilde{\mu}} \sim 1$ GeV

Slepton Masses

Mass difference $M_{\tilde{e}} - M_{\tilde{\mu}}$

is not sinsitive to uncertainties

of bino mass measurement.

→ $\delta(M_{\tilde{e}} - M_{\tilde{\mu}})$
~ 100 MeV

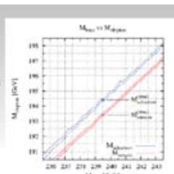

This level of accuracy for the mass difference measurement provides us information of SUSY breaking mechanism.

- Loop effects (muon Yukawa) $\sim O(100\ \mathrm{MeV})$ for the large tanβ
- SUGRA effects $\sim m_{3/2}^2/m_{\tilde{l}}$ ← $m_{3/2} \sim O(1\ \mathrm{GeV})$ case?

Squark Masses

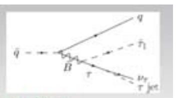

2-step SUSY decay chain:

squark → q + bino,

bino → τ + stau ; followed by τ → τ-jet + ν_τ

τ's momentum is reconstructed by $m_{\tilde{B}}^2 = (r p_{\tau\text{-jet}} + p_{\tilde{\tau}_1})^2$

Then, $\longrightarrow M_{\tilde{q}} = \sqrt{(p_{jet} + r p_{\tau\text{-jet}} + p_{\tilde{\tau}_1})^2}$

Event Selection

(1)(2) At least one pair of stau and τ-tagged jet

(3) At least one jet with p_T > 100 GeV

(4) No isolated leptons with p_T > 15 GeV

Squark Masses

We use upto leading 4 jets (p_T), and again charge subtraction.

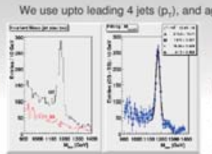

determined underlying
$M_{\tilde{q}}$ = 1172 ↔ 1180 (R)
1230 (L)

Uncertainties
- Statistics + Systematic error ± 10 GeV ???
- Stau mass measurement ± 100 MeV
- Bino mass measurement ± 1 GeV

→ Squark mass measurement : $\delta m_{\tilde{q}} \sim 10$ GeV

Somewhat small value is obtained... this may be improved?

Jet algorism? Cone size? Event selection? Or...

Conclusions

We discuss mass measurements of superparticles in the long-lived stau scenario at the LHC experiments.

- Neutralino Masses
  by endpoint analysis : $\delta m_{\tilde{B}} \sim 1$ GeV, $\delta m_{\tilde{W}^0} \sim 5$ GeV
  charge subtraction method is useful.
- Selectron & Smuon Masses
  particularly in the case $m_{\tilde{B}} > m_{\tilde{e}_R} > m_{\tilde{\tau}_1}$
  as a sharp peak : $\delta m_{\tilde{e}} \sim \delta m_{\tilde{\mu}} \sim 1$ GeV
  - mass difference : $\delta(M_{\tilde{e}} - M_{\tilde{\mu}}) \sim 100$ MeV
- Squark Masses
  as a clear peak : $\delta m_{\tilde{q}} \sim 10$ GeV

Another Example; Sweet Spot Model [Ibe,Kitano(07)]

slepton masses

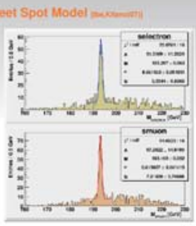

Another Example; Sweet Spot Model [Ibe,Kitano(07)]

The size of the mass difference

(for the fixed N_5 and Λ)

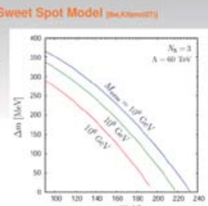

In situ NMR imaging of lithium- ion batteries during charge/discharge cycle

Institute for Multidisciplinary Research of Advanced Materials, Tohoku University

Yoshiki Iwai, Daiki Ohno, Junichi Kawamura

1. Introduction

Lithium ion battery

・High voltage・Hight energy density

Problem

・explosion & capacity fading for long cycling

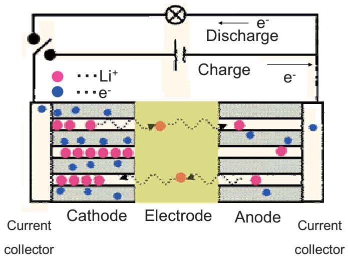

What's happened inside the Li-ion battery ?

Aim of my study

Visualizing the degradation in Li-ion battery with NMR imaging (= MRI) technique

Merits of NMR imaging for batteries

・Nondestructive

・High sensitivity for light atoms (^{1}H and ^{7}Li) composed of electrolyte for batteries

Need to observe inside the cell under operation

2. Experimental

Li-ion Battery

・Cathode: $LiCoO_2$ coated on Al foil

・Anode: Li metal

・Electrolyte: $LiClO_4$+ Propylene carbonate (PC) (1mol/L)

NMR imaging

・Instrument: Bruker Avance 400 (9.4T)

・mini imaging probe : Φ40mm

・Pulse sequence: Spin-echo imaging

・Field of View: 40mm×40mm

・Spatial resolution 160 mm (^{1}H) & 320 mm (^{7}Li)

・Nuclear: ^{1}H (400 MHz) and ^{7}Li (155 MHz)

Electrochemical measurement (CV)

・Instrument: Hokuto Denko HSV-100

・Voltage: 3.0∼4.2 (V)

・Scan rate: 1.0 (mV/sec)

Cell design

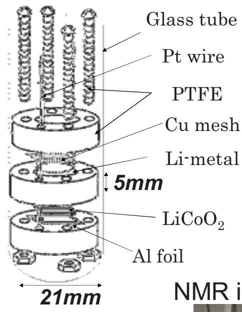

NMR instrument

3. Result and Discussion (^{1}H NMR imaging)

^{1}H intensity =Propylene carbonate (PC) in electrolyte

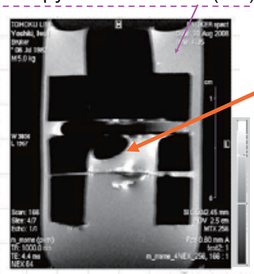

Observation of gas generation inside the Lithium ion battery

Gas formation

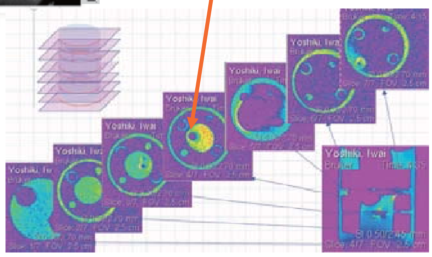

Mechanism of gas generation

PC + e- + Li+ →$CH_3CHCH_2OCO_2Li$

$2CH_3CHCH_2OCO_2Li$
→ $CH_3CH(OCO_2Li)CH_2OCO_2Li$ ↓
+ $CH_3CH=CH_2$ ↑

Lithium-Ion Batteries: Solid-Electrolyte Interphase
Perla B. Balbuena, Yixuan Wang, Imperial College Press, (2004)

Enhancement of MRI intensity near $LiCoO_2$ cathode

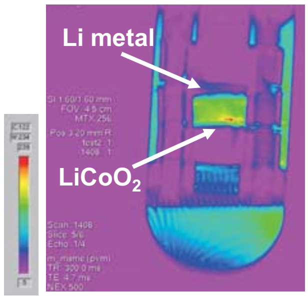

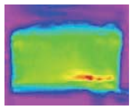

Enhancement of MRI intensity near cathode material

Possibility

・Effect of Co ion

・ Artifact due to electrode and current collector (Al)

Relationship between concentration of $CoCl_2$ in PC electrolyte and MRI intensity

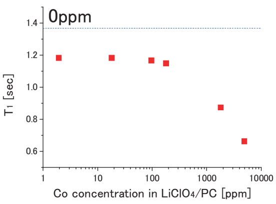

High concentration of Co ion
↓
Decreasing relaxation time T_1 in electrolyte
↓
emphasis MRI intensity

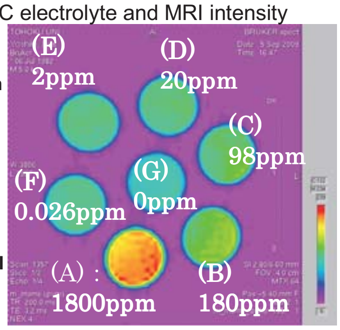

Relationship between MRI intensity & T_1, T_2

$$I(x,y) \propto \rho(x,y)(1-e^{-TR/T_1})\cdot e^{-TE/T_2}$$

In-situ NMR imaging under cyclic voltammetry (CV)

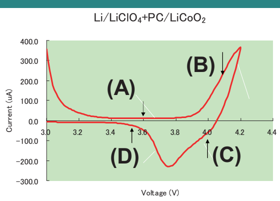

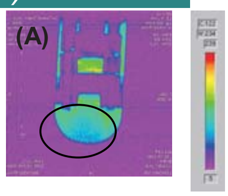

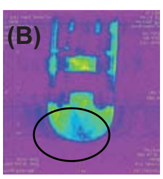

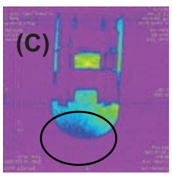

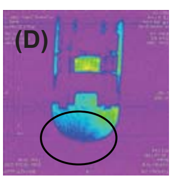

Decreasing the MRI intensity bottom part of electrolyte

It suggests・・・

Polymerization of Propylene carbonate ⇒ suppression motility of ^{1}H ⇒lowering T_2 ⇒decreasing MRI intensity

^{7}Li NMR imaging in Li-ion battery

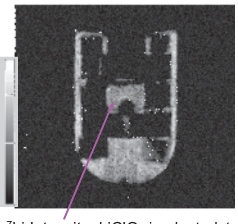

^{7}Li Intensity=$LiClO_4$ in electrolyte

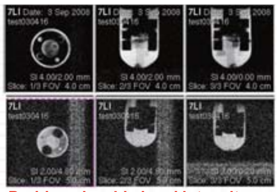

We succeed ^{7}Li NMR imaging of Li-ion battery in practical spatial resolution (320μm) for the first time in the world!

Problem: low Li signal intensity compared with ^{1}H

・Low S/N ratio : Noise commingling from electrochemical instruments

・Long acquisition time (~10 hour): impossible to detect motion

4. Summary

NMR imaging is powerful tool for nondestructive imaging of Li-ion battery

^{1}H imaging: It can detect gas generation, Co-ion elution to electrolyte, polymerization of electrolyte under electrochemical cycling

^{7}Li imaging: We measured ^{7}Li NMR imaging of Li-ion battery successfully in practical spatial resolution (320μm) for the first time in the world.

Future work

Visualization of ionic motion in Li-ion battery with NMR imaging

Crack propagation in largely deformed rubber sheet

Daiki Endo
Physics, D1, Tohoku University

Previous study of quasistatic crack propagation

- An experiment conducted by Yuse and Sano（Nature (London) 362, 329 (1993)) motivates researchers to study about crack pattern especially in brittle materials such as glasses. Glasses can be regarded as linear elastic body.
- As we change temperature difference ΔT or descent speed V, crack pattern changes.

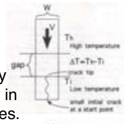

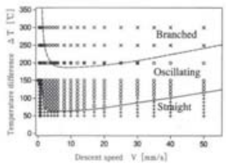

Fracture in large deformation

- Unlike glasses, many materials exhibit nonlinear elasticity and large dissipation when they fracture under large deformation.
- $dE_{\mathrm{elastic}} = dE_{\mathrm{surface}} + dE_{\mathrm{dissipation}}$
- $dE_{\mathrm{dissipation}}$ depends on viscosity, viscoelasticity, and plasticity.

An experiment of rupture of rubber sheets

- Rubber is a typical material which can deform largely. It shows nonlinear elasticity and creep.

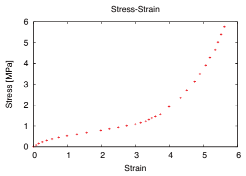

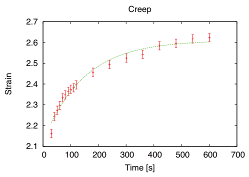

a=0.37,c=2.61,T=146

Experimental procedure

1. Prepare a cylindrical rod and cover it with very viscous silicon oil.
2. As shown in figure, cover the rod with a stretched cylindrical rubber sheet (an inflated balloon) on oil and wait until the rubber sheet is relaxed to be under uniform strain.
3. Create a small initial crack at one end of the sheet to create a spontaneous crack. Then observe the crack propagation.

Experimental set up

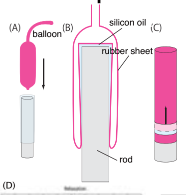

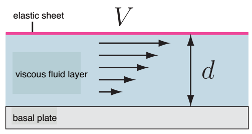

(D)

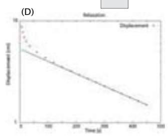

Thickness of a balloon in a natural state	0.37mm
Circumferential length of a balloon in a natural state	20mm
Kinematic viscosity of silicon oil	10000cSt
Diameter of a rod	15, 17.5, 20, 22.5, 25, 30, 35mm

Note

- If we change the amount of silicon oil covering the rod, we can change characteristic relaxation time of the sheet by changing viscous resistance. And if we change diameter of the rod, we can change strain of the sheet.

Five typical crack patterns

【Straight crack】Straight crack propagates in a longitudinal direction of the rod.

【Oscillating crack】Oscillatory crack propagates in a longitudinal direction of the rod.

【Helical crack】Crack keeps a constant angle to the longitudinal direction of the rod.

【Irregular crack】Crack exhibits several irregular turns and stops after that.

【Stagnating crack】Crack propagates in a very short distance and stops after that.

Pattern diagram

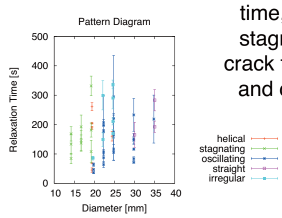

- As we increase strain of the sheet or shorten characteristic time, pattern changes from stagnating crack to straight crack through helical, irregular and oscillating in this order.
- The order of oscillating crack and straight crack is opposite to result of quasistatic fracture of glasses.

Computer simulation

- We use viscoelastic spring model which follows time evolution described by

$$\gamma \frac{d\mathbf{r}^i}{dt} = \sum_j \mathbf{F}^{ij}, \gamma_{in}\frac{d\ell_{in}^{ij}}{dt} = F^{ij}$$

$$F^{ij} = k\ell^{ij} = k_{\mathrm{in}}\ell_{\mathrm{in}}^{ij} + \gamma_{\mathrm{in}}\frac{d\ell_{\mathrm{in}}^{ij}}{dt}$$

- characteristic length a_0
- characteristic time $\frac{\gamma_{\mathrm{in}}}{k_{\mathrm{in}}}$=$T_{in}$
- characteristic force ka_0

$$\ell^{ij} + \ell_{\mathrm{in}}^{ij} = |\mathbf{r}^i - \mathbf{r}^j| - a_0$$

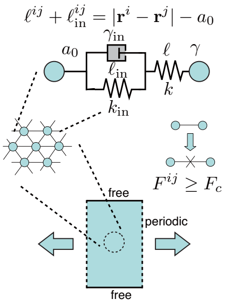

Comparing stress-strain curve

- The model shows nonlinear elasticity and viscoelasticity like a rubber sheet.

model

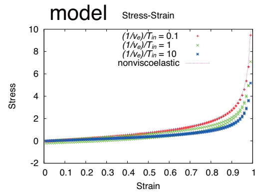

rubber

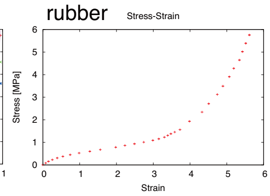

Pattern diagram 1 (computer simulation)

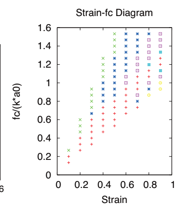

- This diagram is result in nonviscoelastic condition. In large deformation regime, we can see oscillating pattern and straight pattern which may correspond to oscillating crack and straight crack in the experiment.

Crack patterns (computer simulation)

- As we increase strain or decrease F_c, wave length and amplitude decrease.

strain=0.6

F_c

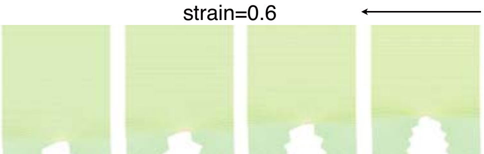

Pattern diagram 2 (computer simulation)

$$\frac{F_c}{ka_0} = 1.0$$

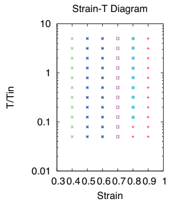

- This diagram is result of computer simulation which corresponds to pattern diagram in the experiment. Unlike the experiment, we can see no change of the crack pattern by changing characteristic time.

Conclusion

- We observe five typical crack patterns in the experiment of rupture of rubber sheets.
- From computer simulation, oscillating pattern and straight pattern appear in large deformation regime in same order of the experiment.
- We conclude that in large deformation regime, very large dissipation arises and causes shortening crack path length per unit length of the rod.

Optical response of photonic crystal with multi-layered structure

Rihei Endo Physics, D2, Tohoku University

Ⅰ. Introduction

Tunneling photons in frustrated total internal reflection

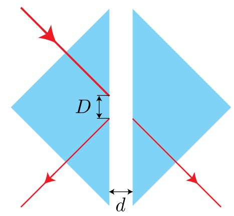

Fig.1: Air gap between double prism
D : Goos-Haehnchen shift

In the condition that total reflection happens in geometrical optics, any light can't penetrate into next medium. However, when two prisms are set as shown in figure, we can observe the penetration light in the second prism, so called "light tunneling effect".

【History】
In 1927, light tunneling effect was first discovered [1].
In 1947, Goos-Haehnchen effect was discovered [2].
In 1992, superluminal barrier traversal was discovered [3].

【Motivation】
We want to calculate the light pulse propagation of superluminal barrier traversal.

[1] J. Ch. Bose, in Collected Physical Papers of Sir Jagadis Chunder Bose (Longmans, London, 1927), p. 42.
[2] F. Goos and H. Ha¨nchen, Ann. Phys. (Leipzig) 1, 333 (1947).
[3] Enders and G.Nimtz, J. Phys. I France 2, 1693-1698 (1992).

Ⅱ. Theory

Ⅱ- i . Boundary condition

$n_1 > n_2$

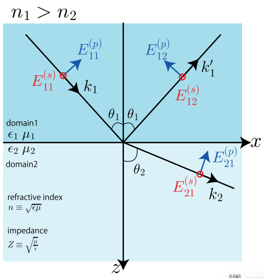

【Snell's law】
$n_1 \sin\theta_1 = n_2 \sin\theta_2$

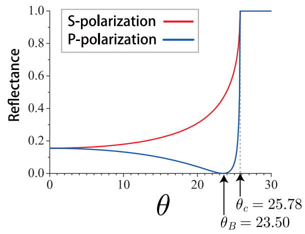

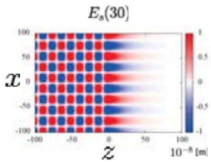

Brewster's angle: $\theta_B = \arctan\left(\frac{n_2}{n_1}\right)$
Critical angle: $\theta_c = \arcsin\left(\frac{n_2}{n_1}\right)$

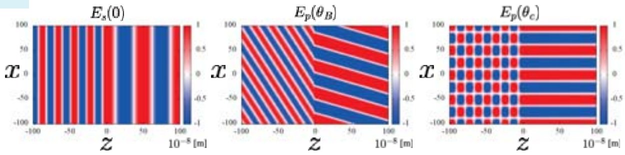

Ⅱ - ii . Refrecrance of Sandwiched layer

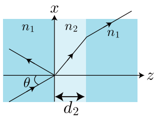

$n_1 = 2.3$
$n_2 = 1.0$
$d_2 = \lambda_0 / n_2$

Resonance angle
$\theta_{d_2} = \arcsin\left(\frac{n_2}{n_1}\sqrt{1 - \frac{m\lambda_0}{2n_2 d_2}}\right)$

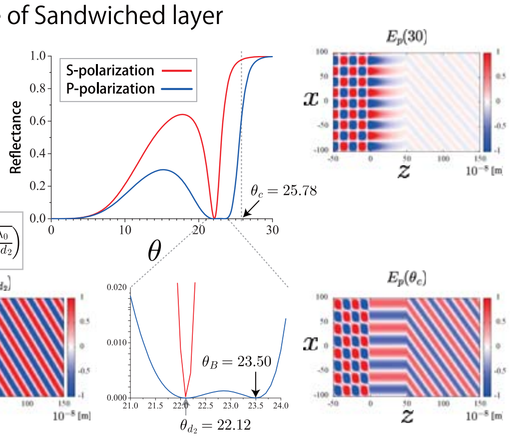

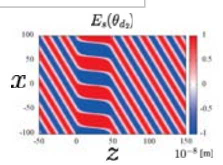

Ⅱ - iii . Light tunneling effect of Sandwiched layer

The amount of penetration of light is decided according to the incident angle and the width of the barrier. We calculated the reflectance of light vs barrier width in the case of critical angle. We got the result that reflectance of P-polarization light is smaller than that of S-polarization.

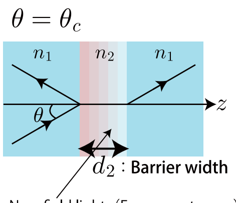

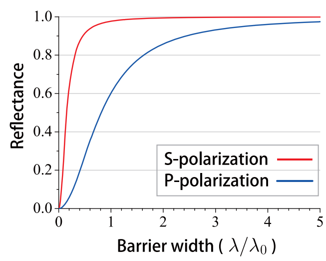

Ⅲ. Model

We consider about one dimension photonic crystal with the periodic multilayer structure as a model. To enhance "light tunneling effect", we can adjust the refractive indices(n_1, n_2), the number of layers (N), and the width of the layer (d_1, d_2). When the angle of incidence is the critical angle, tunneling and propagating are occurred alternately. To examine the behavior of the propagating of the light pulse in this system, we calculate the Maxwell equation.

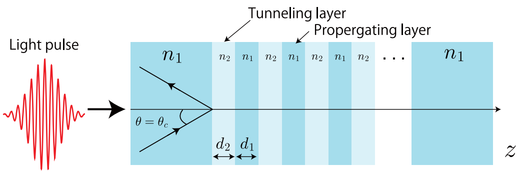

■ parameters

Refractive index
$n_1 = 2.3$
$n_2 = 1.0$

LayerNumber
$N = 17$

layer width
d_1 d_2

Center of weve length
$\lambda_0 = 500$ [nm]

■ What is photonic crystals ?

In generally, photonic crystal (PC) is comprised identical dielectric structures replicated in one-, two-, three-dimensional periodic arrangement as illustrated in Fig.

■ Many kinds of photonic crystals

1D-Fabry-Perot cavity

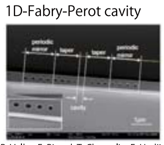

P. Velha, E. Picard, T. Charvolin, E. Hadji, J. C. Rodier, P. Lalanne, and D. Peyrade, Opt. Express 15, 16090 (2007)

M. W. Takeda, S. Kirihara, Y. Miyamoto, K. Sakoda, and K. Honda, Phys. Rev. Lett. 92, 093902 (2004)

3D-Photonic fracral

2D-Crystal Slab Defect Waveguide

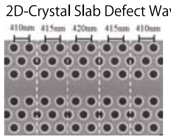

BS Song, S Noda, T Asano, Y Akahane, Nature Materials 4, 207 - 210 (2005)

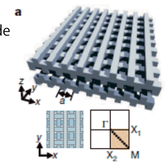

K Ishizaki, S Noda Nature 460, 367-370 (2009)

3D-photonic crystal

Ⅳ. Results

At first, we examined the resonance condition of the "light tunneling effect" (Fig1). Next, we examined the relation between reflectivity and the circular frequency when the resonance condition was filled (Fig.2). Finally, we calculated the time evolution of the Gauss pulse that centered on the number of resonance vibrations (Fig.3). In comparison with light propagation of 1D-photonic crystal and that of vacuum, the front velocities quicken more than the light that propagates in the vacuum.

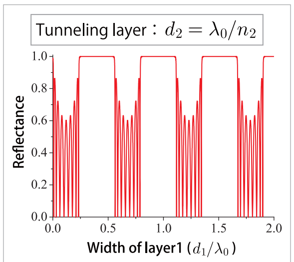

fig.1: reflectance of light vs width of layer1

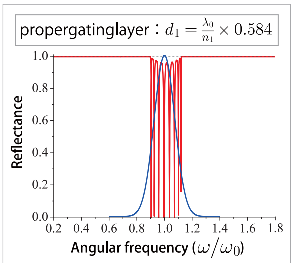

fig.2: reflectance of light vs Angular frequency

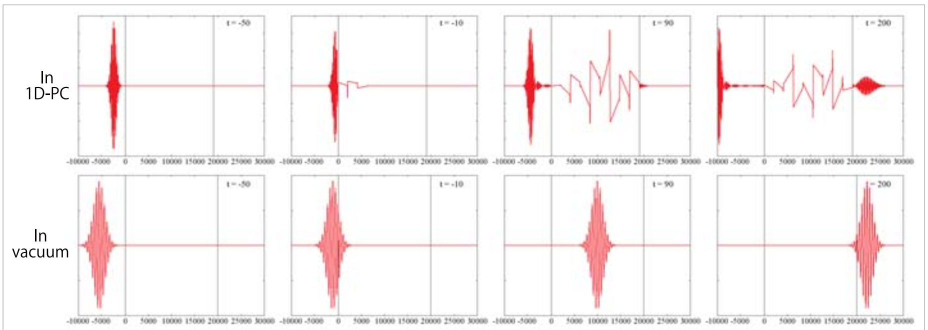

fig.3: comparison with light propagation of 1D-photonic crystal and that of vacuum

Ⅳ. Conclusion

We have understood the following from calculating the Maxwell equation in one dimension photonic crystal with "light tunneling effect".

1. We got the condition of enhancing "light tunneling effect" in the 1D-photonic crystal.

2. In using "Light tunneling effect", the front velocities quicken more than the light that propagates in the vacuum.

7

Pseudo-spin Kondo effect in a capacitively-coupled parallel double quantum dot

February 18th by Yuma OKAZAKI

Kondo singlet and parallel QD

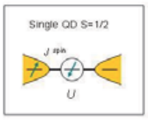

Kondo singlet : many body spin singlet between a local spin at the QD and conduction electrons via an effective antiferromagnetic interaction.

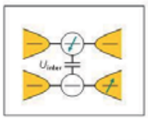

A **parallel double QD** consists of two QDs with a capacitive interaction.
Each QDs are tunnel-coupled to separated lead electrodes.

Each QDs are individually accessible and controllable

Orbital degrees of freedom can be regarded as a pseudo-spin which can play an equivalent role to spin.

A wide variety of Kondo correlation is expected with entangled spin and pseudo-spin.

Motivation : Investigation of Kondo correlation in the parallel QD.

DC current through the Kondo singlet

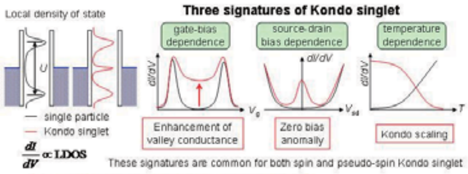

$\frac{dI}{dV} \propto$ LDOS

These signatures are common for both spin and pseudo-spin Kondo singlet

Different behaviour in a in-plane magnetic field

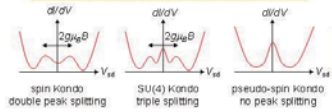

We can distinguish types of Kondo singlet from these differences.

device and controll

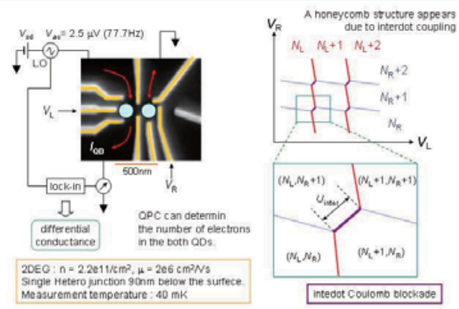

QPC can determin the number of electrons in the both QDs.

2DEG : n = 2.2e11/cm², μ = 2e6 cm²/Vs
Single Hetero junction 90nm below the surface.
Measurement temperature : 40 mK

Charge stability diagram and spin state

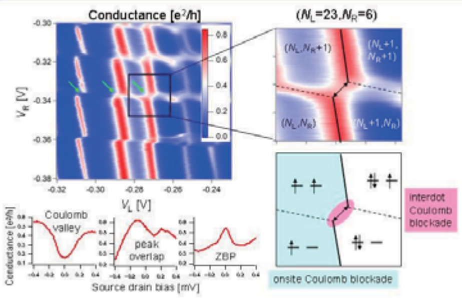

Coulomb diamond and zero bias anomaly

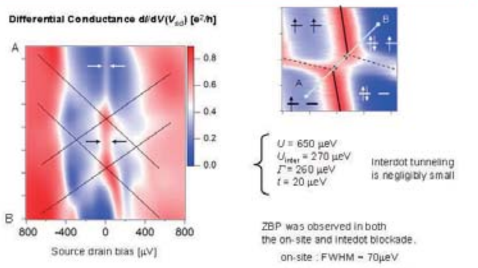

U = 650 μeV
U_{inter} = 270 μeV
Γ = 260 μeV
t = 20 μeV

Interdot tunneling is negligibly small

ZBP was observed in both the on-site and intedot blockade.

on-site : FWHM ~ 70μeV

interdot : FWHM ~ 84μeV

Temperature dependence

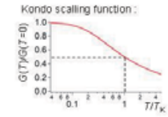

$$\frac{G(T)}{G(T=0)} = \left(\frac{T_K'^2}{T^2 + T_K'^2}\right)^s + B$$

$$T_K' = \frac{T_K}{\sqrt{2^{1/s}-1}} \quad (s \sim 0.22)$$

Fitting parameters are
Normalization factor, Kondo temperature, Background.

$$T_K = 468 \pm 58 \text{ [mK]}$$
$$T_K = 863 \pm 124 \text{ [mK]}$$

A good fit was obtained.

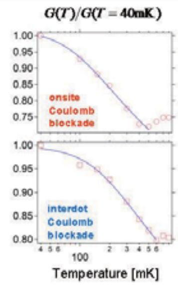

Peak splitting in a finite inplane magnetic field

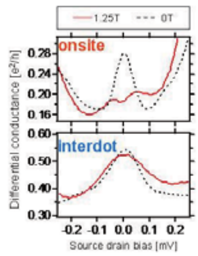

Why B = 1.25T ?
A strong magnetic field affects the orbital state, due to poor alignment of the 2DEG.
This magnetic field did not change the orbitals.

Onsite Coulomb blockade
Double peak splitting was observed, indicating a formation of the spin Kondo singlet.

Interdot Coulomb blockade
ZBP were slightly broaden, might be coming from weak contribution of spin?

No peak splitting was observed, indicating that the pseudo-spin is dominantly contributing to the Kondo correlation.

Why pseudo-spin dominant?

The Kondo singlet is originating from an effective coupling which resulting from second-order spin or pseudo-spin flip process.

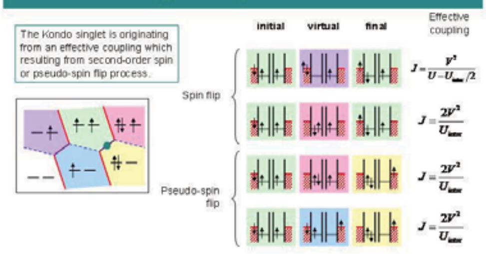

The right lower state has not spin.Thus spin and pseudo-spin can not simultaneously flip.

When U>U_{inter}, The effective coupling of pseudo-spin is stronger than spin

Results

Double dot device was fabricated and measured.

Kondo effect was determined from ZBP and Kondo scaling at both on-site and intedot Coulomb blockade.

No peak splitting was observed at interdot Coulomb blockade in a in-plane magnetic field, indicating that the pseudo-spin dominantly contributes to the Kondo correlation.

I showed you why pseudo-spin domonant.

- The Physical Society of Japan spring meeting 21/3(21aHV-2)
- 30th International Conference on the Physics of Semiconductors (July)

PO no. 8

The 2nd GCOE International Symposium on
"Weaving Science Web beyond Particle-Matter Hierarchy"
Febrary 18 (Thu.), 2010, Sendai, Miyagi, Japan

Spin and charge dynamics in a photo-excited double exchange system

Department of Physics, Tohoku University ,
Sendai National College of Technology[A]

Yu Kanamori, Hiroaki Matsueda[A],
and Sumio Ishihara

Strongly correlated electron systems

Large fluctuation in charge, spin and orbital of electron near phase boundary

By weak external perturbations
- Colossal magneto-resistance effects
- Insulator-to-metal transition
- Photo-induced phenomena

By irradiation femto-second plus laser
- Change in conductance
- Change in magnetic structure
- etc...

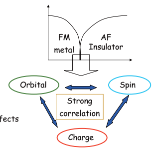

Perovskite manganites

Strongly correlated electron system

$R_{1-x}A_xMnO_3$

(R : Rare earth
A : Alkali earth)

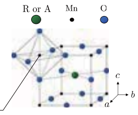

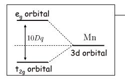

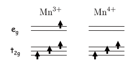

Phase diagram of $R_{1-x}A_xMnO_3$ at x=0.5

$Pr_{0.5}(Ca_{1-y}Sr_y)_{0.5}MnO_3$
(R = Pr, A = Ca, Sr)

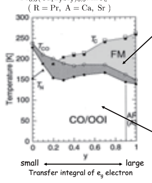

Y. Tomioka and Y. Tokura, Phys. Rev. B **66**, 104416(2002)

Ferromagnetic and metallic phase

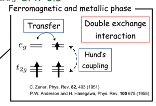

C. Zener, Phys. Rev. **82**, 403 (1951)
P.W. Anderson and H. Hasegawa, Phys. Rev. **100** 675 (1955)

Antiferromagnetic and insulating phase

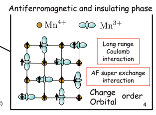

Photo-induced phenomena

Perovskite manganites
$R_{0.5}A_{0.5}MnO_3$ (x = 0.5)

Charge order insulator Antiferromagnet ⟺ Metal Ferromagnet

$Nd_{0.5}Ca_{0.5}MnO_3$
Conductivity spectra

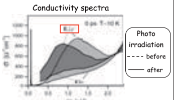

Shift of spectrum → Metallic state

T. Ogasawara et al. J. Phys. Soc. Jpn. **71**, 2380 (2002)

pumping
$Nd_{0.5}Sr_{0.5}MnO_3$

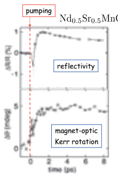

Change in magnetic structure

K. Miyasaka et al. Phys. Rev. B **74**, 012401 (2006)

Purpose

Photo-induced spin and charge dynamics
after photo-irradiation in charge-ordered (C.O.) insulator
associated with antiferromagnetic (AF) order

model: Extended 1D double exchange model → Calculations by exact diagonalization
- Lanczos method
- Density-Matrix Renormalization-Group

Model : Extended double exchange model

$$\mathcal{H}_0 = \mathcal{H}_t + \mathcal{H}_H + \mathcal{H}_U + \mathcal{H}_V + \mathcal{H}_S$$
$$= -t\sum_{i,\sigma}(c^\dagger_{i,\sigma}c_{i+1,\sigma} + h.c.) - J_H\sum_i \boldsymbol{S}_i\cdot\boldsymbol{s}_i \quad \text{Ferromagnet · Metal}$$
$$+U\sum_i n_{i,\uparrow}n_{i,\downarrow} + V\sum_i n_i n_{i+1} + J_S\sum_i \boldsymbol{S}_i\cdot\boldsymbol{S}_{i+1} \quad \text{AF · Insulator}$$

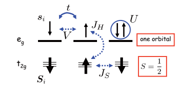

- One dimension
- Open boundary
- 1/4-filling

Perovskite manganites
$R_{1-x}A_xMnO_3$

Initial state

L = 9, N_{e_g} = 5, U = 20t
V = 5t, J_H = 15t, J_S = 0.3t

Ground state: C.O. insulating Ferrimagnetic state

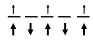

Charge and spin correlation functions

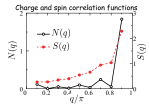

Optical absorption spectrum

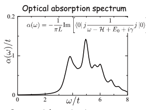

One-particle excitation spectra

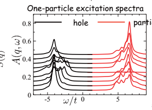

Formulation for photo-excited states and transient spectra

- One-photon excited state at time τ

$$|\tau\rangle = \frac{1}{N}e^{-iH\tau}\mathrm{Im}\left[\frac{1}{\omega_0-\mathcal{H}+E_0+i\gamma_0}\right]j\,|0\rangle \qquad \left[j = i\sum_{i,\sigma}t\left(c^\dagger_{i,\sigma}c_{i+1,\sigma}-h.c.\right)\right]$$

- Transient spectra
  - Optical absorption spectra

$$\alpha(\omega,\tau) = -\frac{1}{L\pi}\mathrm{Im}\left[\langle\tau|j\frac{1}{\omega-\mathcal{H}+E_p+i\gamma}j^\dagger|\tau\rangle\right]$$

  - One-particle excitation spectra

$$A(q,\omega,\tau) = \begin{cases} -\frac{1}{\pi}\mathrm{Im}\left[\langle\tau|c_q\frac{1}{\omega-\mathcal{H}+E_p+i\gamma}c^\dagger_q|\tau\rangle\right] \\ -\frac{1}{\pi}\mathrm{Im}\left[\langle\tau|c^\dagger_q\frac{1}{-\omega-\mathcal{H}+E_p+i\gamma}c_q|\tau\rangle\right]\end{cases} \qquad \left[E_p = \langle\tau|\mathcal{H}|\tau\rangle\right]$$

- Multi-photon excited state at time τ

$$\mathcal{H}(\tau) = -t\sum_{\langle i,j\rangle}\exp\left[-\frac{ie}{\hbar}\int_{R_i}^{R_j}\boldsymbol{A}(\tau)\cdot d\boldsymbol{r}\right]c^\dagger_i c_j + \mathcal{H}_{\text{other}} \qquad \left[A^x(t) = A_0 e^{-\frac{(t-t_0)^2}{2\gamma^2}}\cos[\omega_0(t-t_0)]\right]$$

$$i\hbar\frac{\partial}{\partial\tau}|\psi(\tau)\rangle = \mathcal{H}(\tau)|\psi(\tau)\rangle \Rightarrow |\psi(\tau)\rangle = \exp\left[-\frac{i}{\hbar}\int_{\tau_0}^{\tau}d\tau'\mathcal{H}(\tau')\right]|\psi(\tau_0)\rangle$$

Transient absorption spectra

One-photon absorbed state
$\omega_0 = 3.8t$, $\gamma_0 = 0.4t$

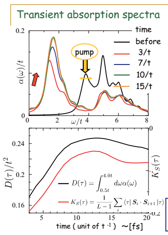

Correlation functions

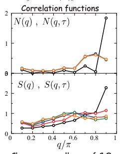

Charge : collapse of C.O.
Spin : collapse of AF

- Appearance of a peak inside of a gap
- Strong correlation between growth of in-gap state and collapse of AF

Transient one-particle excitation spectra

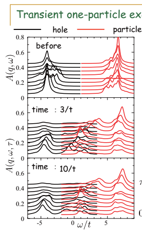

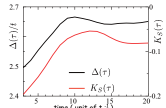

$\Delta(\tau) = \int_{-2.5t}^{5.0t}\sum_q A(q,\omega)(\omega-\omega_c)^2 d\omega$ ~ band width

(ω_c : A medium point)

$K_S(\tau) = \sum_i\frac{\langle\tau|\boldsymbol{S}_i\cdot\boldsymbol{S}_{i+1}|\tau\rangle}{L-1}$: Localized spin correlation

- Appearance of a band inside of the gap
- Increasing of the band width

Transient charge excitation spectra

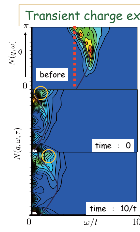

: energy of induced photon
: peak position (q=0.9π)

$E_S(\tau) = \frac{1}{L-1}\sum_i\langle\tau|\boldsymbol{S}_i\cdot\boldsymbol{S}_{i+1}|\tau\rangle$

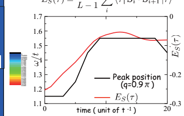

- Appearance of the low energy excitation
- Peak position shifts to high energy region.

Scale of the time evolution

α	Amplitude of transfer integral
1.0 ↕ 0.6	large ↕ small

$$\mathcal{H}_t = -t\sum_{\langle i,j\rangle,\sigma}c^\dagger_{i\sigma}c_{j\sigma} \rightarrow \mathcal{H}_t = -\alpha t\sum_{\langle i,j\rangle,\sigma}c^\dagger_{i\sigma}c_{j\sigma}$$

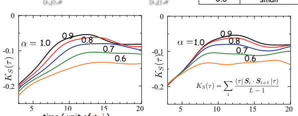

Time-dependence is scaled by "αt".

Multi-photon excitation

$$n_{\text{ph}} = \frac{\Delta\langle\mathcal{H}\rangle}{\omega_0 L}$$

$a_0 = \frac{eR}{\hbar}A_0$: Photon intensity

(R : lattice constant)

$\omega_0 = 5.0t$, $\gamma_0 = 2.0t$

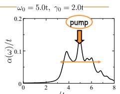

Absorbed photon density

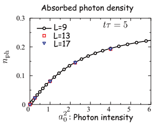

Absorbed photon density

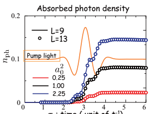

Photon intensity dependence of spin and charge dynamics

Differences in spin and charge correlations

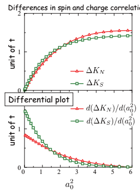

at time $t\tau = 5$

Differences per an absorbed photon

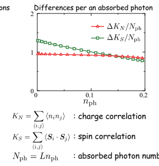

$K_N = \sum_{\langle i,j\rangle}\langle n_i n_j\rangle$: charge correlation

$K_S = \sum_{\langle i,j\rangle}\langle\boldsymbol{S}_i\cdot\boldsymbol{S}_j\rangle$: spin correlation

$N_{\text{ph}} = Ln_{\text{ph}}$: absorbed photon number

- Magnetic energy is more sensitive than charge energy with respect to photon intensity.

Conclusions

Spin and charge dynamics after photo-irradiation in C.O. insulator and AF order in DE model

- Time development
  - Optical absorption → Increasing of in-gap state
  - One-particle excitation → Broadening of photo-carrier band
  - Charge excitation → Appearance of low energy excited states and shift of those to high energy region
  - Spin excitation → Weak momentum dependence

  Scaling of the time-evolution by conduction electron hopping.

  → Strong coupling between spin and charge sectors

- Photon intensity dependence
  - spin sector is more sensitive than charge sector with respect to photon intensity.

  → Separation between spin and charge sectors

Observation of ^{8}B Solar Neutrinos with KamLAND

Yoshiaki Kibe
Department of Physics, Tohoku University,
Research Center for Neutrino Science

(1), History

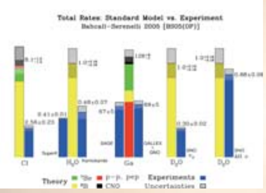

The Standard Solar Model (SSM) attempts to describe the solar processes. Various solar neutrino experiments have yielded results in conflict with SSM predictions.

The most plausible solution for this anomaly is neutrino oscillation, which describes neutrino flavor changing while the neutrino propagates. An additional effect happens in the Sun, the neutrino weakly interacts with other particles and the behavior of the oscillation changes. This effect is called the MSW effect.

KamLAND revealed a significant deficit of electron anti-neutrinos from distant power reactors and suggested the LMA-MSW solution.

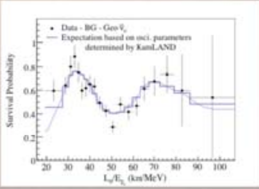

(2), Motivation

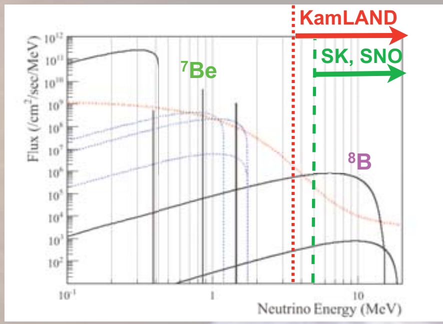

KamLAND has the possibility to observe ^{8}B solar neutrinos with an energy thresold of 3.5 MeV. This provides the transition of vacuum to matter oscillation, which has not been observed yet. The measurement of solar neutrinos provides the test for the theories of steller evolution and structure. Furthermore, The direct measurement of the transition of vacuum to matter oscillation will be good test for the oscillation parameter space.

(3), Detection Method

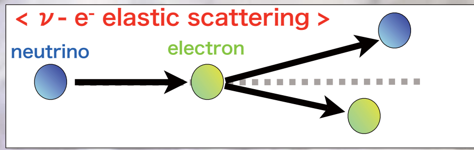

The ν-e⁻ elastic scattering is used to detect the solar neutrino events. In anti-neutrino detection like reactor neutrinos, the inverse βdecay reaction, ν_e+p -> e^++n and the neutron is thermalized in the liquid scintillator. Prompt signal from e^+ gives information on the incident ν_e energy. Neutron capture on hydrogen emits delayed signal with ~200μsec. This delayed coincidence method is effective to the background rejection. The way to detect the solar neutrino is single event, so it is necessary to estimate the background in the ^{8}B solar neutrino energy region in details.

(4), Backgrounds

The dominant background in ^{8}B solar neutrino region(> 5MeV) are from the β-decays of light isotopes produced by muon spallation. The following veto is applied for the light isotopes produced by muon spallation.

- 1 sec whole volume veto after muons
- 5 sec whole volume veto (residual charge > 10^6 p.e.)
- 5 sec veto of 3 m cylindrical volume along muon track (residual charge < 10^6 p.e.)

These cuts are effective for isotopes with half lives less than ~1sec, so ^{8}B, ^{8}Li or ^{11}Be are still significant.

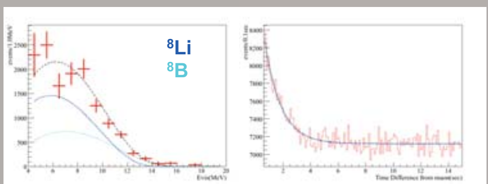

The production rate of ^{8}Li and ^{8}B are estimated with simultaneously fitting the time difference from preceding muon because the lifetime of ^{8}Li (1.21 sec) is close to that of ^{8}B (1.11 sec). The energy spectrum of βdecays of ^{8}Li and ^{8}B is also fitted simultaneously. The estimated event rates are ^{8}Li = 0.52 ± 0.15, ^{8}B = 0.21 ± 0.04 ev/d/kt.

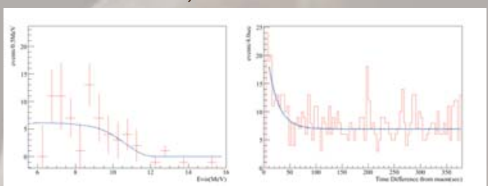

The production rate of ^{11}Be is estimated from the fitting of time difference from muons with tight track correlation. The estimated event rate of ^{11}Be is 0.91 ± 0.30 ev/d/kt.

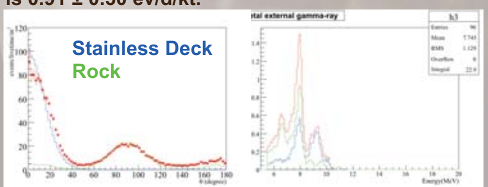

The external γ-rays come from (α, n) and (n, γ) reaction produced in mainly surrounding rock and stainless. The estimation for external γ-rays make use of MC simulation, providing 0.24 ± 0.04 and 0.38 ± 0.14 ev/d/kt for before/after purification.

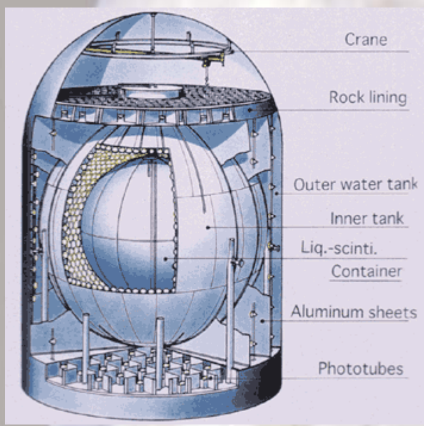

KamLAND
(Kamioka Liquid scintillator Anti-Neutrino Detector)
17inch PMTs; 1325 tubes
20inch PMT; 554 tubes
Outer Detector; 229 20inch PMTs
1000 tons Liquid scintillator;
Dodecane(80%) + Psuedocumene(20%) + PPO(1.36g/l)
Number of target; 3.429×10^{32} electron

(6), Uncertainty

	Before Pur.	After Pur.
Fiducial volume	3 m cylinder	3.5 m spherical
Livetime	952 days	63 days
	Uncertainty(%)	
Trigger Eff.	---	---
Fiducial volume	2.17	11.23
Livetime Calc.	0.03	0.03
Energy Threshold	2.44	3.00
χ2TQ Cut	0.30	0.30
Number of Target	< 0.1	< 0.1
Cross Section	0.50	0.50

Fiducial volume before purification is defined as a cylindrical due to the effect of external γ-rays. On the other hand, fiducial volume after purification is defined as a spherical since ^{208}Tl is a dominant background with an energy threshold of 3.5 MeV, then the signal-to-noise ratio gets better.

(5), Purification

The newly developed purification system reduces the radioactive impurities in a liquid scintillator. This purification system is mainly composed of the distillation tower and nitrogen purge tower. The purification provides a lower energy threshold.

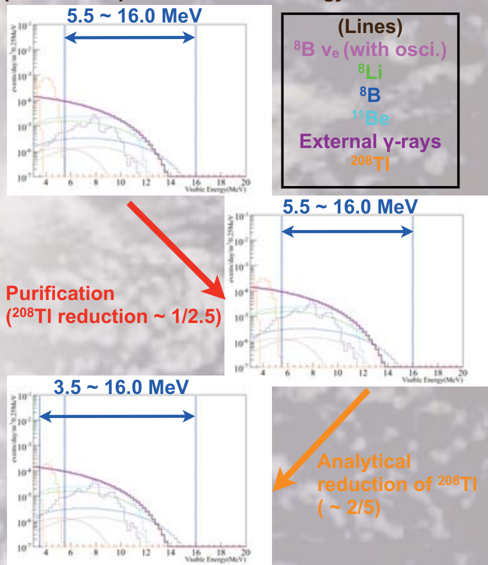

Analytical reduction of ^{208}Tl makes use of the delayed coincidence between prompt ^{212}Bi α-decay and delayed ^{208}Tl β-decay. The lifetime of ^{208}Tl is 3.053 min. Due to this analytical reduction, we can explore 8B solar neutrinos with an energy threshold of 3.5 MeV.

(7), Conclusion

The study of ^{8}B solar neutrinos with KamLAND at energy threshold of 3.5 MeV will provide the observation of the transition of vacuum to matter enhanced neutrino oscillation in addition to the result of ^{7}Be solar neutrino observation (energy is 0.875 MeV). For instance, 2-year livetime provides statistical uncertainty of ~10%.

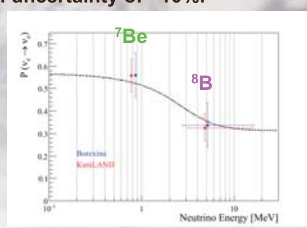

Poster Session
The 2nd Scienceweb GCOE International Symposium on
"Weaving Science Web beyond Particle-Matter Hierarchy"

z〜3 LYMAN BREAK GALAXY CLUSTER SURVEY IN SSA22 WITH VIMOS

Katsuki Kousai
Physics, D2, Tohoku University

We report our redshift survey of z~3 Lyman break galaxies (LBGs). We have obtained spectral redshifts (spec-z) of 94 LBGs in SSA22 (22:17:34, +00:15:04) 912 arcsec^2 field to study three dimensional distribution of LBGs.
SSA22 is a field in which Steidel et al discovered high density region of LBGs at z=3.09 (Steidel et al 1998) . They determined spec-z of 99 LBGs at z~3 in 162 arcsec^2 field. They found density peak of LBGs from their redshift distribution.
We have detected a lot of Lyman alpha emitters (LAEs) at z=3.09 in 912 arcsec^2 field which contains the high density region discovered by Steidel et al, in our narrowband survey for LAEs with Suprime-Cam to find a large scale structure of LAEs (Hayashino et al 2004) . Also, we are carrying out LBG redshift survey in our LAE survey area. We obtained spectral redshifts of 94 LBGs in 2006 and 2008 VIMOS observation.
We have found spike not only at z=3.1, z=3.3 and z=3.7 in our redshift distribution of LBGs.

1. High redshift galaxy

There is two major types of high redshift galaxy Lyman α emitter (LAE) and Lyman break galaxy (LBG) .The LAEs has a strong Lyman α emission line (λ_{rest} =1216 Å) . The emission line are observed by narrow-band imaging technique. The LBGs are observed with strong break at λ_{rest} = 912 Å ; Lyman break. These UV photons of z > 3 galaxies are shifted to visible wave length by redshift. We obtained these candidate by observation of visible range.

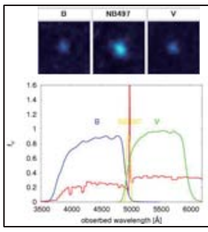

Observed z=3.1 LAE image(upper panel) and z=3.1 LAE model spectrum with filter response curve (bottom panel). We detected Lyman α photon with NB497 filter(: band pass centered at 4977 Å, bandwidth of FWHM 77 Å)

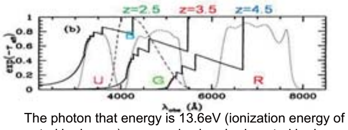

The photon that energy is 13.6eV (ionization energy of neutral hydrogen) or more, is absorbed neutral hydrogen in HI region. The absorption makes Lyman break.
Additionally, UV continuum receives Lyman series absorption by neutral hydrogen in IGM. That make UV continuum break at λ_{rest} =1216 Å .

2. SSA22

Steidel et al discovered high density region of Lyman Break galaxies (LBGs) in SSA22 at z=3.09 (Steidel et al 1998). They observed 81 arcsec2 ×2 in their spectroscopic LBG survey.
We have detected Lyman alpha emitters (LAEs) at z=3.06~3.12 in 912 arcsec^2 field that contain the high density region which was discovered by Steidel et al (Hayashino et al 2004).

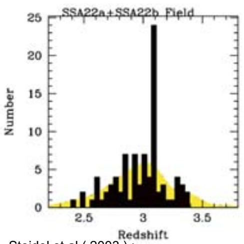

Steidel et al (2003) :
Redshift distribution of LBGs at z~3 in SSA22ab

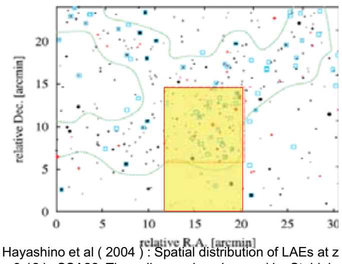

Hayashino et al (2004) : Spatial distribution of LAEs at z = 3.06 ~ 3.12 in SSA22. The yellow region observed by Steidel et al. The Green contour is high density region of LAEs

3. Observation parameter

The parameter of our LBG survey with VIMOS at 2006 and 2008.

	VIMOS 2006	VIMOS 2008
Survey area	900 [arcsec^2]	500 [arcsec^2]
EXP time	2.5 [hour]	4.0 [hour]
Selection criteria of LBGs	(U−V)−1.8×(V−R)≧0.8 R−i'≦0.3 20≦V≦25.5	(U−V)−1.8(V−R)≧1.0 R−i'≦ 0.2 24≦R≦25.5
Grism	OS−Blue (Spectral res : R=180(1″ slit), Spectral range : 3700−6700 Å)	

Field of View

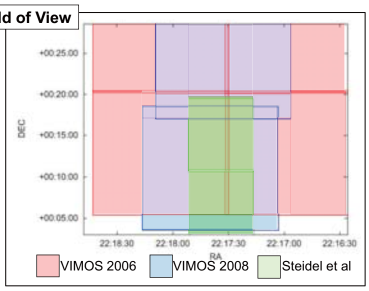

4. Redshift distribution

We obtained spec-z of **34** LBGs by the data that observed at **2006** and **60** LBGs by the data that observed at **2008**.
We have found spike at z=**3.1** and z=**3.3** in the VIMOS2006 redshift distribution. We found another spike at z=3.7 in the VIMOS2008 redshift distribution. The magenta histogram represent the over all redshift selection function , normalized to the observed number of galaxies . We derived the selection function by Monte Carlo simulation.

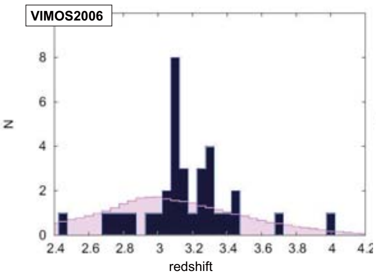

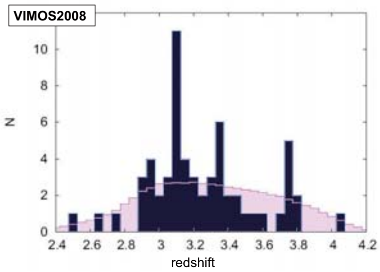

Property of spike

VIMOS2006

redshift	LBG / (selection function)	significance
3.1	5.1	5.1 σ
3.3	3.2	2.4 σ

VIMOS2008

redshift	LBG / (selection function)	significance
3.1	4.0	5.0 σ
3.35	2.3	2.1 σ
3.75	2.7	2.4 σ

5. Three dimensional Spatial distribution

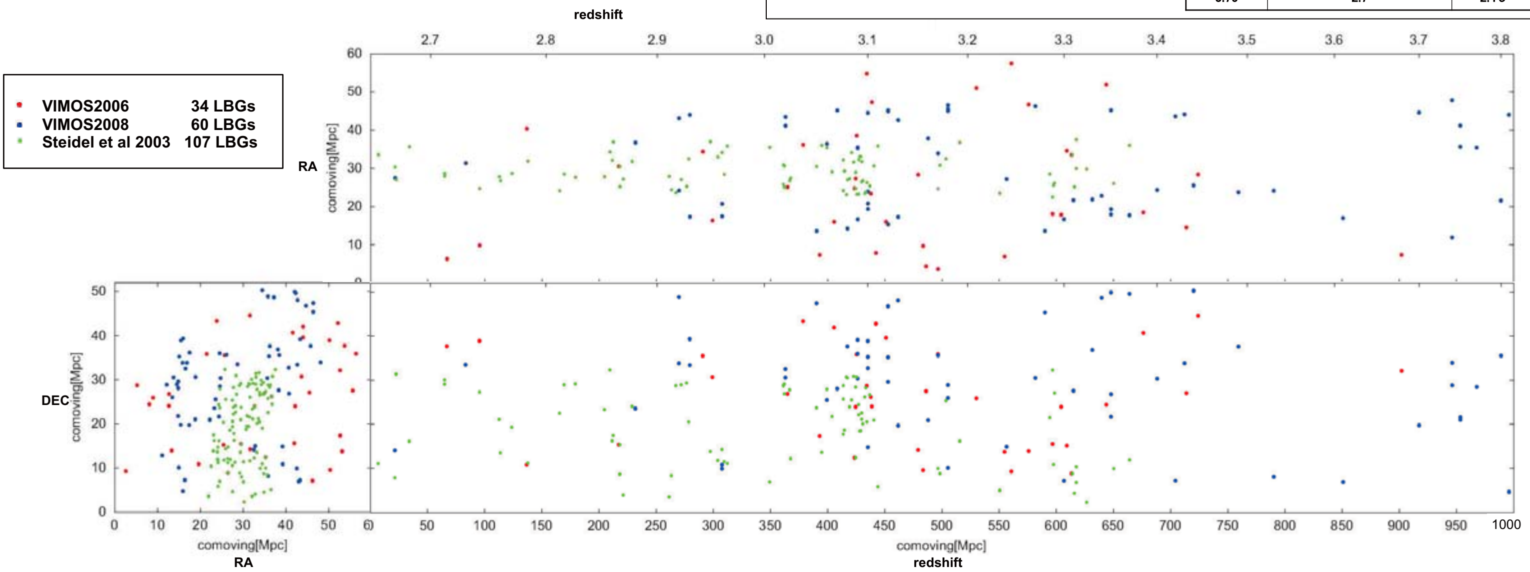

6. 2D Sky map

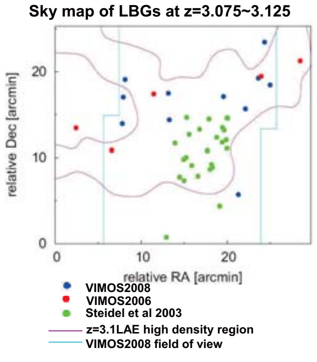

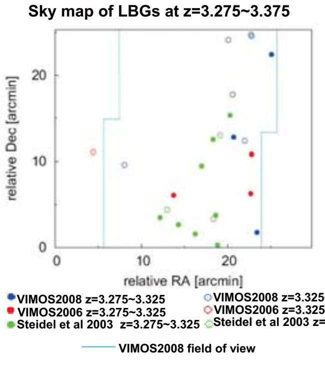

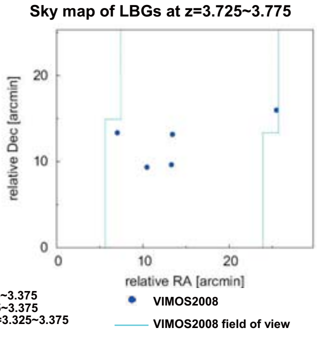

7. SUMMARY

- We have obtained spec-z of **94** LBGs at z~3.
- We have found spikes not only at z=3.1 discovered by Steidel et al but also at z=**3.3** and **3.7** in our redshift distribution of LBGs.
- Most of the LBGs at z=3.075~3.125 distribute inside the high density region of LAE skymap at z=3.06~3.12.
- It seems that LBGs in other spike z=3.3 and 3.7 are also clustered in 2D sky maps.

The 2nd GCOE International Symposium on "Weaving Science Web beyond Particle-Matter Hierarchy"
PO no. 11.

EELS and SXES studies of electronic structures of Al-TM alloys

S. Koshiya (Physics, D1, Tohoku University)

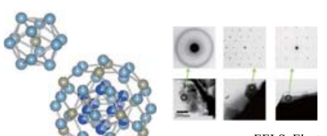

EELS: Electron energy-loss spectroscopy
SXES: Soft-X-ray emission spectroscopy

Abstract

After the discovery of an icosahedral symmetry material (quasicrystals) in a melt-quenched Al_6Mn alloy [1], great effort has been spent for understanding the presence of quasiperiodic structured materials. In recent years, Hume-Rothery mechanism, which predicts an existence of a pseudogap around Fermi level (E_F), is accepted as a major reason for the stabilization of quasicrystals. The presences of pseudogap structures in quasicrystals were experimentally confirmed by X-ray photoemission spectroscopy and EELS. **EELS experiments also pointed out characteristic chemical shifts in Al L-shell excitation spectra of Al-based quasicrystals** [2], which suggested a decrease of valence electron charge at Al sites. Recently, a covalent bonding nature in quasicrystals was reported by MEM/Rietveld analysis of 1/0-Al_{12}Re and 1/1-$Al_{73}Re_{27}Si_{10}$ [3]. Thus, it is interesting to investigate the relation between chemical shift and bonding nature of quasicrystals. On the other hand, the systematic measurements of electronic structures of the 'normal' Al-transition metal (Al-TM) alloys help the understanding of the bonding nature of the Al-based quasicrystal.

[1] D. Schechtman, *et al.*, Phys. Rev. Lett., **53**, 1951, (1984). [2] M. Terauchi, *et al.*, Phil. Mag, **87**, 2947, (2007).
[3] K. Kirihara, *et al.*, Phys. Rev. B, **64**, 212201, (2001).

01

Background 1: Quasicrystals and Approximants

Quasicrystal

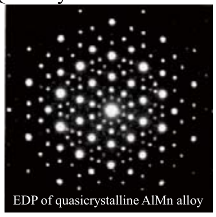

EDP of quasicrystalline AlMn alloy

D. Shechtman, *et al.*, Phys. Rev. Lett. **53**, 1951, (1984).

QC's anomalous properties
- Quasi-periodicity (luck translation symmetry)
- High electronic resistance
- Hard and brittle

Approximants
- Local structure is similar with a QC
- Characterized by **degree of approximation**
  1/0→1/1→1/2→2/3→・・・→1/τ (τ = (1+√5)/2)

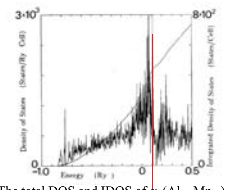

The total DOS and IDOS of α-($Al_{114}Mn_{24}$)
T. Fujiwara, Phys. Rev. B, **40**, 942, (1989).

Quasicrystal and approximants
→Presence of pseudogap near the E_F
→Complicated structure was stabilized?? 02

Background 2: EELS studies

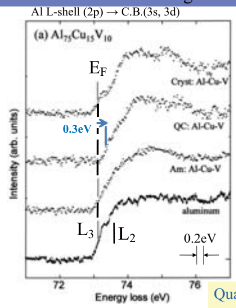

M. Terauchi, *et al.*, Phil. Mag., **87**, Nos.18-21, 2947, (2007).

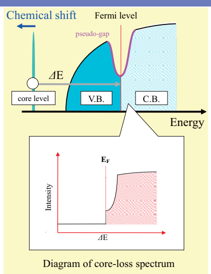

Diagram of core-loss spectrum

Quasicrystal shows chemical shift
→ Decrease of valence electron charge
→ Presence of covalency ??

03

Background 3: MEM/Rietveld analysis

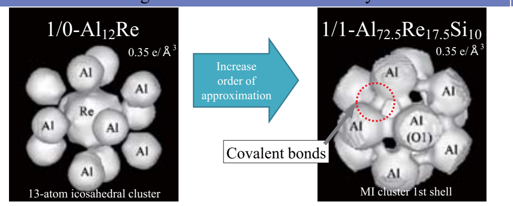

Interatomic bonds: Metallic — Interatomic bonds: **Covalent**

K. Kirihara, *et al.*, Phys. Rev. B, **68**, 014205 (2003).

Covalent bonds between Al atoms
→ Decrease of valence electron charge ??
⟷ Chemical shift (EELS)

04

Background 4: Chemical shifts

			Chemical shift (eV)
[1] Al	in $Al_{65}Cu_{15}V_{10}$		
	Amorphous	$2p_{3/2}$	0
	Quasicrystal	$2p_{3/2}$	+0.3
	Crystal	$2p_{3/2}$	0
[2] Al	in d-$Al_{70}Ni_{15}Co_{15}$	$2p_{3/2}$	+0.4
Ni	in d-$Al_{70}Ni_{15}Co_{15}$	$2p_{3/2}$	+0.3
Co	in d-$Al_{70}Ni_{15}Co_{15}$	$2p_{3/2}$	+0.7
[3] Al	in i-$Al_{70}Pd_{20}Mn_{10}$	2s	+0.2
		$2p_{3/2}$	+0.2
Pd	in i-$Al_{70}Pd_{20}Mn_{10}$	3s	+1.8
		$3p_{3/2}$	+1.4
		$3d_{5/2}$	+1.7
Mn	in i-$Al_{70}Pd_{20}Mn_{10}$	$2p_{3/2}$	0

Different ordered states

All constituent atoms of quasicrystals

[1] M. Terauchi, et al., Phil. Mag., **87**, 2947, (2007).
[2] Esther Belin-Ferré, et al., J. Phys. Condens. Matter, **8**, 6213, (1996).
[3] Z. M. Stadnic, et al., Phys. Rev. B, **51**, 11358, (1995).

The measurements of all constituent atoms of different ordered states have not been reported.

05

Purpose of this study

Investigate the relation between chemical shifts and crystalline order by using EELS and SXES

I. Approximants vs Chemical shifts
1/0-Al_{12}Re , 1/1-$Al_{73}Re_{17}Si_{10}$

II. Crystalline order vs Chemical shifts
Am, QC, Cryst phases of $Al_{53}Si_{27}Mn_{20}$

III. Normal Al-TM alloy vs Chemical shifts
B2 structure ($Pm\bar{3}m$) Al-TM (TM=Fe, Co, Ni, Pd, Pt)

06

High resolution EELS-TEM instrument

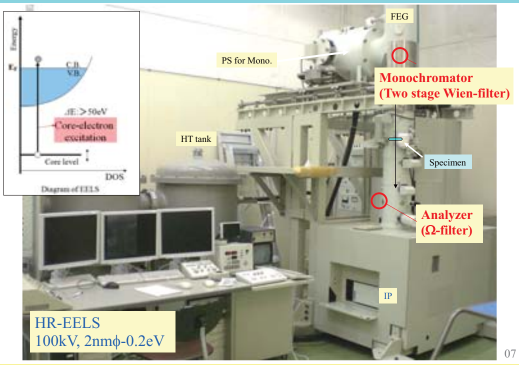

HR-EELS
100kV, 2nmϕ-0.2eV

07

High resolution SXES-TEM instrument

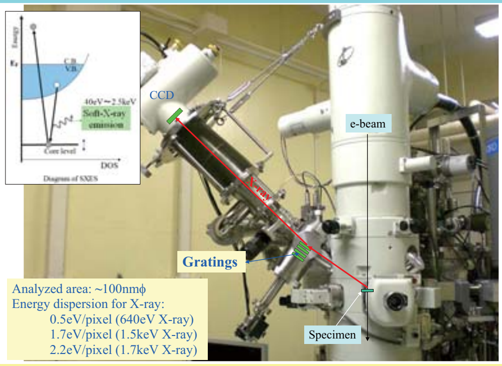

Analyzed area: ~100nmϕ
Energy dispersion for X-ray:
0.5eV/pixel (640eV X-ray)
1.7eV/pixel (1.5keV X-ray)
2.2eV/pixel (1.7keV X-ray)

08

I-a. Approximants vs Chemical shifts: EELS

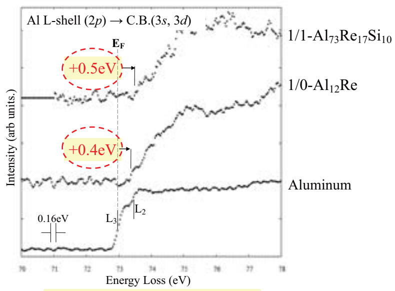

Chemical shift 1/0 ≤ 1/1

09

I-b. Approximants vs Chemical shifts: SXES

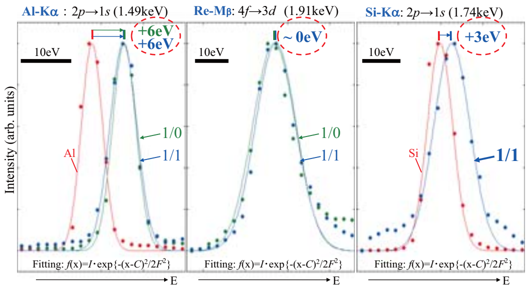

Chemical shift: 1/0, 1/1 — No difference for 1/0, 1/1 — Chemical shift: 1/1

10

Results I: Approximants vs Chemical shifts

	Al L-shell excitation	Al-Kα emission	Re-Mβ emission	Si-Kα emission
Comparison with	Pure Al	Pure Al	1/0, 1/1	Pure Si
1/0-Al_{12}Re	+0.4eV	+6eV	~0eV	---
1/1-$Al_{73}Si_{17}Re_{10}$	+0.5eV	+6eV	~0eV	**+3eV**

This result suggests that the covalent electrons between Al sites was provided from Si sites in 1/1 approximants.

11

II-a. Crystalline order vs Chemical shifts: EELS

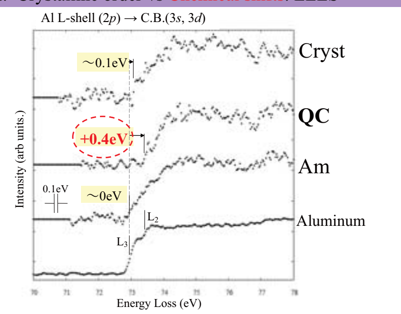

Chemical shift: QC phase

12

II-b. Crystalline order vs Chemical shifts: SXES

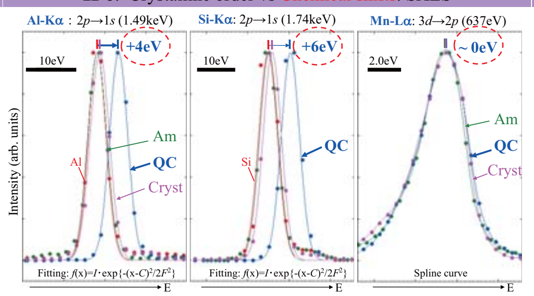

Chemical shift: QC phase — No difference

13

Results II: Crystalline order vs Chemical shifts

	Al L-shell excitation	Al-Kα emission	Si-Kα emission	Mn-Lα emission
Comparison with	Pure Al	Pure Al	Pure Si	Am, QC, Cryst
Amorphous	~0eV	~0eV	~0eV	~0eV
Quasicrystal	**+0.4eV**	**+4eV**	**+6eV**	**~0eV**
Crystal	+0.1~0.2eV	~0.5eV	~1eV	~0eV

Chemical shift is characteristic for QC phase
→Al and Si atoms change those valence electron states
Mn site does not change its valence electron charge
→Because of localization of Mn 3*d* electron ??

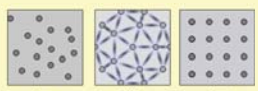

Am QC Cryst

14

III-a. Normal Al-TM alloy vs Chemical shifts: EELS

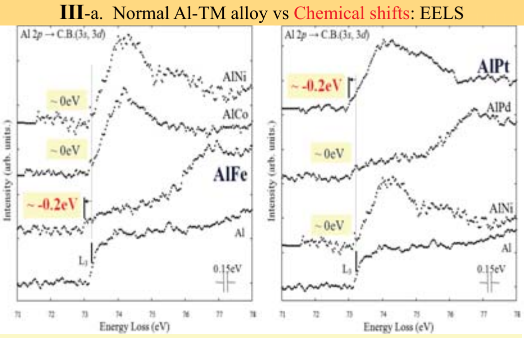

AlFe, AlPt: chemical shift to smaller binding energy side (increase the valence electron)
The amount of shift: AlFe, AlPt > AlPd ≒ AlCo ≒ AlNi ≒ pure Al

15

III-b. Normal Al-TM alloy vs Chemical shifts: SXES

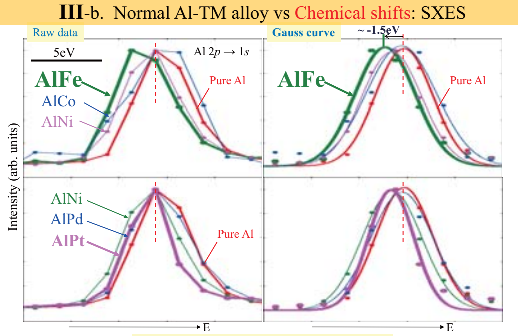

AlFe: shift to small binding energy side
(Consistent with EELS results)

16

Summary

The relations between chemical shifts and crystalline order have been investigated by using EELS and SXES

I. Approximants vs Chemical shifts:
Al, Re: Chemical shift in 1/0, 1/1 but no difference
Si: Chemical shift in 1/1
→ Added Si supply the charge for the covalency

II. Crystalline order vs Chemical shifts:
Al, Si: Chemical shift is characteristic for QC phase
Mn: No difference → Because of localization of 3*d* electron ??

Chemical shift
→ Decrease of valence electron charge
Covalent bonds between Al or Si atoms in QC

III. Normal Al-TM alloy vs Chemical shifts:
AlFe, AlPt: Chemical shift to smaller binding energy side
→ Charge transfer, different from quasicrystal
Larger atomic radius of TM → Larger shift

17

Comparison of membrane physical property changes between DMPC membrane and DMPE membrane induced by melittin

Atsuji Kodama

Introduction

Melittin, an amphipathic peptide composed of 26 amino acid residues from honeybee venom, has been widely used in the study of lipid-peptide interaction in biomembranes.

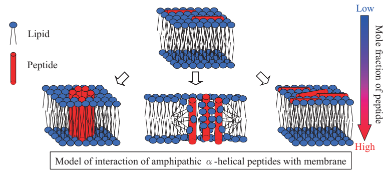

Model of interaction of amphipathic α-helical peptides with membrane

It has been reported that the strongest interaction of melittin observed in 1,2-dimyristoyl-sn-glycero-3-phosphocholine (DMPC) membrane among PC membranes which have different length of fatty acyl chains because of matching of hydrophobic regions between melittin and DMPC membranes. In this study, we have investigated the interaction of melittin with PC and PE membranes which have same length of fatty acyl chains with respect to effect of melittin on phase transition of phospholipids.

Methods

Synthetic phospholipids were purchased from Avanti Polar Lipids (Alabaster, AL). Melittin was purchased from Sigma Chemical Co. (St Louis, MO). Laurdan and Prodan were purchased from Molecular Probes (Eugene, OR).

Vesicle Preparation

The desired phospholipid was taken from the chloroform solution into a test tube. In the study of GP measurement, laurdan or prodan dissolved in DMSO was also added (0.5mol%). The solvent was evaporated first by a nitrogen stream, then under reduced pressure overnight. The lipid was dispersed into buffer (HEPES 50mM, EDTA 5mM, PH 7.3) containing desired concentration of melittin in a bath-type sonicator and incubated for an hour above the phase transition temperature. The total lipid concentration was 1mM for DSC and 0.2mM for fluorescene spectrometry.

Differential Scanning Calorimetry

Calorimetric scans were performed with a differential adiabatic microcalorimeter (Privalov calorimeter DASM-4, Sinku Riko, Yokohama, Japan) at a heating scan rate of 0.5K/min in 0.5ml cells under a pressure of 2.0 atm to prevent bubble formation.

Fluorescence Spectrometry

Fluorescence spectrometry were performed with an AmincoBowman Series 2 luminescence spectrometer (SLM Instruments, Urbama, IL) and rf-5000 (shimazu). The temperature of the sample was controlled by a water-circulating bath.

Materials

Melittin

- European honey bee venom
- 26 amino acid residues
- α-helix structure (interact with membrane)

α-helix structure of melittin

Phospholipid

DMPC (diC14:0) $T_m = 23$℃

DMPE (diC14:0) $T_m = 49$℃

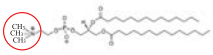

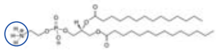

DMPC has larger headgroup than DMPE

Differential Scanning Calorimetry

Thermogram of DPPC

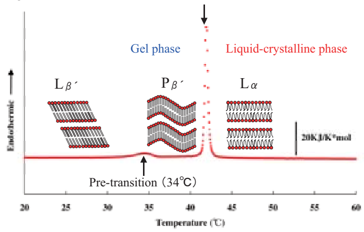

The peaks on the thermogram of the liposomal system indicate phase transition of lipid membrane. The shape of the peak informs us extent of cooperativity.

DSC thermograms of DMPC/Melittin and DMPE/Melittin

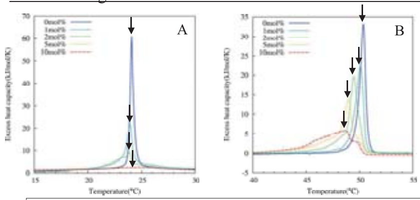

DSC thermograms of DMPC/Melittin (A) and DMPE/Melittin (B) at different mole fraction of melittin.

Lipid	T_m	Peak width
DMPC	No change	Broading
DMPE	Shift to lower	Broading

The scan times dependence of DSC thermograms

DMPC/Melittin (2mol%) DMPE/Melittin (5mol%)

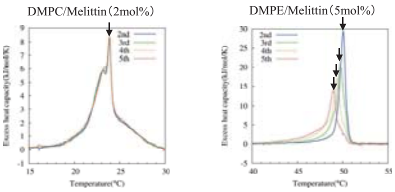

The scan times dependence of peak temperature and width with increasing of concentration of melittin

Lipid	T_m	Peak width
DMPC	No change	No change
DMPE	Shift to lower	Broading

DSC thermograms of membranes with additives (1)

J.M.Sturtevant (1982)

$$\frac{T_0}{T} = 1 + RT_0\left\{\frac{1}{\Delta H_{vH}} ln\left(\frac{1-\alpha}{\alpha}\right) - \frac{lnX_2}{\Delta H_{cal}}\frac{1}{\frac{K}{1-K}+\alpha}\right\}$$

Red part of the equation

van't Hoff equation for two state transition

[redacted] van't Hoff enthalpy
Mole fraction of LC phase
Midle temperature of phase transition

Blue part of the equation

Freezing point depression in solid solution

[redacted] Phase transition enthalpy
Mole fraction of additives
Partition coefficient of additives (Gel phase / LC phase)

- The partition of additives for water phase is not taken into account.

partition coeeficient of melittin (membrane / water) ⟶ 10000

DSC thermograms of membranes with additives (2)

Additives prefer liquid-crystalline phase Additives prefer gel phase

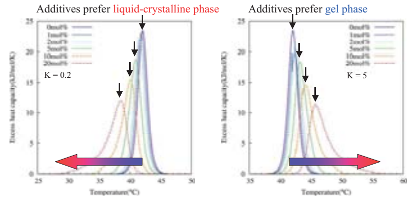

K	Preference	Peak temperature	Peak width
K > 1	Gel phase	Elevation	Broading
K < 1	Liquid-crystalline phase	Depression	Broading

Summary of DSC measurment

The dependence of concentration of melittin on DSC thermograms

DMPC/Melittin

The behaviors of DSC thermograms could not be explained qualitatively by the equation because the peak position of phase transition did not change even though it became broadened with increasing of concentration of melittin.

DMPE/Melittin

The behaviors of DSC thermograms could be explained qualitatively by the equation at K < 1.

The dependence of the scan times on DSC thermograms

DMPC/Melittin

There was no dependence of scan times on DSC thermograms.

DMPE/Melittin

The behaviors of DSC thermograms could be explained qualitatively by the equation at K < 1.

⟶

It indicates melittin inserted into with increasing of DSC scan times.

Laurdan

Structure

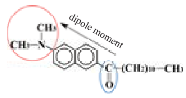

Generalized Polarization (GP)

$$GP = \frac{I_{440} - I_{490}}{I_{440} + I_{490}}$$

[Parasassi et al (1990)]

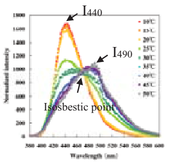

Laurdan spectra in DMPC membrane.

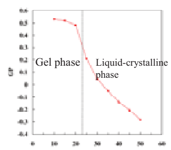

GP value for DMPC membrane.

Temperature dependence of GP value for DMPC/Melittin and DMPE/Melittin

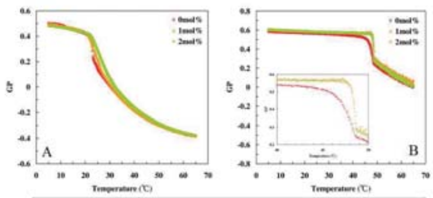

Temperature dependence of GP value for DMPC/Melittin (A) and DMPE/Melittin (B) at different mole fraction of melittin.

Changing of GP value for DMPC in phase transition became moderate with increasing of melittin, whereas GP value for DMPE changed drastically in the presence of melittin compared with in the absence of melittin at the phase transition temperature.

Tryptophan fluorescence

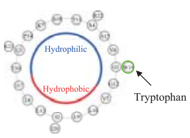

Property of emission spectra

Hydrophilic environment

Shift to longer wavelength

Hydrophobic environment

Shift to shorter wavelength

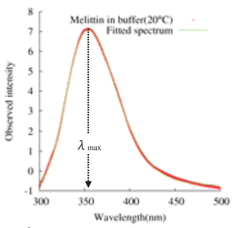

λ_{max} was obtained from tryptophan spectrum fitted by log-normal distribution. [Alexey S. Ladokhin et al (2000)]

Temperature dependence of λ_{max} for tryptophan residue in DMPC and DMPE

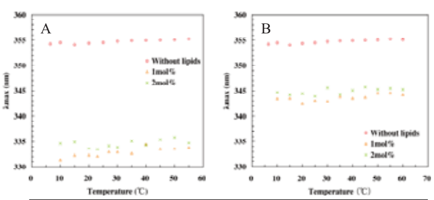

λ_{max} of tryptophan fluorescence in DMPC (A) and DMPE (B) at different mole fraction of melittin. Excitation wavelength was 280nm.

In DMPC/Melittin systems, λ_{max} at all mole fractions of melittin were between 330nm and 335nm through all temperature ranges. In DMPE/Melittin systems, λ_{max} were at about 345nm.

Model for interaction of melittin with PC and PE membrane

PC membrane

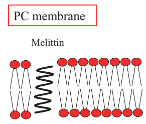

Melittin inserted into membranes and the system achieved equilibrium.

The reason why transition temperature did not change with increasing of concentration of melittin has to be revealed.

PE membrane

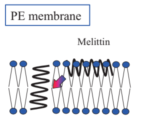

Melittin oriented pallarel to the membrane at the initial state.

Melittin oriented pallarel to the membranes disturbed penetration of water into membranes.

Heating - cooling cycles induced insertion of melittin into membranes.

Resonant x-ray scattering experiment on $Pr(Ru_{1-x}Rh_x)_4P_{12}$

Kotaro Saito, Kazuaki Iwasa

Department of Physics, Tohoku University, Sendai

Multipole ordering

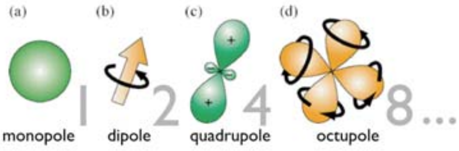

Fig.1 Schematics of multipoles [3]

Fig.2 Antiferro-hexadecapole ordering in $PrRu_4P_{12}$ [6]

High order multipoles as an order parameter

Rh-Substitution effect

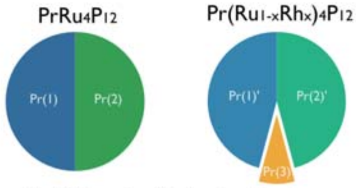

Fig.3 Schematics of Pr ions in ordered state

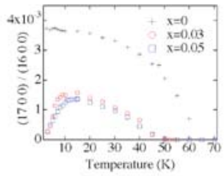

Fig.4 Temperature dependence of superlattice reflection

Effect on 4f electron state & lattice distortion

Resonant x-ray scattering

Scattering factor of resonant process = tensor

⟶ able to detect anisotropy of charge distribution

Promising method to detect multipole ordering

quadrupole	✓
octupole	✓
hexadecapole	predicted

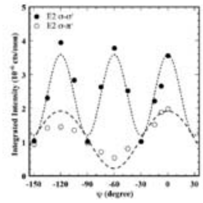

Fig.5 Azimuthal dependence of resonant signal in octupole ordering phase of $(Ce_{0.7}La_{0.3})B_6$ [3]

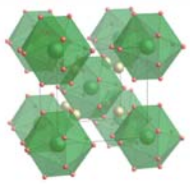

Objective

To investigate electronic state in multipole ordered phase of $Pr(Ru_{0.97}Rh_{0.03})_4P_{12}$, we have carried out resonant x-ray scattering experiment.

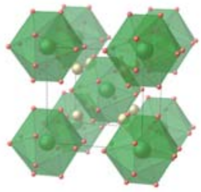

Results

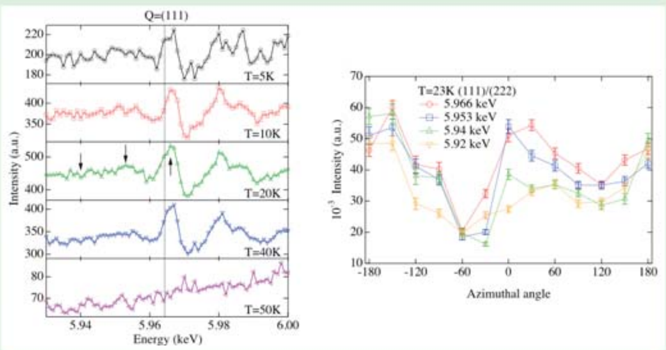

Fig.6 Temperature dependence of energy scan (left) and azimuthal plot of omega scan intensities at sereral incident energies (right)

Resonant signal appears below transition temperature then weaken below about 10 K.

➡ **Electronic state has temperature dependence same as lattice distortion**

No clear difference in azimuthal dependence between resonant and non-resonant range.

Periodicity in energy scan profile with different azimuthal angle

➡ **Anisotropy of electronic state (resonant range)**

Conclusion

In multipole ordered phase of $Pr(Ru_{0.97}Rh_{0.03})_4P_{12}$, electronic state shows similar temperature dependence as lattice distortion and has anisotropic charge distribution.

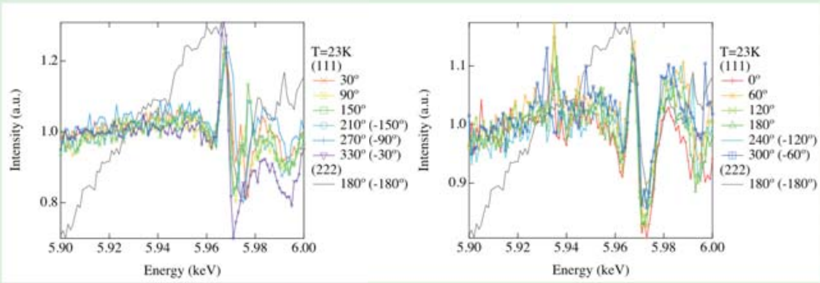

Fig.7 Energy scan with different azimuthal angle.

Reference

[1] H. Kusunose, JPSJ Online - News and Comments (Sep. 10, 2007) [2] Y. Kuramoto, PTPS 176 77
[3] D.Mannix et al., PRL 95 117206

Acknowledgement

Author thank to Dr. Hironori Nakao for helping us at BL-4C, Photon Factory.

Study of geo neutrinos with KamLAND

Yuri Shimizu, D3, RCNS

Geo-Neutrino

Radioactive sources in Earth emit electron anti-neutrinos (geo-neturinos) via beta-decays.

$$^{238}\mathrm{U} \rightarrow {}^{206}\mathrm{Pb} + 8\,{}^{4}\mathrm{He} + 6e^- + 6\bar{\nu}_e + 51.7\,\mathrm{MeV}$$
$$^{232}\mathrm{Th} \rightarrow {}^{208}\mathrm{Pb} + 6\,{}^{4}\mathrm{He} + 4e^- + 4\bar{\nu}_e + 42.7\,\mathrm{MeV}$$
$$^{40}\mathrm{K} \rightarrow {}^{40}\mathrm{Ca} + e^- + \bar{\nu}_e$$
$$^{40}\mathrm{K} + e \rightarrow {}^{40}\mathrm{Ar} + \nu_e$$

Geo-neutrino measurement is the only direct way to investigate chemical composition of the Earth's interior.

KamLAND detects geo-neutrinos with inverse beta-decay because it has high sensitivity for low energy neutrinos.

KamLAND detector

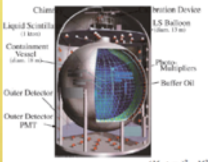

6.5-m radius balloon

1-kton liquid scintillator (LS=NP80%+PC20%+PPO)

1,879 PMTs

inverse beta-decay
→ U, Th geo-neutrinos

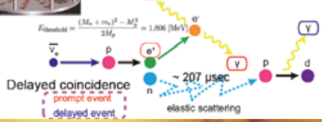

Earth's internal structure

Seismic wave measurements have revealed the detailed structure of Earth.

Core : mainly Fe and Ni. No U and Th exist

Mantle : Unknown composition by direct measurement → estimated using $\boxed{\text{CI chondrites}}$

Bulk Silicate Earth model ← Crust's samples
Crust + Mantle
+ Seismic wave measurement
+ Lithology
↓
Reference Earth model
Calculate geo-neutrino flux

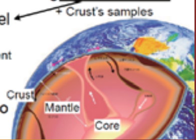

Meaning of geo-neutrino observation

The geo-neutrino observation can directly measure the Earth's internal structure.

U and Th mass in the mantle

Radiogenic heat from U and Th in Earth

Total heat flow 44 or 31 TW

BSE model prediction 19 TW
(U 8TW, Th 8TW, ^{40}K 3TW)

The contribution of radiogenic heat is about half of total heat flow. → U and Th are main heat sources in Earth.

Problems and solutions for geo-neutrino observation

✓ **Statistics**

➡ Analysis using 2076.6-day data set (KL08+586.0days)

✓ **Backgrounds**

➡ LS purification reduced the (α, n) background by 1/16.

✓ **Uncertainties**

➡ LS purification caused a decrease of light yield. Before the analysis, reconstructed energy is calibrated for positions and time.

LS purification

LS purification (distillation + N_2 purge) campaign was performed from May, 2007 to Feb, 2009.

Distillation reduced ^{210}Pb which is the parent of the dominant (α, n) source, ^{210}Po.

After the purification, ^{210}Po decay rate decreased by 1/16. It means the (α, n) background was also reduced by the same factor.

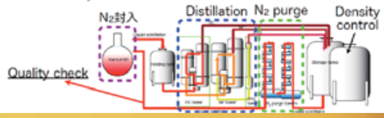

Background Reduction

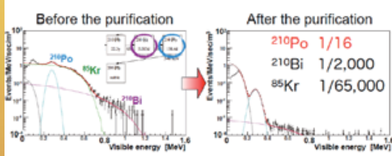

	Geo-neutrino prediction	(α, n)	S/N
After purification	11.1	1.1	10.1
Before purification	71.9	217.7	0.3

Energy correction

After the purification, light yield decreased by 20% and reconstructed energy has large time variation and an ununiformity.

That significantly affects an uncertainty of energy scale. → ~~The post-purification period is dead time...~~

Energy is calibrated for z-axis, off-axis and time using ^{60}Co gamma and n-capture gamma.

That suppresses the increase of the uncertainty of energy scale. Time variation and an uniformity are the same as before the purification.

Before the correction

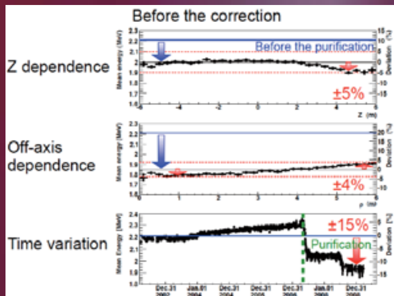

After the correction

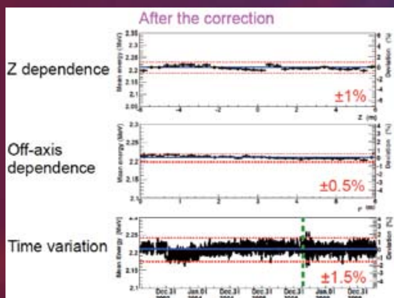

Expected spectra

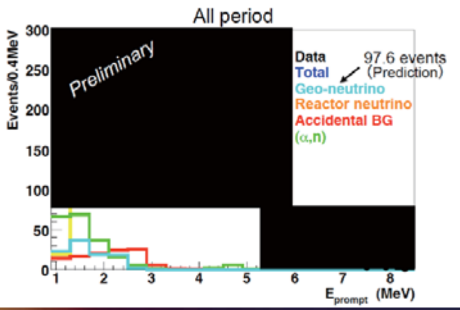

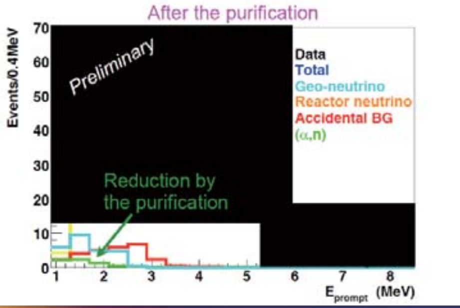

Analysis

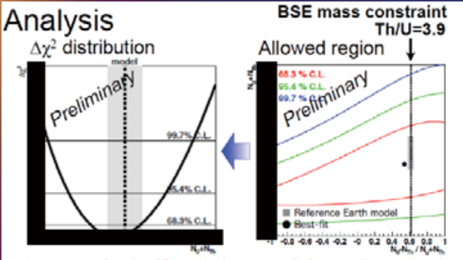

Accuracy is significantly improved due to the reduction of the (α, n) background.

The hypothesis of zero signal is excluded at over 3σ C.L.. (investigation → **evidence**)

Restrict for radiogenic heat

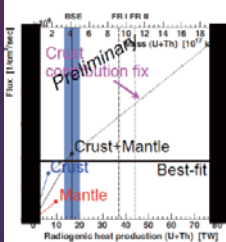

Models of radiogenic heat

- BSE model **16TW**
- Fully-radiogenic model I **37TW** ($H_U+H_{Th}+H_K=H_{Earth}$)
- Fully-radiogenic model II **44TW** ($H_U+H_{Th}=H_{Earth}$)

Fully-radiogenic models are excluded at over 2σ C.L..

Conclusion

Geo-neutrino analysis was performed with 2076.6-day data set (KL08**+586.0days**).

(α, n) background was reduced by 1/16 resulted in **the significant improvement of accuracy**.

The energy shift due to the decrease of light yield was carefully calibrated.

The analysis provided the evidence of geo-neutrinos and excluded fully-radiogenic models at the first time.

Pressure dependence of B-T phase diagram in heavy-fermion superconductor $CeRhSi_3$

T. Sugawara [1], N. Kimura [1], H. Aoki [1], T. Terashima [2], F. Lévy [3] and I. Sheikin [4]

[1] Graduate School of Science, Tohoku University

[2] National Institute for Materials Science

[3] DPMC, Université de Genève, Geneva, Switzerland

[4] Grenoble High Magnetic Field Laboratory, CNRS

Introduction

$CeRhSi_3$ is a pressure-induced heavy-fermion superconductor discovered in 2005 by N. Kimura *et al*. It crystallizes in the $BaNiSn_3$-type tetragonal structure which lacks an inversion center. It exhibits the antiferromagnetic ordering below the Néel temperature T_N = 1.6 K at ambient pressure. The superconductivity emerges above 0.2 GPa and its transition temperature T_c becomes comparable to T_N at P_c = 2.4 GPa.

We have measured the resistivity of $CeRhSi_3$ for magnetic field along the tetragonal *c*-axis under several pressures. We obtained a novel superconducting B-T phase diagram, suggesting the existence of multiple superconducting phases.

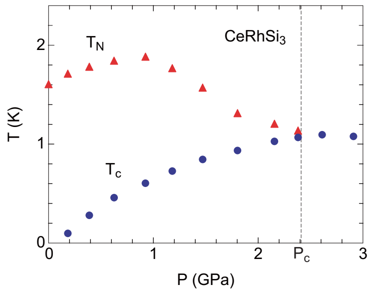

Crystal structure

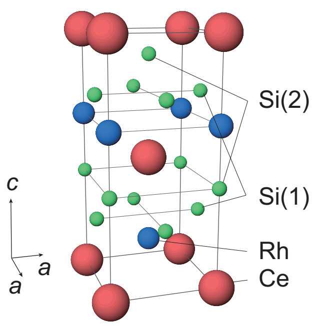

Sample

Starting materials: Ce(4N), Rh(2N8), Si(5N)

Czochralski pulling method in a tetra-arc furnace

Anneal: 900°C, 2×10^{-6} Torr, 1 week

RRR > 100 (l > 2000Å: from dHvA)

Experimental method

Pressure: Ni-Cr-Al / Cu-Be piston cylinder cell
i- and n-propanol
0~2.85GPa

Resistivity: 4 wires AC method
0.02~1.6K, 0~16T(~28T at 2.85GPa)

4 wires DC method
1.5~300K, 0T
(for obtaining the absolute values)

B-T phase diagram

There is a bend point on the superconducting transition line ($B_{c2}(T)$) above P_c.

Below the bend point field (B_{BP}), the form of $B_{c2}(T)$s are quite similar.

Above B_{BP}, an obvious change of the slope is observed at T_a on the temperature dependence of the resistivity $\rho(T)$ (see below section).

T_a may emerge from the bend point.

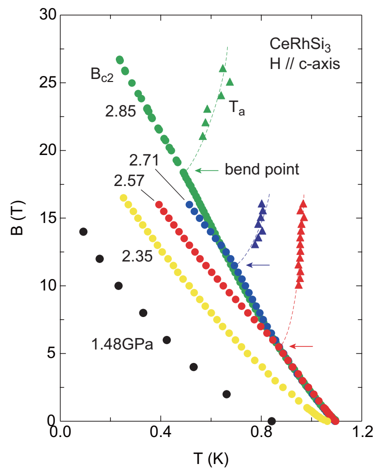

Pressure dependence of several parameters

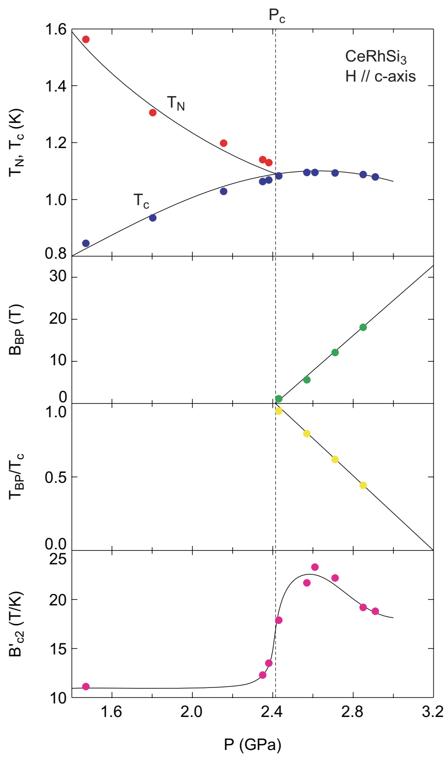

B_{BP} and the bend point temperature (T_{BP}) have P-linear dependence.

Considering a linear extrapolation, the bend point vanishes at 3.20 GPa.

The initial slope of $B_{c2}(T)$ at T_c, $B_{c2}' = -dB_{c2}(T)/dT\,|_{T=T_c}$ shows abrupt change at P_c.

This and the bend on the $B_{c2}(T)$-line suggest the existence of three (at least two) distinct superconducting phases and the superconducting state changes at P_c and the bend point.

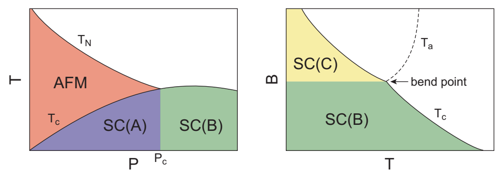

$\rho(T)$ under several pressures

2.35GPa (< P_c)

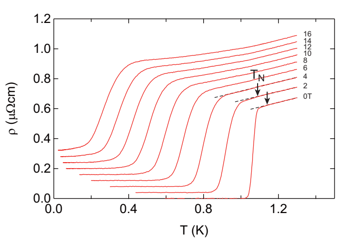

As increasing magnetic field, T_N becomes ambiguous and $\rho(T)$ turns to have a positive curvature.

2.57GPa (> P_c)

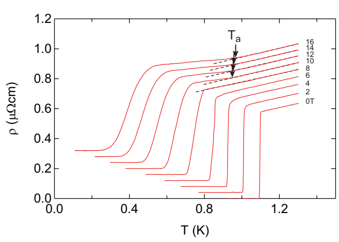

Above B_{BP}, the slope of $\rho(T)$ changes at T_a. This behaviour is different from that of T_N.

2.85GPa

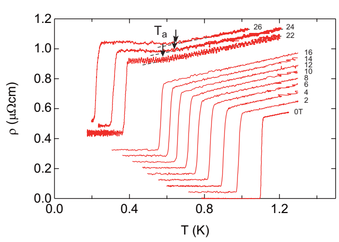

The change of the slope of $\rho(T)$ becomes obvious with increasing pressure.

Neutral meson photoproduction experiments with electromagnetic calorimeter complex FOREST

Reserch Center for Electron Photon Science, Tohoku University K. Suzuki

1. Motivation

Recently, a new baryon resonance was observed at W=1670 MeV in the γd→ηnp reaction, as shown in Fig. 1. The resonance width is narrow compared with that of a typical baryon resonance. No indication appears in the γp→ηp reaction in the same energy region.

Fig. 1

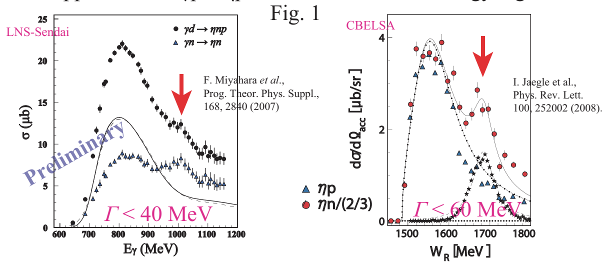

The narrow baryon resonance would be a member of anti-decouplet?

Figure 2 shows baryon states of Octet and Anti-decuplet which have spin 1/2 on the *SU(3)* quark model. From *U-spin* conservation, "p_8" can not be excited to "$p_{\overline{10}}$" in photo-reaction since the photon carries *U-sipn* 0. The new baryon resonance as well as the Θ^+ might be a member of anti-decuplet states (five-quark state). **It is important to determine the spin and parity of the narrow baryon resonance to elucidate five-quark states.**

Fig. 2

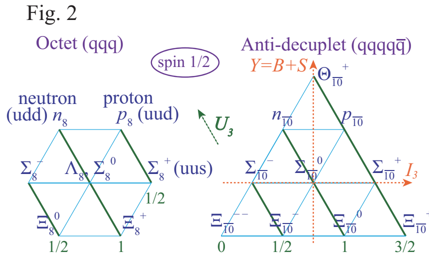

2. Accelerator and beam

For photoproduction experiments, we use a bremsstrahlung photon beam. We have an electron synchrotron, called STB, accelerating electrons up to 1.2 GeV. The bremsstrahlung photon beam is generated by employing a radiator placed just upstream from a bending magnet of the STB ring. The radiator made of a carbon fiber, 11 μm in diamitor, is inserted into the circulating electrons. Recoiled electrons are analyzed by the bending magnet and detected with the STB-Tagger II system which consists of 116 telescopes of two-layer scintillating fibers (Fig. 3). The energy Eγ of a generated photon is determined by the energy of the recoiled electron Ee and that of the circulating electron E_0 as

$$E\gamma = E_0 - Ee.$$

Fig. 3

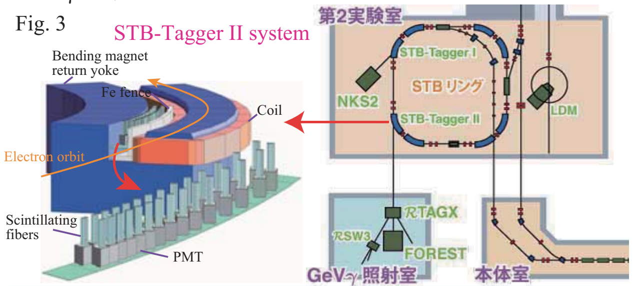

Tagging counter rate : ~20 MHz
Tagged photon energy : 750 ~ 1150 MeV/c @ 1.2 GeV electron

3. Electro-magnetic calorimeter FOREST

We developed a 4π electro-magnetic calorimeter, FOREST, for neutral meson (π^0 and η) photo-production experiments. Figure 4 shows FOREST which consists of 3 different types of electro-magnetic calorimeters called SCISSORS III (192 pure CsI crystals), Backward Gamma (252 lead scintillating fiber blocks), and Rafflesia II (62 lead glass cherenkov counters), respectively. Plastic Scintillator hodoscopes were constructed in front of these calorimeters, called SPIDER, IVY, and LOTUS, respectively. They can identify charged particles, and measure the position of the incident particles. FOREST covers about 90% of 4 π [str], thus it has large geometrical acceptances for the γp→π^0p and γp→ηp reactions. FOREST is powerful in suppressing background events (missing γ-ray events from 2π^0 or 3π^0...) since the missing γ-ray happens with a low probability under the large geometrical acceptance.

Fig. 4

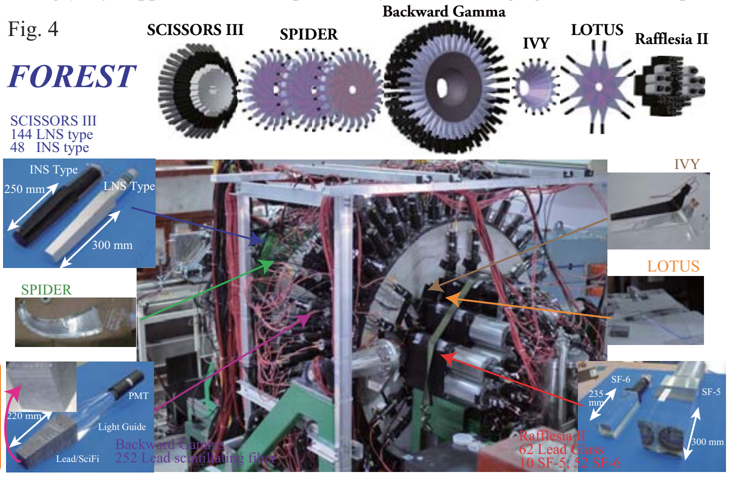

Detectors	covered angle ([str])	energy reso.	radiation length ($1X_0$)
SCISSORS III	4~24° (0.17π)	2.3%	16.2X_0 (18.5 mm)
BG	30~100° (2.08π)	7.2%	13.8X_0 (16.0 mm)
Rafflesia II	110~175° (1.31π)	4.9%	11.8X_0 (25.4 mm)

4. Experimental data and analysis

Photo-production experiments have been carried out with a hydrogen/deuterium target. Up to now, more than 2×10^9 events were obtained for each target. A typical trigger rate and DAQ efficiency are 1.8 kHz and 80%, respectively.

Fig. 5

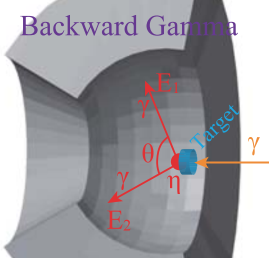

The π^0 and η mesons decay into 2γ-rays as soon as they are generated. The decay branching ratios of π^0 and η mesons are 99% and 39%, respectively. FOREST measures energies and positions of γ-rays comming from these mesons (Fig. 5). The γγ invariant mass can be calcurated by using the energy and position information for 2γ-rays as,

$$M_{\gamma\gamma} = \sqrt{2 E_1 E_2 (1 - \cos\theta)}.$$

The π^0 and η mesons are observed in Fig. 6.

Fig. 6

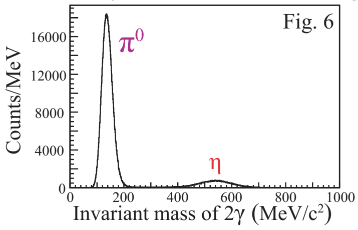

To select γp→ηp and γd→ηnp events, we require the following conditions:

1. 2γ-rays are deteced by Backward Gamma, and
2. 1 charge or 1 neutral is detected by SCISSORS III.

In the 2-nd requirement, we choose Mx < 1100 MeV events as indicated in Fig. 7 (Mx : missing mass of γN→ηX) to ensure that the charged or neutral particle is a proton or neutron. Background events are suppressed through these event selections as shown in Fig. 8.

Fig. 7

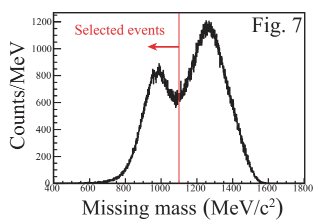

Fig. 8

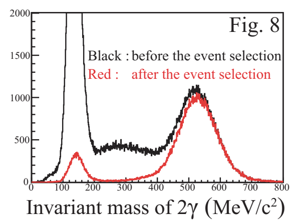

The η meson yield, Yη, for every tagged energy is calcurated by using counts of η mesons, Nη, and counts and efficiency of the tagging counters, Nγ and εγ, as

$$Y\eta = N\eta/(N\gamma\ \varepsilon\gamma).$$

Figures 9 and 10 show the η meson yields of the γp→ηp and γd→ηnp reactions.

Fig. 9

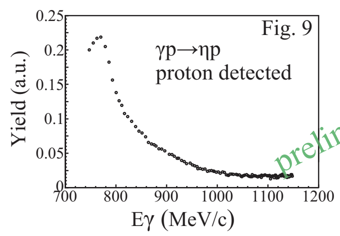

Fig. 10

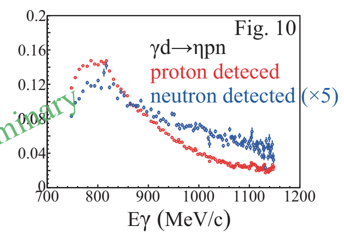

5. Future plan

The goal of this analysis is to determine the spin and parity of the new baryon resonance N*(1670). It is necessary to simulate the acceptances of FOREST to obtain the cross sections for the γp→ηp and γd→ηnp reactions. And a partial wave analysis will be made to determine the spin and parity of N*(1670).

Micro-photoluminescence
around spin phase transition of ν=2/3 fractional quantum Hall regime

J. Hayakawa[A], K. Muraki[B], G. Yusa[A]

[A] *Department of Physics, Tohoku University*
[B] *NTT Basic Research Laboratories, NTT Corporation*

Quantum Hall Effect

・Quantum Hall effect can be observed in two-dimensional electron systems subjected to low temperatures and strong magnetic fields, in which the Hall resistance takes on the quantized values $h/\nu e^2$ and longitudinal resistance vanishes at the same time.

※Landau level filling factor ν

$$\nu = \frac{n_{2D}}{(e/h)B} = \frac{n_{2D}}{n_\phi}$$

n_{2D} : 2 dimensional electron density
n_ϕ : density of magnetic flux

Transport

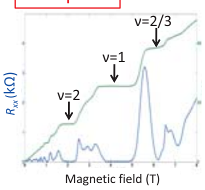

Photoluminescence

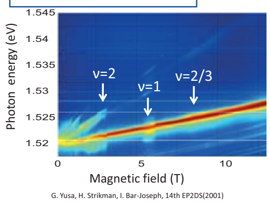

G. Yusa, H. Strikman, I. Bar-Joseph, 14th EP2DS(2001)

Photoluminescence of 2DEG under magnetic field

(schematic diagram)

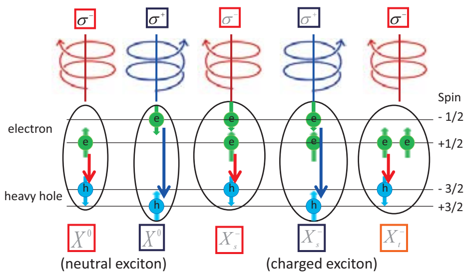

Plan of experiments ~ micro PL ~

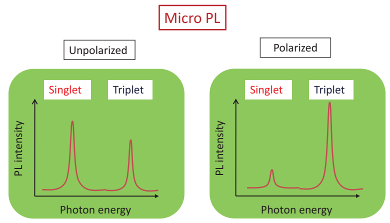

The peak intensity of charged excitons can be used as a probe to detect local spin polarization.

Motivation
Special features of ν=2/3 FQHS

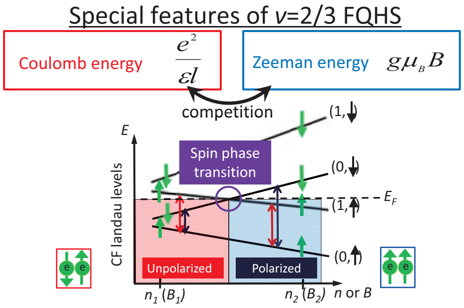

Theory:
・N.Shibata *et al.*, *JPJS* 76, 103711 (2007).

Experiment:
・O.Stern *et al.*, *PRB* 70 075318 (2004).
・B.Verdene *et al.*, *Nature physics* 3 392 (2007).

formation of domains with two polarizations at transition point

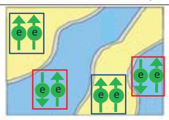

domain size > 500nm
→How large is the domain?
→What shape is the domain?
→How dose behave the domain dynamics?

◆ Optical study
can reveal local configurations of electrons

How to assign photoluminescence peaks ?

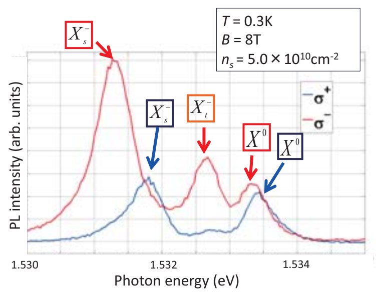

Local probe techniques for luminescence

Optical local probe techniques

☑Confocal laser scanning microscope(CLSM)
☑CLSM + solid immersion lens (resolution: ～sub μm)
☐CLSM + nonlinear optics (eq. two photon microscopy)
☐Scanning near-field optical microscope (SNOM)
(resolution:1～100nm)

High spatial resolution

・Domain size is expected to be comparable to CLSM resolution
・High spatial resolution experiment requires high detection efficiency & very long exposure time …

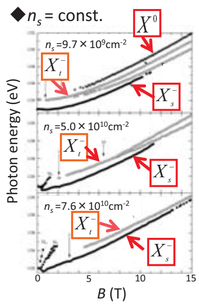

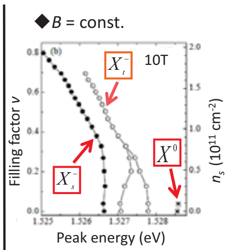

G. Yusa *et al.*, Physica E 12,49 (2002).

Quasi-confocal microscopy

◆Confocal microscopy:
・point excitation, point collection
・resolution depends on N.A. of objective lens

for imaging spin domain…

◆Quasi-confocal microscopy:
・uniform excitation, point collection
→replace single-mode fiber to multi-mode(square) fiber for illumination

※In this case, PM single-mode fiber's core play a role of 'pinhole'

Experimental setup

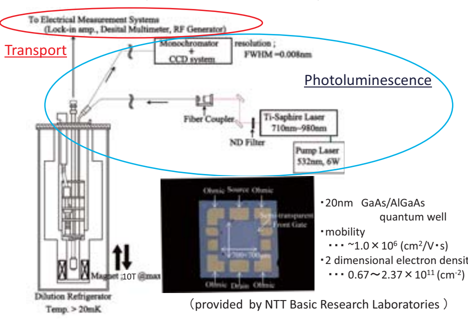

・20nm GaAs/AlGaAs quantum well
・mobility ･･･~1.0×10^6 (cm^2/V･s)
・2 dimensional electron density ･･･0.67～2.37×10^{11} (cm^2)

(provided by NTT Basic Research Laboratories)

Longitudinal resistance in the vicinity of ν=2/3

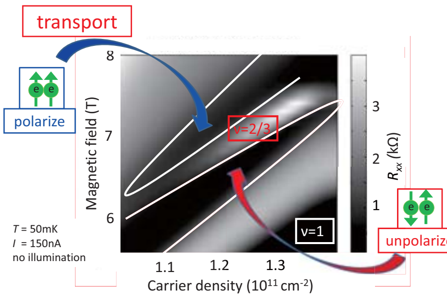

New experimental setup

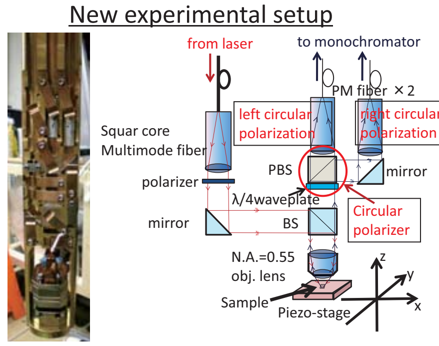

Photoluminescence of 2DEG at zero magnetic field

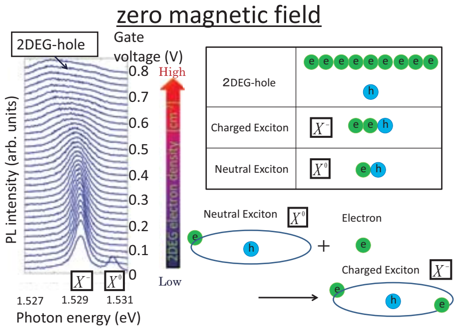

Simultaneous measurement

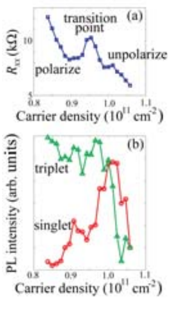

・Simultaneously measured (a) R_{xx} and (b) PL intensity originated from charged excitons in the vicinity of ν=2/3 spin transition point.

	X_s^-	X_t^-
unpolarized region	incrase	incrase
polarized region	decrease	incrase

The tendency of PL intensity by decreasing carrier density

B = 6.3T
T = 150 mK
I = 200 nA
Laser power = 0.65 mW/cm^2

Conclusion

We have found the peak intensity of singlet charged exciton tends to increase up to transition point and it tends to decrease beyond this point by decreasing electron density. On the other hand the peak intensity of triplet charged exciton tends to monotonically increase by decreasing electron density. Thus the peak intensity of charged excitons can be used as a probe to detect local spin polarization.

In order to acquire the image of spin domains, we developed a scanning optical microscope in a dilution refrigerator. This experimental set-up will enable us to directly observe the spin domains with micron order spatial resolution.

Ionic conductivity of Trehalose-Water-Lithium iodide mixture in glass and supercooled liquid state

(IMRAM) Tohoku University
○ Reiji Takekawa, Yoshiki iwai, and Junichi Kawamura

1. Introduction

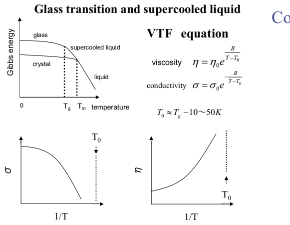

VTF : Vogel-Tammann-Fulcher

Coupling system and decoupling system

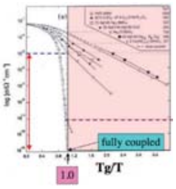

F. Mizuno ea al

Journal of Non-Crystalline Solids 352 (2006) 5147–5155

How do particles behave in coupling system and decouplong system in glass and supercooled liquid state

What is cause by change from coupling to decoupling

LiI-H_2O-trehalose system

LiI-6H_2O (14.3 : 85.7)

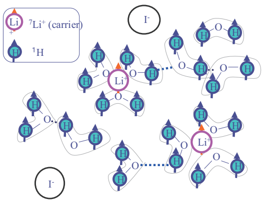

Li$^+$ and water is strong coupling

○ Suitable things of containing sugar

Stable supercooled liquid and glass

The dynamics of the salt is variously changed depending on the kind of the sugar. (see below figure)

trehalose

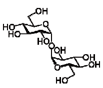

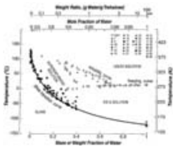

Tani chen et al

Cryobiology **40,** 277–282 (2000)

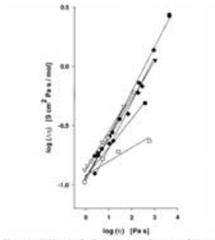

Figure 3. Walden plot for the conductivity of aqueous solutions of (●) trehalose/NaCl, (○) maltose/NaCl, (▼) sucrose/NaCl, (▽) sucrose/KCl (ref 23), (■) glucose/NaCl, (□) glycerol/NaCl, and (◆) trehalose/LiCl. In all cases, the NaCl or LiCl concentration was nominally 0.01 M.

Danforth P. Miller, et al

J. Phys. Chem. B, Vol. 104, No. 44, 2000

How does the change of the ion dynamics by adding trehalose to LiI-H_2O systems?

2. Experiment

NMR	Composition analysis
DSC	Determination of glass transition temperature Tg
AC impedance	Measurement ionic conductivity

3. Result and discussion

^{1}H NMR result

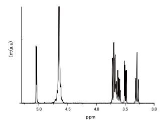

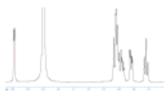

[BMRB data base]

4.7ppm is from water

Another is from trehalose

Result of composition analysis and Tg in preparation samples

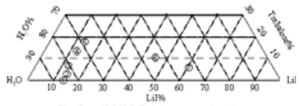

Fig1 Part of LiI-H_2O-Trehalose ternary phase diagram

	LiI : H_2O : Trehalose	Tg(℃)
①	14.3 : 85.7 : 0	-130.0
②	15.7 : 83.3 : 1.0	-119.2
③	12.5 : 81.1 : 6.4	-68.6
④	13.0 : 74.0 : 13.0	-45.6
⑤	14.0 : 68.4 : 17.7	-8.6
⑥	46.0 : 43.4 : 10.7	-9.4
⑦	61.4 : 32.8 : 5.8	2.0

Table.1 Composition (mole ratio) of the samples and Grass transition temperatures.

Tg increase

Increase trehalose ratio

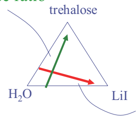

Increase LiI ratio

Temperature dependence of ionic conductivity

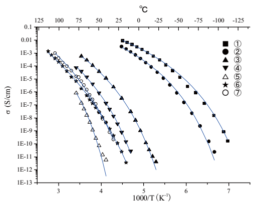

Fig.2 Temperature dependence of conductivity in LiI-H_2O-Trehalose compounds

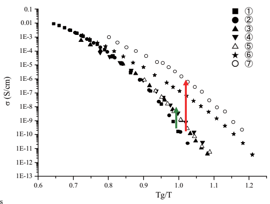

Fig.3 Tg scaled plot of temperature dependence of conductivity

Line is shift to left with increase Tg

At Tg,

σ Increase 1 order of magnitude

σ Increase 4 order of magnitude

① 14.3LiI-85.7H_2O

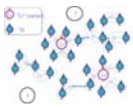

Coupling system

⑤ 14.0LiI-68.4H_2O-17.7trehalose

Li ion mobility increase slightly

⑦ 61.4LiI-32.8H_2O-5.8trehalose

Li ion density is increase and ion have high mobility. Changing decouple system.

meaning trehalose-water region

4. Summary

LiI-H_2O-trehalose system can make glass in wide component region.

Systems of which the properties are changed from coupling to decoupling by changing their molar ratio only.

It is possible to study how to change couple glass to decouple glass using this system in detail.

Progress of the new DAQ system for wide-band solar neutrino observation with KamLAND

Yasuhiro Takemoto (Physics, D1, Tohoku Univ.) PO.19

Backgrounds

Physics

Standard Solar Model

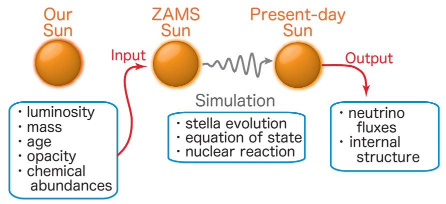

Solar Composition Problem

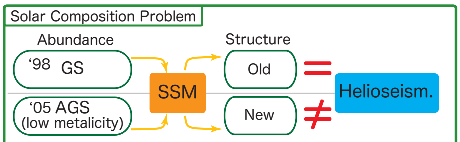

Predicted Solar Neutrino Fluxes (cm^{-2} s^{-1})

Source	SSM Flux (GS)	SSM Flux (AGS)	Scale	Diff[%]	σ[%]
PP Chain					
pp	5.97	6.03	10^{10}	+ 1.0	± 0.5
pep	1.41	1.44	10^{8}	+ 2.1	± 1.0
hep	7.90	8.18	10^{3}	+ 3.5	± 15
^{7}Be	5.07	4.64	10^{9}	- 8.5	± 6
^{8}B	5.94	4.85	10^{6}	- 18.4	± 12
CNO Cycle					
^{13}N	2.88	2.07	10^{8}	- 28.1	+14 -13
^{15}O	2.15	1.47	10^{8}	- 31.6	+16 -15
^{17}F	5.82	3.48	10^{6}	- 40.2	+17 -16

Sensitive to Difference

Flux(GS) : BPS08(GS)
Flux(AGS): AGSS09(AGS)

PP Chain

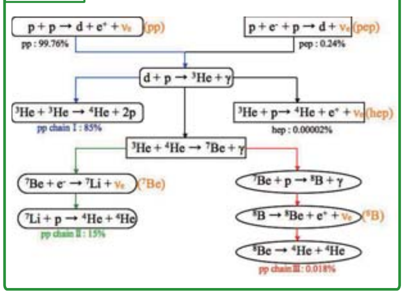

CNO Cycle

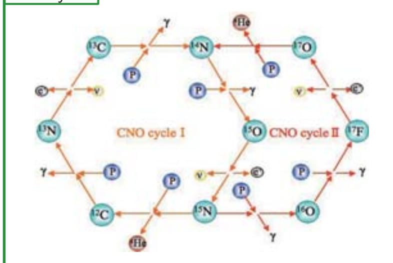

Precise measurement of multiple Solar Neutrinos is the key to investigate "Solar Composition Problem".

Observation

KamLAND

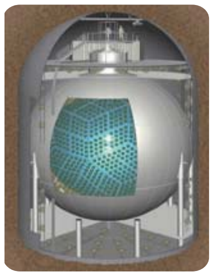

KamLAND:
Kamioka Liquid scintillator Anti-Neutrino Detector.

- 10^{-5} cosmic ray fluxes by the 2700 m.w.e. overburden
- 1000 tons of pure liquid scintillator
- 1879 high-accuracy PMTs
- Sensitive > ~250 [keV]
- Resolution
  Vertex: 12 [cm]/√E[MeV]
  Energy: 6.5 [%]/√E[MeV]
- Additional purification of LS enabled low energy solar neutrino observation.

Background Reduction

More powerful DAQ electronics enables additional reduction of background against wide-band solar neutrino observation.

ν	B.G.	Reduction Scheme
^{7}Be	^{210}Bi	α PSD
	^{210}Po	α PSD
	^{75}Kr	Delayed Coincidence
CNO /pep	^{210}Bi	α PSD
	^{11}C	One by one tagging
^{8}B	^{208}Tl	α PSD of parent ^{212}Bi
	^{10}C	One by one tagging

^{11}C Tagging

Analytical 3-fold coincidence, with tagging by-product neutrons' position.

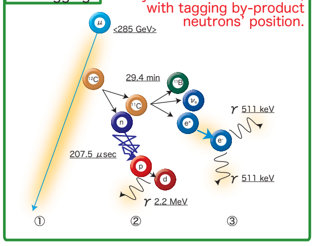

Roll-back Trigger

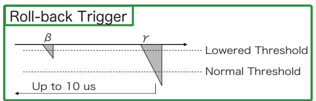

Electronics

System Design

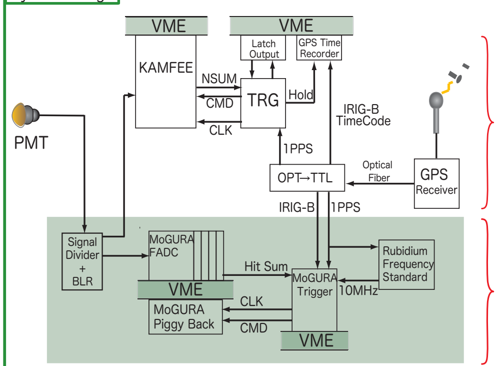

Pallarel DAQ system insures data with the same quality as before, enables shortest dead time on installation of new system and leads opputunity of cross check of data between the systems.

Modules

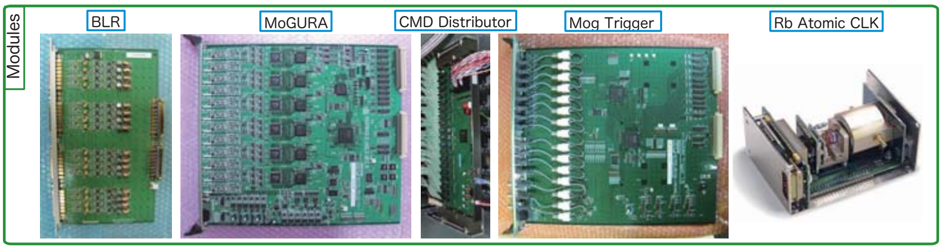

BLR (BaseLine Restorer)

Overshoot restoration after muons for triggering following signals

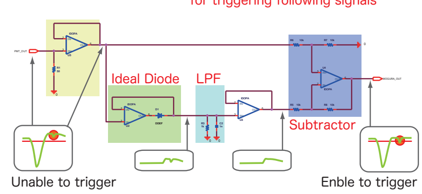

MoGURA(Module for General-Use Rapid Application)

Deadtime-free ADC and on board data reduction DSP

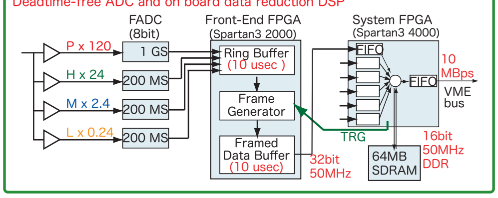

DAQ System Construction

Installation

KamLAND EHut Crate Reassignment

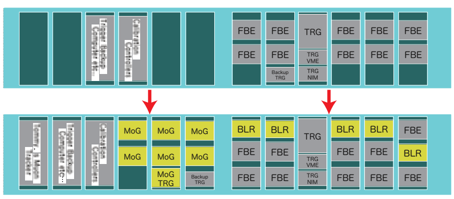

Cable delay due to this installation was caluculated in advance, and event reconstruction method was modified just after this installation.

Installation Works

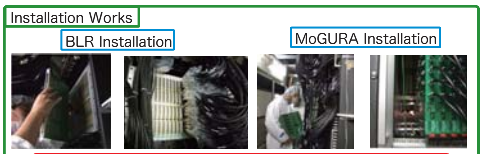

BLR Installtion was done by one crate by one crate.

DAQ System

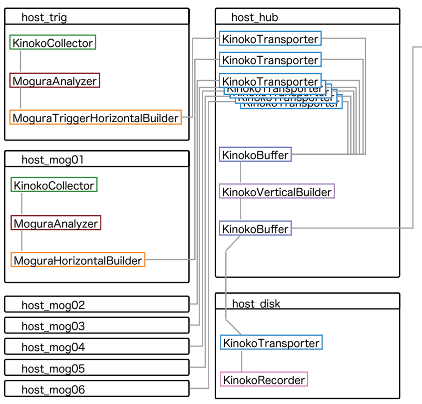

KiNOKO is used for this DAQ System.
Inline event building is the new idea.
Spreading builders and analyzers lessens loads.

Summary

Physics and Requirements

- Wide-band solar neutrino observation needs less background.
- 3 schemes, event tag with neutrons, α particle PSD and genuine delayed coincidence are required.
- Dead-time free DAQ system solely enables those.

Done

- All electronics are developed, verified, and installed.
- Current DAQ system had cable delay, which was corrected.

On Going

- New DAQ is on construction.
- The DAQ includes inline event building.

Todo & Prospects

- Roll-back trigger for the delayed co-incidence has to be developped before DAQ launches.
- After starting DAQ, tagging method and PSD method have to be established.
- For longer live time, we will start DAQ as soon as possible.

Double Chooz PMT preparation

The 2nd GCOE International Symposium @ Tohoku University,18-19/Feb/2010

TABATA Hiroshi

What is Double Chooz?:

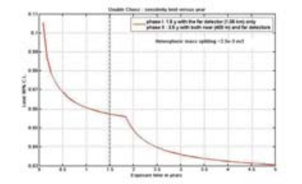

New concept of Double Chooz: The Double Chooz experiment is a neutrino oscillation experiment at Chooz nuclear power plant in France to accurately measure the last mixing angle θ_{13}. Double Chooz uses 2 identical detectors at different distances from nuclear reactors to cancel systematic uncertainties on neutrino flux and detector response. Short baseline reactor experiments can provide a clean θ_{13} measurement.

$$P(\bar{\nu}_e \to \bar{\nu}_e) \approx 1 - \sin^2 2\theta_{13} \sin^2\left(\frac{\Delta m^2_{31} L}{4E}\right)$$

Sensitivity: The current upper limit is $\sin^2 2\theta_{13} <$ 0.15. We will measure the $\sin^2 2\theta_{13}$ with 5 times better sensitivity than the current limit measured by the previous CHOOZ experiment.

Double Chooz detector:

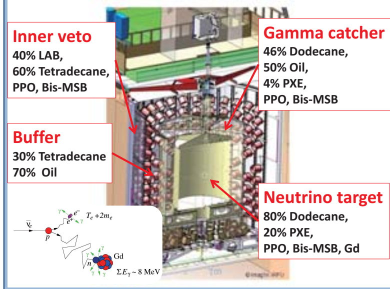

Neutrino target: 10.3 m^3 of liquid scintillator doped with 0.1 g/l of Gd.
Gamma catcher: 22.3 m^3 of liquid scintillator
Buffer: 110 m^3 of non scintillating oil & 390 PMTs (10 inch)
Inner veto: 90 m^3 of liquid scintillator & 78 PMTs (8 inch)
PMT (Photon Multiplier Tube):Main responsibility of Japanese group is PMT (buffer) system. We developed low background PMT with HAMAMATSU.

Anti neutrino events: $\bar{\nu}_e + p \to e^+ + n$
Prompt: e^+ *with* $T_e = 1-8MeV$ *in the target.*
Delayed: radiative capture of n *on Gd with* $\tau \sim 30\mu s$, $r < 1m$ *and* $\sum E_\gamma \sim 8MeV$.
Neutrino signals are estimated as 70/day @far and 500/day @near.

Preparation in the lab:

PMT delivery: PMT group purchased 800 PMTs for both detector. After acceptance test in Japan and Germany, cleaning and magnetic shield assembly were held in Germany. Then, 400 PMTs were delivered to Chooz. Other 400 PMTs for near detector are kept in Germany.
Preparation of the lab: Before starting PMT installation, clean and new scaffolding was installed in buffer tank. Then, clean tents were installed. One tent covered tank. Another tent was for dressing area and preparation area.
Cleanliness organization[1]: To keep lab clean, we cleaned all of the lab at least twice everyday. The tunnel in front of the lab was cleaned also. All people have to wear clean suit, clean shoes and clean glove.
Pretest[2]: PMT was tested just before installation. If some kind of problem is found in this test, the PMT is rejected.
PMTs preparation[3]: After testing, legs to fix PMT to wall were mounted on PMT. PMTs were covered by black plastic bag to avoid light and dust. Position survey markers were put on PMT.

Lid PMT installation (Nov-Dec,2009):

Preparation of the buffer lid[1]: After acrylic vessel integration, PMT group worked for lid PMT installation. Since tank was open, it was covered by plastic sheet to avoid any dust.
PMT installation[2]: People worked below buffer lid. Worker paid attention very much not to touch installed PMTs.
PMT cabling[3]: To be passed through cable exit pipe on the buffer lid, we made bundle. Making good bundle, worker was unrolling PMT cable.
Buffer lid closing[4]: After lid PMT installation, buffer lid was closed. Then PMT group routed lid PMT cable to divider module and connected just before Christmas of 2009.

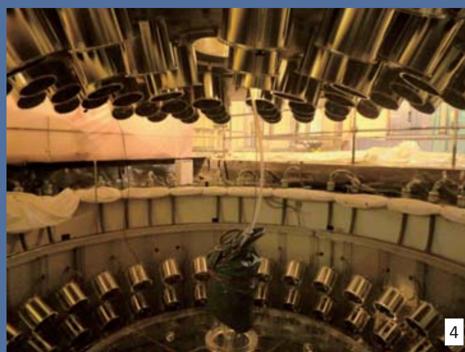

Side and Bottom PMT installation (Jun-Jul, 2009):

PMT transportation[1]: PMTs were transferred to each place. During side and bottom PMT installation, we used a bucket to lowering the PMTs.
PMT installation[2]: As you can see, fixation rails had already been installed on the buffer tank in advance. 2 people mounted PMTs on the rail. We could install 25 PMTs everyday. This was hard work, because they worked in very small space between scaffolding and wall.

PMT cabling[3]: PMTs have a high voltage cable. Cable goes to divider module which installed on wall of the lab. 6 people worked for this cable routing. This task was hardest work because workers went up and down many times.
Done[4]: All PMTs were installed until end of July 2009. After precise PMT position survey was held, plastic bags and survey markers were removed.

Future plan:

Electronics and DAQ integration: Electronics are under production and testing. It will take 3 months for electronics and DAQ integration.
Detector closing: Inner veto lid is open now. Until detector closing, chimney construction (between buffer and veto tank), veto lid closing and chimney construction (above veto lid) have to be done.
Filling: Liquid and gas filling system is under construction by filling group. Since chimney is not so thick, difference of liquid levels is critical for acrylic vessel. Therefore filling operation is very important.
Filling will be finished until July 2010.
Data taking: After filling , we will turn on the high voltage of PMTs to detect first neutrino for Double Chooz experiment. This is scheduled June 2010. Detector commissioning and data analysis will be continued.
Near detector construction: Tunnel construction of near detector will start October 2010. Data taking with double detector is scheduled middle of 2012.

Effects of lanthanoid ion on phosphate head groups in DMPC membrane

Kouya Tamatsukuri[1], Tetsuhiko Ohba[1], Gen Sazaki[2], Kazuo Ohki[1]
tamatuku@bio.phys.tohoku.ac.jp
[1]Department of Physics, Tohoku University, Sendai, 980-8578
[2]Institute for Materials Research, Tohoku University, Sendai, 980-8577

Biomembrane

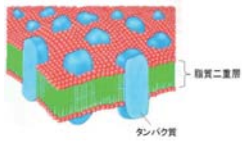

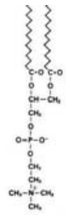

Biomembrane composed of lipid bilayer membrane with occasional proteins interwined.

Liposome

Phospholipid

It composed of hydrophilic head and hydrophobic acyl chain, and have amphipathic character

GUV (Giant Unilamellar Vesicle) ～50μm
LUV (Large Unilamellar Vesicle) ～500nm
SUV (Small Unilamellar Vesicle) ～50nm

MLV (Multi lamellar Vesicle)

Micelle ～50nm

Phase transition of biomembrane

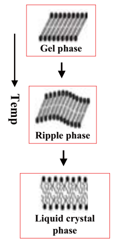

Direct microscopic observation of MLV under a magnetic field (～10T)

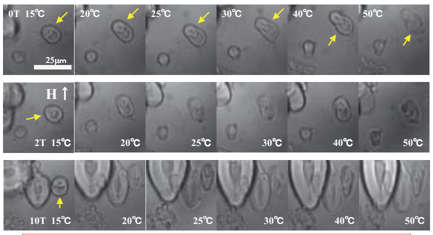

Phospholipids become orientated perpendicular to the static magnetic field due to the anisotropy of magnetic susceptibility $\Delta\chi$, which arises mainly from their fatty acyl chains.

Lanthanoid ions reorient lipids parallel to the magnetic field

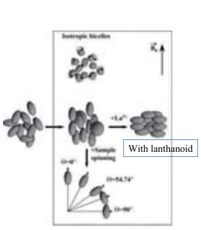

Isabelle Marcotte et al
(2004 Concepts in Mag. Res. Part A)

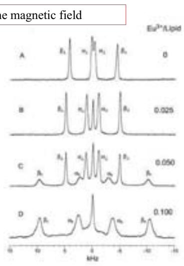

Kevin J et al (2001 Biophis. J.)
DMPC/DHPCによるBicell＋Euの²H-NMR (DMPC-d4)

Conformation of the polar head group in the presence of cations

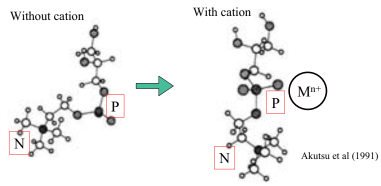

It was reported that cations including lanthanoid ions induce the conformation change of the polar head group of lipids （The figure shows DPPC head group in Lc phase）

We investigated the effects of lanthanoids ion Eu^{3+} on the comformation and dynamics of the polar head group in DMPC membrane.

Fluorescent probes

Polar head group

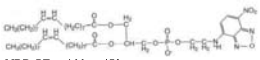

NBD-PE ex466 em470

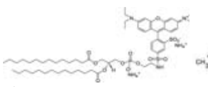

Rh-PE ex530 em590

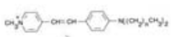

DiA ex470 em585

Acyl chain

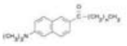

Laurdan ex360 em430

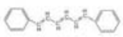

DPH ex360 em430

Fluorescent anisotropy （DPH）

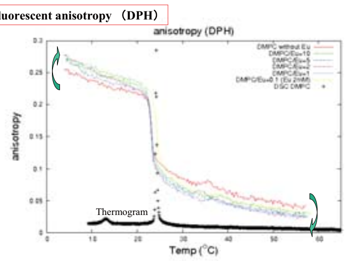

As Eu^{3+} concentration is higher,
the anisotropy is higher in gel phase.
the anisotropy is higher in liquid crystal phase.

Fluorescent anisotropy （DiA、NBD）

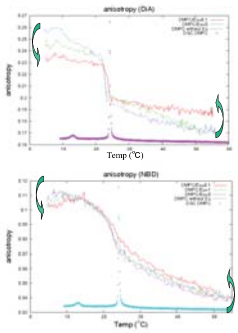

DiA、NBD
As Eu^{3+} concentration is higher,
the anisotropy is higher in gel phase.
the anisotropy is higher in liquid crystal phase.

Fluorescent polarized microscopy of GV

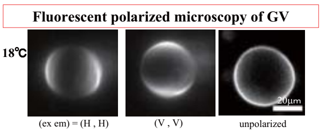

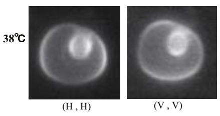

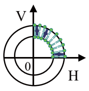

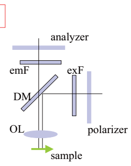

Orientation of probes in membrane is revealed by using linearly polarized light.

DPH

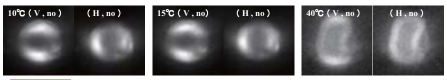

Without Eu

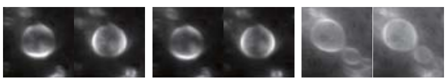

DMPC/Eu=0.1

The orientation of DPH was observed above 40℃ on microscopy, and there is no dependence of orientation of DPH on lanthanoid ion .

Rh-PE

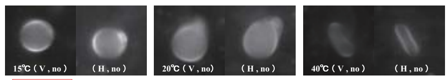

Without Eu

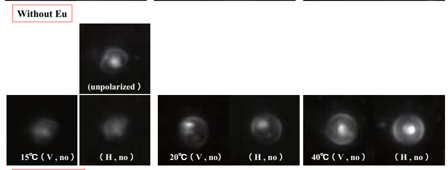

DMPC/Eu=0.1

The orientation of Rh-PE was observed above 40℃ on microscopy, and there is no dependence of orientation of Rh-PE on lanthanoid ion.

Generalized polarization (G.P.)

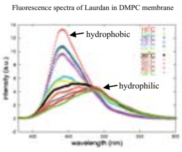

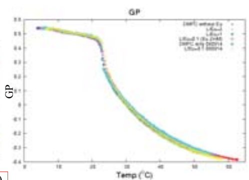

$$GP = \frac{I(440\ nm) - I(490\ nm)}{I(440\ nm) + I(490\ nm)}$$

Dependence of GP on Eu concentration

DSC

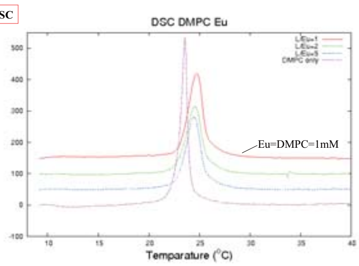

As increasing of Eu concentration , peak temperature is shifted to higher and peak width is broaden.

Optical system

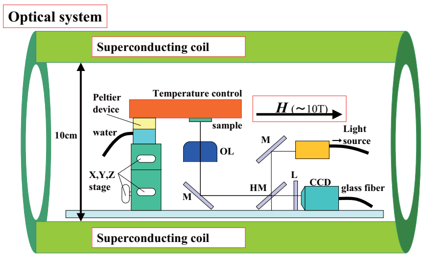

Sample

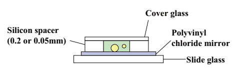

Direct microscopic observation of MLV doped Eu^{3+} under a magnetic field (L/Eu=2)

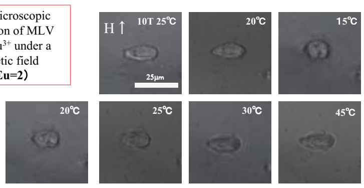

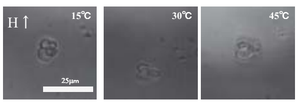

Conclusion

Addition of Eu^{3+}

- Rotational diffusion of acyl chains is facilitated
  polar head group is inhibited
- Main transition temperature is shifted to higher
  →The occupied area of polar head group is relatively small in the liquid crystalline phase.
- there is no dependence of orientation of acyl chain or polar head group on lanthanoid ion.
- Under the static magnetic field, phospholipids became orientated parallel to the static magnetic field.

Status of double beta decay experiment with KamLAND

Azusa Terashima
Research Center for Neutrino Science, Tohoku University

KamLAND (Kamioka Liquid scintillator Anti-Neutrino Detector)

●Location

Placed in Gifu prefecture.
2,700 m.w.e.
μ rate ~ 0.34Hz

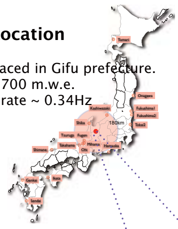

●Current Targets

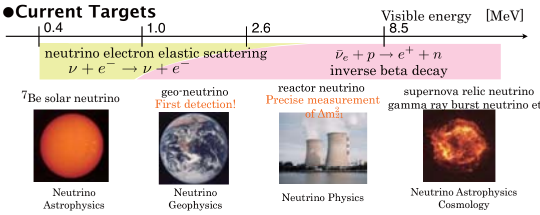

●Inner Detector
(diam. 18m, stainless tank)
Buffer oil: 1,800 m^3,
This density is strictly controlled with LS ~ 0.4%.
PMTs: 1,325 × 17 inch
554 × 20 inch
Photo coverage: 34%
Energy resolution:
6.5%/√E(MeV)

● Outer Detector
(diam. 20m, height 20m)
Ultra pure water: 3,000 ton
PMTs: 20 inch × 225
for muon veto

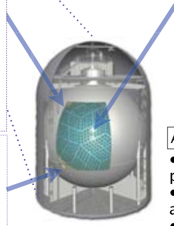

●1,000 ton of highly purified Liquid scintillator(LS) in the balloon(diam. 13m, thickness 135μm, EVOH)

Background level of LS is extremely low.
U (3.4 ± 0.4) × 10^{-18}[g/g] (O(10^{-5} μBq^{214}Bi/kg))
Th (5.7 ± 0.8) × 10^{-17} [g/g] (O(10^{-4} μBq^{208}Tl/kg))
K 2.7 × 10^{-16} [g/g]
This level is already about four or five digits lower than general double beta decay experiment.

Advantage of using KamLAND
- Ultra low radioactivity environment based on ultra pure LS and 9m radius active shield.
- No modification to the detector is necessary to accommodate DBD nuclei.
- Reactor and geo- antineutrino observations continue.
- High scalability for 2nd phase.
  1000 kg ^{136}Xe, improvement of energy resolution with light concentrators and brighter LS

Next target is neutrinoless double beta decay to search the nature of neutrino.

What Can We Learn from Double Beta Decay

Double beta decay could occur if the usual single beta decay is forbidden energetically or suppressed strongly. This transition takes place through the two decay modes.

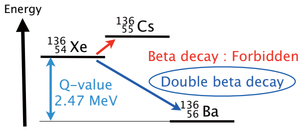

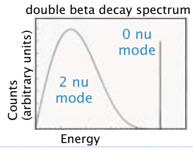

● 2ν mode

$(A,Z) \to (A,Z+2) + 2e^- + 2\bar{\nu}_e$

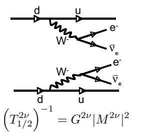

$\left(T^{2\nu}_{1/2}\right)^{-1} = G^{2\nu}|M^{2\nu}|^2$

● 0ν mode

m_{nu} is nonzero & Majorana particle!

$(A,Z) \to (A,Z+2) + 2e^-$

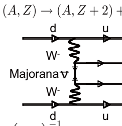

G: phase space factor,
M: nuclear matrix element
<m$_\nu$>: effective neutrino mass

$\left(T^{0\nu}_{1/2}\right)^{-1} = G^{0\nu}|M^{0\nu}|^2\langle m_\nu\rangle^2$

$\langle m_\nu \rangle \equiv \left| |U^L_{e1}|^2 m_1 + |U^L_{e2}|^2 m_2 e^{i\phi_2} + |U^L_{e3}|^2 m_3 e^{i\phi_3} \right|$

This decay is beyond the standard model and if observe this,
- leptonic number violation.
- nature of neutrino: **Majorana/Dirac**? Majorana!!
  if Majorana → see-saw mechanism, leptogenesis?
- absolute neutrino mass and neutrino mass hierarchy.

Double Beta Decay Experiment with KamLAND

●Possible Milestones of Neutrinoless Double Beta Decay Experiment

Neutrino oscillation experiments tell us Δm^2 and allow the possible region of neutrino effective mass <m$_\nu$> (see below pictures).

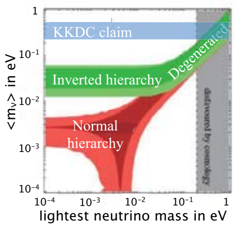

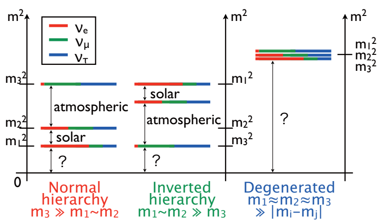

Possible mile stone of neutrinoless double beta decay experiment will be
- Verification of KKDC claim and search degenerated hierarchy
  KKDC claim is the only one observation of 0ν mode by Group of Heidelberg-Moscow(1990-2003) with ~11 kg enriched ^{76}Ge and calorimeter.
  Their claim of observed neutrinos effective mass: 0.24-0.58 eV(4σ)
  This will be needed dozens ~ a few hundreds kg of isotope.
  ⇒ KamLAND 1st phase
- Exploration of inverted hierarchy
  Target effective mass will be a few ten meV, need a few hundred kg ~ ton of isotopes. ⇒ KamLAND 2nd phase

●KamLAND with ^{136}Xe

There are 10 double beta decay nucleus whose Q-value is more than 2 MeV. To take advantage of KamLAND clean environment and its large volume of LS, we choose ^{136}Xe(Q-value: 2.48 MeV) for the experiment. Advantages of using Xe are...
- isotopic enrichment, purification established
- soluble to LS more than 3 wt%, easily extracted
- slow 2ν mode ($T_{1/2}$>10^{22} years) requires modest energy resolution

●1st phase (2011~, 400 kg of ^{136}Xe) → KKDC claim, degenerated hierarchy

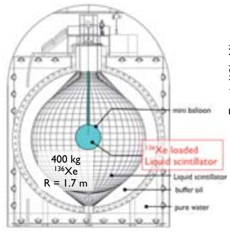

Expected spectrum

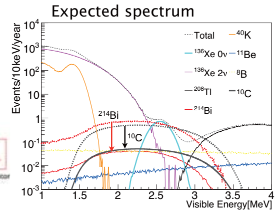

simulation conditions
- <m$_\nu$> = 150 meV
- $T_{1/2}$(0ν) = 9.8 × 10^{25} yr
- $T_{1/2}$(2ν) = 1.0 × 10^{22} yr

- mini balloon(nylon6) thickness 15 um,
  ^{232}Th, ^{238}U = 10^{-12} g/g,
  ^{40}K = 10^{-11} g/g.

- ^{214}Bi tagging(analysis)
- ^{10}C tagging(electronics)

Target sensitivity of the 1st phase is ~60 meV.

Target sensitivity of the 2nd phase is ~25 meV with 5 years.

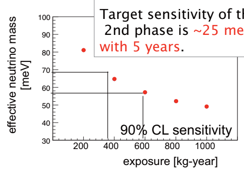

● 2nd phase (end of 2013~, 1 ton of ^{136}Xe) → inverted hierarchy

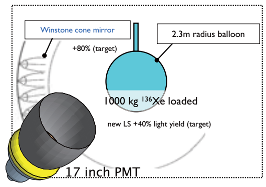

Current image of winston cone.

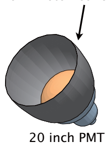

20 inch PMT

●R&D items and current experiment status

●Xe loaded liquid scintillator Already developed!

New Xe loaded LS decane(81.8%), PC(18.2%) and PPO with 2.5 wt% Xe. Density 0.78 g/cm^3	cf.) KamLAND LS dodecane(80%), PC(20%) PPO 1.36 g/l Density 0.78 g/cm^3

Now testing...
- Precise measurement of solubility within 0.1 % error.
- Precise measurement of solubility's temperature and pressure dependency.

Almost same density, light yield, transparency, alpha-ray quenching ratio as current KamLAND liquid scintillator.

●Xe purification, collection system

Target ... collection value 99.7 %/1cycle

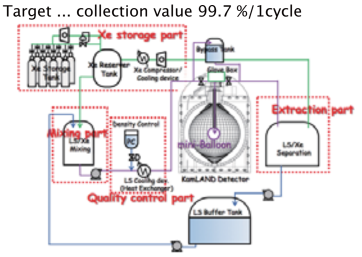

Under excavation the mine area for big tank.

●mini balloon

Need thin, ultra-clean(ex. ^{238}U, ^{232}Th ~ 10^{-12} g/g, ^{40}K ~ 10^{-11} g/g), enough strength and gas-tight balloon. Have experience of 13mφ and 135 um thickness balloon.
Selection of film continue...

13mφ balloon.

1/4 scaled mini balloon
⇒ Adhering test
⇒ Water injection test
(see right pictures)

1/1 scaled mini balloon will come soon for folding test.

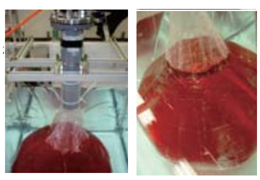

●MoGURA Module for general use rapid application

At KamLAND neutrinoless double beta decay, most dominant background is spallation product ^{10}C generated by cosmic muon.
New dead-time free electronics MoGURA, will allow 90% reduction of ^{10}C with neutron tagging.
Now DAQ construction.

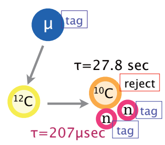

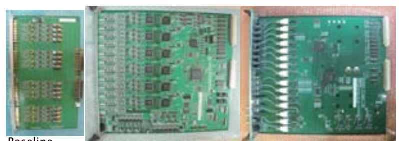

Baseline restorer and signal splitter
1GHz FADC + 3 range 200 MHz FADC for each channel
Trigger module

In detail ⇒ please see Takemoto's poster!

PO no. 23

The 2nd GCOE International Symposium

Simulations on Dynamics of Wormlike Micellar System Using Particle-Field Hybrid Models

Masatoshi Toda
Physics, D3, Tohoku University

February 18, 2010

1

Wormlike Micelle

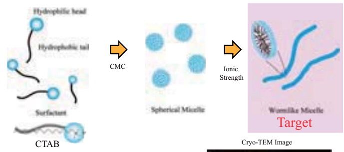

Characteristic Size

Cross Section Diameter: $R_{cs} \sim 5$ nm

Persistence Lengtrh: $l_p \sim 10$nm

Contour Length : $L \sim 1000$ nm

Cryo-TEM Image

Lin (1996)

2

Linear Rheology —Brief Review—

Exponential Relaxation

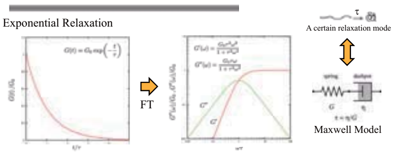

Generally,…

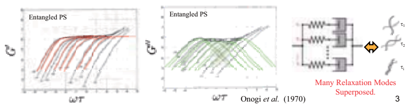

Onogi *et al.* (1970)

3

Linear Rheology —Wormlike Micellar Case—

Shikata *et al.*

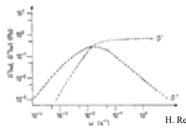

H. Rehage & H. Hoffmann (1988)

One Separated Relaxation Mode Exists!!

What is it ?

A Proposed Relaxation Mechanism (Phantom Crossing Model)

T. Shikata (1987)

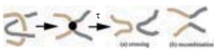

4

Shear Banding

Couette Flow

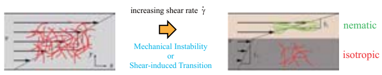

Uniform Flow (Isotropic)

Inhomogeneous Flow (Isotropic to Nematic)

Flow Birefringence

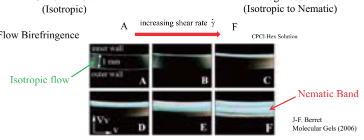

J-F. Berret
Molecular Gels (2006)

5

Purpose

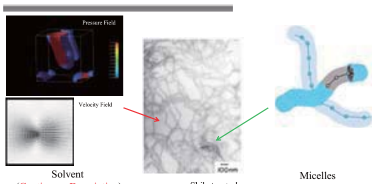

Solvent
(Continuum Description)
Hydrodynamic Interaction

Shikata *et al.*

Micelles
(Particle Description)
Entanglement Relaxation

Particle-Field Hybrid Models ⇨ Microscopic Origins of
- Maxwellian Behavior
- Shear Banding, etc.

6

Hybrid Model —Purely Dissipative Equations— (Non dimensional)

- Solvent Component

$$\frac{\partial \boldsymbol{v}}{\partial t} = -\nabla p + \nabla^2 \boldsymbol{v} + \sum_{i=1}^{N}\left[\frac{\mathrm{d}\boldsymbol{r}_i}{\mathrm{d}t} - \boldsymbol{v}(\boldsymbol{r}_i) - \boldsymbol{\zeta}_i\right]\delta(\boldsymbol{r}-\boldsymbol{r}_i) + \boldsymbol{\theta}$$

(at Low Reynolds Number)

Body Force f_i^B (Coupling Term with Micelles)

$$\nabla \cdot \boldsymbol{v} = 0$$

- Micellar Component

$$\frac{\mathrm{d}\boldsymbol{r}_i}{\mathrm{d}t} = \boldsymbol{v}(\boldsymbol{r}_i) - \frac{\partial H}{\partial \boldsymbol{r}_i} + \boldsymbol{\zeta}_i$$

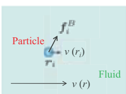

- Fluctuation-Dissipation Relation

$$\langle \boldsymbol{\zeta}_i(t)\boldsymbol{\zeta}_j(t')\rangle = 2T_\mathrm{P}\delta_{ij}\mathbf{1}\delta(t-t')$$

$$\langle \boldsymbol{\theta}(\boldsymbol{r},t)\boldsymbol{\theta}(\boldsymbol{r}',t')\rangle = -2T_\mathrm{F}\mathbf{1}\nabla^2\delta(\boldsymbol{r}-\boldsymbol{r}')\delta(t-t')$$

⇨ $T_F = 0$

7

Bending Elasticity of Membranes

W. Helfrich (1973)

$$H_{\text{Bending Elasticity}} = \int \mathrm{d}\boldsymbol{a}\left[\frac{1}{2}\kappa(C_\mathrm{m}(\boldsymbol{a}) - C_0)^2 + \bar{\kappa}C_{\text{Gauss}}(\boldsymbol{a})\right]$$

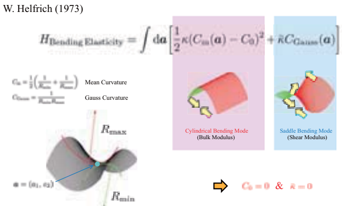

⇨ $C_0 = 0$ & $\bar{\kappa} = 0$

Helfrich's Free Energy ⇨ Bending Elasticity & Cohesive Energy of Micelles

8

Network Structure

without shear
Percolation Prob. = 0.955

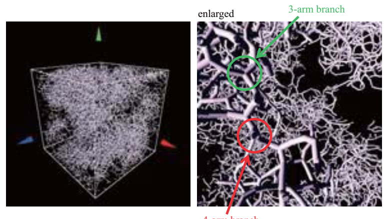

9

Cluster Size Distribution

without shear

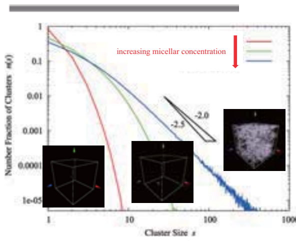

Fischer exponent at Percolation Transition Point

$\tau = 5/2$ (Bethe lattice)

$\tau = 2$ (Triangle lattice)

Only maximum clusters displayed

dilute state ⇨ Exponential distribution

concentrated state ⇨ Power law

10

Conclusion & Future Problems

(1) Modeling of Wormlike Micellar System

Particle-Field Hybrid Model

⇨ Micellar Network Formation

(2) As a Result of a Coarse Graining, Discontinuity in Interparticle Interaction Potential

⇨ Failure of Canonical Distribution

⇨ New Stochastic Methods

11

Magneto-dielectric phenomena in charge ordered system with frustrated geometrical lattice

Department of Physics,
Tohoku University
M. Naka and S. Ishihara

I. Introduction

Conventional ferroelectricity

・Displacive Type (example : $BaTiO_3$)

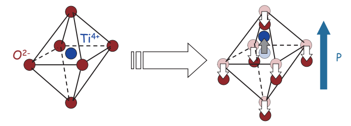

・Order-Disorder Type (example : $NaNO_2$)

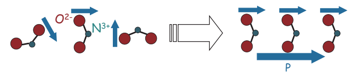

Electronic ferroelectricity

・polarization by charge order

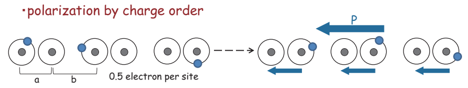

・purpose of study in electronic ferroelectricity

mechanism of polar charge order

prediction of magneto-dielectric phenomena

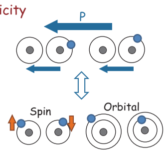

Strongly Correlated electron system

By electron-electron Coulomb repulsion...

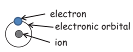

・localization of electron

inter site Coulomb repulsion

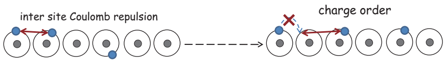

・correlation between degrees of freedom of electron

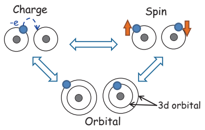

Exotic phenomena
Colossal magneto-resistance
Multi-ferroics

II. Electronic properties in RFe_2O_4

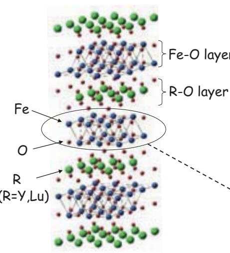

- Exotic ferroelectricity
- New class of multiferroics
- Layered triangular lattice

Fe-O W-layer

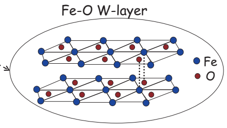

Charge & Spin Orders in $LuFe_2O_4$

Electron Diffraction
(hhl) plane

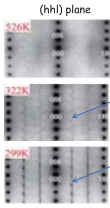

charge	T	spin
disorder	500K	
(1/3 1/3 l) 2D CO	320K	disorder
(1/3 1/3 5/2) 3D CO	247K	(1/3 1/3 m) 3D SO

Charge Order of Fe^{2+} & Fe^{3+}

Neutron Diffraction
(1/3 1/3)

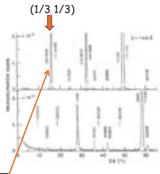

2D : 2 dimensional
3D : 3 dimensional
CO : charge order
SO : spin order

Y.Matsuo et al.
J. Cryst. Soc. Jpn. 50, 150-154 (2008)

K.Siratori et al.
Proc. 6th. Int. Conf. Ferrites, 703 (1992)

Dielectric properties in $LuFe_2O_4$

Spontaneous Polarization

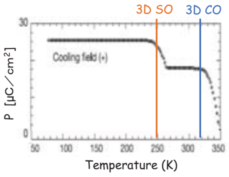

P appears around T_{CO}
P increases around T_{SO}

Charge Order induces P
(electronic ferroelectricity)
+
Spin Order enhances P
(ME effects)

"electronic" multiferroics

N.Ikeda et al.
J.Phys.Soc.Jpn. 69, 1526 (2000)

A Model of "Polar" Charge Order

Charge Structures in W-layer

○ : Fe^{2+}
● : Fe^{3+}
◐ : Fe^{2+}/Fe^{3+}

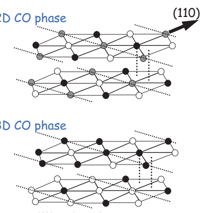

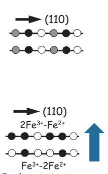

Polarization

Charge	T
disorder	500K
2D CO (1/3,1/3,l) Non-Polar	320K
3D CO (1/3,1/3,5/2) Polar	

Solid State Commun. 692 (1998)

FeO W-layer is a minimal unit of electric polarization

Purpose of this Study

CO/SO in the W-layer

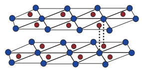

Mechanism of ・・・

Polarization by charge ordering

Correlation between P & SO

Charge	T	Spin
disorder	500K	
2D CO	320K	disorder
3D CO Polar	250K	3D SO

Interactions between Fe ions

・Coulomb interaction H_V

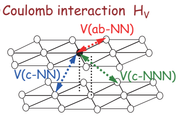

$$H_V = \sum_{ij} V_{ij} n_i n_j = \sum_{ij} V_{ij} Q_i Q_j + const.$$

- Charge pseudo spin Q_i Fe^{3+} : +1/2, Fe^{2+} : -1/2
- Charge conservation $\sum_i Q_i = 0$

・Exchange interaction H_J

Extended p-d model
2p orbital (O) & 3d orbital (Fe)

Effective Hamiltonian

$$H_J = H_{22} + H_{23} + H_{33}$$

Fe^{2+}-Fe^{2+} Fe^{2+}-Fe^{3+} Fe^{3+}-Fe^{3+}

(perturbation with respect to the p-d transfer)

One term of H_{22}

$$H^1_{22} = -J^1_{22} \sum_{\langle ij \rangle} \left(\frac{I_i \cdot I_j}{2} + 3 \right) \left(\frac{1}{2} - Q_i \right) \left(\frac{1}{2} - Q_j \right)$$

spin charge

Approximation: Magnetic anisotropy ⋯⋯ I_i : Ising spin

Calculation Methods

・Charge Structure & Polarization

$$H_V = \sum_{ij} V_{ij} Q_i Q_j$$

Mean-Field Approximation &
Multi-Canonical Monte Carlo Method

・Charge & Spin Structures & Polarization

$$H = H_V + H_J$$

Multi-Canonical Monte Carlo Method

Mean-Field
・periodic boundary
・non-uniform solution along (110) & (100)

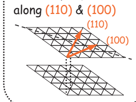

Multi-Canonical Monte Carlo
・periodic boundary condition
・6×6 or 12×12 sites
paired triangular lattices

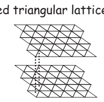

Charge Structure (Mean Field)

phase diagram

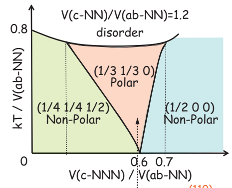

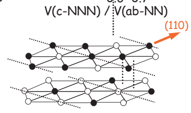

$LuFe_2O_4$ charge	T
disorder	500K
(1/3 1/3 l) 2D CO	320K
(1/3 1/3 5/2) 3D CO Polar	

YFe_2O_4 charge	T
(1/3 1/3 l) 2D CO	250K
(1/3 1/3 5/2) 3D CO	225K
(0 1/2 0) 3D CO	190K

Charge structures are consistent with experiments in $LuFe_2O_4$ & YFe_2O_4

Charge Structure (Monte Carlo)

Charge correlation function

$$\langle Q(k)Q(-k) \rangle = \frac{1}{N} \sum \langle Q_i Q_j \rangle e^{-ik(r_i - r_j)}$$

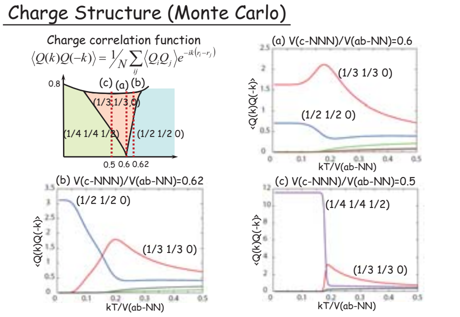

Charge correlation functions are consistent with the MF phase diagram

Electric Polarization (Monte Carlo)

Polarization

$$P = \sum_i^{U} Q_i - \sum_i^{L} Q_i$$

$$\Delta P = \sqrt{\langle P^2 \rangle}$$

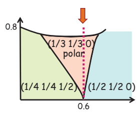

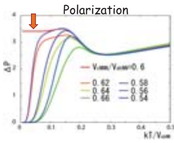

Polar CO states & a lot of non Polar CO states are degenerate at ↓

ΔP is smaller than maximum value of 12.0
Other weak interaction induces P
(example : inter W-layer interaction)

(1/3 1/3 0) CO tends to polarize in comparison with other COs

Mechanism of Polar (1/3,1/3,0) CO

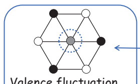

Valence fluctuation by charge frustration

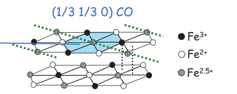

- Large entropy gain by charge fluctuation
- Charge imbalance without energy loss of V(ab-NN)

Charge imbalance (Polarization)

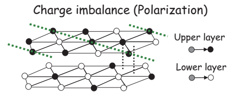

(1/3 1/3 0) CO is stabilized in finite temperatures and tends to polarize by charge frustration

Charge & Spin Structure and Polarization

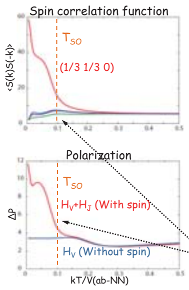

Hamiltonian $H = H_V + H_J$

Charge correlation function

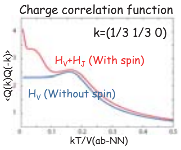

Spin order (1/3 1/3 0) enhances the electric polarization

Mechanism of Magneto-dielectric effect

Charge Structure in $T < T_{so}$

Polar (1/3 1/3 0) CO

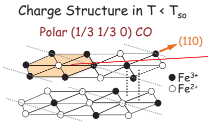

Spin structure in $2Fe^{3+}$-Fe^{2+} layer

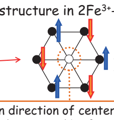

Fe^{3+}-Fe^{3+} Antiferromagnetic Spin alignment

Spin direction of center site is not determined by frustration

The number of ◯ sites is N/3
N : the number of sites in a triangular lattice
$2^{N/3}$ degenerate spin states

Polar CO gains large entropy

Polar CO is stabilized by
- Spin frustration
- Spin-Charge coupling

III. Conclusion

RFe_2O_4

A new class of Multiferroics based on
- "Electronic" Ferroelectricity
- Magneto-Electric effects

(1/3 1/3 0) CO is stabilized in finite temperature

Charge fluctuation accompany with (1/3 1/3 0) CO by charge frustration

Electric polarization is enhanced with spin ordering

Enhancement of electric polarization is attributed to large spin entropy gain by spin frustration

Pi-mesonic decays of Λ hypernuclei

Yoji Nakagawa (physics, D1)

Introduction

Decay of free Λ particle

$$\Lambda \rightarrow \begin{cases} p+\pi^- \sim 64\% \\ n+\pi^0 \sim 36\% \end{cases}$$

$\tau_\Lambda \sim 2.6\times10^{-10}$[sec]

$\Gamma_{\pi^-}/\Gamma_{\pi^0} = 1.79$

ΔI = ½ rule

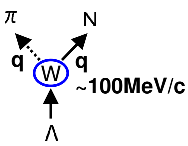

Decay of Λ hypernucleus

O. hashimoto, H. Tamura, PTP57 (2006) 564

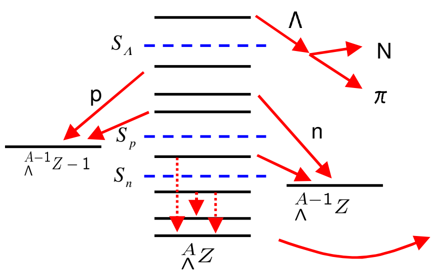

Weak decay
mesonic
non-mesonic

Weak decay of Λ hypernucleus

Mesonic decay

Pauli suppression (cf. $\mathbf{k}_F \cong 280$MeV/c)

Non-mesonic decay

Non-mesonic decay mode is dominant in medium-heavy nucleus

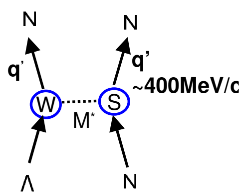

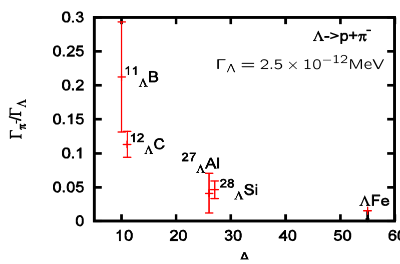

Mesonic decays of neutron-rich Λ hypernuclei

✓Decay widths of C, O, Ne, Mg, Si - isotopes

✓Distortion effect of the π wave function (Especially in neutron-rich region)

Method

Solve Hartree-Fock equation with Skyrme-like interaction

- ✓Core nucleus ･･･ spherical and even-even
- ✓Λ particle ･･･ the lowest state
- ✓Continuum states ･･･ Box descretization (15fm)
- ✓Pairing ･･･ BCS approximation with density dependent δ interaction

Ground state of Λ hypernucleus、single-particle w.f.

Input of the decay interaction

$$\begin{cases} \Gamma_\pi^{(\mathrm{free})} = \dfrac{2q_0}{1+\frac{\omega_\pi}{m_N}}\left(|s_\pi|^2+|p_\pi|^2\right) \\ \Gamma_{\pi^-}/\Gamma_{\pi^0} \sim 2 \end{cases} \Rightarrow \begin{cases} s_{\pi^-} = 0.96\times10^{-7}, \quad p_{\pi^-} = -0.35\times10^{-7} \\ s_{\pi^0} = -s_{\pi^-}/\sqrt{2}, \quad p_{\pi_0} = -p_{\pi}/\sqrt{2} \end{cases}$$

Decay width in nucleus

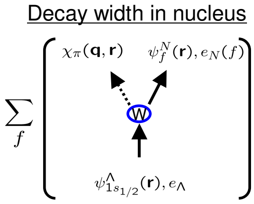

$$\Gamma_\pi = \sum_f \frac{2q}{1+\frac{\omega_\pi}{M_A}}(1-v_f^2)\frac{2j+1}{2}\left[s_\pi^2\eta_f^{(s)} + \left(\frac{p_\pi q}{q_0}\right)^2\eta_f^{(p)}\right]$$

$\eta_f^{(s)} = |\langle\psi_{nlj}^{(N)}|\tilde{j}_l(q,r)|\psi^\Lambda_{1s1/2}\rangle|^2$, $\eta_f^{(p)} = \sum_{L=l\pm1}|\langle\psi_{nlj}^{(N)}|f_l^L(q,r)|\psi^\Lambda_{1s1/2}\rangle|^2$

$$f_l^L(q,r) = \frac{\tilde{j}'_L}{q} + \left[1-\frac{l(l+1)-L(L+1)}{2}\right]\frac{\tilde{j}_L}{qr}$$

v_f^2 ･･･ Occupation probability of the final single particle state

(cf. $\tilde{j}_l(q,r) = j_l(qr)$, if no distortion)

Result

NN :: SIII, ΛN :: #13 (M. Rayet), π - nucleus :: set A (K. Stricker) M.Beiner et al. NPA238(1975)29, M. Rayet, NPA367(1981)381, K. Stricker et al. PRC22(1980)2043

✓O, Ne, Mg, Si - isotopes

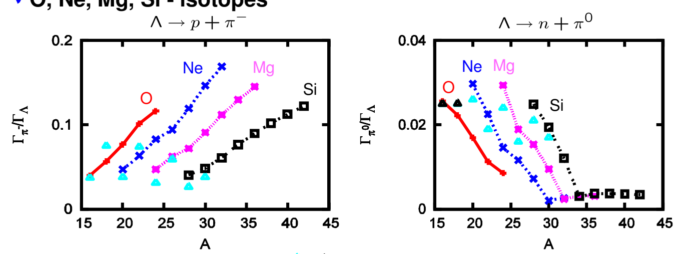

△ ▲ ･･･ T. Motoba, K. Itonaga, PTPS117(1994) 477

✓Distortion effect on π⁻ decay mode

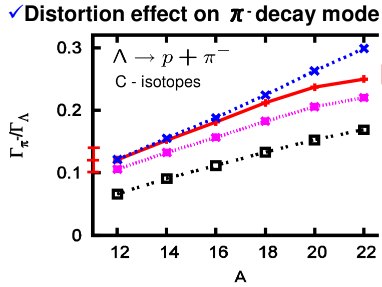

$\delta\rho = \rho_n - \rho_p$

Isospin dependence in the optical potential

･･･ KEK-PS E462

Mesonic decays of $^5{}_\Lambda$He

π momentum distribution of double Λ hypernucleus

Method

Emulsion data of $^5{}_\Lambda$He decay W. Gajewski et al., NPB14(1969)11

$\Lambda \rightarrow p+\pi^-$

Consider only α + N + π decay mode

✓**Initial state**

- α - Λ model

B_Λ=3.1 [MeV] ⟷ SG, Isle potential

- Spectroscopic amplitude

NN		ΛN
Minnesota	+	D2'
G3RS	+	SC97e

•ΛN-ΣN coupling
•Tensor force

✓**Final state**

Scattering states of α + N

Kanada-Kaneko's α-p potential

Descritized states by L³ -box (L=15[fm])

✓**Input of the decay interaction**

$$\Gamma_{\pi^-}/\Gamma_{\pi^0} = 1.79 \Rightarrow \begin{cases} (s_\pi/p_\pi)^2 = 9 \\ s_{\pi^0}^2 = s_{\pi^-}^2/1.79, \quad p_{\pi^0}^2 = p_{\pi^-}^2/1.79 \end{cases}$$

Result

	$\Gamma_{\pi^-}/\Gamma_\Lambda$	$\Gamma_{\pi^0}/\Gamma_\Lambda$
SG (α-Λ)	0.27 (0.21)	0.17 (0.13)
Isle (α-Λ)	0.35 (0.27)	0.21 (0.17)
Minnesota + D2'	0.33 (0.26)	0.21 (0.16)
G3RS + SC97e	0.314 (0.244)	0.195 (0.153)
G3RS + SC97e	0.312 (0.242)	0.193 (0.152)
(KEK-PS E462)	0.340± 0.016	0.202 ± 0.011

Our results are comparable with the previous study

I. Fuse et al., The 59th JPS annual meeting

✓**Difference between the initial states**

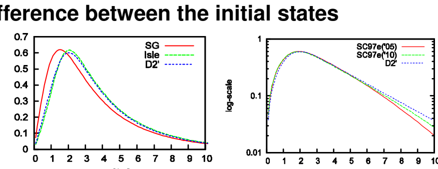

Conclusion

- In neutron-rich region, π⁰ decay mode is suppressed (as expected), π⁻ decay mode is enhanced because of a strong proton - neutron interaction.
- For π⁻ decay mode, the effect of the δρ term is important in neutron-rich region.
- Our method can reproduce the experimental value of the mesonic decay of $^5{}_\Lambda$He.

超対称性の破れのアクシオニック･ミラージュ伝播機構

理学研究科物理学専攻
中村俊太郎

素粒子物理学には標準理論と呼ばれる様々な実験結果を説明する理論がある

しかし、近年その存在が確定的となった暗黒物質(DM)は説明することができない

標準模型を超える物理を知ることが目標

超対称性(SUSY)：ボソンとフェルミオンの間の対称性

電子（スピン1/2） ⟷ スカラー電子（スピン0）

Rパリティ(標準理論粒子＋超対称粒子ー)が保存してれば最も軽い超対称粒子(LSP)は安定になる

超対称粒子はまだ見つかっていないので超対称性は破れている

超対称粒子は対の粒子よりも重い

neutralinoなどが暗黒物質の候補になる

超対称粒子の質量スペクトルは超対称性の破れ(~~SUSY~~)によっている

どのように~~SUSY~~が伝わっているかを理解することは重要

注目を浴びているのがmirage mediation

||

moduli mediation + anomaly mediation

余剰次元を特徴づけるmoduliが~~SUSY~~を伝える

場のスケール変換に対するanomalyが~~SUSY~~を伝える

これら二つの寄与は常にあるのでmirage mediationはとても自然な~~SUSY~~のメカニズム

しかし、mirage mediationには問題がある

moduli 問題

mirage mediationにおけるmoduli 問題

Endo, Hamaguchi, Takahashi ’06
S.N., Yamaguchi ’06

$H \simeq m_X$ のときにmoduliはポテンシャルの最小値のまわりを初期振幅 $\mathcal{O}(M_{\rm Pl})$ で振動し始める

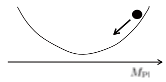

振動エネルギーはすぐに宇宙を支配し様々な粒子へと崩壊していく

とりわけ次の過程が重要

$$X \longrightarrow 2\,\psi_{3/2} \longrightarrow \tilde{\chi}\,\tilde{\chi}$$

$\psi_{3/2}$: gravitino　$\tilde{\chi}$: neutralino LSP

neutralinoは大量に存在するので対消滅する

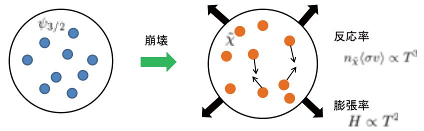

宇宙は膨張しているので対消滅は $n_{\tilde{\chi}}\langle\sigma v\rangle \simeq H(T_{3/2})$ のとき終わる

これが最終的な $\tilde{\chi}$ の残存量　($T_{3/2}$: gravitino崩壊時の熱浴の温度)

$T_{3/2}$ が十分高くない(10MeV)ため消滅効果が一番効くwino LSPでも

$m_{\tilde{\chi}}\dfrac{n_{\tilde{\chi}}}{s} = \dfrac{m_{\tilde{\chi}}}{\langle\sigma v\rangle M_{\rm Pl} T}$ は暗黒物質量を超えてしまう

我々はmirage mediationを拡張することでmoduli問題を解決する

Axionic mirage mediation ＝ mirage mediation ＋ axion

強いCP問題の解決方法として最も有力視されている

Axionic mirage mediationにはaxionの超対称粒子であるaxinoも入ってくる

質量スペクトル

$$m_\lambda = \frac{F_X}{2X_R} - \frac{b_a - N}{4\pi}\alpha(M_{\rm GUT})F_\Phi$$

$$A_i = q_i\frac{F_X}{2X_R} - \frac{1}{2}\gamma_i(M_{\rm GUT})F_\Phi$$

$$m^2_{Q\,1,2} = q_i\left|\frac{F_X}{2X_R}\right|^2 - \frac{1}{2}\gamma_i(M_{\rm GUT})\left(F_\Phi^\dagger\frac{F_X}{2X_R} + {\rm h.c.}\right) - \frac{1}{4}\frac{d\gamma_i'}{d\ln\mu}|F_\Phi|^2$$

(q_i : modular weight)
(γ_i : 異常次元)

$$\mathcal{O}(100){\rm GeV} - \mathcal{O}(1){\rm TeV}$$

axinoの質量は

$$m_{\tilde{a}} = \frac{5N}{16\pi^2}\lambda^2 \underbrace{A_{S\Phi\Phi}}_{\mathcal{O}(m_{\rm soft})}\left\langle\frac{\hat{S}^\dagger}{\hat{S}}\right\rangle \simeq \mathcal{O}(1){\rm GeV}$$

axinoがLSPになる ⟹ DMの候補

axinoはneutralinoよりも軽いのでmirage mediationのmoduli問題を解決できそう

moduliの崩壊で生成されたaxinoが現在のDM量を説明できるかどうかを見る必要がある

axinoの生成過程

$$X \longrightarrow \Psi_{3/2}\Psi_{3/2} \longrightarrow \tilde{\chi}\,\tilde{\chi} \longrightarrow \tilde{a}\,\tilde{a}$$

axinoの残存量

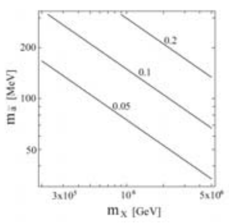

($\Omega_{\rm DM}h^2 = 0.105^{+0.007}_{-0.013}$)
Spergel, et. al ’06

質量が $\mathcal{O}(100){\rm MeV}$ のaxinoで暗黒物質を説明できた

moduli問題の解決

mirage mediationは有望な超対称性の破れの機構だがmoduli問題と呼ばれる宇宙論的な問題があった

我々はmirage mediationにaxionを加える拡張をすることによってneutralinoよりも軽いaxino LSPを実現できた

質量が $\mathcal{O}(100){\rm MeV}$ のaxinoで暗黒物質を説明でき moduli問題も解決することができた

The Study of the Origin of Lyman Alpha Emitters with Large Wquivalent Widths

SSA22 AT Z=3.1

Yuki Nakamura, Toru Yamada, Tomoki Hayashino, Katsuki Kousai, Nana Morimoto, Mitsunori Horie, Eri Nakamura (Tohoku University),
Yuichi Matsuda (Durhum University) and Masayuki Umemura (Tsukuba University)

Our wide-area (2.4deg^2 in total) and deep narrow-band survey detected ~2000 LAEs and reveal that there are a number of large EW objects in "SSA22" and general fields EW$_0$>=240Å; 240 LAEs at SSA22, 95 LAEs at general fields). In order to discriminate the origin of large EW objects, first we should make large EW samples which include objects enhanced for EW by mechanism of Lyman alpha scattering and/or galactic superwind. We measured the both Lyman alpha emission and continuum components by pseudo total magnitude (2.5 × kron radius of SExtractor software) as the Lyman alpha emission of these objects have extended shape. (Noteworthy, we measured Lyman alpha emission and continuum within a given aperture in previous work. When we focus on the EW at the exact position where the star-formation occur to know the stellar age, this measurement is effective.) In results, we found the larger number of high EW objects by this method than that by previous method and the ratio of large EW objects (EW$_0$=400-700Å) to small EW objects (EW$_0$<100Å) is 1.6 times larger in "SSA22" fields than general fields. Furthermore we investigate the statistic properties of these objects such as the size of Lyman alpha emission, Luminosity Function and colors.

1. Observation

We conducted wide-area (2.4deg2 in total) and deep narrow-band survey with Suprime-Cam of Subaru Telescope.

Field	Number of LAEs	Volume (Mpc^3)	Density (Mpc^{-3})
SSA22	1438	9.9 * 10^5	1.4 * 10^{-3}
General Fields	764	7.7 * 10^5	0.99 * 10^{-3}
SDF	196	1.6 * 10^5	1.2 * 10^{-3}
GOODS-N	186	1.9 * 10^5	0.98 * 10^{-3}
SXDS	382	4.2 * 10^5	0.90 * 10^{-3}

Number density of LAEs in SSA22 region is 1.5 times larger than it in general fields.

SSA22 region is a high-density region of LAEs

2. Calculation of EW

We calculated EW of our detected LAEs by two methods.

If Lyα photons emitted from star-forming regions are scattered by neutral hydrogen gas and the emission regions are extended,

A) focus on the EW of the exact position where star-formation occurs to know the stellar age
"EWap": EW measured by Lyα emission and continuum fluxes within aperture=2"φ (psf=1".0 at SSA22)

B) include objects enhanced for EW by mechanism of Lyα scattering and/or galactic superwind
"EWto": EW measured by pseudo total magnitudes of Lyα emission (within 2.5*kron radius defined in NB image) and continuum (within 2.5*kron radius defined in BV image)as the Lyα emission of objects have extended shape (using SExtractor)

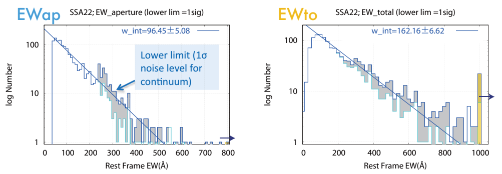

EWap ≧ 300Å: 104 LAEs
EWto ≧ 300Å: 388 LAEs

Some LAEs have very extended Lyα emission due to Lyα scattering and/or galactic superwind.

3. Relationship between EWap and EWto

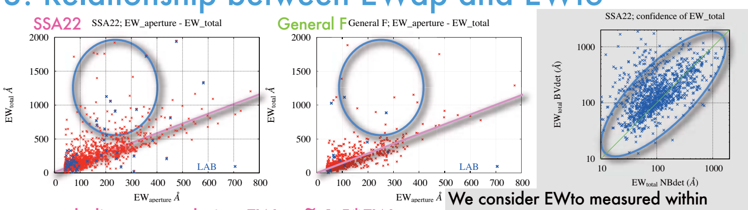

mostly linear correlation EWap ~ 1.5*EWto
→ most LAEs have extended Lyα emission.
objects with extremely extended emission which makes EWto very large.

We consider EWto measured within radius for continuum flux defined in NB image as conservative case(EWtoNBdet).
Most of objects are measured accurately, while some objects are overestimated.
It is necessary to check some large EWto objects.

4. Size of Lyα as a Function of EWto

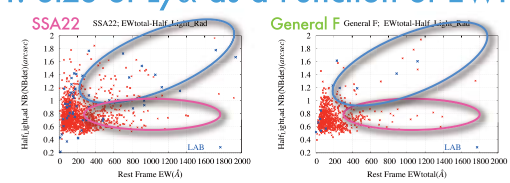

Some large EWto objects have compact Lyα emission,

Others have extended Lyα emission.

5. Luminosity Function of Lyα as a Function of EWto

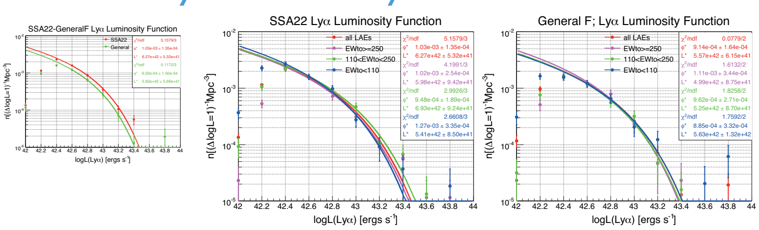

There are no significant differences in the shape of Lyα luminosity function between large EWto objects and small EWto objects.

6. EWto Distribution of LAEs

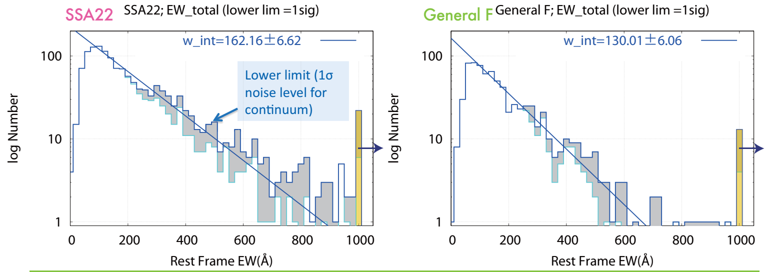

EWto Distribution in SSA22 have flatter slope than it in General Fields
N = C*exp (-EW/w$_0$): SSA22 w$_0$ = 162.16 ± 6.62, General Fields w$_0$ = 130.01 ± 6.06

Ratio of the LAE number within each range of EWto to that within EWto<100Å

Field	100≦EWto<200	200≦EWto<400	400≦EWto<700	EWto≧700
SSA22	1.11 ± 0.08	0.920 ± 0.066	0.393 ± 0.037	0.170 ± 0.022
General Fields	1.09 ± 0.10	0.709 ± 0.070	0.230 ± 0.034	0.098 ± 0.021

Higher ratio of large EWto LAEs in SSA22 than it in General fields.

Is the EWto distribution a function of surface density of LAEs
or
Is it an unique characteristic of LAEs in SSA22?
→ We investigate the difference in EWto distribution of samples within given number density range of LAEs.

7. EWto Distribution as a Function of LAE-Density in SSA22

High Density Region: $\rho \geqq 1.15*\rho_{SSA22}$
Medium Density Region: $0.9*\rho_{SSA22} \leqq \rho < 1.15*\rho_{SSA22}$
Low Density Region: $\rho < 0.9*\rho_{SSA22}$

ρ: local number density of LAEs,
ρ_{SSA22}: average number density of LAEs at entire SSA22

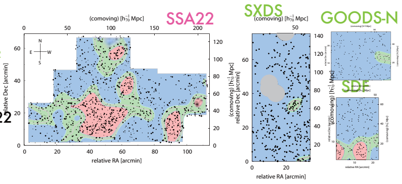

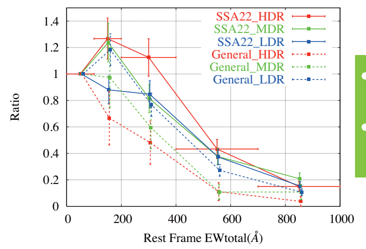

- The most highest ratio of large EWto objects SSA22-HDR.
- No trend is seen in other case.

→ SSA22-HDR → unique region ?

8. Discussion

Characteristics of large EWto objects in SSA22

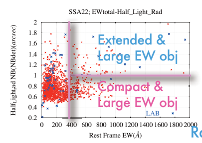

Among the large EWto objects (EWto ≧ 400Å),
A) Compact Sample
Half_Light_Radius < 1".0
B) Extended Sample
Half_Light_Radius ≧ 1".0

Ratio of the number of LAEs with EWto ≧ 400Å to the number of extended sample

	SSA22	General Fields
Entire Region	63/225 (0.25±0.04)	17/80 (0.21±0.06)
High Density Region	13/70 (0.19±0.06)	0/4 (0)
Medium Density Region	26/76 (0.34±0.08)	2/8 (0.25±0.20)
Low Density Region	24/79 (0.30±0.07)	15/68 (0.22±0.06)

- No trend of Lyα size toward an increase/decrease in LAE number density.
- More compact sample in HDR than it in LDR???

Hypothesis	Size of Lyα	Lyα - UV size ratio
1. Young / low-metal	compact?	Comparable?
2. Cooling Radiation	extended	More extended than UV?
3. Galactic Wind	extremely extended	Much more extended than UV?

Future work,
to investigate the Lyα - UV size ratio (it is necessary to increase the S/N value of continuum),
the color of large EW objects,
the luminosity function of large EW objects

Summary

We made the large sample of ~2000 LAEs in SSA22 and general fields.
The number density of LAEs in SSA22 region is 1.5 times larger than it in general fields.

We calculated EW of LAEs by two methods: "EWap"- aperture-photometry and "EWto" - total magnitude.
We can newly find a large number of LAEs with high EWto objects which have extremely extended emission.
There are the large EWto objects with compact Lyα emission and extended Lyα emission.
The large EWto LAEs in SSA22 region have higher ratio than in General fields.
→ It is the unique characteristic of SSA22-HDR (?)

Ultrafast broadband THz response of photo-induced metallic state in charge ordered insulator α-(BEDT-TTF)$_2$I$_3$

H. Nakaya[1], Y. Takahashi[1], K. Itoh[1], S. Iwai[1,2], K. Yamamoto[3], K. Yakushi[3], S. Saito[4]

[1]*Department of Physics, Tohoku University, Sendai 980-8578, Japan,* [2]*JST-CREST*

[3]*Institute of Molecular Science, Okazaki 444-8585*

[4]*Kobe Advanced ICT Research Center, NICT, Kobe 651-2492*

Photo-induced insulator to metal (I-M) transition in correlated electron system

Melting of "frozen electron"
(Mott insulator, Charge order)

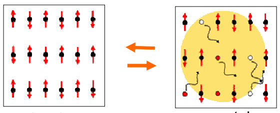

- *3d* transition metal compounds (Oxides and complexes) U, V (5-10 eV)>>t (1 eV)

Fiebig et al, APB71, 211(2000)
Cavalleri et al PRL87, 237401(2001)
Iwai et al. PRL91, 057401(2003)
etc.....

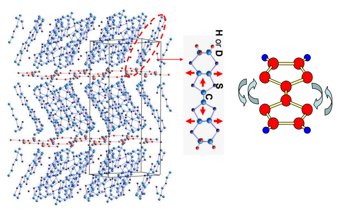

- Organic salts (molecular solids) U, V (0.5-1 eV) >> t(0.1 eV)

Chollet et al. Science 307, 86 (2005).
Iwai et al. PRL98, 097402(2007).

- small t (0.1 eV)<< U, V
  0.1 eV ⇔ 40 fs
- molecular re-arrangements (libration etc...)
  c.f. coherent control
  Iwai et al. PRL96, 057403(2006).

Objective

Clarifying electronic nature of photo-induced metallic state

⟶ Ultrafast broadband terahertz (THz) spectrum

(Charge-ordered gap ~ 50-100 meV)

c. f. Hilton et al., PRL 99, 226401 (2007). , Averitte et al., PRL87, 017401(2001).
Kuber et al., PRL99, 116401(2007).

BEDT-TTF based salts

bis(ethylenedithio)-tetrathiafulvalene
→ BEDT-TTF, ET

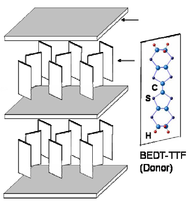

(ET)$_2$X → 3/4 filled band

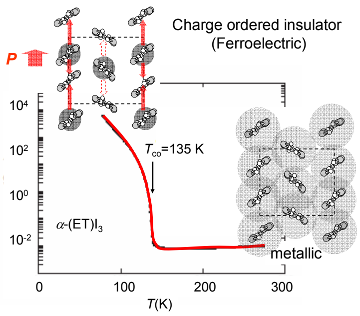

Mott ins., Charge Order
Ferroelectricity
Metal, Superconductor

Yamamoto, Iwai et al. JPSJ(2007)
Tajima et al. JPSJ69,543 (2000)
Kino, Fukuyama (1996, theory).
Takano, et al. (2001, NMR).

Mid- and Far IR spectroscopy of α-(BEDT-TTF)$_2$I$_3$

Ultrafast Mid-IR spectroscopy
Iwai et al. (PRL2007,PRB2008)

THz response of PIMT ?

Thermal insulator-metal transition

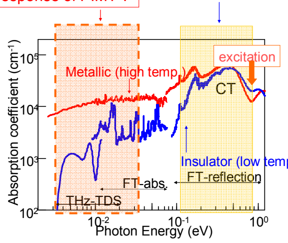

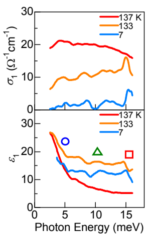

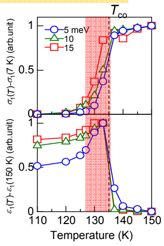

c.f. Zelezny et al., J. Phys. France51, 869(1990)
Dressel et al., J. Phys. I France 4, 579(1994)

→ Relaxer-like behavior

Nakaya et al. to be published

Photo-induced insulator-metal transition (2-11 meV)

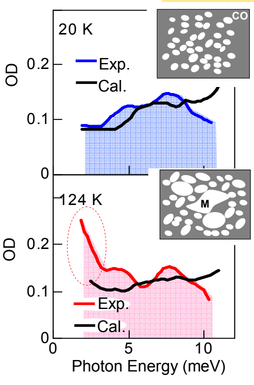

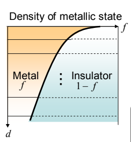

- Inhomogeneous along d
  ⟶ Multi-layer model
- Inhomogeneous mixture (metal and insulator)
  ⟶ Effective-medium theory

Fraction of metal

$$f=\exp[-\frac{d}{a}]$$

(d :depth, a :penetration depth)

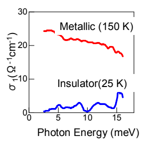

Hanai's equation

$$f\,\frac{\varepsilon_{\mathrm{eff}}-\varepsilon_{\mathrm{I}}}{\varepsilon_{\mathrm{M}}+2\varepsilon_{\mathrm{I}}}\left(\frac{\varepsilon_{\mathrm{M}}}{\varepsilon_{\mathrm{eff}}}\right)=(1-f)$$

$\varepsilon_{\mathrm{eff}}$:effective dielectric function
ε_{M} :dielectric function of metallic state
ε_{I} :dielectric function of insulator
f :fraction of metallic state

→ 20 K<<T_c Photo-induced metal is analogous to the thermal metal.
124 K~T_c is differ from the thermal metal.

Nakaya et al. to be published

Setup of optical-pump THz-probe measurement

1.4 μ m-pump,THz (2 - 36 meV)-probe,1 kHz

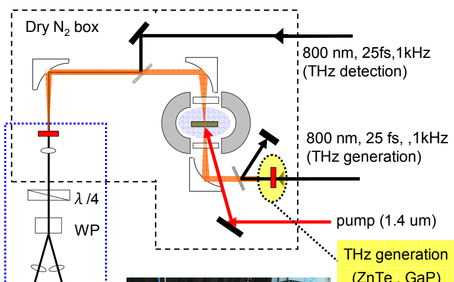

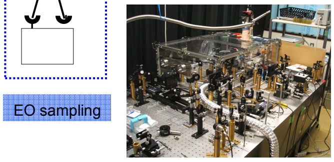

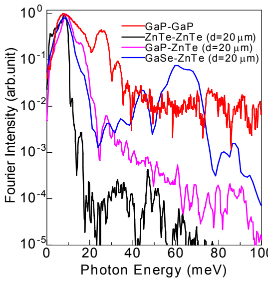

Generation	Detection	Bandwidth (meV)
ZnTe	ZnTe	2 - 11
GaP	ZnTe	2 - 20
GaP	GaP	2 - 36
GaSe	ZnTe	2 – 20, 50-70

Time evolution of the broadband transient spectra

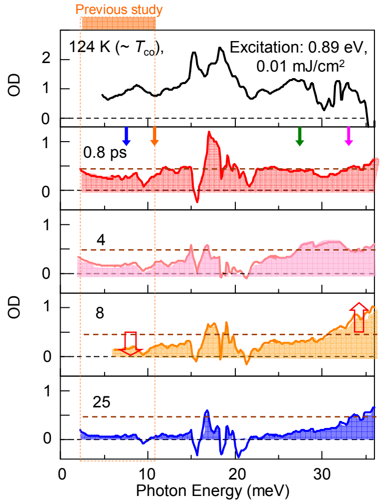

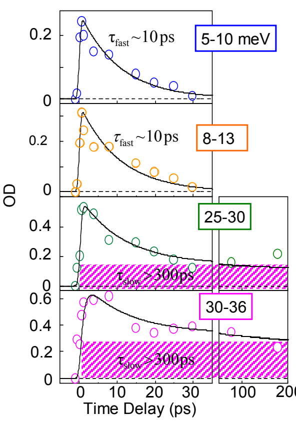

- 5 13 meV :fast (~10 ps)
- 25 36 meV :slow (> 300 ps)

Spectral weight (low energy ⇒ high energy) ⟹ Formation of charge-ordered gap ?

Dynamics of photo-induced metallic state

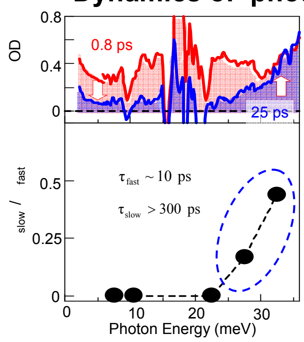

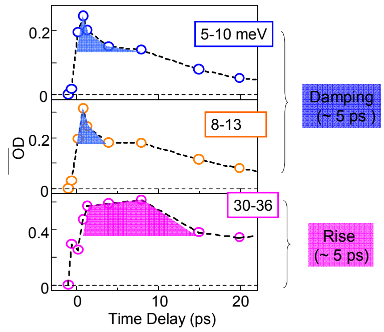

Formation of charge-order gap

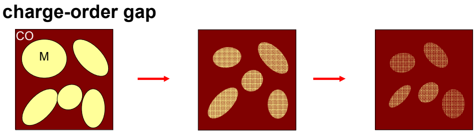

0 (< 2 meV) ------ ~10 ps ------→ ~ 30 meV

In summary, we investigated the ultrafast dynamics of photo-induced I-M transition by using optical pump-broadband (2 - 36 meV) THz probe spectroscopy in charge ordered insulator α-(BEDT-TTF)$_2$I$_3$. At 124 K (~T_{co}), OD spectrum at 0.8 ps has a broad absorption increase, exhibiting generation of the metallic state. Then, the spectral weight shifts to high energy region within several picoseconds. Such spectral behavior in THz region indicates the formation of the charge-ordered gap.

Po-no. 29

Ring-Exchange Interaction in Orbital Degenerate System

J. Nasu, S. Ishihara,
Department of Physics, Tohoku University

Orbital degree of freedom

Crystal Field (High symmetry) ⟹ Orbital degeneracy partially remains

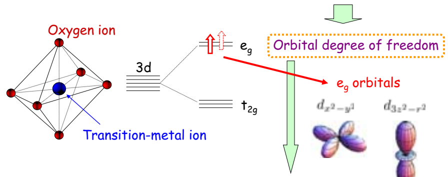

Anisotropy of electronic distribution
- Exchange interaction of spins
- Anisotropy of electric conductance
- Coupling with lattice distortion

Property of Orbital Degree of Freedom

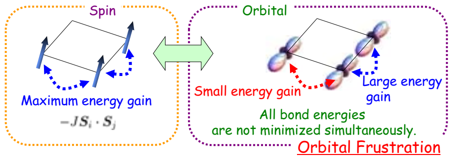

e_g orbital model

$$H=\sum_{k}\vec{T}(-k)^t\hat{J}(k)\vec{T}(k)$$

Orbital pseudo-spin T: $d_{3z^2-r^2}$ up, $d_{x^2-y^2}$ down

$J(k)$: Effective orbital interaction

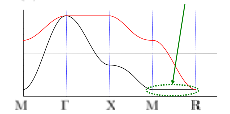

Ring-Exchange Interaction

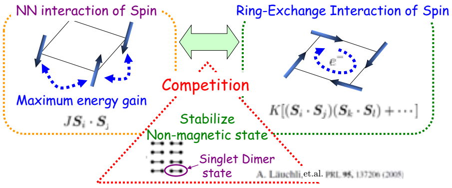

Orbital Degree of Freedom

Frustration exists in NN interaction

Many-Body interaction of Orbitals
(Effect of higher order perturbation) is prominent

Purpose

Orbital symmetry → Intrinsic Frustration → Macroscopic degeneracy in the classical ground state

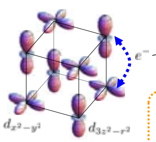

Within the nearest neighbor interaction

Purpose : Orbital effect
by the long range interaction
or the ring-exchange interaction

Thermal fluctuation
Quantum fluctuation

Model Hamiltonian

$t_l^{\mu\mu'}$: transfer integral from μ to μ' for l bond

Spinless (Ferromagnetic) two-orbital Hubbard model

$$H=\sum_{\langle ij\rangle_l}\sum_{\alpha\beta}\left[t_l^{\alpha\beta}c^\dagger_{i\alpha}c_{j\beta}+h.c.\right]+\tilde{U}\sum_i n_{i\uparrow}n_{i\downarrow}=H_t+H_U$$

$$\begin{cases}|\phi_u\rangle=|3z^2-r^2\rangle\\|\phi_v\rangle=|x^2-y^2\rangle\end{cases}$$

Transfer integrals

$$t_x=\begin{pmatrix}-\frac{1}{4}t & \frac{\sqrt{3}}{4}t\\ \frac{\sqrt{3}}{4}t & -\frac{3}{4}t\end{pmatrix},\quad t_y=\begin{pmatrix}-\frac{1}{4}t & -\frac{\sqrt{3}}{4}t\\ -\frac{\sqrt{3}}{4}t & -\frac{3}{4}t\end{pmatrix},\quad t_z=\begin{pmatrix}-t & 0\\ 0 & 0\end{pmatrix}$$

$$t_l\equiv\begin{pmatrix}t_l^{uu} & t_l^{uv}\\ t_l^{vu} & t_l^{vv}\end{pmatrix}$$

$H=H_t+H_U$ — perturbation term

Perturbational expansion

The effective Hamiltonian up to the 4th order of t/U

$H_{\rm eff}=H_2+H_4$ — Ring-Exchange interaction

Effective Hamiltonian (1)

$$H_{\rm eff}=H_2+H_4 \xrightarrow{\text{Dominant term}} H=H_J+H_K$$

$$H_J=H_2=J\sum_i\left(\tau_i^x\tau_{i+\hat{x}}^x+\tau_i^y\tau_{i+\hat{y}}^y+\tau_i^z\tau_{i+\hat{z}}^z\right)\qquad J=\frac{2t^2}{U}\quad K=\frac{40t^4}{U^3}$$

: conventional e_g orbital model

- Prefer the antiferro-orbital order ($J>0$)
- Macroscopic degeneracy in classical ground state on T^z-T^x plane

Orbital pseudo-spin

$d_{3z^2-r^2}$: $T^z\to+\frac{1}{2}$

$d_{x^2-y^2}$: $T^z\to-\frac{1}{2}$

$$\begin{cases}\tau_i^x=-\frac{1}{2}T_i^z-\frac{\sqrt{3}}{2}T_i^x\\ \tau_i^y=-\frac{1}{2}T_i^z+\frac{\sqrt{3}}{2}T_i^x\\ \tau_i^z=T_i^z\end{cases}$$

Effective Hamiltonian (2)

$$H_K=K\sum_{[ijkl]_{lm}}\frac{1}{2}\left(\tau_i^{a+}\tau_j^{a-}\tau_k^{a+}\tau_l^{a-}+h.c.\right)$$: Ring-Exchange interaction

- Prefer the up-up-up-down structure (compete with H_J)
- Include octupole interaction

$$\begin{cases}\tau_i^{a+}=\tau_i^a+i\frac{\sqrt{3}}{2}T_i^y\\ \tau_i^{a-}=\tau_i^a-i\frac{\sqrt{3}}{2}T_i^y\end{cases}\qquad a=x,y,z$$

Real space

$T^z\propto 3l_z^2-l^2$, $T^x\propto l_x^2-l_y^2$: Electric quadrupole (E_g)

$T^y\propto\overline{l_xl_yl_z}$: Magnetic outupole (A_{2g}) $l=2$

Classical Phase Diagram

$r_R=\sqrt{K/(20J)}$

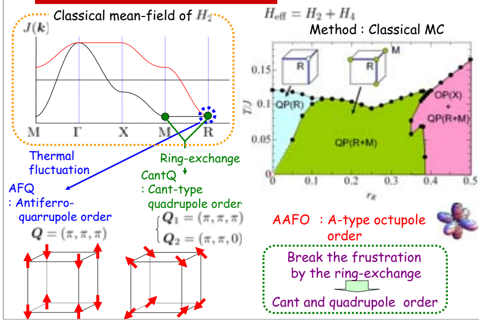

AFQ : Antiferro-quarrupole order $Q=(\pi,\pi,\pi)$

CantQ : Cant-type quadrupole order $Q_1=(\pi,\pi,\pi)$, $Q_2=(\pi,\pi,0)$

AAFO : A-type octupole order

Break the frustration by the ring-exchange

Cant and quadrupole order

八極子秩序の形成

$r_R=\sqrt{K/(20J)}$

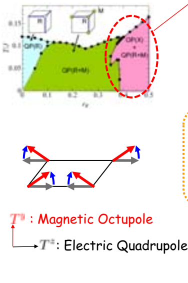

Ring-exchange interaction is large

Strong competition between H_J and H_K in the T^z-T^x plane

Ferro-type Octupole T^y order appear at low temperature

$$H_K=\frac{3}{4}KT_i^yT_j^yT_k^yT_l^y+\cdots$$

Antiferro / Ferro

T^y : Magnetic Octupole

T^z: Electric Quadrupole

Quatrupole C-type AF $Q=(\pi,\pi,0)$

Octupole A-type AF $Q=(0,0,\pi)$

Quantum Effect

$H=H_J+H_4$ $r_R=\sqrt{K/(20J)}$

Bethe approximation

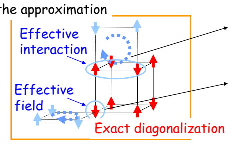

Approximate four-body term to two-body interaction $\tau\tau\tau\tau\to\langle\tau\rangle\tau\tau$

One-body approximation $\tau\tau\tau\tau\to\langle\tau\rangle\langle\tau\rangle\langle\tau\rangle\tau$

→ Calculate self-consistently

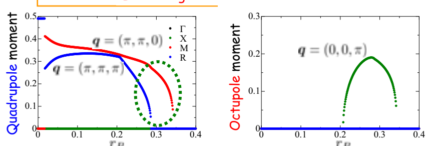

Moment suppression

Appear the octupole correlation

Extension of model Hamiltonian

Ring-Exchange interaction

$$H_K=K\sum_{[ijkl]_{lm}}\frac{1}{2}\left(\tau_i^{a+}\tau_j^{a-}\tau_k^{a+}\tau_l^{a-}+h.c.\right)\qquad\begin{cases}\tau_i^{a+}=\tau_i^a+i\frac{\sqrt{3}}{2}T_i^y\\ \tau_i^{a-}=\tau_i^a-i\frac{\sqrt{3}}{2}T_i^y\end{cases}\quad a=x,y,z$$

Containing both Quadrupole τ^a and Octupole T^y

Introduction of parameter η : Coefficient of Octupole operator

$\eta=\frac{3}{4}$

$$H_K(\eta)=K\sum_{[ijkl]_{lm}}\frac{1}{2}\left(\tau_i^{a+}(\eta)\tau_j^{a-}(\eta)\tau_k^{a+}(\eta)\tau_l^{a-}(\eta)+h.c.\right)\qquad\begin{cases}\tau_i^{a+}=\tau_i^a+i\sqrt{\eta}T_i^y\\ \tau_i^{a-}=\tau_i^a-i\sqrt{\eta}T_i^y\end{cases}$$

$\eta\to0$: Quadrupole interaction

$$H_K(\eta)/K\to\sum_{[ijkl]_{lm}}\tau_i^a\tau_j^a\tau_k^a\tau_l^a$$

$\eta\to\infty$: Octupole interaction

$$H_K(\eta)/K\to\eta^2\sum_{[ijkl]_{lm}}T_i^yT_j^yT_k^yT_l^y$$

Extension of model Hamiltonian

$r_R=\sqrt{K/(20J)}$

$r_R\to\infty$

$$H_K=K\sum_{[ijkl]_{lm}}\frac{1}{2}\left(\tau_i^{a+}\tau_j^{a-}\tau_k^{a+}\tau_l^{a-}+h.c.\right)$$

r_R : Intensity of Ring-Exchange

η : Intensity of Octupole

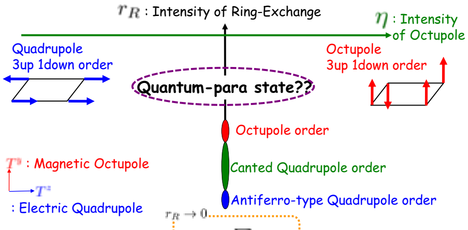

T^y : Magnetic Octupole

T^z : Electric Quadrupole

$r_R\to0$

$$H_J=J\sum_{\langle ij\rangle_l}\tau_i^l\tau_j^l$$

Effect of Ring-Exchange interaction

$H=H_K(\eta)$

Mechanism of the para-orbital state at $T=0$

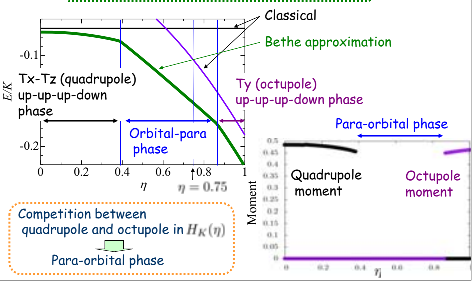

Competition between quadrupole and octupole in $H_K(\eta)$

Para-orbital phase

Spin-wave Approximation

$H=H_J+H_K(\eta)$

Assumption

Holstein-Primakoff method in four sublattice

Bogoliubov transformation

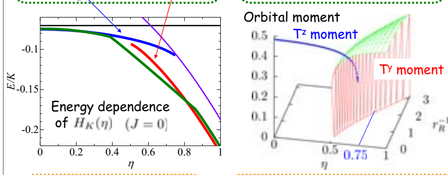

Orbital-para phase does exist in $J=0$

Introduction of H_J → Reduction of orbital moment

Orbital Structure by Exact Diagonalization

$T=0$

$H=H_J+H_K(\eta)$

$$K^{zz}(q)=\frac{4}{N^2}\sum_{ij}\left(\langle T_i^zT_j^z\rangle+\langle T_i^zT_j^z\rangle\right)e^{iq(r_i-r_j)}$$: quadrupole correlation

2x2x4 cluster

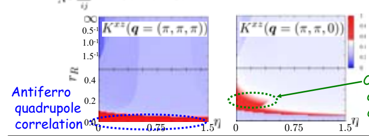

$$P^a=\frac{1}{3N}\sum_{\square_{ijkl}}\left(1-16\langle T_i^aT_j^aT_k^aT_l^a\rangle\right)/2$$: Energy gain on a plaquette

Quadrupole 3up 1down order $P_Q=(P^x+P^z)/2$

Octupole 3up 1down order $P_O=P^y$

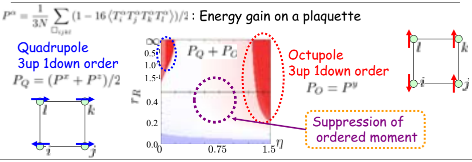

Suppression of ordered moment

Summary

Orbital degenerate system ⟹ Intrinsic frustration

Effects of Ring-Exchange interaction

- Classical Monte-Carlo method
- Exact diagonalization method
- Spin-wave approximation method
- Bethe approximation mathod

Preprint arXiv:1002.0178 JN and SI

Orbital Frustration ⟹ Ring-Exchange interaction

Degeneracy is lifted → Canted quadrupole order

Octupole interaction → Octupole order

Quadrupole & Octupole Competition → Suppression of ordered moment

Phase diagram at $T=0$

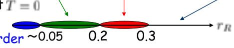

Shape Memory Effect Induced by Magnetic-Field Rotation in MnV_2O_4 Spinel Compound

Yoichi Nii, Takamichi Yagi, Nobuyuki Abe, Kouji Taniguchi[1], Hajime Sagayama[1], Taka-hisa Arima[1]
Department of Physics, Tohoku University
[1]Institute of Multidisciplinary Research Laboratory, Tohoku University

Introduction

What is shape memory effect?

A schematic representation of shape memory effect

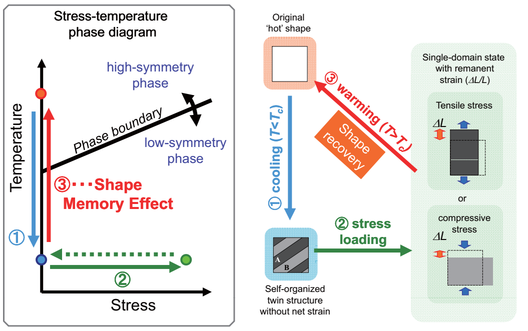

Is it possible to produce
magnetic shape memory effect
in a system with *strong magnetoelastic coupling*?

Magnetic-field control of crystal structure

A candidate material : MnV_2O_4 spinel compound

[1] T. Suzuki *et al.*, Phys. Rev. Lett. **98** 127203 (2007)
[2] H. Tsunetsugu and Y. Motome, Phys. Rev. B **68**, 060405(R) (2003).
[3] V. O. Garlea *et al.*, Phys. Rev. Lett. **100**, 066404 (2008)

Crystal structure

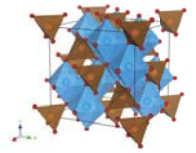

MnV_2O_4
☆ Space group : $Fd\bar{3}m$
☆ Structural transition from cubic to tetragonal (c<a) occurs at *Ts*, accompanying ferrimagnetic transition

⇒ $T_s = T_N \sim 57K$

Orbital pattern

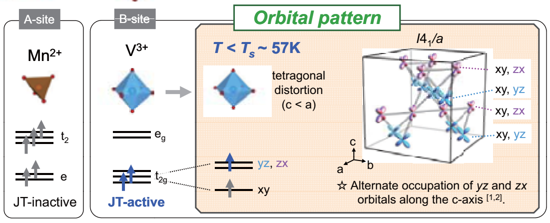

☆ Alternate occupation of *yz* and *zx* orbitals along the c-axis [1,2].

Magnetic structure [3]

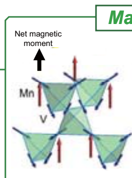

★ Noncollinear ferrimagnetic structure ($T<T_N\sim 57K$)

☆ Mn (S=5/2) moments along c axis
☆ V (S=1) moments canted by about 65°

Strong orbital-spin coupling

Magnetic-field dependence of strain at various temperatures.

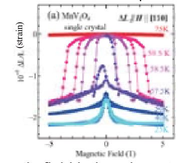

★ Magnetic-field induced crystal structure switching has been observed[1].

MnV_2O_4 has a possibility to exhibit ***magnetic shape memory effect***.

Purpose

★ Magnetic-field control of macroscopic shape
★ Demonstration of *magnetic shape memory effect*

Experimental

★ Sample preparation
☆ Single crystal was grown by a floating zone method in an Ar atmosphere.

★ Physical properties
☆ Strain ($\Delta L/L$) was measured by using a conventional strain-gauge in an applied magnetic field.
☆ Magnetization (*M*) was measured by a SQUID magnetometer.
☆ Dielectric constant (ε) was measured at 10kHz using an LCR meter.

Results

Magnetoelastic effect through a strong orbital-spin coupling

Temperature dependence of magnetization(*M*), strain($\Delta L/L$) and dielectric constant(ε)

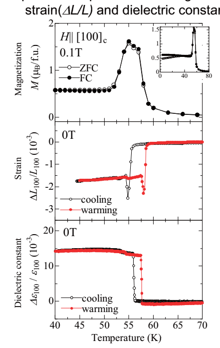

Around the ferrimagnetic transition temperature, a sharp decrease in $\Delta L/L$ and increase in $\Delta\varepsilon/\varepsilon$ were observed with decreasing temperature.

Temperature dependence of strain($\Delta L/L$) at various magnetic field strength.

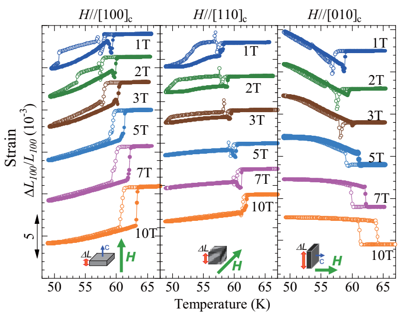

Anisotropic magnetostriction dependent on the applied *H* direction was observed. This suggest that the c axis of each tetragonal domain preferentially aligns along *H*.

Crystal structure switching by a magnetic-field rotation

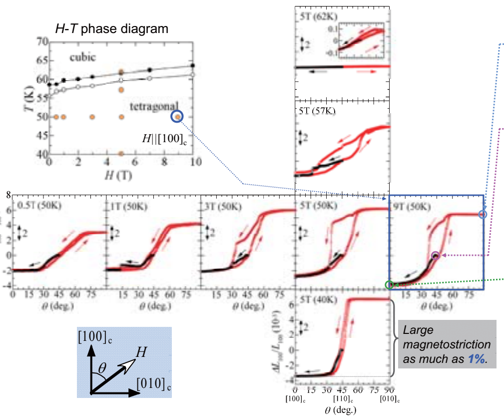

Single-domain state c // $[010]_{cubic}$

Multi-domain state c // $[100]_{cubic}$, c // $[010]_{cubic}$

Single-domain state c//$[100]_{cubic}$

By oscillating the magnetic field direction between $[100]_c$ and $[010]_c$, a single tetragonal domain state switches to another single-domain state, exhibiting a strain-angle hysteresis loop.

Magnetic-field-induced shape memory effect

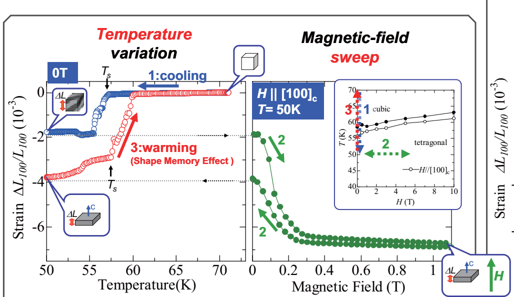

Combination of a magnetic field sweep and temperature variation.

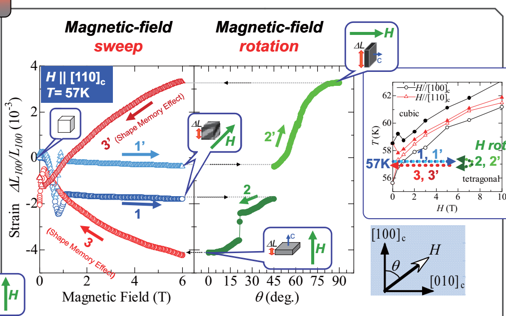

Combination of a magnetic field ***sweep*** and ***rotation*** without temperature variation

Magnetic-field-induced shape memory effect

Conclusions

★ By rotating a magnetic field from $[100]_c$ to $[010]_c$, successful switching between two tetragonal variants (c//$[100]_c$, c//$[010]_c$) has been achieved.

★ By sweeping a magnetic field along $[110]_c$, a multi-domain state of the two tetragonal variants has been obtained.

★ Combining these processes, a magnetic shape memory effect without temperature variation has been demonstrated.

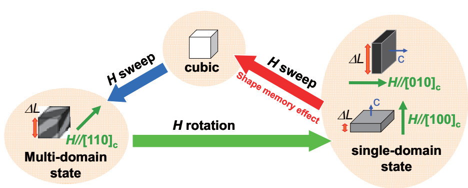

A high speed control of macroscopic shape is possible by using this process where temperature variation are not necessary.

The ω meson photoproduction on the nucleon in the threshold region

Ryo HASHIMOTO (Department of Physics, D3)
Research Center of Electron Photon Science, Tohoku University

The ω meson is one of vector mesons having a spin parity of 1^-. Studying near-threshold ω meson photoproduction is interesting theme to search for new baryon resonance states. Recently, the CLAS collaboration has reported that a missing baryon state with $J^P = 5/2^+$ contributes to ω photoproduction around the incident photon energy of 2 GeV. Paying attention to other vector mesons, the anomaly of the cross section near the threshold region is observed for ϕ photoproduction by the CLAS collaboration. A local maximum has observed around Eγ = 2 GeV. Is such a local maximum observed in the ω photoproduction cross section? We plan to measure it from threshold up to 1145 MeV.

ω meson - *one of vector mesons*

$J^P = 1^-$

mass	782.65 ± 0.12 MeV	
width	8.49 ± 0.08 MeV	
decay mode	$\pi^+\pi^-\pi^0$	89.1%
	$\pi^0\gamma$	8.9%

Near threshold photoproduction processes of the ω meson

one-pion-exchange (OPE) in t-channel   resonance contribution in s- and u-channels

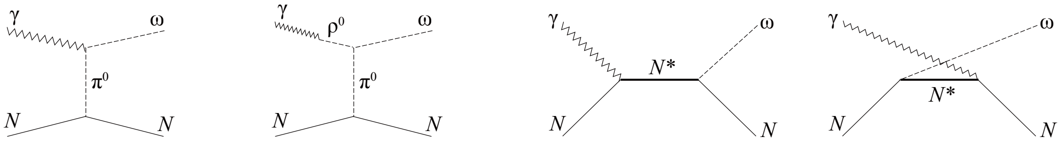

Interesting topics of vector meson photoproduction

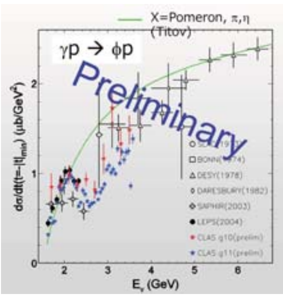

T. Mibe et al.

A local maximum appeared in the γp → ϕ p cross section (CLAS collaboration)

How about *ω* meson?

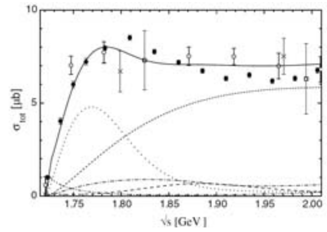

Fig. 17. γp → ωp total cross-section Data: ●: this experiment; ○: [18]; ×: [5]; □: [19]. Partial-wave decomposition [17]: dotted line: $J^P = \frac{1}{2}^+$; short-dashed line: $J^P \geq \frac{3}{2}^+$ (stemming from π^0 exchange); dashed line: $J^P = \frac{1}{2}^-$; dashed-dotted line: $J^P = \frac{3}{2}^+$; dashed-double-dotted line: $J^P = \frac{3}{2}^-$.

G. Penner and U. Mosel calculated the total cross section for the γp → ωp reaction from threshold up to 2 GeV. The P_{11} resonance contribution and OPE process are dominant.
However, near the threshold, main contribution for the total cross section is the D_{13} resonance.
→ We expect a local maximum in our data.

ω-photoproduction @ ELPH

Eγ range   747.6 - 1147.8 MeV
  Photoproduction threshold   1109 MeV
Detector   FOREST in the Gev-γ experimental hall
Target   Liquid hydrogen/deuterium
Selected events   3*γ* from $\pi^0\gamma$ (and 1p)

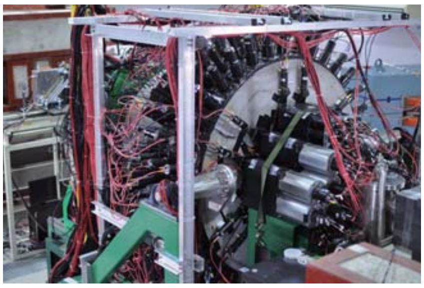

Simulation

to study kinematics of $\pi^0\gamma$ from *ω* or $2\pi^0$

generated events   *ω*   50,000 events
  $2\pi^0$ 5,000,000 events

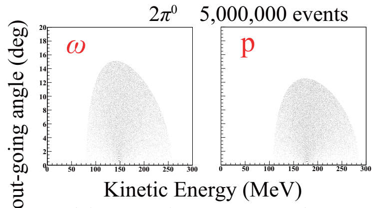

kinematics of *ω* and p

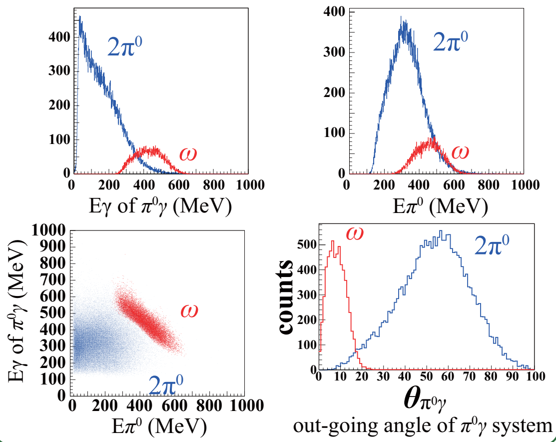

Analysis

ΔE-E plot

Selection of proton detected events

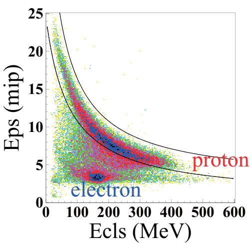

Selection of a π^0 combination from 3*γ*

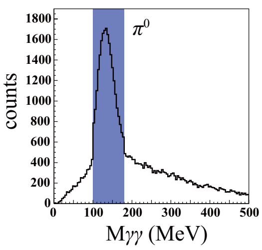

make *γγ* invariant mass for 3 combination
choose 1 pair whose mass is closer to π^0 mass.

Invariant mass of $\pi^0\gamma$

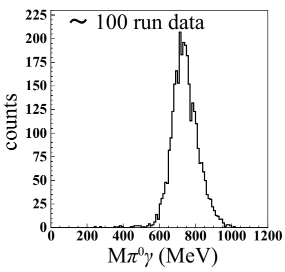

including background events
・accidental coincidence
・$\pi^0\gamma$ from $2\pi^0$ events

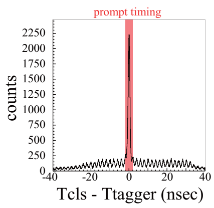

↓ subtract background

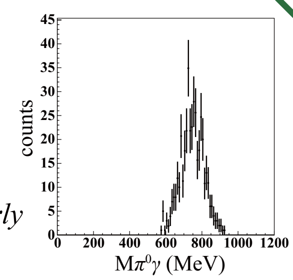

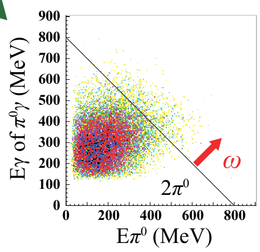

ω peak is clearly appeared!

using 500 run data - check *ω* yield

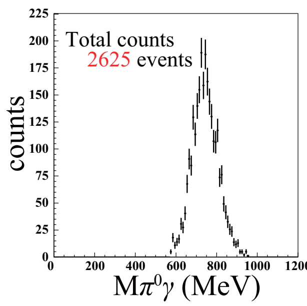

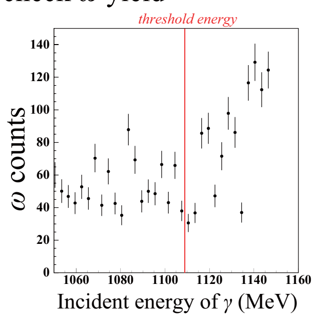

Prototype fast imaging detector for Hyperon Nucleon (YN) -scattering

Ryotaro Honda
Dept. of Physics M1, Tohoku Univ.

1.Introduction

Nuclear force shows different behavior depending on the range between two nucleons. In the long range around nucleon radius, its potential is attractive. However in a short range, potential becomes to be repulsive rapidly. This repulsive part is called repulsive core. **Anything cannot explain the figure of the hard core.**

Nuclear force is often divided to three parts.
Region Ⅰ ($\sim \lambda_\pi$). Pion exchange dominant region; It's explained by OPEP.
Region Ⅱ ($\lambda_\pi \sim \lambda_B$). Heaver meson exchange described by OBEP.
Region Ⅲ ($\lambda_B \sim r_B$). Phenomenological region.
λ_π and λ_B are Compton wave length of pion and baryon. r_B is a size of baryon.

We can study nuclear force as BB-interaction based on SU(3) symmetry by introducing *s*-quark. Nijmegen model [1] and Kyoto-Niigata RGM model [2] extend the nuclear force to YN-sector.
Nijmegen :
Interaction in the short range is described by **meson exchange** model.
Kyoto-Niigata RGM :
Interaction in the short range is described by **direct quark** model.

These two models adopt different model in a short range. However experimental data have not proven which model is consistent yet.

$^1S_0$ potential predicted by fss2

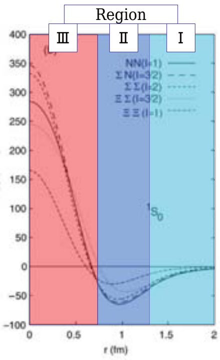

Progress in Particle and Nuclear Physics 58(2007) 439-520

[1]. Physical Review C, Vol. 40, No. 5, 2226
[2]. Progress of Theoretical Physics, Vol. 94, No. 3, 353

2.YN-scattering

A scattering experiment is a most effective way to investigate 2-body interaction between two baryons. Especially in **$\Sigma^+ p$ channel** where four *u*-quarks exist, one pair of *u*-quarks has an identical quantum number of spin and color. Therefore strong **repulsive force is expected** due to Pauli principle. Obtaining the cross section of this channel is important to discriminate the two models are correct, meson exchange or direct quark.

Many experiments have been performed on NN-scattering. However **statistics of YN-scattering is still poor** [3]. This fact is due to hardness of YN-scattering experiments.
1st : Hyperons must be created.
2nd : They need to be scattered before decaying.

Imaging detector, which records all process, is one solution to detect YN-scattering events. Imaging detector using Image Intensifying Tube (IIT) readout was applied to E289 in KEK. However **IIT cannot be used under high intensity condition (~100 kHz) due to image overlaps**. We have to develop a fast imaging detector to solve this problem.

$\Sigma^+ p$ elastic scattering

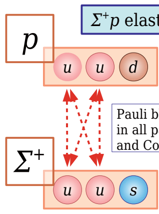

Pauli blocking will occur in all parts, Spin, Flavor and Color.

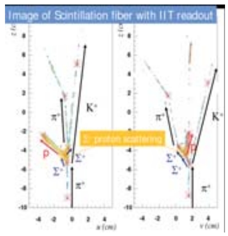

[3]. Physical Review A 761(2005) 41

3.Experimental setup

Now we are developing a new fast imaging detector using MPPC readout. In order to check the performance of new readout system, we performed a test experiment at Cyclotron facility in Tohoku University.
We made two detectors. One was an **active target** as imaging detector. The other was **half-circle detector** used for determination of scattering angle.

Active target
*Scintillation Fiber(Scifi) + MPPC
*36ch fast imaging device.

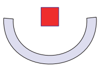

Half circle detector(Barrel)
*Plastic scintillator + MPPC
*Determine scattering angle.

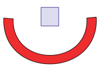

We performed experiment on **proton double scattering**. A primary beam of proton was irradiated to a primary target of ^{12}C and the scattered proton was used as the secondary beam. **The secondary beam rate was about 50 kHz.** All detectors including MPPC ware installed in a vacuum chamber. Normal run trigger is following.

1st layer(OR) & 2nd layer(OR) & Barrel(OR) & RF
Secondary target

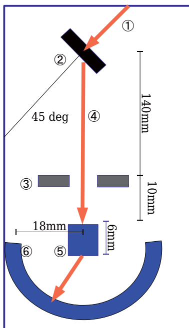

①Primary beam
Proton 65MeV
~10^{11}Hz
②Primary target
Carbon 1mm
③Collimator
Lead φ=4mm
④Secondary beam
~58MeV
~50kHz
⑤Secondary target
Active target
⑥Barrel

All detectors were installed in vacuum chamber.

Experimented at CYRIC Beam line 42. (Cyclotron in Tohoku Univ.)

4.MPPC

MPPC (Multi-Pixels Photon Counter) is a **semiconductor photon sensor** of HAMAMATSU. It consists of many APD operated in Geiger mode. Characteristics are following.

*Very small (Sensitive area is a few mm^2)
*Large gain. ($10^5 \sim 10^6$)
*High photon counting resolution.
***Fast time response.** (< 10ns)
***Possible to operate in magnetic field.**

MPPC is suitable for the readout of a counters that of segments are dense, detectors used under high intensity condition. In this time, we used 400pixels MPPC which has enough gain per pixel and the number of pixels.

MPPC

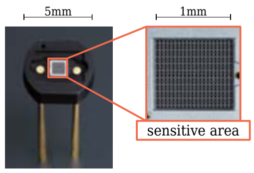

Black part is made by ceramic. All pixels are independent. Output charge is sum of them.

Spectrum of LED

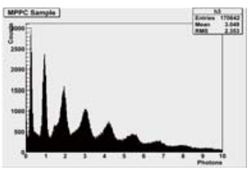

X-Axis represents the number of photons. Pedestal was shifted due to failure of amplifier.

5.Active target

An active target is made by scintillating fibers. **Each fiber is read by MPPC.** We used fibers which size was 1mm×1mm. Because fibers consist of Hydrogen and Carbon, proton-proton and proton-carbon scatterings will occur in this target.

Structure of the active target

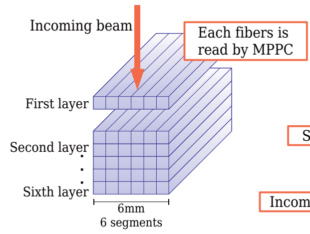

Active target

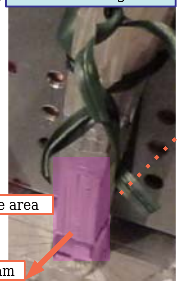

6.Barrel

Barrel is a name of half-circle detector used to **determine scattering angle of proton** scattered by secondary target. This detector had 14 channels and each channel was read by MPPC. A 3mm×3mm×5mm sized plastic scintillator was attached to each MPPC. Characteristics of this detector are following.

*Angular resolution 12.4 deg/ch (Lab sys.)
*Acceptance 9.5 deg/ch (Lab sys.)
*Total acceptance -80 ~ 80 deg (Lab sys.)
*Solid angle 28 msr/ch (Lab sys.)

Barrel

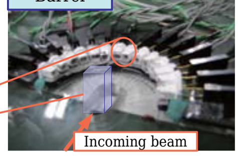

Heads of scintillator of front 2channels were touch to count the number of secondary beam. **These channels were not used for trigger.**

7.Result

Detectors were operated well under hard condition. Tracks are clearly identified **without an overlap.**

Event display, pp scattering

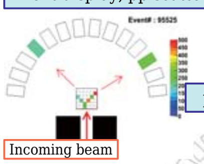

pC scattering

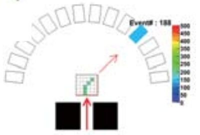

8.Analysis

Using a imaging detector, while we can observe scattering events visibly, **we must analyze data as image**. 8 million events were token by DAQ. It's quite hard to identify scattering events by human eyes. Therefore we made an analysis routine to select scattering events.
Vertex was limited to 4 segments in the center of the active target to get enough length of each track.

Procedure for pC

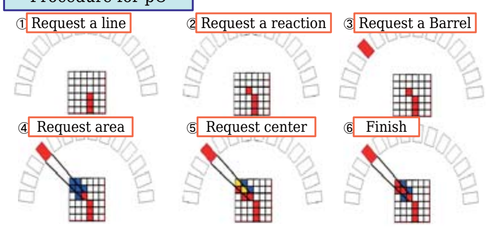

Procedure for pp

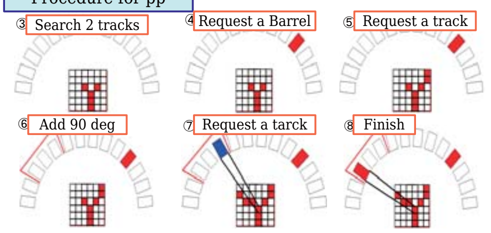

If an event was pp scattering, two barrels should be fired. However it's a rare case. Therefore pp event was selected by the number of tracks. A track with hit a barrel was analyzed by the same procedure for pC and **the other side was not requested a barrel TDC**. Virtual hit is created to determine a scattering angle.

9.Cross section

Obtained cross section are shown in figures. Red points are data of proton scattered to right side of barrel. Greens are left side.

pC.
Blue dots are reference data [4]. Some points are quite different due to trigger quality.

pp.
Blue area data are not consistent. A scattered proton with scattering angle 70 degree was stopped immediately. Such tracks cannot be identified.

Obtained cross section was **one order of magnitude smaller** than well known value. However the tendency of cross section is consistent.

Cross section of pC

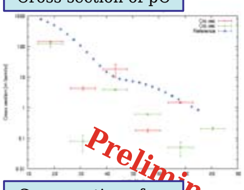

Cross section of pp

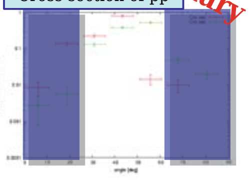

[4]. Physical Review C 78(2008), 044610

10.Summary

*The prototype fast imaging device with active target and barrel using MPPC.

*Detectors worked well under rather hard condition

*Image is clearly identified without overlaps. Scattering events were selected by off line algorithm.

*Obtained cross section is one order smaller than the reference, but trend is consistent.

Ground state phase diagram of graphene in a high Landau level: A density matrix renormalization group study

Tatsuya Higashi

Dept. of Physics, Tohoku U.

Low-energy states of electrons in graphene

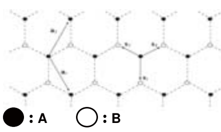

$$\mathcal{H}_K = v_F\begin{pmatrix} 0 & p_x - ip_y \\ p_x + ip_y & 0 \end{pmatrix} \quad \begin{matrix}(K,A)\\(K,B)\end{matrix}$$

$$\mathcal{H}_{K'} = v_F\begin{pmatrix} 0 & p_x + ip_y \\ p_x - ip_y & 0 \end{pmatrix} \quad \begin{matrix}(K',A)\\(K',B)\end{matrix}$$

$\hbar v_F = 3ta/2$ a: Lattice constant, t: Nearest neighbor hopping

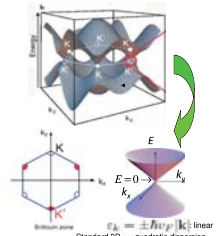

$\varepsilon_k = \pm\hbar v_F|\mathbf{k}|$: linear

Standard 2D ⋯quadratic dispersion

Fermi levels are located at the two inequivalent points (K, K').

K,K' (valley) are particular internal degree of freedom of graphene (pseudospin).

Graphene is a new type of 2D electron system.

e.g. Unconventional quantization pattern of IQHE

Electronic states of graphene in magnetic fields

Effects of a magnetic field

$\vec{p} \rightarrow \vec{\pi} = \vec{p} + e\vec{A}/c$

$a = \frac{l_B}{\sqrt{2}\hbar}(\pi_x - i\pi_y)$ Lowering operator

$a^\dagger = \frac{l_B}{\sqrt{2}\hbar}(\pi_x + i\pi_y)$ Raising operator

$l_B = \sqrt{\frac{\hbar c}{eB}}$ Magnetic length

Landau levels

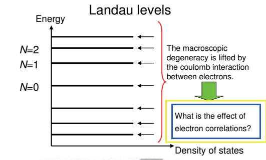

$E_n = \mathrm{sgn}(n)\hbar v_F\sqrt{2|n|}/\ell_B$

Hamiltonian

K : $H_K = \sqrt{2}\frac{\hbar v_F}{l_B}\begin{pmatrix} 0 & a \\ a^\dagger & 0 \end{pmatrix}$ (K,A) (K,B) ⇒ $\Psi_{Kn} = \frac{1}{\sqrt{2}}\begin{pmatrix}\mathrm{sgn}(n)\phi_{|n|-1} \\ \phi_{|n|}\end{pmatrix}$

K' : $H_{K'} = \sqrt{2}\frac{\hbar v_F}{l_B}\begin{pmatrix} 0 & a^\dagger \\ a & 0 \end{pmatrix}$ (K',A) (K',B) ⇒ $\Psi_{K'n} = \frac{1}{\sqrt{2}}\begin{pmatrix}\phi_{|n|} \\ \mathrm{sgn}(n)\phi_{|n|-1}\end{pmatrix}$

Eigenfunction $(n \neq 0)$

ϕ_n : The standard Landau wave function of electrons in the nth Landau level.

CDW ground states of standard 2D electron systems in high Landau levels

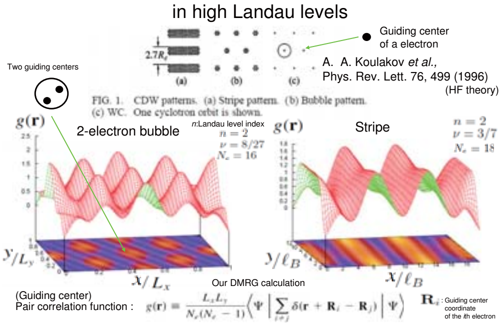

(Guiding center) Pair correlation function : $g(\mathbf{r}) = \frac{L_xL_y}{N_e(N_e-1)}\left\langle\Psi\left|\sum_{i\neq j}\delta(\mathbf{r}+\mathbf{R}_i-\mathbf{R}_j)\right|\Psi\right\rangle$ $\mathbf{R}_i$: Guiding center coordinate of the ith electron

Motivation

Effective inter-electron interaction of Nth Landau level

Standard 2D systems

$H_s = \sum_{i<j}\sum_{\mathbf{q}} e^{-q^2/2}[L_N(q^2/2)]^2 V(q)e^{i\mathbf{q}\cdot(\mathbf{R}_i-\mathbf{R}_j)}$ $V_{\mathrm{eff}}(r)$

Graphene

$H_G = \sum_{i<j}\sum_{\mathbf{q}} e^{-q^2/2}[F_n(q)]^2 V(q)e^{i\mathbf{q}\cdot(\mathbf{R}_i-\mathbf{R}_j)}$

"Mixture" of the nth and n-1th Landau levels of the standard 2D

$$F_{n\neq0}(q) = \frac{1}{2}\left[L_n\left(\frac{q^2}{2}\right) + L_{n-1}\left(\frac{q^2}{2}\right)\right]$$

The eigenfunction of nth Landau level of graphene $(n \neq 0)$

$\Psi_{Kn} = \frac{1}{\sqrt{2}}\begin{pmatrix}\mathrm{sgn}(n)\phi_{|n|-1} \\ \phi_{|n|}\end{pmatrix}$

The two effective interactions (H_S, H_G) are different.

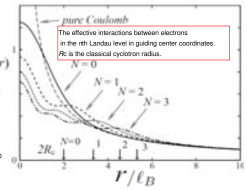

$V(q)$: Transform of the Coulomb interaction

$\mathbf{R}_i$: Guiding center coordinate of the ith electron

$L_N(x)$: Laguerre polynomials

What happens to the ground state ?

Purpose

Previous works

- Hatree-Fock theory (C.-H.Zhang *et al*, PRB 75, 245414 (2007))
  - Charge density waves (CDW) called stripes and bubbles realize in the ground state in high Landau levels of graphene.
  - But, quantum fluctuations are neglected in HF theory.
  - Can the CDW ground states survive under quantum fluctuations?
- Exact diagonalization (ED) (H.Wang *et al*, PRL 100, 116802 (2008))
  - The system size treated by ED is quite small.
  - The filling factor studied is limited.

Because of these limitations, such studies cannot determine the phase diagram of the present system.

In the present study, we investigate the ground state of graphene in the Landau levels of N=2,3 at various filling factors by the use of the DMRG method, and determine the ground state phase diagram.

Graphene N=3, N=2 is Mixture of Standard 2D N=2 and N=3, N=1 and N=2 → CDW; → Liquid type ground states at some filling factors

Model

Periodic boundary condition is imposed both in the x and y directions the period being L_x and L_y, respectively. (Torus geometry)

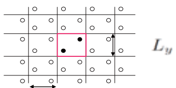

● : Electron

○ : Image of the electron in □.

Approximations

- assume spin-polarized ground state
- assume valley-polarized ground state
- neglect Landau level mixing

Relevant energy scales

LL Separation between 0th and 1th Landau level: $\sqrt{2}\hbar v_F/\ell_B \simeq 400\sqrt{B[T]}[K]$

Typical Coulomb energy between electrons : $e^2/\epsilon l_B \simeq 100\sqrt{B[T]}[K]$

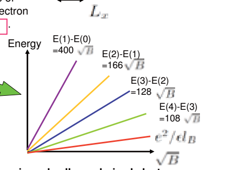

Solve the inter-electron interaction Hamiltonian for spin and valley-polarized electrons at various filling factors in high Landau levels (N=2,3) of graphene.

filling factor : $\nu = 2\pi N_e/L_xL_y = N_e/N_\phi$ N_ϕ : Total number of flux quanta in □.

DMRG method for quantum 2D electron systems in a high magnetic field

The DMRG method was originally developed for 1D lattice models, short range interactions.

$|\psi\rangle = \sum\sum \psi_{ij}|i\rangle|j\rangle$ Target states

Map to a 1D model (N. Shibata *et al.* Phys. Rev. Lett. 86, 5755 (2001))

One-particle states of free electrons in 2D under perpendicular magnetic field : $\Psi_{NX}(x,y)$, $X_n = 2\pi n/L_y$

Two quantum numbers: N : Landau level index, Xn : Guiding center (n : integer)

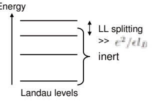

The ground state is determined only by the electrons in top most Landau level.

We can omit the Landau level index, N.

The quantum number is only Xn, which is a discrete number.

1D lattice model !

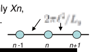

$$H = \sum_{n_1}\sum_{n_2}\sum_{n_3}\sum_{n_4} A_{n_1n_2n_3n_4}c^\dagger_{n_1}c^\dagger_{n_2}c_{n_3}c_{n_4}$$

$1 \le n_1, n_2, n_3, n_4 \le N_\phi$ Long-ranged hopping !!

[redacted]

N=3, ν =0.4 (N_ϕ=30,Ne=12)

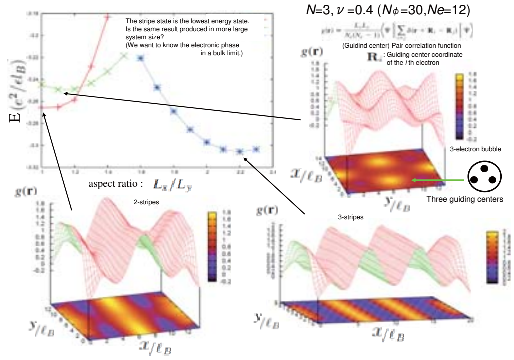

N=3, ν =0.4 (N_ϕ=45,Ne=18)

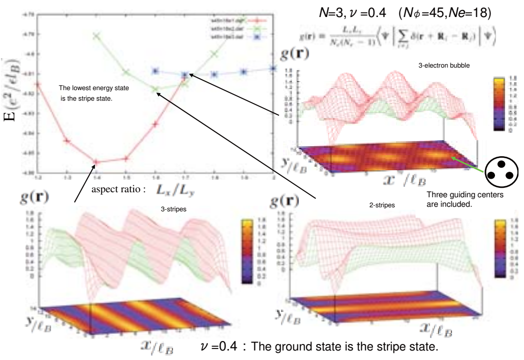

ν =0.4 : The ground state is the stripe state.

Ground state phase diagram of N=3 Landau level of graphene

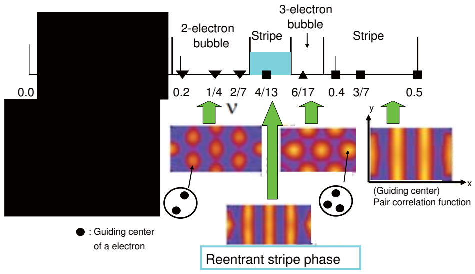

● : Guiding center of a electron

Reentrant stripe phase

Comparison with the result of the HF theory

DMRG (present study)

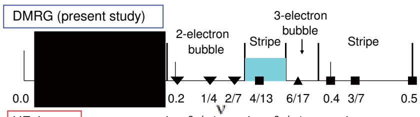

HF theory

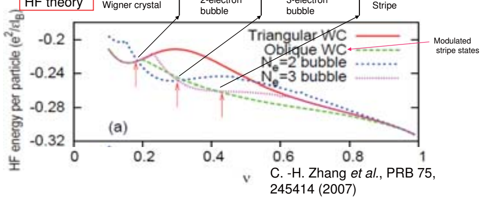

C. -H. Zhang *et al.*, PRB 75, 245414 (2007)

Ground state phase diagram of N=2 Landau level of graphene

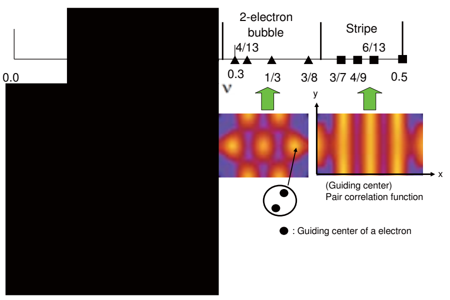

● : Guiding center of a electron

Comparison with the result of the HF theory

DMRG (present study)

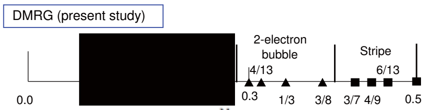

HF theory

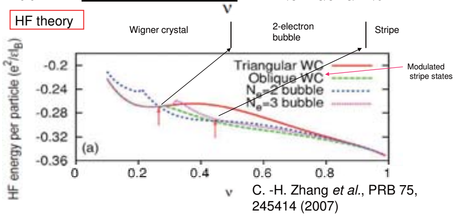

C. -H. Zhang *et al.*, PRB 75, 245414 (2007)

Summary

- By the use of DMRG method, we determined the ground state of electrons at various filling factors of the N=2,3 Landau level of graphene.
- By analyzing the (guiding center) pair correlation function, we obtained the reliable phase diagram of electrons in the N=2,3 Landau level of graphene.
- [redacted]
- Possibility of realizing the reentrant stripe phase around ν =0.3 of N=3 Landau level

Investigation of the $n(\gamma,K^0)\Lambda$ reaction near the threshold

K. Futatsukawa for NKS2 collaboration, Tohoku Univ.

Introduction

Kaon photoproduction

Kaon production on a nucleon or a nucleus by the electromagnetic interaction provides invaluable information on the strangeness production mechanism and strengths of meson-hadron coupling constant. Because the electromagnetic interaction is better understood than the hadronic interaction. Other subject in the investigation of photo- and electro- production of kaon is searching for 'missing resonances' which are predicted by QCD models but not confirmed experimentally in hadronic reaction such as πN. Quark model studies suggest some of these resonances may strongly couple to strange channels. Kaon photoproduction can be a good probe to find missing resonance states.

However the elementary processes of kaon photoproduction are far from well understood. The precise measurement such as each polarization of beam and target, hyperon have an essential information on kaon photoproduction mechanism. On the other hand, the experimental data for the lack of isospin channel are eagerly waited, as they provide an other approach to the investigation of kaon photoproduction.

Total cross section for 6 isospin channels of kaon photo-production

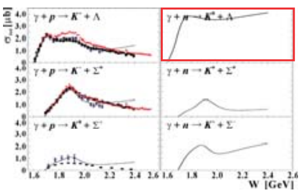

solid lines : Kaon-MAID [T. Mart and C. Bennhold, Phys. Rev. C 61 012201(R) (1999)]
data : SAPHIR(98) [M. Q. Tran et al., Phys. Lett B445, 20 (1998)] [S. Goers et al., Phys. Lett B445, 20 (1998)]
SAPHIR(04) [K. –H. Glander et al., Eur. Phys. J. A 19, 251 (2004)] [R. Lawall et al., Eur. Phys. J. A 24, 275 (2005)]
CLAS [R. Bradford et al.(CLAS Collaboration), Phys. Rev. C 73, 035202 (2006)]

$n(\gamma, K^0)\Lambda$ reaction in the threshold region

$n(\gamma, K^0)\Lambda$ process has unique features in the investigation of kaon production process by electromagnetic interaction as follows,

- no charge in initial and final state
  → t-channel Born term does not contribute
- isospin symmetry to $p(\gamma, K^+)\Lambda$ process
  → sign of coupling constant in u-channel is opposite
  $g(K^0\Sigma^0 n) = -g(K^+\Sigma^0 p)$
- the electromagnetic coupling constants of resonances in the *s*- and *t*-channels
  → It's different from K^+ process : e.g., $g(N^* n\gamma)$ and $g(K^* K^0\gamma)$

Feynman Diagrams for isobar model

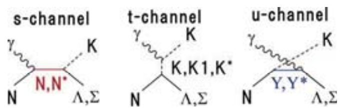

Due to these characteristics, the interference among the diagrams in the K^0 production process is quite different from that in the K^+ process.

For the elementary reaction of $\gamma n \to K^0\Lambda$, photon energy dependence and angular distribution at $E\gamma = 1.05$ GeV are calculated using Kaon-MAID model and Saclay Lyon model(SLA). These two models agree well with the $\gamma p \to K^+\Lambda$ process, while those are quite different for the $\gamma n \to K^0\Lambda$ process.

- Photon energy dependence
  - 0.9-1.0 GeV
    - KaonMAID~SLA(-1.9)
  - 1.0-1.1 GeV
    - KaonMAID~2*SLA(-1.9)

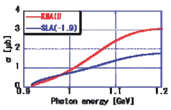

- Angular distribution
  - Using SLA with various rkk
  → angular distribution in center of mass system
  Backward peak is suggested

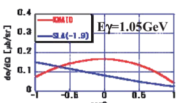

Restraint on diagram contributions in theoretical models

Experimental apparatus

Tagged photon beam

NKS2 was installed at Laboratory of Nuclear Science, Tohoku (LNS-Tohoku).

The photon beam is generated via bremsstrahlung and scattered electron is tagged by STB-Tagger system.

- Energy Region 0.8 - 1.1 GeV
  $n(\gamma, K^0)\Lambda$ threshold (915 MeV)
- Energy Resolution 10 MeV
- Beam Intensity 2×10^6 Hz
- Duty Factor 65 - 85 %

Schematic view of the experimental hall at LNS-Tohoku

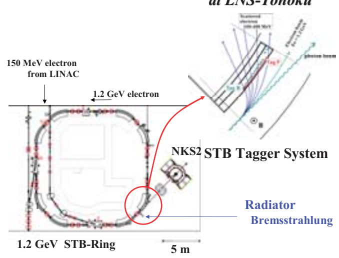

NKS2 Setup

K^0 are measured with Neutral Kaon Spectrometer (NKS2) by detecting the $K^0_S \to \pi^+\pi^-$ decay channel .

NKS2 is a spectrometer dedicated to measure the $n(\gamma, K^0)\Lambda$ reaction in the threshold region. It consists of a dipole magnet and two types of drift chamber, TOF counter. The liquid deuterium target is located at the center of NKS2. The acceptance covers the very forward region, making it possible to measure much larger kinematical region for K^0

- $n(\gamma, K^0)\Lambda$ reaction
  $K^0_S : K^0_L = 1 : 1$
- K^0_S decay channel
  K^0_S ($c\tau = 2.68$ cm)
  : $\pi^+\pi^-$ (69 %)
  $\pi^0\pi^0$ (31 %)

Schematic view of NKS2

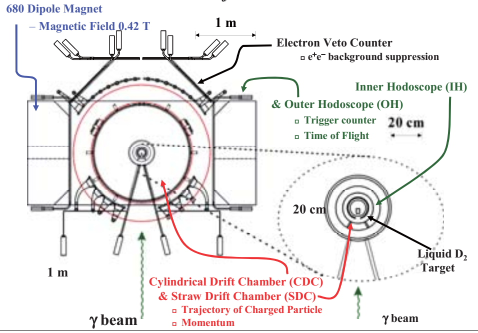

$p\pi^+\pi^-\pi^-$ Event Distribution

Particle Identify (PID)

An example from two tracks events

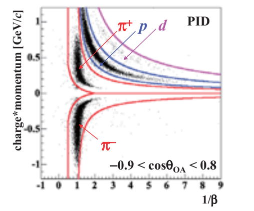

The red, blue and magenta line represents the pion, proton and deuteron region, respectively

This figures is the correlation between momentum and inverse velocity. The sign of momentum represents the charge of the particle.

Correlation between $p\pi^-$ and $\pi^+\pi^-$ Invariant Mass

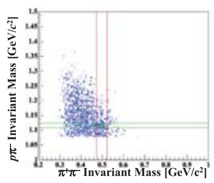

The red and blue line represents $|m_{\pi+\pi-} - m_{K0}| < 25$ GeV/c^2 and $|m_{p\pi-} - m_{\Lambda}| < 7.5$ GeV/c^2 region, respectively

This figures is the correlation between $p\pi^-$ and $\pi^+\pi^-$ invariant mass distribution. The $K^0\Lambda$ coincidence events can be confirmed.

Correlation between $p\pi^+$ and $\pi^-\pi^-$ Invariant Mass

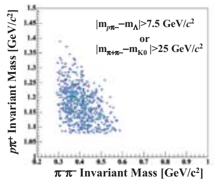

This figures is the correlation between $p\pi^+$ and $\pi^-\pi^-$ invariant mass distribution. The events which are candidate for $K^0\Lambda$ coincidence events weren't filled.

Background Estimation

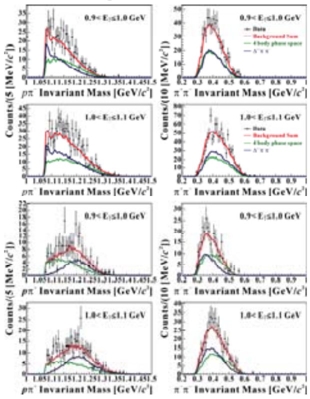

Data : Experimental data

Background estimation(simulation)
R : Background Sum
G : 4 body phase space
B : $\Delta^{++}\pi^-\pi^-$

$|m_{p\pi-} - m_{\Lambda}| > 7.5$ GeV/c^2
or
$|m_{\pi+\pi-} - m_{K0}| > 25$ GeV/c^2

This figures represent the background estimation from the invariant mass distribution. The invariant mass distribution of background events are simulated by Monte-Carlo method. The ratio and amount of the background events was gotten by fitting.

Invariant Mass Distribution

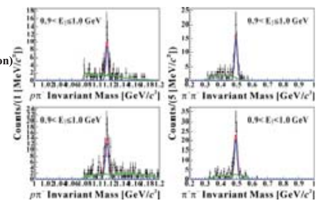

This figures represent the invariant mass distribution of $p\pi^-$ and $\pi^+\pi^-$ in each energy. The $p\pi^-$ invariant mass is shown with the region of $|m_{\pi+\pi} - m_{K0}| < 25$ GeV/c^2 . The $\pi^+\pi^-$ invariant mass represents with the region of $|m_{p\pi-} - m_{\Lambda}| < 7.5$ GeV/c^2. The greed line is shown the estimated background.

Detector Acceptance

K^0 Acceptance

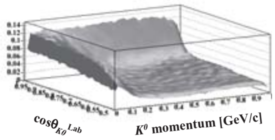

Simulation Condition :
Generate K^0 isotropically in Lab frame,
$0 < p_{K0} < 1.0$ GeV, $0.5 < \cos\theta_{K0}^{Lab} < 1.0$
Use the same analyzer for the experimental data.

Λ Acceptance

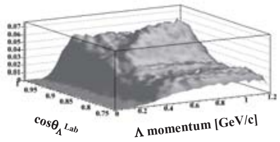

Simulation Condition :
Generate Λ isotropically in Lab frame,
$0 < p_{\Lambda} < 1.2$ GeV, $0.75 < \cos\theta_{\Lambda}^{Lab} < 1.0$
Use the same analyzer for the experimental data.

Momentum Distribution

After acceptance correction

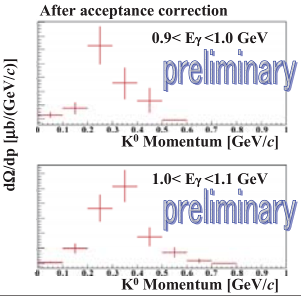

Summary

- **The $\gamma + n \to K^0 + \Lambda$ process plays a unique role in the investigation of kaon photoproduction mechanism.**
- **We have finished the construction of Neutral Kaon Spectrometer (NKS2)**
- **We performed the physics data taking with the deuteron target.**
- **The momentum distribution was obtained for two photon energy region, 0.9 to 1.0 GeV and 1.0 to 1.1 GeV.**
- **It is ready to contact the theorists and to discuss these results.**

35. Traffic flow of two lanes with a bottleneck

Sho Furuhashi
Dept. of Phys. , Tohoku Univ.

Introduction

Networks around us
- Internet
- Power grid
- Airline

Flows on networks
- Packet
- Electricity
- Airplane

Focus
- Robustness
  e.g. Keeping the connectivity of Internet against the failure of routers
- Efficiency
  e.g. Prevention of packet jam

http://www.atmarkit.co.jp/fwin2k/network/tcpip001/tcpip04.html

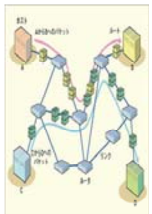

Traffic flow on road network is one of them.

Road network

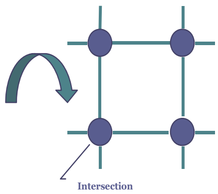

Intersection

Bottleneck is a factor which interrupts traffic flow.
At an intersection, cars on one lane interrupt cars on the other lanes. Road network consists of bottlenecks linked each other.

Traffic flow

Macroscopic viewpoint
- Burgers equation
- Lighthill-Whitham model

Microscopic viewpoint
- Cellular automaton model
- Optimal velocity model

Cellular automaton (CA) model
- 184 model
- Asymmetric Simple Exclusion Process (ASEP)
- Nagel-Schreckenberg (NS) model

In one dimensional case, the fundamental diagrams (flow-density relationship) of these models can reproduce the major characteristic of the ones of real traffic flow.

NAGARE 22(2003)95−108

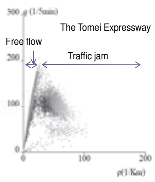

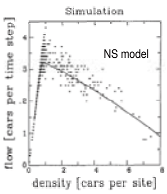

Simplified model of bottleneck

Two lane road which has a one lane road in a part

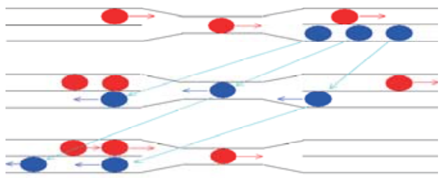

Previous studies
- Y. Ishibashi and M. Fukui J. Phys. Soc. Jpn. 65 (1996) 2793
- M. E. Foulaadvand and M. Neek-Amal EPL. 80 (2007) 60002

Objective

Real traffic flow is reproduced by the model (CA model) in the previous studies?

Road network is complex.
⇓
CA model might be no good for road network.

We check the adequacy of the model.

Model

System
Two lane circuit having one lane in a part

- Total length of a lane L
- The length of a bottleneck L_b
- Initial density ρ_1, ρ_2

Car dynamics
ASEP with parallel update.

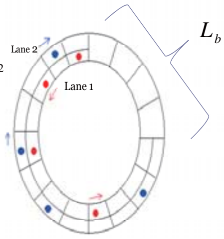

ASEP

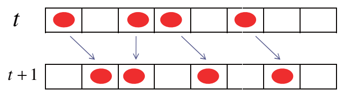

- Hop to the next cell with probability p.
  (Self-driven nature of cars)
- Stop when the next cell is occupied.
  (Excluded volume effect)

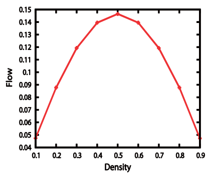

Observation

Recorded with video camera

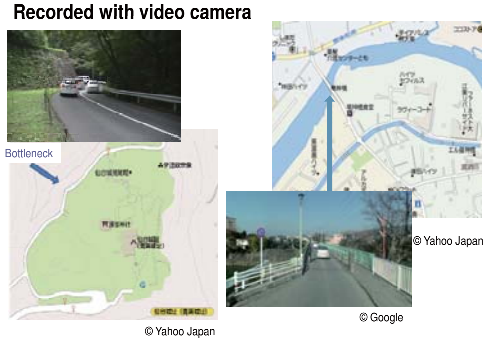

Index for characterization

The number of passing cars $N_i(j)$

Sendai castle

The number of passing cars on first lane in j-th cycle.

$N_1(j) \Rightarrow N_2(j) \Rightarrow N_1(j+1) \Rightarrow$

One cycle

- No distinction between lanes

$$N(j)=\begin{cases} N_1(k) & (j=2k) \\ N_2(k) & (j=2k+1) \end{cases}$$

$$F(N_i)=\int_{N_i}^{\infty} f(x)dx$$

$(f : N_i \text{ distribution function})$

- Cumulative

$$\langle (N_i(j)-\bar{N}_i)(N_i(j+\Delta)-\bar{N}_i) \rangle$$

The cumulative distribution of the number of passing car

Simulation $L-L_b=500, L_b=1, p=0.5$ Observation

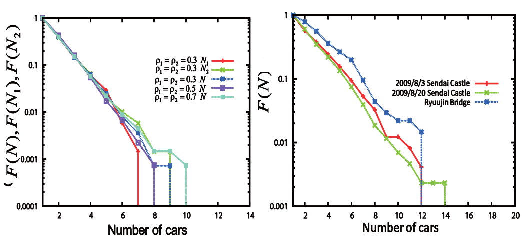

Exponential distribution

Cycle correlation

Simulation $L-L_b=500, L_b=1, p=0.5$ Observation

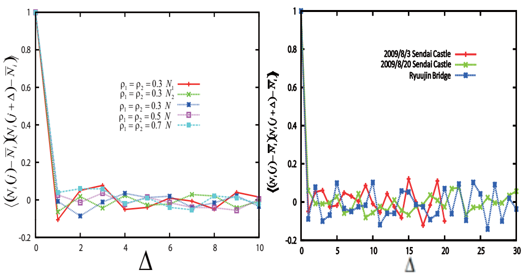

No cycle correlation

Result and assignment

Result
The model agrees with real traffic flow in the two indexes.
These are Poisson process.

Assignment
We have to check that this result is independent of the density of cars.

⇓

When the density is over the critical value, traffic jam occurs.
The mental condition of drivers in a traffic jam is different from of drivers in a free flow.

Staggered Order with Kondo and Crystalline Field Singlets

Tohoku University, D1

Shintaro Hoshino, Junya Otsuki, Yoshio Kuramoto

Properties of $PrFe_4P_{12}$

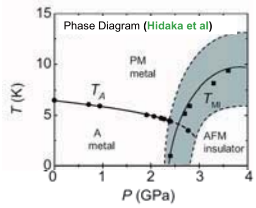

Resistivity (Hidaka et al)

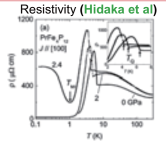

Neutron Scattering (Iwasa et al)

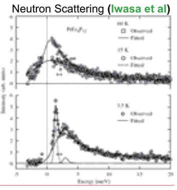

■CEF states is singlet-triplet quasi-quartet by microscopic theory (Otsuki et al)
■Scalar Order has been suggested theoretically (Kiss and Kuramoto) and experimentally (Kikuchi et al)

Band Structure in $LaFe_4P_{12}$

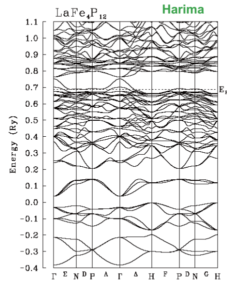

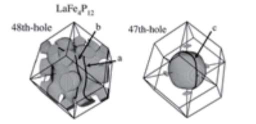

We consider **two-band model** coupled with crystalline electric field (CEF) singlet-triplet systems:
two-band singlet-triplet Kondo model

Purpose:
Investigation of the competition between Kondo singlet and CEF singlet.

2band Singlet-Triplet Kondo Model

Local Picture

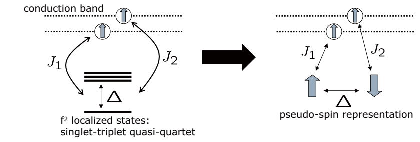

Hamiltonian

$$\mathcal{H}=\sum_{k\gamma\sigma}(\varepsilon_{k\gamma}-\mu)c^\dagger_{k\gamma\sigma}c_{k\gamma\sigma}+\sum_{i\gamma}J_\gamma \boldsymbol{S}_{\gamma i}\cdot \boldsymbol{s}_{c\gamma i}+\sum_i \Delta \boldsymbol{S}_{1i}\cdot\boldsymbol{S}_{2i}$$

Conditions
■put $J_1=J_2=J$ for simplicity
■ n_c=1: one conduction filling per site (quarter filling)

Methods

■Two-Sublattice Dynamical Mean-Field Theory

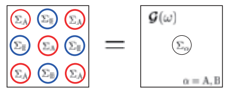

Georges et al (1996)

Half Brillouin Zone

■Continuous-Time Quantum Monte Carlo

●without approximation
●absence of negative sign
●finite temperatures

Rubtsov et al (2005)
Werner et al (2006)
Otsuki et al (2007)

Density of States (hypercubic lattice)
perfect nesting property at half filling

$$\rho(\omega)=\frac{1}{D}\sqrt{\frac{2}{\pi}}e^{-2(\omega/D)^2}$$

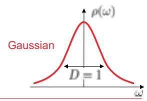

Phase Diagram for Kondo Lattice

$$\mathcal{H}_{\rm KLM}=-t\sum_{\langle i,j\rangle\sigma}(c^\dagger_{i\sigma}c_{j\sigma}+{\rm h.c.})+J\sum_i \boldsymbol{S}_i\cdot\boldsymbol{s}_{ci}$$

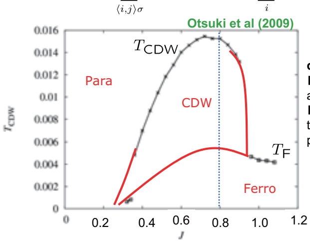

quarter filling:
■Charge density wave (CDW) arise.
■At sufficiently low temperatures there is magnetically ordered phase.

We concentrate on the case with J = 0.8 , and investigate the effect of the CEF splitting Δ.

Inverse Susceptibilities

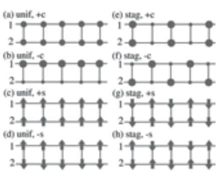

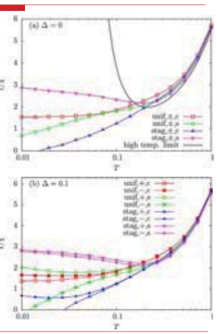

Charge density wave shown in (e) is stabilized by the CEF singlet.

Δ-T Phase Diagram for $J=0.8$

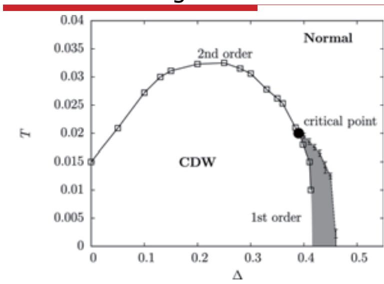

■The CEF splitting stabilizes the CDW order up to $\Delta\sim0.25$.
■ Large enough Δ destroy the CDW (Every site forms CEF singlet).

Ordered Moments

$$n_{c\boldsymbol{Q}}=\frac{1}{2}(n_{cB}-n_{cA})\qquad (n_{cA}<n_{cB})$$

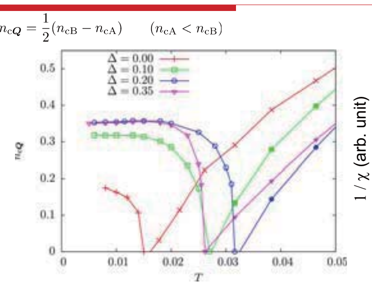

■Increase of ordered moments due to the CEF splitting.
■Initial rise of moments becomes sharper with increasing Δ.

Local Magnetic Susceptibility

$$\chi_{\rm M}^{\gamma\delta}=\int_0^\beta\left[\langle T_\tau S^z_\gamma(\tau)S^z_\delta\rangle-\langle S^z_\gamma\rangle\langle S^z_\delta\rangle\right]{\rm d}\tau.$$

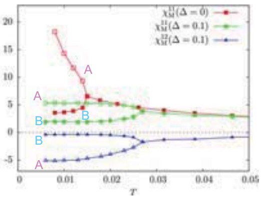

■Δ=0 (Kondo Lattice, red line)
A: Local magnetic fluctuation increase
→ ***Free localized spin***
B: suppresion of the magnetic fluctuation
→ ***Kondo singlet***

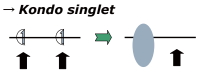

■Δ=0.1 (green and blue lines)
Every susceptibility shows van Vleck-type behavior in the CDW phase.
→ What happen?

Equal-Time Correlations for Δ=0.2

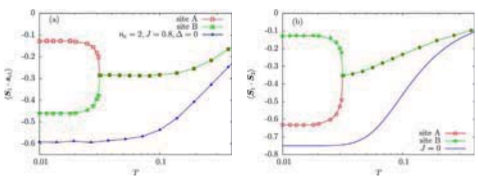

A: $\langle \boldsymbol{S}\cdot\boldsymbol{s}_c\rangle$ decrease and $\langle \boldsymbol{S}_1\cdot\boldsymbol{S}_2\rangle$ increase.
B: $\langle \boldsymbol{S}\cdot\boldsymbol{s}_c\rangle$ increase and $\langle \boldsymbol{S}_1\cdot\boldsymbol{S}_2\rangle$ decrease.

The CDW turns out to be
Staggered order with Kondo and CEF singlets.

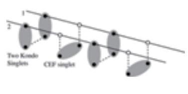

Density of States for $\Delta=0.2$

$$\rho(\omega)=\frac{1}{2}\sum_\lambda\left[-\frac{1}{\pi}{\rm Im}\,G^\lambda_{\rm loc}(\omega+i\delta)\right]$$: summation over sublattices

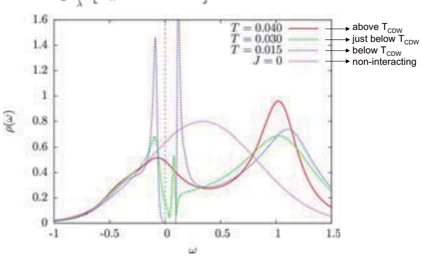

The CDW transition is accompanied by the metal-insulator transition

Local Magnetic Spectrum for Δ=0.2

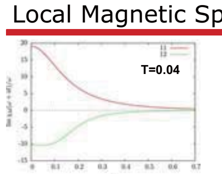

Above $T_{\rm CDW}$:
■Broad quasi-elastic peak which is characteristic for Kondo effect.

Below $T_{\rm CDW}$:
■Inelastic peak
■Intensity in CEF singlet site is much stronger than Kondo singlet site.

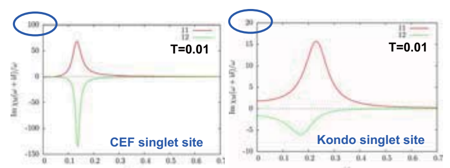

Origin of Charge Fluctuations

Kondo Lattice Model:

$$\mathcal{H}=J\sum_i \boldsymbol{S}_i\cdot\boldsymbol{s}_{ci}-t\sum_{\langle i,j\rangle\sigma}c^\dagger_{i\sigma}c_{i\sigma}=\mathcal{H}_0+\mathcal{V}$$

Model Space: "Local Singlet" or "Free Spin without Conduction electron"

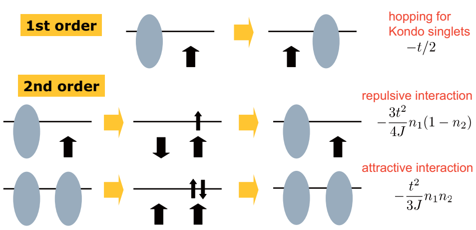

Summary and Discussions

We have first revealed the novel electronic order with staggered Kondo and crystalline electric field (CEF) singlets.

■ Kondo effect plays an essential role for the formation of the charge density wave (CDW).
■ This order is important especially in the CEF singlet system.
■ The CDW at quarter filling is accompanied by the metal-insulator transition.

Relevance to $PrFe_4P_{12}$
●The CDW in the present model is non-magnetic scalar order.
●The inelastic peak in local magnetic spectrum.
●Reduction of the number of carriers at transition temperature.

Remaining Issues
The more concrete calculation aimed at the understanding of the behaviors in $PrFe_4P_{12}$.

Proton elastic scattering of ^{9}C at 290 MeV

Y.Matsuda
Department of Physics, Tohoku University

The differential cross-section for proton elastic scattering on ^{9}C at 290 MeV/u was measured in inverse kinematics.
The experimental method, results and discussion are shown below.

1. Introduction

Goal : Deduce nuclear matter density distributions of unstable nuclei

☆The (p, p) reaction at intermediate energies(～300 MeV) is suitable probe.

♩The proton has the longest mean free path in nuclei.

↳ interior structure → accuracy of surface distributions (halo, skin)

♪A proton interacts with not only protons but also neutrons.

↳ neutron density distribution

♫A one-step direct reaction is dominant.

↳ simple and exact treatment, respectively; Relativistic impulse approximation

♬The effective interaction has been well studied using polarized beams for stable nuclei.

↳ nicely reproduce cross-sections and spin observables from small to large momentum transfer

Experiments until now

♠Stable nuclei

For example, neutron density distributions of Sn isotopes extracted from proton elastic scattering at Ep=300 MeV at RCNP.

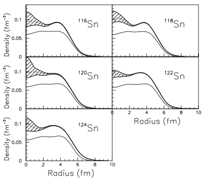

Point nucleon density distributions for $^{116-124}$Sn
S.Terashima et al ,Phys. Rev. C 77, 024317 (2008)

♠Unstable nuclei.

GSI : He and Li isotopes at E=700 MeV/u.
RIKEN etc. : various nuclei at E <100 MeV/u.

※ At E=300 MeV/u, experiments have not been performed.

2. Elastic Scattering of Protons with RI beams (ESPRI) equipment

Inverse kinematics

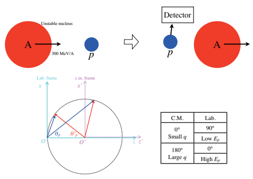

C.M.	Lab.
0° Small q	90°
	Low E_p
180° Large q	0°
	High E_p

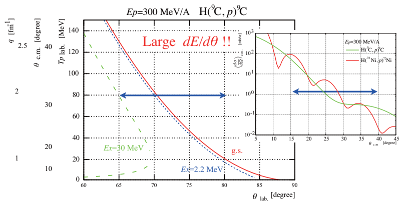

Experimental setup

- Missing mass (MM) spectrometer : $p^{\mu}{}_{beam} + p^{\mu}{}_{p} \Rightarrow$ MM (target point : σ_{Ex} ～400 keV)
- Cover extensive momentum transfer region : up to ～2 fm^{-1}

Large momentum transfer region , θ_{lab} = 66° - 80°, Ep=20-120 MeV $\Delta\Omega$～10 msr/deg.		
Recoil spectrometer	Recoil drift chamber	436x436 mm^2 (x-y-x'-y')
	plastic scintillator	440x440 mm^2 x 2 mm^t
	NaI(Tl) calorimeter	431.8x45.72 mm^2 x 50.8 mm^t
Target	Solid hydrogen	Φ35 - 5 mm^t / Φ30 - 1 mm^t

Small momentum transfer region (θ_{lab} = 75° - 85°), $\Delta\Omega$～14 msr/deg.		
Telescope	Si strip	70x50 mm^2 x 300 μm^t
	CsI(Tl)	70x50 mm^2 x 25.5 mm^t
Target	CH$_2$ - C	70x50 mm^2 x 0.3 mm^t

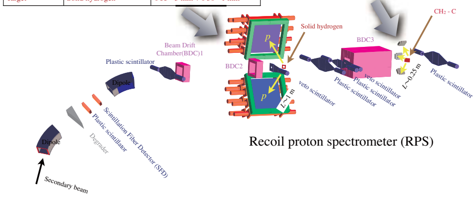

Recoil proton spectrometer (RPS)

3. Experimental results of the H(^{9}C,p) reaction at 300 MeV/nucleon

National Institute of Radiological Science(NIRS)
SB2 course @ Heavy Ion Medical Accelerator in Chiba(HIMAC)

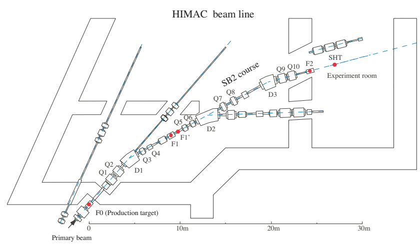

Angular acceptance	±13 mrad
Momentum acceptance	±2.5%
Production target	^{9}Be 50 mm^t
Energy degrader	Al 10.58 mm^t (wedge 1°)
Magnetic rigidity (D1/D3)	4.3855 Tm / 4.0865 Tm
Momentum dispersion (F1')	20 mm/%
Magnification factor (SHT)	1(x), 3(y)

Primary beam : ^{12}C	430 MeV/u	6x10^9 counts/spill
Secondary beam : ^{9}C	277-300 MeV/u	4x10^4 counts/spill
Spill structure	3.3 seconds(duty factor 50%)	
Total number of ^{9}C	4.5x10^8 counts/52.8 hours (SHT) 0.39x10^8 counts/5.2 hours (B.G.)	
Target	Solid hydrogen 5 mm^t (43 mg/cm^2)	

Scatter plot of $\theta_{lab.}$ and T_p/E_x

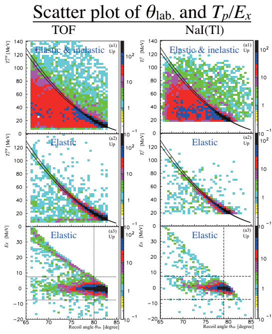

E_x spectrum

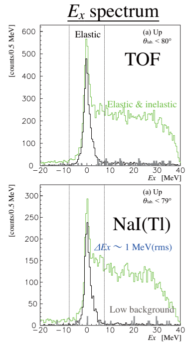

4. Comparison of the experimental data and some calculations

Density distribution

(1) Relativistic Hartree Approximation (RMF)
[C.J.Horowitz and B.D.Serot, NPA368(1981)503.]

(2) Antisymmetrized Molecular Dynamics (AMD)
[Y.Kaneda-En'yo and H.Horiuchi, Prog.Theor.Phys.Suppl.142(2001)647]

Optical potential

(1) Relativistic Impulse Approximation (RIA)
[D.P.Murdock and C.J.Horowitz, Phys. Rev.C35(1987)1442.]

(2) Hamburg G-matrix Approximation (G-matrix)
[L.Rikus and H.V.von Geramb, NPA426(1984)496.]

Density distributions of $^{9\text{-}12}$C

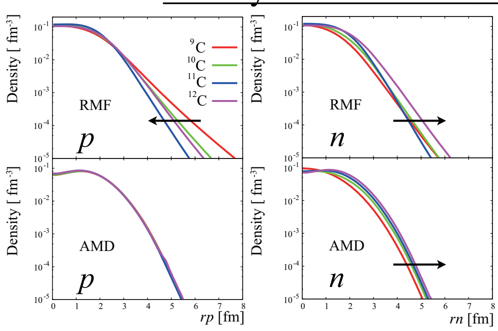

	RMF [fm]		
	r_p	r_n	r_m
^{9}C	2.58	2.06	2.42*
^{10}C	2.36	2.12	2.27*
^{11}C	2.16	2.07	2.12*
^{12}C	2.35**	2.32	2.34
	AMD [fm]		
^{9}C	2.37	2.10	2.28
^{10}C	2.36	2.24	2.31
^{11}C	2.34	2.28	2.31
^{12}C	2.35**	2.33	2.34

* A.ozawa et al., NPA693(2001)32.
** W.Ruckstuhl et al., NPA430(1984)685.

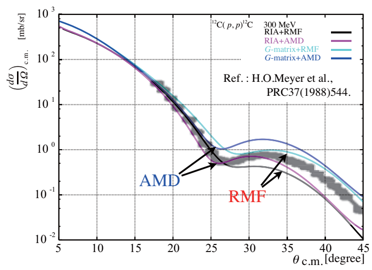

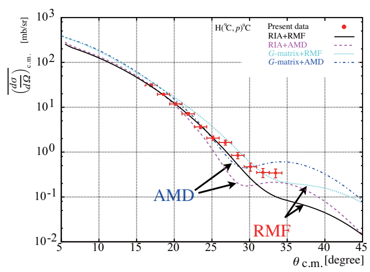

5. Summary

- The differential cross-section for ^{9}C was measured in the momentum transfer region of 1 to 2 fm^{-1}.
- This measurement is the first at the energy region at which the proton has the longest mean free path in nuclei.
- The experiment was performed with very low background using the 5 mm thick solid hydrogen target.
- The excitation energy resolution was about 1 MeV.
- Compared with ^{12}C data, the angular distribution does not show a clear diffraction minimum.

- The angular distribution is compared with microscopic model calculations.
  Optical model description is performed with the RIA and the G-matrix approximation. Description of nuclear structure is done with the RMF and the AMD.
- The unclear diffraction minimum is comparatively reproduced by the RMF.
  It is considerd that this reproduction is derived from that the tail of the proton distribution grow longer than that of the AMD result.
- The RMF calculation is performed by adjusting the scalar mass so as to reproduce the matter radius 2.42(3) fm.
  The calculation suggests that there might be a large differentce between the proton and neutron radii, which are 2.58 fm and 2.06 fm respectively.
- Though more detailed discussion could be done by comparing with more backscattering data, a lack of data and an inaccurateness of nuclear reaction models at the angle make it difficult.
  In future, it is desired to improve these two points.

High Resolution and High Statistics Λ Hypernuclear Spectroscopy by the (e,e'K+) Reaction

A. Matsumura (Tohoku Univ.) for the JLab E01-011 collaboration

The 2nd GCOE
International Symposium on
"Weaving Science Web beyond Particle-Matter Hierarchy"
Feb. 18 (Thu.) – Feb. 19 (Fri.), 2010
Main Lecture Hall, Faculty of Science
Aobayama Campus of Tohoku University,
Sendai, Japan

Dept. of Phys. Tohoku Univ.
D.Kawama, Y. Fujii, O. Hashimoto, H. Kanda, M. Kaneta, K. Maeda, N. Maruyama, A. Matsumura, S.N. Nakamura, K. Nonaka, Y. Okayasu, M. Sumihama, H. Tamura, K. Tsukada, Y. Miyagi
Dept. of Phys. Hampton Univ.
O.K. Baker, L. Cole, M. Christy, P. Gueye, C. Jayalath, C. Keppel, S. Malace, E.K. Segbefia, L. Tang, V. Tvaskis, L. Yuan
Dept. of Phys. Florida International Univ.
A. Acha, W. Boeglin, L. Kramer, P. Markowitz, N. Perez, B. Raue, J. Reinhold, R. Rivera
Dept. of Phys. Yamagata Univ.
S. Kato
Institute of Particle and Nuclear Physics High Energy Accel. Res. Org. (KEK)
H. Noumi, Y. Sato, T. Takahashi
Laboratory of Phys. Osaka Electro-Comm. Univ.
T. Motoba
Dept. of Phys. Univ. of Houston
Ed. V. Hungerford, K.J. Lan, Y. Li, N. Elhayari, S. Randeniya, N. Klantrains
Thomas Jefferson National Accel. Facility
P. Bosted, R. Carlini, V. Dharmawardane, R. Ent, H. Fenker, D. Gaskell, M. Jones, D. Mack, J. Roche, G. Smith, W. Vulcan, S. Wood, C. Yan
Yerevan Physics Institute
R. Asaturyan, H. Mkrtchyan, A. Margaryan, S. Stepanyan, V. Tadevosyan
Nuclear Physics InstituteLanzhou Univ.
X. Chen, B. Hu, S. Hu, Y. Song, W. Luo, B. Wang
Dept. of Physics / Applied Phys. Univ. of Zagreb
D. Androic, M. Furic, T. Petkovic, M. Planinic, T. Seva
Dept. of Phys. North Carolina A&T State Univ.
A. Ahmidouch, S. Danagoulian, A. Gasparian
Dept. of Phys. Louisiana Tech Univ.
N. Simicevic, S. Wells
Dept. of Phys. James Madison Univ.
G. Niculescu, M.-I. Niculescu
Dept. of Phys. Univ. of North Carolina at Wilmington
L. Gan
Dept. of Phys. Duke Univ.
M.W. Ahmed
Dept. of Phys. Univ. of Maryland
F. Benmokhtar, T. Horn
Dept. of Phys. Southern Univ. at New Orleans
M. Elaasar
Phys. and Astro. Dept. California State Univ.
Ed F. Gibson

Λ hypernucleus

- Normal nucleus : proton(s) + neutron(s)
  (e.g. ^{12}C = 6 protons, 6 neutrons)
- Λ hypernucleus : proton(s) + neutron(s) + Λ
  (e.g. $^{12}_{\Lambda}$B = 5 protons,6 neutrons, Λ)

Λparticle :
Consist of u,d,s quarks (lightest hyperon, strangeness = -1)
Free from Pauli exclusion principle by nucleons (proton and neutron)
➔ can be bound deeply inside nucleus

Quark	Charge	s
u	+2/3	0
d	-1/3	0
s	-1/3	-1

s : strangeness

Particle	Quarks	Charge	s	Mass(MeV/c^2)
Proton	uud	+1	0	938.3
Neutron	udd	0	0	939.6
Λ	uds	0	-1	1115.7

s : strangeness

•Binding energy of hypernuclei
➔ Structure of nucleus
➔ Hyperon – Nucleon (YN) interaction

Motivation

Investigate the fine structure of various Λ hypernuclei by the (e,e'K$^+$) reaction

- ^{12}C(e,e'K$^+$)$^{12}_{\Lambda}$B
  - Fine structure of p-shell hypernucleus
  - Mirror-symmetric hypernucleus (vs. $^{12}_{\Lambda}$C @ (π^+,K$^+$))
- ^{7}Li(e,e'K$^+$)$^{7}_{\Lambda}$He
  - Neutron rich hypernucleus
  - ΛN-ΣN coupling
- ^{28}Si(e,e'K$^+$)$^{28}_{\Lambda}$Al
  - Single-particle potential
  - First challenge to study beyond the p-shell region

➔ New information on ΛN interaction

Second generation hypernuclear spectroscopy @ JLab Hall C (E01-011, 2005)

Upgrade of first generation experiment @JLab (E89-009, 2000)

➢High-resolution Kaon Spectrometer(HKS)
- Specialized for hypernuclear spectroscopy
  - Large acceptance
  - Short orbit

➔ < 0.5 MeV energy resolution w/ high quality primary electron beam from CEBAF@JLab

➢「Tilt method」 for scattered electron
- Optimization of detection angle of e'
  - Suppress a huge background from Bremsstraglung and Møller scattering
- e' spectrometer vertically tilted by 8 degree

➔Higher Luminosity w/ better S/N ratio

E01-011 setup

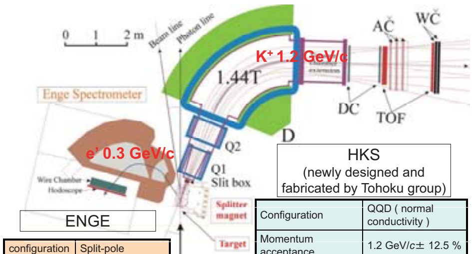

HKS
(newly designed and fabricated by Tohoku group)

Configuration	QQD (normal conductivity)
Momentum acceptance	1.2 GeV/c± 12.5 %
Momentum resolution	2 × 10^{-4} (FWHM)
Angular acceptance	1° ~ 13°
Solid angle	16 msr (w/ splitter)

ENGE

configuration	Split-pole
Momentum acceptance	0.316 GeV/c± 30 %
Momentum resolution	4 × 10^{-4} (FWHM)

Scheme of Data analysis

Particle ID — *Select K$^+$* Time Of Flight, Cherenkov

True coincidence — *Select true coincidence event* Coincidence time

Optical matrices

Missing mass

HKS : New spectrometer
ENGE : Optically new spectrometer (Tilt method)
Tune Angular and momentum matrices
Sieve slit run (angle)
Λ,Σ, and $^{12}_{\Lambda}$B g.s. (momentum)

Estimation of systematic errors depend on the tuning procedure

•Blind analysis with simulation data
CH$_2$ data : well-known mass
^{12}C data : binding energies and cross sections were arbitrarily changed and hidden from analyzers
•Analyze simulation data w/ the same method as experimental data

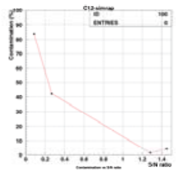

Systematic error ….
for major peak (S/N > 1),
Accuracy of binding energy ~ 100 keV
cross section ~ 5%
for core excited states(S/N <1),
Accuracy of binding energy ~ 400 keV
cross section ~ 90 %

Background estimation by mixed event analysis

•Background source : accidental coincidence between e' and K$^+$
•Mixed background ➔ random combination of e' and K$^+$ with different event ID
Much higher statistics (less statistical fluctuation)

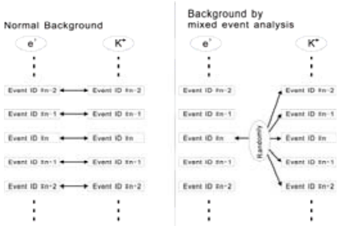

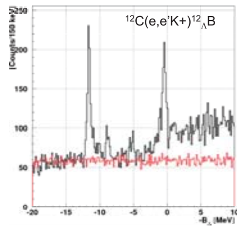

Normal background (red)

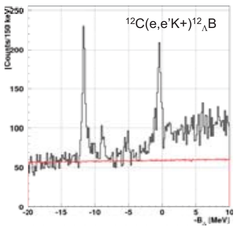

Background by mixed event analysis (red)

Efficiencies for cross section estimation

Cross section of the (γ^*, K$^+$):

$$\overline{\left(\frac{d\sigma}{d\Omega}\right)} = \frac{1}{N_T}\frac{1}{N_\gamma}\sum_{i=1}^{N_K}\frac{1}{\varepsilon_{total} d\Omega}$$

N_T : # of target
N_γ: # of V.P.
dΩ: solid angle acceptance of HKS
N_K : yield of Λ, Σ^0, or hypernuclear state

$$\varepsilon_{total} = \varepsilon_{htrk}\cdot\varepsilon_{AC}\cdot\varepsilon_{WC}\cdot\varepsilon_{bk}\cdot f_{abs}\cdot f_{decay}\cdot\varepsilon_{etrk}\cdot f_{comp}$$

ε_htrk: ~ 0.96
HKS tracking efficiency
ε_AC: ~0.96
AC cut efficiency
ε_WC: ~0.95
WC cut efficiency
ε_bk: ~0.98
beta cut efficiency
ε_etrk: ~0.88
ENGE tracking efficiency
f abs: ~0.82
Kaon absorption factor
f decay: ~0.35
Kaon decay factor
f comp: ~0.97
Computer dead time factor

Systematic error [%]

Target	Thickness	N_γ	dΩ	ε_{total}	*Tune (S/N>1)*		Total
7Li	5	22	1	3	5		23
12C	2						22
28Si	5						23

Λ and Σ spectra (CH$_2$)

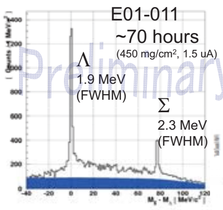

c.f. E89-009, 183 hours
(8.8 mg/cm^2, 0.5 or 1.0 uA)
T. Miyoshi *et al.*,
Phy. Rev. Lett. **90**, 232502(2003)

Better resolution and statistics

^{12}C(e,e'K$^+$)$^{12}_{\Lambda}$B (preliminary)

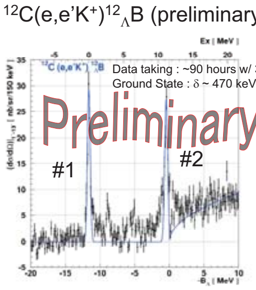

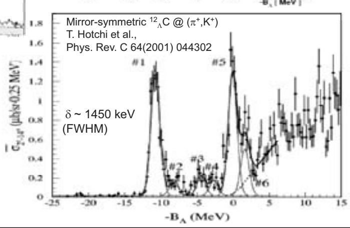

^{7}Li(e,e'K$^+$)$^{7}_{\Lambda}$He (preliminary)

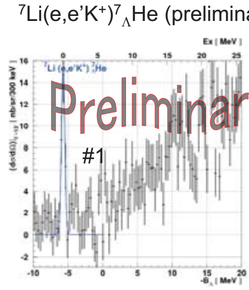

Data taking : ~30 hours w/ 30 μA

First observation of $^{7}_{\Lambda}$He
w/ sufficient statistics

Emulsion data of $^{7}_{\Lambda}$He
M.Jurič et al.,
Nucl. Phys. B52(1973) 1

^{28}Si(e,e'K$^+$)$^{28}_{\Lambda}$Al (preliminary)

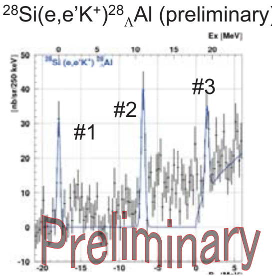

Data taking : ~140 hours w/ 30 μA, Ground State : δ ~ 470 keV (FWHM)
First spectroscopy beyond the p-shell by (e,e'K$^+$) reaction

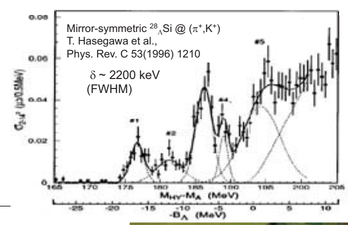

Summary

•The second generation Λ hypernuclear spectroscopy by (e,e'K+) reaction has been carried out successfully at JLab in 2005
•New configurations, **HKS** and **Tilt method**, significantly improved both energy resolution and statistics
•New background estimation method (mixed event analysis)
•Neutron rich hypernucleus $^{7}_{\Lambda}$He was observed with sufficient statistics
•First spectroscopy of *sd*-shell hypernucleus $^{28}_{\Lambda}$Al by (e,e'K$^+$) reaction was successfully performed

•Analysis is in the final stage

External Gamma-ray Backgrounds of the KamLAND Detector

Yukie Minekawa
Physics, D2, Tohoku University

KamLAND Detector

The KamLAND Detector is located 1000 meters under the mountain in Gifu prefecture.
It is searching neutrinos, especially low energy ones like reactor neutrino, solar neutrinos and so on.

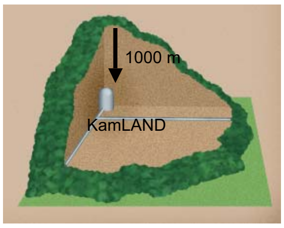

In order to detect low energy signals, it is necessary to reduce harmful signals. The reason why it is underground is to shield from cosmic muons by mountain rock.

The detector was made of as pure materials as possible and have been kept clean.
However there are some radioactive impurities in every components and surroundings. They generate gamma-rays and they can be background. They are called the external gamma-ray background.
It can affect especially precise ^{7}Be neutrino observation.

External Gamma-ray Sources

The KamLAND detector's main components are oils, EVOH films, Kevlar strings, PMTs, water and stainless.
And it is surrounded by rocks.

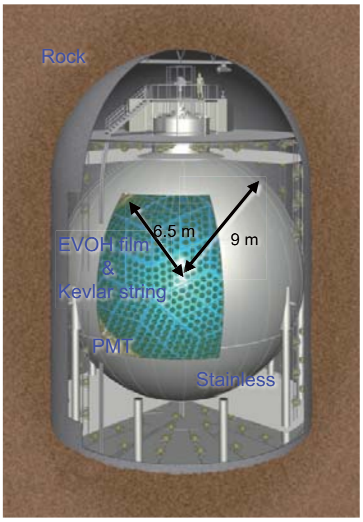

Simulation for Background Estimation

Simulation tool ･･･geant4
a toolkit for the simulation of particles through matter
(reference : http://geant4.web.cern.ch/geant/)

- Construction of the detector geometry.

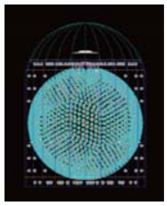

KamLAND geometry

using geant4

- Generation :
  generate gamma-rays from each materials.
- Reconstruct :
  reconstruct energy deposits in the detector as signals in order to compare with real KamLAND data.

Simulation : ^{40}K in EVOH film and Kevlar string

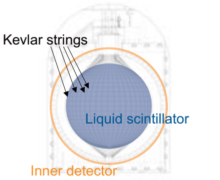

EVOH film : The KamLAND inner detector is 9 meters radius stainless tank. It contains 6.5 meters radius liquid scintillator at the center. This liquid scintillator is separeted by a balloon made from EVOH films.

Kevlar string : The balloon (that was made by EVOH films) is held by grid-like Kevlar strings.

Gamma-ray generation

• Energy	1.4 MeV
• Position	EVOH and Kevlar
• Dirction	uniform

simulation data (Kevlar)

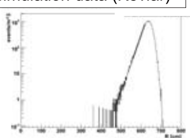

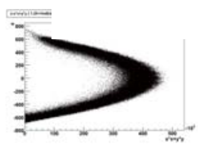

Attenuation length
KamLAND data
19.55 ± 0.02 cm
simulation data
19.78 ± 0.2 cm

KamLAND data

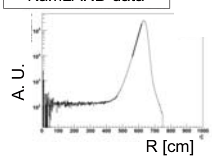

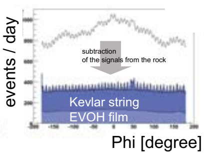

Estimation
The amount of gamma-ray from ^{40}K was estimated by comparing phi distribution with KamLAND data.
The gamma-rays from the Kevlar string make a pattern in the phi distribution.
The heights of the projections of it show the amount of the gamma-ray from the Kevlar strings.

The table shows the estimation result with analysis' .

	Result	ICP-MASS
Kevlar	34 Bq	31 Bq
EVOH	14 Bq	7.2 Bq
total	48 Bq	38 Bq

Simulation : ^{208}Tl in Rock, Glass (PMT), Stainless

Gamma-ray generation

• Energy	2.6 MeV
• Position	Rock, glass (PMT surface) and stainless
• Dirction	uniform

Energy : 2 ~ 4 MeV
Radius : 6.0 ~ 7.5 m

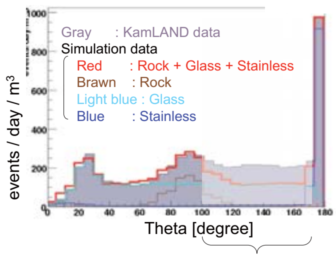

Not consistent

Estimation
Fit theta distribution using the fitting functions which was gotten by the simulation.

Theta distributions of the simulation and KamLAND data are almost consistent.

Summary

- We can estimate the amount of external gamma-ray backgrounds by comparing the simulation data with KamLAND data.
- This time, ^{40}K and ^{208}Tl are generated in the simulation and get the result that almost consistent with analysis's.
- The ^{40}K background rate is
  1.0 [events / day] (90% C.L.)
  in 4.0 meters fiducial volume and within energy 1.3 ~ 1.6 MeV.

^{7}Be neutrino events
~ 80 events / day

- The ^{208}Tl backgraund rates are
  < 7.1 × 10^3 [events / day] from rock
  < 8.5 [events / day] from Glass (PMT)
  < 0.33 [events / day] from stainless
  in 4.0 meters fiducial volume and within energy 2.4 ~ 3.0 MeV.

- We needs more simulation events to estimate precisely.
- We plan to estimate the amount of gamma-rays from others.

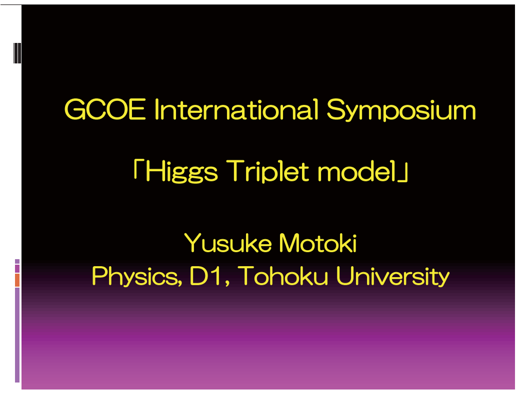
GCOE International Symposium
「Higgs Triplet model」
Yusuke Motoki
Physics, D1, Tohoku University

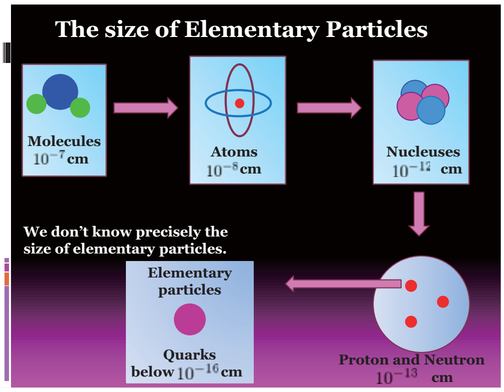
The size of Elementary Particles
Molecules 10^{-7}cm
Atoms 10^{-8}cm
Nucleuses 10^{-12} cm
We don't know precisely the size of elementary particles.
Elementary particles
Quarks below 10^{-16}cm
Proton and Neutron 10^{-13} cm

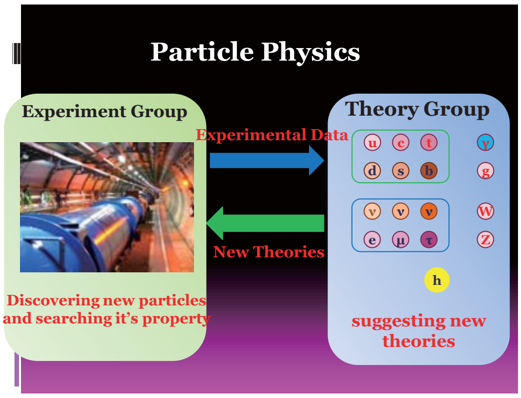
Particle Physics
Experiment Group
Theory Group
Experimental Data
New Theories
Discovering new particles and searching it's property
suggesting new theories

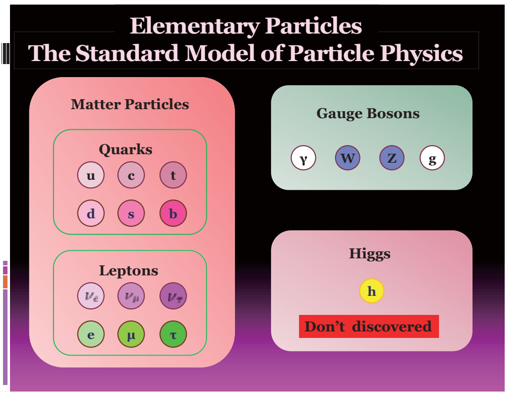
Elementary Particles
The Standard Model of Particle Physics
Matter Particles
Quarks
u c t
d s b
Leptons
ν_e ν_μ ν_τ
e μ τ
Gauge Bosons
γ W Z g
Higgs
h
Don't discovered

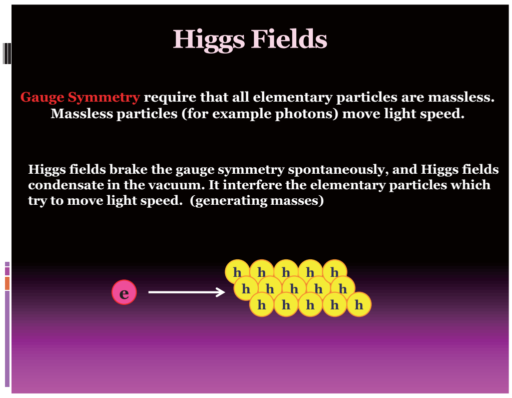
Higgs Fields
Gauge Symmetry require that all elementary particles are massless. Massless particles (for example photons) move light speed.
Higgs fields brake the gauge symmetry spontaneously, and Higgs fields condensate in the vacuum. It interfere the elementary particles which try to move light speed. (generating masses)

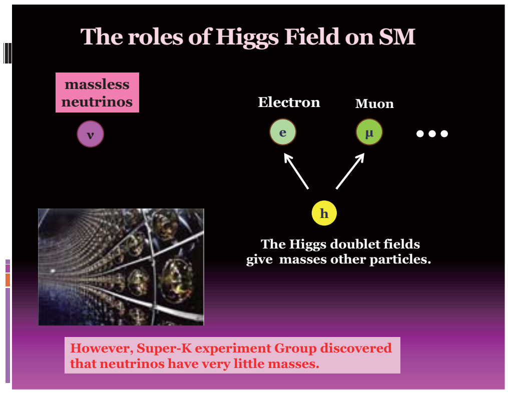
The roles of Higgs Field on SM
massless neutrinos
Electron
Muon
The Higgs doublet fields give masses other particles.
However, Super-K experiment Group discovered that neutrinos have very little masses.

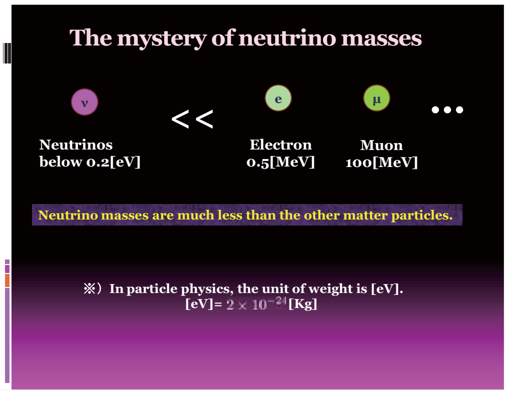
The mystery of neutrino masses
Neutrinos below 0.2[eV]
Electron 0.5[MeV]
Muon 100[MeV]
Neutrino masses are much less than the other matter particles.
※) In particle physics, the unit of weight is [eV]. [eV]= 2×10^{-24}[Kg]

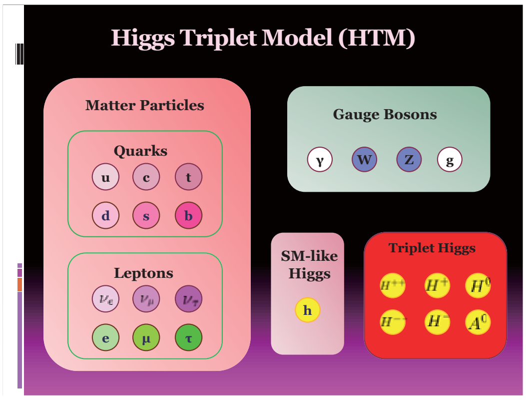
Higgs Triplet Model (HTM)
Matter Particles
Quarks
Leptons
Gauge Bosons
SM-like Higgs
Triplet Higgs
H^{++} H^{+} H^{0}
H^{--} H^{-} A^{0}

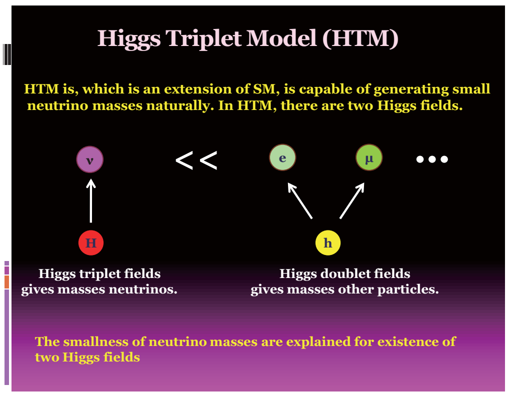
Higgs Triplet Model (HTM)
HTM is, which is an extension of SM, is capable of generating small neutrino masses naturally. In HTM, there are two Higgs fields.
Higgs triplet fields gives masses neutrinos.
Higgs doublet fields gives masses other particles.
The smallness of neutrino masses are explained for existence of two Higgs fields

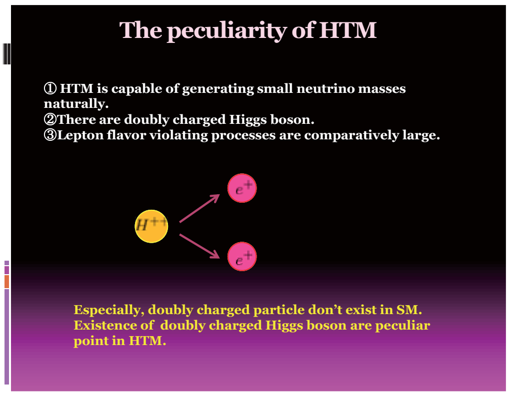
The peculiarity of HTM
① HTM is capable of generating small neutrino masses naturally.
②There are doubly charged Higgs boson.
③Lepton flavor violating processes are comparatively large.
Especially, doubly charged particle don't exist in SM.
Existence of doubly charged Higgs boson are peculiar point in HTM.

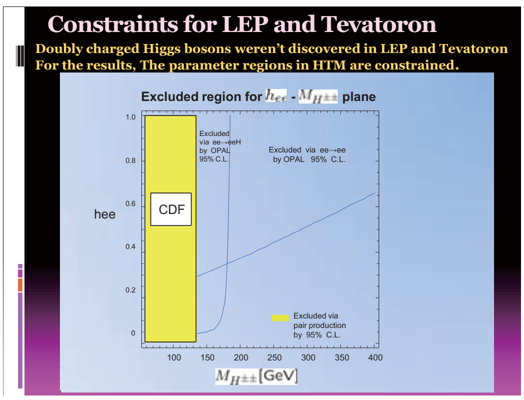
Constraints for LEP and Tevatoron
Doubly charged Higgs bosons weren't discovered in LEP and Tevatoron
For the results, The parameter regions in HTM are constrained.
Excluded region for h_{ee} - $M_{H^{\pm\pm}}$ plane
hee
CDF
$M_{H^{\pm\pm}}$[GeV]

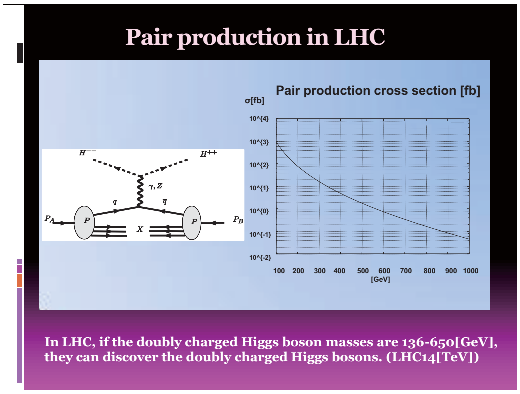
Pair production in LHC
Pair production cross section [fb]
In LHC, if the doubly charged Higgs boson masses are 136-650[GeV], they can discover the doubly charged Higgs bosons. (LHC14[TeV])

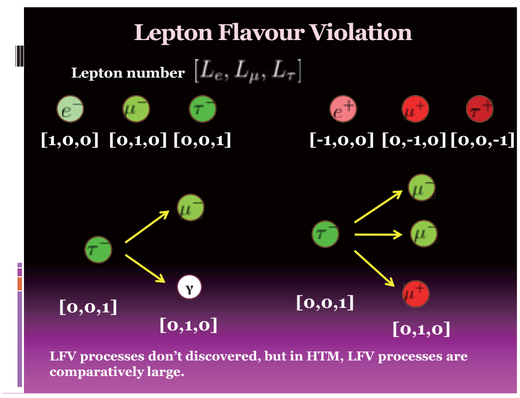
Lepton Flavour Violation
Lepton number $[L_e, L_\mu, L_\tau]$
[1,0,0] [0,1,0] [0,0,1]
[-1,0,0] [0,-1,0] [0,0,-1]
[0,0,1]
[0,1,0]
[0,0,1]
[0,1,0]
LFV processes don't discovered, but in HTM, LFV processes are comparatively large.

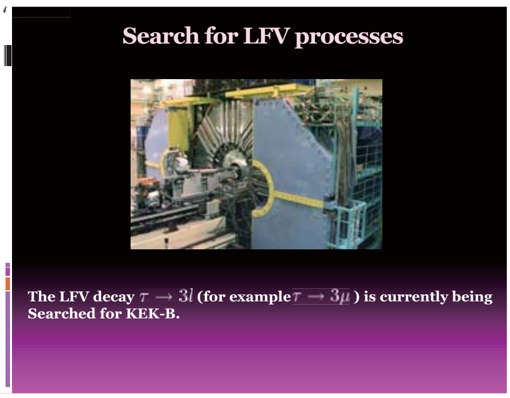
Search for LFV processes
The LFV decay $\tau \to 3l$ (for example $\tau \to 3\mu$) is currently being Searched for KEK-B.

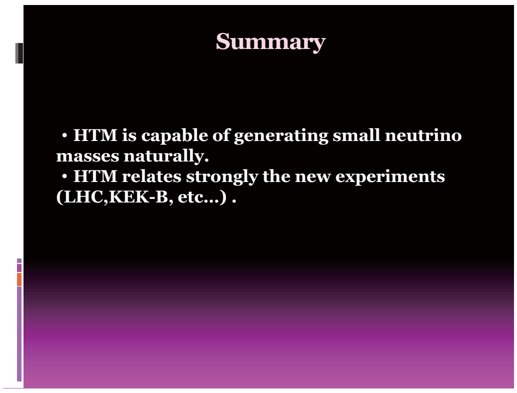
Summary
• HTM is capable of generating small neutrino masses naturally.
• HTM relates strongly the new experiments (LHC,KEK-B, etc...) .

41.

Electron diffraction study of the low temperature phase of Hollandite-type oxide $K_2Cr_8O_{16}$

Daisuke Morikawa
Physics, D1, Tohoku University

Introduction

Recently, the high quality single crystal of Hollandite-type oxide $K_2Cr_8O_{16}$ has been successfully made by high-pressure synthesis and the metal-insulator transition keeping ferromagnetism was formed at 95K [1]. This phenomenon is very rare in the strongly-correlated electron materials. The crystal structure of the low temperature phase and the origin of the metal-insulator phase transition have been unclear yet. The purpose of this study is to examine the phase transition at the nano-scale area of $K_2Cr_8O_{16}$ using Convergent-beam electron diffraction (CBED) and Selected-area electron diffraction (SAED).

[1] K. Hasegawa *et al.*, *Phys. Rev. Lett.* **103**, 146403 (2009).

Objective

Crystal structure of the low temperature phase

Investigation of the metal-insulator transition

Backgroud.1

Hollandite-type oxide $K_2Cr_8O_{16}$

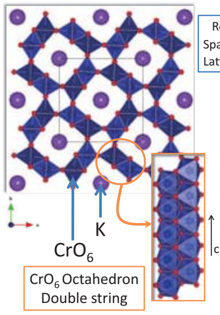

Room temperature phase
Space group : ***I4/m***
Lattice parameter : a=9.7792(7) Å , c=2.9379(3) Å

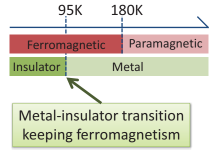

Single crystal : high-pressure synthesis[1]
TEM sample : crush + Ag paste

Backgroud.2

Synchrotron X-ray diffraction data

Observation of (½ ½ 0) super spot under 20K

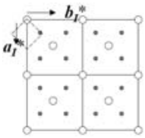

I4/m (room temperature)

Candidate of crystal structure at low temperature

Tetragonal ***$P4_2/n$***
Monoclinic ***$P2_1/a$* or *$P2_1/n$***

A. Nakao *et al.*, personal communication

Crystal structure analysis at nm scale area using electron microscopy

Experimental.1

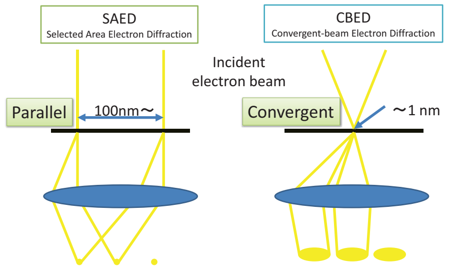

Average structure

Rocking curve
Space group determination
Crystal structure and electrostatic potential

Experimental.2

CBED method

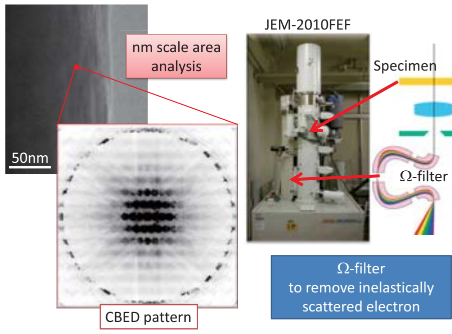

Ω-filter to remove inelastically scattered electron

Result.1-1

[100] incidence CBED pattern (whole pattern)

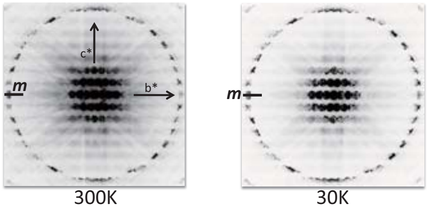

Whole pattern symmetry ***m***

Whole pattern symmetry & Intensity distribution → No temperature dependence

Result.1-2

[100] incidence SAED pattern

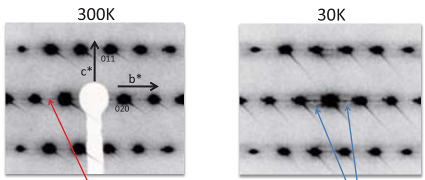

Diffuse streak in b* direction → Stacking fault (010) plane

Diffuse scattering — Sharp at low temperature

Result.2

[001] incidence SAED pattern

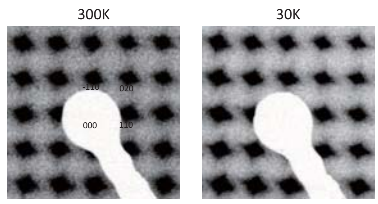

-No super spot
-Spot are diffuse
-Low crystalline (difficult for CBED pattern)

Result.3

[201] incidence SAED pattern

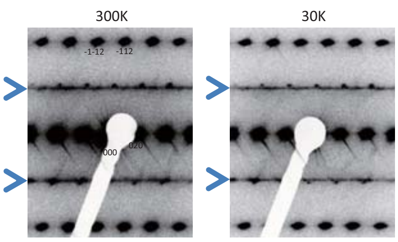

Super spot(?) and diffuse scattering
But no temperature dependence

Result.4

Other incidence SAED pattern (30K)

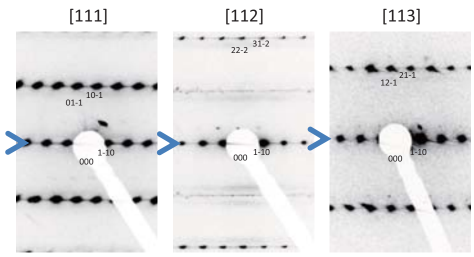

No super spot & Streak to <110> direction → Stacking fault (110) plane

Result.5

[100]? incidence SAED pattern

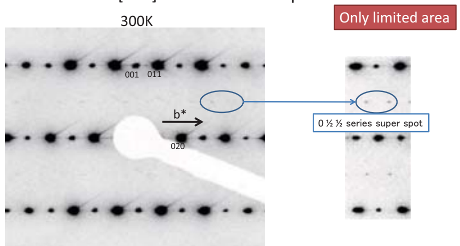

Forbidden reflection for *I* lattice + Super spot

→ Different lattice type? ***P* lattice + b,c axis ×2?**

Need more information

Discussion.1

Diffuse scattering (compare with other Hollandite oxide)

Comparison of [100] incidence SAED pattern

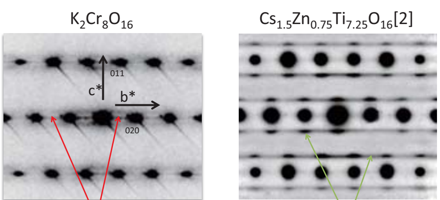

Streak
Stacking fault

Different type

Interstitial A-site ion
Long period structure

[2] M. L. Carter and R. L. Withers, *J. Solid State Chem.* **178**, 1903 (2005).

Discussion.2-1

CBED pattern symmetry (compare with simulation)

MBFIT

Many-Beam dynamical-simulation and least-square FITting
K. Tsuda *et al.*, *Acta Cryst.* A (1999,2002)

-Multiple-scattering calculation
electron has high scattering power
-Non-linear least-square fitting
direct comparison between experimental CBED 2D disk and calculation
fitting parameter (atom position, DW-factor, low-order crystal structure factor etc)
-Preprocessing of experimental data
-PC clusters
96 node PC cluster system were installed

Discussion.2-2

[100] incidence CBED pattern comparison

ZOLZ : zeroth-order Laue Zone
HOLZ : higher-order Laue Zone

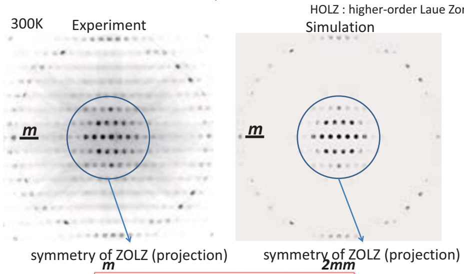

Good agreement at only HOLZ pattern
But ZOLZ symmetry are different!

Discussion.2-3

[100] incidence CBED pattern

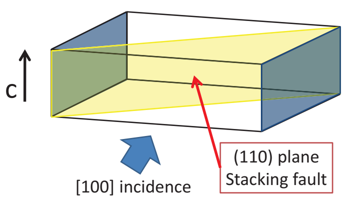

Stacking fault make low CBED symmetry
Main influence are shown at ZOLZ reflection

Need more high-crystalline single crystal

Summary

Metal-insulator transition keeping ferromagnetism

No structure transition were found

CBED pattern symmetry⇒ no contradiction for space group *I4/m*

Sharp diffuse scattering at low temperature

[100]? incidence SAED pattern

No *I* lattice type area exist

Streak in SAED pattern

Stacking fault at (010) and (110) plane

Make low symmetry ([100]incidence CBED pattern)?

Future prospects & Other works

i. Visualization of orbital and/or charge ordering state
direct determination of 3 dimensional electrostatic potential using CBED method
spinel type ($FeCr_2O_4$), perovskite type ($TbMnO_3$, $Pr_{0.6}Ca_{0.4}MnO_3$, $Sm_{0.5}Ba_{0.5}MnO_3$)

ii. Investigate the relation with Physical property and crystal structure
$RBaMn_2O_6$ series ($NdBaMn_2O_6$ etc)

iii. Space group determination
$BaCeO_3$, Li_2TiO_3, κ-$Ce_2Zr_2O_8$, ($K_2Cr_8O_{16}$)

iv. Estimate crystalline and composition of single crystal
$BaFe_{2-x}Cr_xAs_2$, (Pr, La)$FeAsO_{1-x}F_x$, $Pr_{1-x}Sr_xFeAsO$

v. Polarization determination
AlGaN, GaN

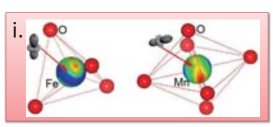

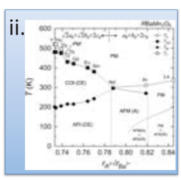

Light scattering by collective excitation of phonon in quantum paraelectrics

Ryuta Takano

Physics, D1, Tohoku University

Quantum Paraelectrics

The polarization arrangement in these materials is disturbed by the zero point vibration at extremely low temperatures. So they do not undergo a ferroelectrics phase transition.

⟹ $SrTiO_3$, $KTaO_3$ etc.

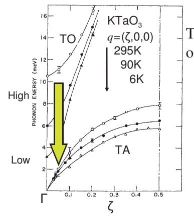

J.D.Axe, J.Harada, and G.Shirane, Phys. Rev. B **1**, 1227 (1970).

The TO-mode softens at the neighborhood of the Γ point.

⇒The density of state of phonon increases at the Γ point.

(TO-phonon＋TA-phonon)

Importance of the state of collective excitation of phonon at low temperature.

Relaxation Time in the Phonon-Phonon Scattering

$$\frac{1}{\tau_N} \approx \frac{\varepsilon^{1/2}}{\tau_U}$$

V.L. Gurevich and A.K. Tagantsev, Sov. Phys. JETP **67**, 206 (1988).

ε : dielectrics constant

τ_U : relaxation time of the "Umklapp process"

τ_N : relaxation time of the "Normal process"

The dielectrics constant of quantum paraelectrics is a value high at low temperature.

K.A.Müller and H.Burkard, Phys.Rev. B**19**(1979)3593.

(A ferroelectrics phase transition is not caused.)

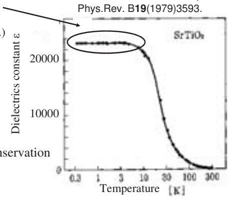

$$1/\tau_U << 1/\tau_N$$

⇒The Normal process (the momentum conservation process) is predominant.

Energy Transportation in the Phonon Gas

< Thermal Diffusion and Second Sound >

< Diffusion of heat >

The Umklapp process and the impurity scattering is predominant.

(Umklapp+impurity+..+etc=Resistive process:τ_R)

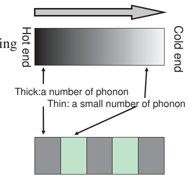

< Propagation of heat >

The Normal process is predominant.

A compression wave of the phonon gas is propagated.

= Second Sound

Change in phonon number = Change in the temperature

There is a possibility that heat is propagated as a wave in a gas.

Quasi Elastic Light Scattering (QELS) and Broad Doublet

B.Hehlen, A.L.Pérou, E.Courtens, and R.Vacher, PRL **75**,2416(1995).

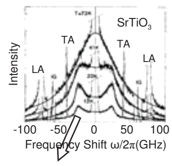

P.A.Fleury and K.B.Lyons, PRL.**37**,161(1976).

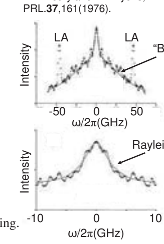

Second Sound?

It is necessary to decide the relaxation time of τ_R,τ_N in the phonon-phonon scattering.

It is necessary to experiment in a wide temperature region and a wide frequency domain.

Objective

We measure the spectrum in the Brillouin scattering region in $SrTiO_3$ and $KTaO_3$,and understand a temperature dependence of the spectrum according to the model of collective excitation of phonon.

・We aim to understand a picture of the phonon gas at each temperature, obtaining τ_R and τ_N from the analysis of the light scattering spectrum.

Thermal Diffusion and Second Sound

$$\begin{cases} \rho C_p \dfrac{\partial \delta T}{\partial t} + \dfrac{\partial Q}{\partial x} = 0 & \text{Conservative low of energy} \\ Q = -\kappa \dfrac{\partial \delta T}{\partial x} & \text{Fourier's low} \end{cases}$$

Usual thermal equation

$$\frac{\partial \delta T}{\partial t} = \frac{\kappa}{\rho C_p}\frac{\partial^2 \delta T}{\partial x^2}$$

ρ :density C_p:specific heat κ:thermal conductivity

Q :energy current density δT :temperature fluctuation

The finite lengths of time is necessary for the establishment of a regular heat flow.

$$Q + \tau_R \frac{\partial Q}{\partial t} = -\kappa \frac{\partial \delta T}{\partial x}$$ (Cattaneo's expression)

It becomes a wave equation including decay for the temperature.

⇒ A wave of temperature fluctuation **(Second Sound)**.

$$\frac{\partial^2 \delta T}{\partial t^2} + \frac{1}{\tau_R}\frac{\partial \delta T}{\partial t} = \frac{D_{th}}{\tau_R}\frac{\partial^2 \delta T}{\partial x^2}, \quad \frac{1}{\sqrt{3}}c$$

:propagation velocity (**c : average speed**)

$D_{th} = \frac{1}{3}c^2\tau_R$: thermal diffusivity coefficient

Spectrum of a Wave Equation

$$S \sim \frac{\omega_0^2/\tau_R}{(\omega^2-\omega_0^2)^2 + \omega^2/\tau_R^2} \qquad \omega_0 = \frac{1}{\sqrt{3}}cq \quad , q = \frac{4n\pi}{\lambda}\sin\frac{\theta}{2}$$

・$\omega_0 << 1/\tau_R$ (overdamping)

・$1/\tau_R << \omega_0$ (underdamping)

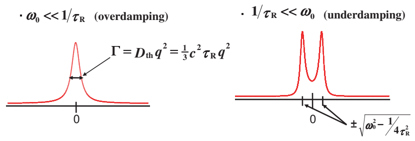

Propagation as a wave of heat

Underdamping

Local thermal equilibrium

$$1/\tau_R << \omega_0 << 1/\tau_N$$

Window condition of Second Sound

Spectrum Expression by Extended Thermodynamics

H.Dreyer and H.Struchtrup, Continuum Mech. Thermodyn. 5(1993)3-50

$$S_{total}(q,\omega) = P_1 S_1(q,\omega) + P_2 S_2(q,\omega) + \text{const}$$

$$\begin{cases} S_1(q,\omega) = \dfrac{\omega_0^2\left(\gamma_3 + \frac{1}{\tau_R}\right)}{\left(\omega_0^2 - \omega^2 - \gamma_3''\omega\right)^2 + \omega^2\left(\gamma_3' + \frac{1}{\tau_R}\right)^2} \\ S_2(q,\omega) = \dfrac{1}{2\pi cq}\left[\tan^{-1}\tau(\omega+cq) - \tan^{-1}\tau(\omega-cq)\right] \end{cases}$$

$$1/\tau = 1/\tau_N + 1/\tau_R \qquad \omega_0 \equiv \frac{1}{\sqrt{3}}cq$$

$$\gamma_3 = \gamma_3' + i\gamma_3'' = \cfrac{\alpha_3 c^2 q^2}{i\omega + \frac{1}{\tau} + \cfrac{\alpha_4 c^2 q^2}{i\omega + \frac{1}{\tau} + \cfrac{\alpha_5 c^2 q^2}{i\omega + \frac{1}{\tau} + \cdots}}} \qquad \alpha_n = \frac{(n-1)^2}{4(n-1)^2 - 1}$$

parameter ⟹ $P_1, P_2, \omega_0, \tau_N, \tau_R$, **const**

τ_R is decided from thermal diffusivity coefficient obtained by the light scattering experiment in the time domain. ($\omega_0 << 1/\tau_R$)

Optical System 1 (back scattering) and Crystals

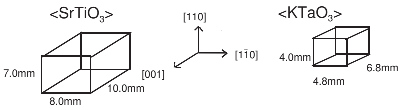

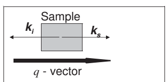

$q = 6.00\times10^7$ [m^{-1}]($SrTiO_3$)

$q = 5.56\times10^7$ [m^{-1}]($KTaO_3$)

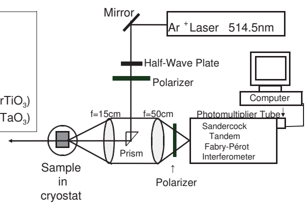

Optical System 2 (forward scattering)

< Impulsive Stimulated Thermal Scattering >

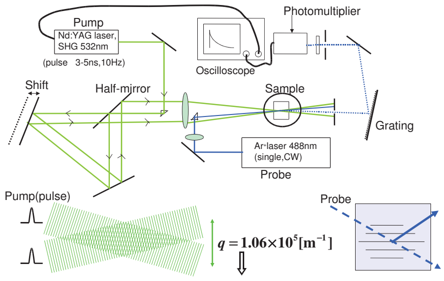

This q has the value of about 1/100~1/1000 compared with the backscattering experiment.

Decision of "τ_R"

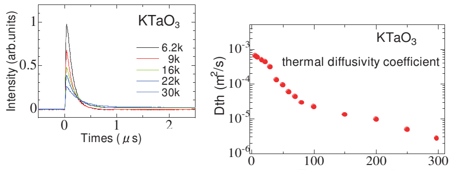

・ Thermal diffusion : exponential decay

$$I = A\exp(-2\Gamma t) + \text{const}$$

Thermal diffusivity coefficient : $D_{th} = \Gamma/q^2$ ⟹ $D_{th} = \frac{1}{3}c^2\tau_R$

$q = 1.06\times10^5$[m^{-1}]

Spectrum and Fitting

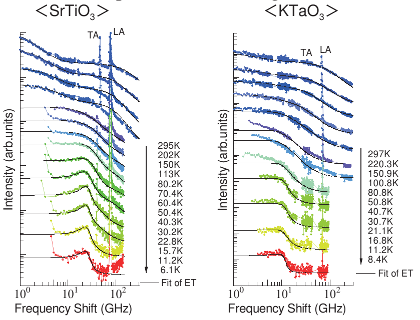

Temperature Dependence of τ_N and τ_R

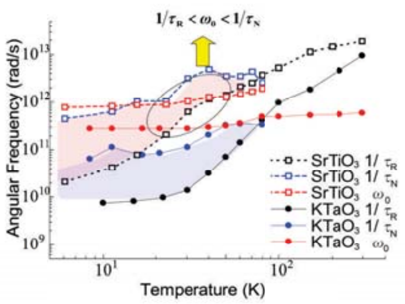

Conclusion

1. A narrow quasi-elastic scattering component in the high temperature region is a light scattering spectrum by thermal diffusion. It has been understood that the frequency of the resistive process falls when lowering the temperature in $SrTiO_3$, and this thermal diffusion mode (the second-sound wave that over dumped) shifts to the second-sound wave (propagating mode).

2. It cannot be said that the phonon gas is in the state of the collective excitation in the observation scale of the actual experiment. It should be interpreted that the observed BD for $KTaO_3$ only as the second order Raman scattering involving pairs of individual phonons.

Formation of the Milky Way Based on the Analysis of Kinematics and Chemical Abundance of the Outer Halo Stars

Miho Ishigaki (Astronomy, D3)
Co-I. Chiba, M. (Tohoku U.); Aoki, W. (NAOJ)

GCOE 2010/2/18-09

NAOJ (http://www.nao.ac.jp/Gallery/index.html)

Stars in the solar-neighborhood

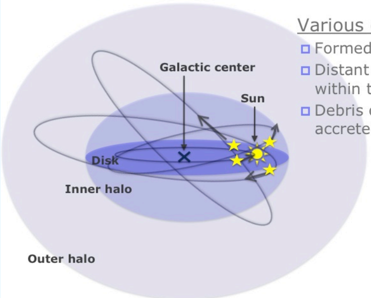

Various origins
- Formed *in situ*
- Distant location within the MW
- Debris of accreted galaxy

The MW *inner* and *outer* stellar halo

Results from SDSS (Carollo et al. 2007, 2009)

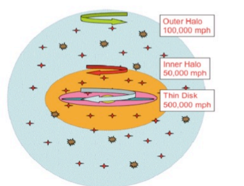

Inner halo
- Modest prograde rotation
  - $0<V_\phi<50$ km s^{-1}
- [Fe/H] ≈ −1.6
- Flattened
- *[α/Fe]~0.4*

Outer halo
- Retrograde rotation: $-70<V_\phi<-40$ km s^{-1}
- [Fe/H] ≈ −2.2
- Spherical
- *Chemical abundance?*

Different formation mechanisms?

Picture from the SDSS press release (http://www.sdss.org/news/releases/20071212.dblhalo.html)

Observation

- Subaru Telescope High-Dispersion Spectrograph (HDS)
- Date of observations
  - 2003-2005 : N~28
  - June, July 2008: N~29
- Wavelength coverage ≈ 4000-7000 A
- Spectral resolution R ≈ 50000
- S/N>100@5000A

Subaru/HDS

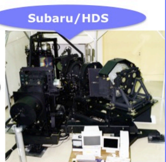

Raw data

Results(2) neutron-capture element

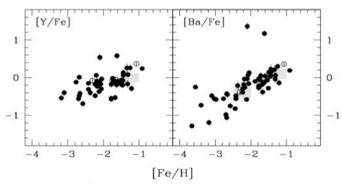

Inner halo Result

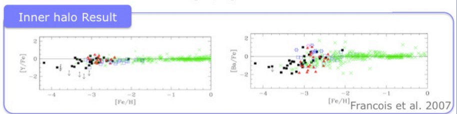

Francois et al. 2007

Comparison with the MW dwarf satellites

[Mg/Fe]-[Fe/H]

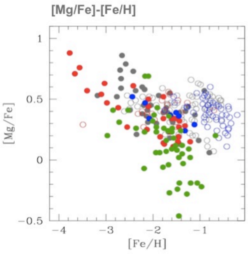

Histogram -2<[Fe/H]<-1

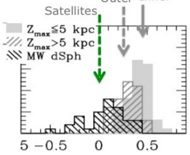

Nearby dSphs: ● (Dra, Umi, Sex, Car, Scl, Fnx, Leo)
Shetrone et al. 2001, 2003, Koch et al. 2008, Geisler et al. 2005

Outline

1. What can we learn from chemical abundance (+ kinematics) of nearby stars regarding the formation of the Milky Way Galaxy
2. The main results of our study on the chemical abundance of the outer stellar halo of the MW
   - Sample selection using kinematics
   - Abundance results of key-elements
   - Implication for the formation of the MW outer halo

Formation of elements

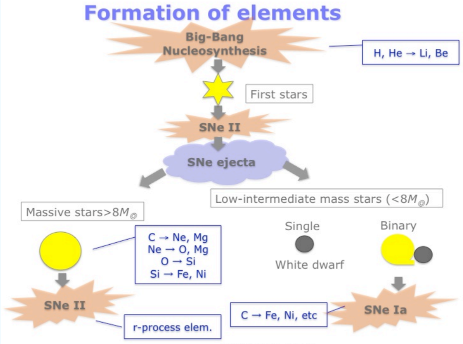

[α/Fe] ratios: The halo vs. dwarf satellites

[Mg/Fe] @-2<[Fe/H]<-1
Halo: +0.3~+0.5 dex
Satellite galaxies: -0.5~+0.4 dex

Venn et al. 2004

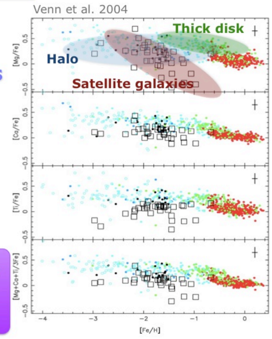

Simple assembly of the nearby satellites cannot explain abundances of the current inner stellar halo of the MW

- Data reduction: Standard IRAF routines

Example of reduced spectrum: BD-03 5215, S/N=370

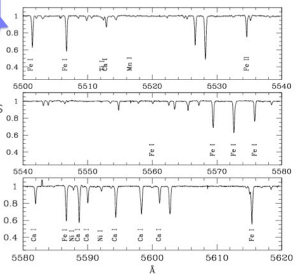

- Abundance analysis (Aoki et al. 2009)
  - Alpha: Mg, Si, Ca, Ti
  - Iron-peak: Cr, Mn, Fe, Ni, Zn
  - Neutron-capture: Y, Ba
  - Odd-Z: Na

Cumulative distributions of [α/Fe] ratio at -2<[Fe/H]<-1

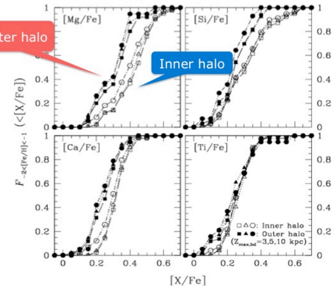

Interpretations of the lower [Mg/Fe]

Possible building blocks of the inner/outer halo may be different

- Star formation efficiency (v_{SF})
  - Inner halo: High
    Mg (SNe II) > Fe (SNe Ia)
  - Outer Low
    Mg (SNe II) < Fe (SNe Ia)

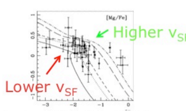

Lanfranchi & Matteucci 2003

- Epoch of the accretion
  - Early
    No time for Fe enrichment
  - Recent
    Enough time for Fe enrichment

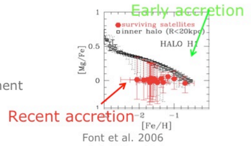

Font et al. 2006

The Milky Way Galaxy: "Laboratory of galaxy formation"

- Stellar over density

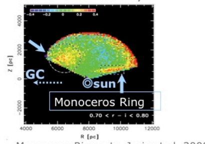

Monoceros Ring, etc. Juric et al. 2008

- Stellar streams

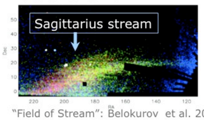

"Field of Stream": Belokurov et al. 2006

- Clumps in an angular momentum (L_z-L_{tan}) space

Fossil records of the Milky Way Formation

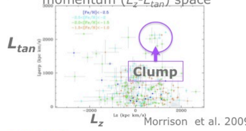

Morrison et al. 2009

SNe Yields

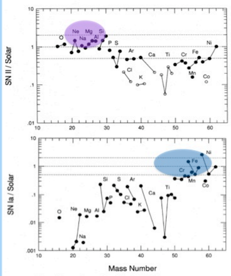

Tsujimoto et al. 1995

- Type II SNe
  - α elements
    Mg, Si, etc
  - Short timescale (<100Myr)
- Type Ia SNe
  - Fe-peak elements
    Fe, Cr, Ni, etc
  - Long timescale (>1Gyr)

Abundance Ratios

$$[A/B]=\log_{10}\{(N_A/N_B)/(N_A/N_B)_{solar}\}$$

[α/Fe] ≈ Relative fraction of Type II/Type Ia SNe in the past

Kinematics of the sample stars

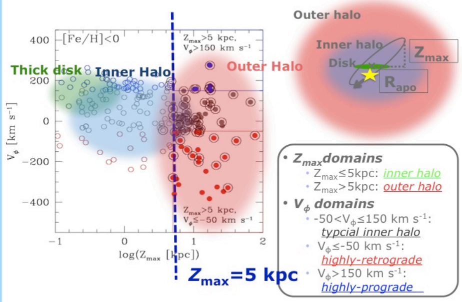

- Z_{max} domains
  - Z_{max}≤5kpc: *inner halo*
  - Z_{max}>5kpc: *outer halo*
- V_ϕ domains
  - $-50<V_\phi\leq150$ km s^{-1}: typcial inner halo
  - $V_\phi\leq-50$ km s^{-1}: *highly-retrograde*
  - $V_\phi>150$ km s^{-1}: *highly-prograde*

Result(1) α-elements (Mg, Si, Ca, Ti)

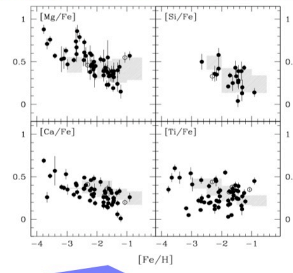

Decreasing trend with increasing [Fe/H]

[Mg/Fe]-Orbital parameters

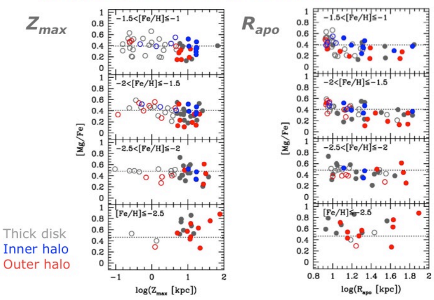

- Thick disk
- Inner halo
- Outer halo

Summary

- *Motivation:* Examination of chemical abundance of the outer halo stars
- *Methods:* Subaru/HDS observation + homogeneous abundance analysis
- *Results:*
  - At -2<[Fe/H]<-1, the outer halo sample show systematically lower [Mg/Fe]
  - The [Mg/Fe] ratios for the outer halo sample spans intermediate range between the inner halo and the MW satellites
- *The implication for the halo formation:*
  - Certain fraction of the outer halo was formed through merging/accretion of dwarf galaxies.
  - *Later accretions and disruption of stellar systems with lower star formation rates* were important.

Searching for Luminous Core-Collapsed Supernovae in a High-z Proto-Cluster

N. Morimoto, T. Yamada, T. Hayashino, Y. Nakamura, K. Kousai (Tohoku Univ.) and Y.Matsuda (Durham Univ.)

It has been revealed that SSA22 region at redshift z=3.1 is an extremely high density region of LAEs (Lyman α emitters). In addition to this, star formation in this region is supposed to be biased to very large mass from the evidence such as a large number of large LyA EW objects. Therefore core- collapsed supernovae (SNe) of massive stars are expected to occur frequently in this region. While SNe has not been detected beyond z>2 to date, it is very important not only to detect core-collapsed SNe at z=3.1 but also to obtain any useful information to understand star formation in early universe. So we estimated the expectation of observing core-collapsed SNe in SSA22 region at z=3.1 based on our own sample of star-forming galaxies, and carried out preliminary observations and data analysis to search for variable objects to investigate the detectability of core-collapsed SNe at high-z by searching for variability of LAEs in this region.

Purpose

Approaching Galaxy formation & evolution in the early universe by studying star formation of LAEs & LBGs (Lyman Break Galaxies)

- Usual way (using UV, H α etc...) have uncertainties.
- Searching Core-Collapsed Supernovae(SNe)

Core-Collapsed Supernovae

Their progenitors are massive stars.

= Direct indicator of star formation because they are short-lived.

- Setting lower-limit on star formation rate of host galaxies
- Showing trend of IMF of host galaxies

(Whether to be biased large mass or not?)

Where? How?

Target Field

The high density region of star-forming galaxies at z=3.1

= The SSA22 field (R.A. = $22^h 17^m$, Dec = + 00°15')

Subaru Telescope / Suprime-Cam 7 FoVs (4726 arcmin²)

= named Sb1~Sb7

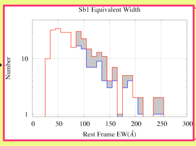

A Distribution of equivalent width(EW) of Lyman α emission line (Sb1). There are LAEs with large EW in the SSA22 field.

↓ Distribution of LAEs

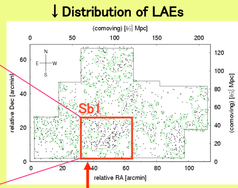

Sb1, which has a highest density among 7 FoVs, is a target field this time.

Why in the SSA22-Sb1 field?

① High density region of LAEs & LBGs

→ We can get large samples of LAEs & LBGs. ⇨ Efficient survey

LAE : 614 obj.
(1) NB497 < 26.0
(2) BV-NB497 > 0.8

LBG : 985 obj.
(1)U-V-2×(V-i')≧1.0
(2)U-V ≧ 0.5
(3)V-i' ≦ 0.6 (4)24 ≦ R ≦ 25.5

② In the SSA22 field, there are LAEs with large Equivalent Width.

→ Probability of the star formation biased to very large mass.

The stars whose mass > 8 M_{sun} become core-collapsed SNe.

Frequent SNe explosions by massive star? = Frequent Core-collapsed SNe

But observed most distant core-collapse SN is at z<1 …

Probability of detecting SNe at z~3

Brightness

Richardson et al. (2002)

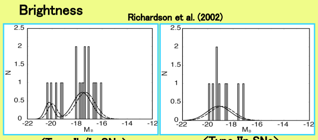

<Type Ib/Ic SNe> <Type IIn SNe>

Expected brightness at Maximum light

M_{1700}~ -17.9 ➡ m_{6500}~27.7

But more luminous SNe could exist.

Expected number

- Consider constant, continuous star formation history.
- Initial mass function (IMF) :Salpeter IMF α=2.35 (0.1-130Msun)
- Star Formation Rate (SFR)
  - LAE:SFR=2 Msun/yr
  - LBG:SFR=40 Msun/yr

⇩ One SN could be observed for 2 weeks in the rest-frame

z~3 LAE sample : ~0.05 SN / 614objs.

z~3 LBG sample : ~0.2 SN / 985objs.

In case of star formation biased very large mass α=0.5

LAE:~0.3 SN、LBG:~3 SN

Method

- Observing data (Subaru Telescope / Suprime-Cam)

Band	date	PI	Exposure (hr)	5σ-limit (ABmag)
B	2002/9	Hayashino et al.	0.7	26.6
	2003/9	Capak et al. (archive)	1.1	27.1
V	2002/9	Hayashino et al.	0.7	26.6
	2003/9	Capak et al. (archive)	0.8	26.8
z'	2001/10	Capak et al. (archive)	1.2	26.0
	2002/9	Capak et al. (archive)	1.4	26.0

→ Using for detecting flux variances

<Filters of Suprime-Cam>

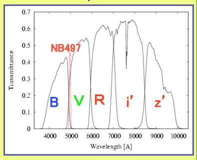

<Flux variance>

① Star-forming galaxies in the SSA22 field
② The background objects in the same images

Aperture photometry (V / z'-band images, 2 epochs)

Flux variance between 2-epochs of the star-forming galaxies and the background objects ⇨ Comparing their flux variances

Selection of variable objects (Δflux ≧ 3σ of thebackground objects)

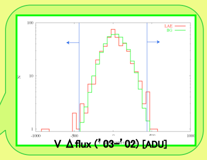

<Estimation of flux variance by noise>

Selecting objects those which might be non-variable objects as a control sample.

Selection criteria for the background objects

(1) same magnitude range as LAEs / LBGs

LAE : 25 < V < 27.3 , LBG : 24 < V < 25.5

(2) eliminate blue objects (AGN) : 0.2 < R-i' < 0.4

Aperture photometry in the B-band images (2-epoch)

Δflux ≦ 3σ → Aperture photometry in the V/z'-band images

→ control sample

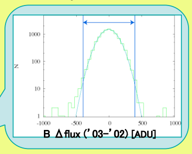

Result

Variable objects candidates: LAE : 13 objs. LBG : 14 objs.

⇨ what are the origins of variances showed by these variable object candidates?

<LAE>

ID	V Δmag	V year+	z' Δmag	z' year+	Spectrum
35	0.65 (3.6σ)	03	–	–	–
102	–	–	1.1 (3.0σ)	02	–
120	1.86 (3.8σ)	03	–	–	–
135	0.58 (3.3σ)	03	–	–	–
157	0.41 (3.4σ)	03	–	–	–
216	0.77 (3.4σ)	03	–	–	LAE?
335	0.67 (3.0σ)	02			–
384	–	–	0.29 (3.6σ)	02	AGN
392	0.25 (6.2σ)	02	–	–	AGN
457	0.37 (43.6σ)	03	–	–	AGN
489	–	–	0.07 (3.8σ)	02	–
645	0.22 (3.0σ)	03	–	–	LAE
686	0.17 (3.5σ)	02	0.48 (7.8σ)	01	–

(year+ ; The year when luminosity of galaxies increase)

<LBG>

ID	V Δmag	V year+	z' Δmag	z' year+	Spectrum
32	0.29 (11.4σ)	03	–	–	–
72	0.3 (3.1σ)	03	–	–	LBG
168	–	–	0.18 (3.4σ)	01	–
491	–	–	0.29 (3.6σ)	02	AGN
500	0.25 (6.2σ)	02	–	–	AGN
614	0.33 (3.1σ)	03	–	–	–
691	0.3 (3.4σ)	03	–	–	AGN?
699	0.35 (3.4σ)	02	–	–	–
701	0.3 (3.4σ)	03	–	–	–
818	–	–	0.37 (3.2σ)	01	–
869	0.15 (5.2σ)	02	–	–	–
927	–	–	0.5 (3.0σ)	02	–
984	0.16 (3.6σ)	02	–	–	–

Consideration

Candidate1・・・Supernova

unidentifiable now (Because only 2-epoch images exist.)

⇨ Need more photometric and spectroscopic data !!

Candidate2・・・Active Galactic Nuclei (AGN)

<Spectrum Features>

- Width of Lyman α emission line

Type I : 50~100Å、Type II : >10Å ⇔ LAE : <10Å (Observing frame)

- N V emission line (Observing wave length~5080Å)

⇨ Some of the candidates those have spectrum-data have been confirmed as AGNs.

Images

<Identified>

LAE 645

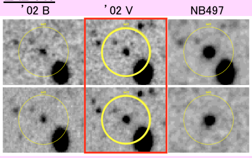

V Δflux : 3.0σ (year+=03)

➡ Δmag=27.21

Lyman α emission FWHM~10Å

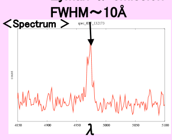

LBG 72

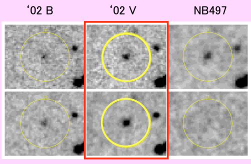

V Δflux : 3.1σ (year+=03)

➡ Δmag=27.13

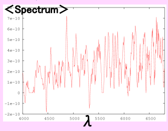

<Unidentified>

LAE 102

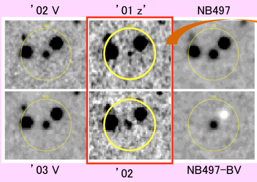

z' Δflux : 3.0σ (year+=02)

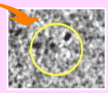

~3pixels difference

||

SN-like variance

z'-band subtracted image ('02-'01)

➡ Δmag=26.32

Summery

✦ 2 variable objects remain as candidates of star-forming galaxies without evidence of AGN contributions, which are potential candidates of SNe at z=3.1.

(And there was an unidentified variable object candidate showing SN-like variance.)

➡ There is possibility of detecting high-z SNe.

✦ Multi-epoch photometric data and spectra can prove the origins of the variability.

A study of light curves from rapidly rotating neutron stars

Astronomy, D3, Kazutoshi Numata

Two types of X-ray phenomenon

X-ray pulsar(High Mass X-ray Binary)

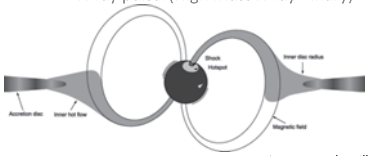

Accretion-powered oscillation

X-ray burst(Low Mass X-ray Binary)

Nuclear-powered oscillation

Accreting Millisecond X-ray Pulsars (AMXPs)

Periodic millisecond X-ray oscillation

•Accretion-powered millisecond oscillation (10 AMXPs)

•Nuclear-powered millisecond oscillation (16 AMXPs)

The properties of AMXPs

- Small amplitudes
- Sinusoidal pulse shapes
- Variable oscillation amplitudes

small amplitudes: a few %
sinusoidal pulse shapes:
fundamental ≧ 10 × first overtone

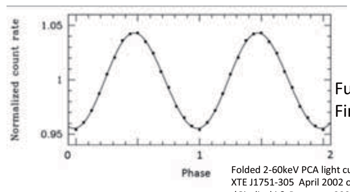

Folded 2-60keV PCA light curve
XTE J1751-305 April 2002 outburst
(Gierlinski & Poutanen 2005)

Fundamental: 3.28±0.03
First overtone: 0.11±0.03

Variable oscillation amplitudes:
factor 1 → 2 ~10

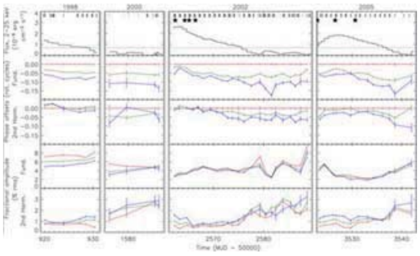

SAX J1808.4-3658 outbursts
Red 2-5keV; green 5-10keV; blue 10-20keV
(Hartman et al. 2009)

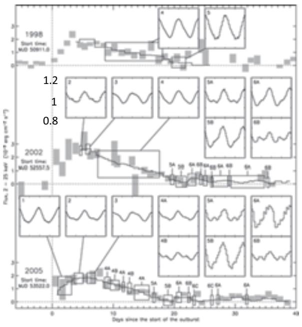

SAX J1808.4-3658 outbursts
(Hartman et al. 2008)

To explain these properties,Lamb et al. (2009) proposed

Spot model

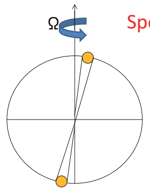

fractional rms amplitudes

Lamb et al. (2009)

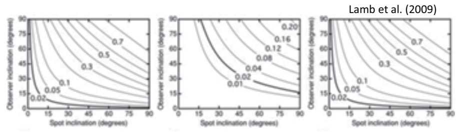

fundamental First overtone total

- Small amplitudes
- Sinusoidal pulse shapes
- Variable oscillation amplitudes

This model can explain all properties of observations !

model

Parameters in Spot-model

Mass: M
Radius: R
Spin frequency: f_{NS}
Observer inclination: i_o
Spot position: i_s
Spot radius: s_r
➢1 spot
➢Blackbody radiation

Curvature of space-time (Mass, Radius)

→ observable (Spin frequency)

assumption (1 spot, Blackbody radiation)

RS model (new model)

•Spot model
•R-mode model
•R-modes are excited by gravitational wave radiation (Andersson 1998; Friedman & Morsink 1998)
•RS model
R mode plus hot Spot model

We examine some properties observed from AMXPs

Core r-mode

Lee (2009)

Neutron star model composed of fluid ocean, solid crust, fluid core

Rotating and magnetized neutron star

We consider the amplitudes at the surface of the star

Contribution to light curves

1. Temperature perturbation on the surface
2. Periodic disturbance to the hot spot

Temperature perturbation on the surface

$l' = m = 1$ $\boxed{l' = m = 2}$

l': spherical harmonic degree
m: azimuthal wave number

$$T = T_0\{1 + A_c f(\theta)\cos(m\phi + \sigma t)\}$$

The frequency of r-mode in inertial frame

$$\sigma = -\frac{4}{3}\Omega - \delta$$

$T_0 = 1$

$A_c = 0.05$

T_0 mean temperature of the surface

A_c Fractional amplitude of temperature perturbation due to r-mode

Pattern by f(θ)cos2 Φ

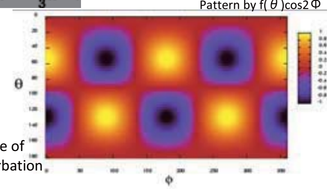

Result light curves

R-mode model
M=1.4 M_{sun}
R=16.4 km
f_{NS}=600 Hz

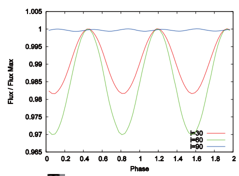

RS model
M=1.4 M_{sun} is=40°
R=16.4 km sr=20°
f_{NS}=600 Hz Th=1.02

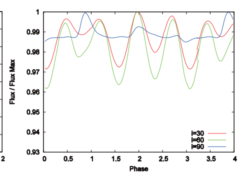

RS model
M=1.4 M_{sun} is=10°
R=16.4 km sr=20°
f_{NS}=600 Hz Th=1.02

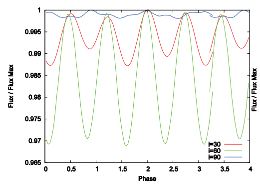

RS model
M=1.4 M_{sun} io=60°
R=16.4 km sr=20°
f_{NS}=600 Hz Th=1.02

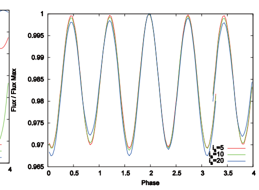

T_h:temperature ratio of the hot spot to the mean surface temperature

RS model
M=1.4 M_{sun}
R=16.4 km
f_{NS}=600 Hz
is=40°
sr=20°
Th=1.05,
1.15,
1.5,
2.1,
4.2,
10.5

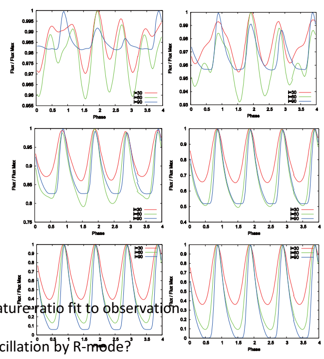

•What do the temperature ratio fit to observation from AMXP?
•Can we detect the oscillation by R-mode?

RS model
M=1.4 M_{sun} io=60°
R=16.4 km sr=20°
f_{NS}=600 Hz

Th=2.1

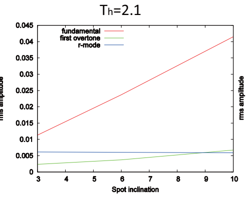

Th=4.2

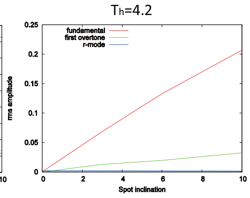

Contribution to light curves

1. Temperature perturbation on the surface
2. Periodic disturbance to the hot spot

radial component / horizontal and toroidal components

around the spin axis
The hot spot near spin axis can drift !

η : angular radius of circular path
ξ : angular velocity of the spot along the circular path
i_c : angular distance from the spin axis of the center of the circular path

Lamb et al. (2008)

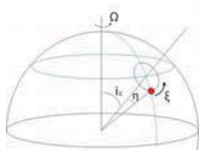

RS model

$T_0 = 1$

$A_c = 0.05$

$T_h = 10.5$

Conclusions

1. temperature perturbation on the surface (Ac=0.05)
   - We can detect the amplitudes of the oscillation by r-mode in Th≦2.
   - The light curves calculated by RS model become similar to those by Spot model when Th≧4.
2. Periodic disturbance to the hot spot
   We can detect the oscillation in η ≧1
   If we detect the oscillation, it will become to an evidence that the l'=m=2 core r-mode is excited by the gravitational radiation.

M=1.4 M_{sun} io=30°
R=16.4 km sr=20°
f_{NS}=600 Hz ξ=4Ω/3

η =0.5°

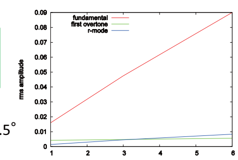

ic

η =1°

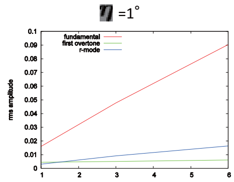

ic

η =3°

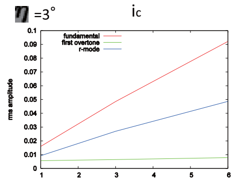

ic

CMB bispectrum from the second-order cosmological perturbations

●Daisuke Nitta (Astronomy D3), Eiichiro Komatsu (the university of Texas at Austin), Nicola Bartrolo (Universita di Padova), Sabino Matarrese (Universita di Padova), Antonio Riotto (CERN).

・Motivation

Detecting the primordial non-gaussianity.

But・・・

We need to deal with the following effects appropriately.

・Primordial non-gaussianity (via inflation etc.)

・The non-linear evolution of the temperature anisotropies via the photon-electron interaction and gravitaty.
→ 2nd-order Boltsmann equations and Einstein equation. ← our work

・Others (non-gaussianity via week lensing etc.)

・2nd order Boltsmann eq.

(Bartoro et al 2006 I,II pitrou et al 2008, 2009)

The photon's distribution function

$$f(\mathbf{x},p,\mathbf{n},\eta)=2\left[exp\frac{p}{T(\eta)e^{\Theta}}-1\right]^{-1}$$

We introduce

$$\Delta^{(i)}(\mathbf{x},\mathbf{n},\eta)=\frac{\int dpp^3 f^{(i)}}{\int dpp^3 f^{(0)}}$$

Relations between Δ and temperature fluctuation Θ are given by

$$\Delta^{(1)}=4\Theta^{(1)}$$
$$\Delta^{(2)}=4\Theta^{(2)}+16[\Theta^{(1)}]^2$$

The Boltsmann equations for each order are

$$\Delta^{(1)\prime}+ik\mu\Delta^{(1)}-\tau'\Delta^{(1)}=S^{(1)}(\mathbf{k},\mathbf{n},\eta)$$
$$\Delta^{(2)\prime}+ik\mu\Delta^{(2)}-\tau'\Delta^{(2)}=S^{(2)}(\mathbf{k},\mathbf{n},\eta)$$

Integral solution:

$$\Delta^{(i)}(\mathbf{k},\mathbf{n},\eta)=\int_0^{\eta_0}d\eta S^{(i)}(\mathbf{k},\mathbf{n},\eta)e^{ik\mu(\eta-\eta_0)-\tau}$$

・Angular averaged bispectrum

We may observe the primordial bispectrum as the temperature anisotropies

The spherical harmonic coefficients of temperature anisotropy: $a_{lm}=\int d^2\hat{n}Y^*_{lm}(\hat{n})\frac{\Delta T(\hat{n})}{T}$

Due to the rotational symmetry

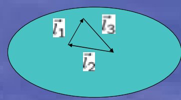

2-poit correlation

$$\langle a_{l_1m_1}a_{l_2m_2}\rangle=(-1)^{m_1}\delta_{l_1l_2}\delta_{-m_1m_2}C_{l_1}$$

C_{l_1} : angular power spectrum

3-point correlation

$$\langle a_{l_1m_1}a_{l_2m_2}a_{l_3m_3}\rangle=\begin{pmatrix} l_1 & l_2 & l_3\\ m_1 & m_2 & m_3\end{pmatrix}B_{l_1l_2l_3}$$

Wigner 3j symbol

$B_{l_1l_2l_3}$: angular averaged bispectrum

$$B_{l_1l_2l_3}=\tilde{B}_{l_1l_2l_3}-3I_{l_1l_2l_3}(C_{l_1}C_{l_2}+cyclic)$$

・Analytic formula of $B_{l_1l_2l_3}$

The 1st-order: $a^{(1)}_{lm}=4\pi(-i)^l\int\frac{d^3k}{(2\pi)^3}g_l(k)Y^*_{lm}(\hat{\mathbf{k}})\zeta(\mathbf{k})$ → $S^{(1)}_{lm}(\mathbf{k})$

The 2nd-order: We assume the source terms are convolution of two curvature perturbations.

$$S^{(2)}_{lm}(\mathbf{k})=\int\frac{d^3k'}{(2\pi)^3}\int d^3k''\delta^3(\mathbf{k}'+\mathbf{k}''-\mathbf{k})S^{(2)}_{lm}(\mathbf{k}',\mathbf{k}'',\mathbf{k})\zeta(\mathbf{k}')\zeta(\mathbf{k}'')$$

$$a^{(2)}_{lm}=\frac{4\pi}{8}(-i)^l\int\frac{d^3k}{(2\pi)^3}\int\frac{d^3k'}{(2\pi)^3}\int d^3k''\delta^3(\mathbf{k}'+\mathbf{k}''-\mathbf{k})\sum_{l'm'}F^{l'm'}_{lm}(\mathbf{k}',\mathbf{k}'',\mathbf{k})Y^*_{l'm'}(\hat{\mathbf{k}})\zeta(\mathbf{k}')\zeta(\mathbf{k}'')$$

The bispectrum is given by

$$\langle a^{(1)}_{l_1m_1}a^{(1)}_{l_2m_2}a^{(2)}_{l_3m_3}\rangle=\frac{(-i)^{l_1+l_2+l_3}}{(2\pi)^3}\sum_{L_3M_3}\prod\int d^3k_i\delta^3(\sum\mathbf{k}_i)Y^*_{l_1m_1}(\hat{\mathbf{k}}_1)Y^*_{l_2m_2}(\hat{\mathbf{k}}_2)Y^*_{L_3M_3}(\hat{\mathbf{k}}_3)$$
$$\times g_{l_1}(k_1)g_{l_2}(k_2)P_\zeta(k_1)P_\zeta(k_2)\{F^{L_3M_3}_{l_3m_3}(\mathbf{k}_1,\mathbf{k}_2,\mathbf{k}_3)+F^{L_3M_3}_{l_3m_3}(\mathbf{k}_2,\mathbf{k}_1,\mathbf{k}_3)\}$$

Performing the integral over angles

We obtain

$$\tilde{B}_{l_1l_2l_3}=\frac{4}{\pi^2}\sum_{\mathrm{all}\,l'\lambda}i^{l_3-l'_3+R}I_{l'_1l'_2l'_3}I_{l_1l'_1\lambda_1}I_{l_2l'_2\lambda_2}I_{l_3l'_3\lambda_3}\begin{Bmatrix} l_1 & l_2 & l_3\\ l'_1 & l'_2 & l'_3\\ \lambda_1 & \lambda_2 & \lambda_3\end{Bmatrix}\sqrt{\frac{4\pi}{\prod_i(2\lambda_i+1)}}$$
$$\times\int dr r^2\prod_{i=1}^{3}\int dk_i k_i^2 P_\zeta(k_i)j_{l'_i}(rk_i)\ldots S_{\lambda_1\lambda_2\lambda_3}(k_1,k_2,k_3,r')+\mathrm{perm}$$

where $I_{l_1l_2l_3}\equiv\sqrt{\frac{(2l_1+1)(2l_2+1)(2l_3+1)}{4\pi}}\begin{pmatrix} l_1 & l_2 & l_3\\ 0 & 0 & 0\end{pmatrix}$

The Wigner 9j symbol

$\begin{Bmatrix} l_1 & l_2 & l_3\\ l'_1 & l'_2 & l'_3\\ \lambda_1 & \lambda_2 & \lambda_3\end{Bmatrix}$ If they satisfy the triangle conditions, then ≠0

We have defined the "angular-averaged source function"

$$S_{\lambda_1\lambda_2\lambda_3}(k_1,k_2,k_3)=i^{\lambda_1+\lambda_2}\sqrt{\frac{2\lambda_1+1}{4\pi}}\sqrt{\frac{2\lambda_2+1}{4\pi}}\sum_{\mu_i}\begin{pmatrix}\lambda_1 & \lambda_2 & \lambda_3\\ \mu_1 & \mu_2 & \mu_3\end{pmatrix}$$
$$\times\int d^2\hat{\mathbf{k}}_1\int d^2\hat{\mathbf{k}}_2 Y^*_{\lambda_1\mu_1}(\hat{\mathbf{k}}_1)Y^*_{\lambda_2\mu_2}(\hat{\mathbf{k}}_2)S_{\lambda_3\mu_3}(\mathbf{k}_1,\mathbf{k}_2,\mathbf{k}_3)$$

If we can know the 2nd-order source terms, then we can calculate the bispectrum.

The 2nd-order source terms (Bartoro et al 2006 I)

$$S_{lm}(\mathbf{k},\eta)=(4\Phi^{(2)\prime}-\tau'\Delta^{(2)}_{00})\delta_{l0}\delta_{m0}+4k\Phi^{(2)}\delta_{l1}\delta_{m0}-8\omega'_m\delta_{l1}-4\tau'v^{(2)}_m\delta_{l1}-\frac{\tau'}{10}\Delta^{(2)}_{2m}\delta_{l2}-4\chi'_m\delta_{l2}$$
$$+\int\frac{d^3k_1}{(2\pi)^3}\Big\{-2\tau'[(\delta^{(1)}_e+\Phi^{(1)})(\mathbf{k}_1)\Delta^{(1)}_0(\mathbf{k}_2)+2iv^{(1)}_0(\mathbf{k}_1)\Delta^{(1)}_1(\mathbf{k}_2)]\delta_{l0}\delta_{m0}$$
$$+4k\Phi^{(1)}(\mathbf{k}_1)\Phi^{(1)}(\mathbf{k}_2)\delta_{l1}\delta_{m0}+\tau'[(\delta^{(1)}_e+\Phi^{(1)})(\mathbf{k}_1)\Delta^{(1)}_2(\mathbf{k}_2)-2v^{(1)}(\mathbf{k}_1)\Delta^{(1)}_1(\mathbf{k}_2)]\delta_{l2}\delta_{m0}$$
$$+[8\Phi^{(1)\prime}(\mathbf{k}_1)+2\tau'(\delta^{(1)}_e+\Phi^{(1)})(\mathbf{k}_1)]\Delta^{(1)}_{l0}(\mathbf{k}_2)\delta_{m0}\Big\}$$
$$-\int\frac{d^3k_1}{(2\pi)^3}\hat{\mathbf{k}}_1\cdot\hat{\mathbf{k}}_2[2\tau'v^{(1)}_0(\mathbf{k}_1)v^{(1)}_0(\mathbf{k}_2)\delta_{l0}-i(-i)^{-l}(2l+1)k_1(\Psi^{(1)}+\Phi^{(1)})(\mathbf{k}_1)$$
$$\times\sum_L(2L+1)\Delta^{(1)}_L(\mathbf{k}_2)\int d\mu P_l(\mu)\frac{\partial P_L(\mu)}{\partial\mu}\delta_{m0}$$
$$-2\left[4\Phi^{(1)}\nabla\Phi^{(1)}+4\tau'(\delta^{(1)}_e+\Phi^{(1)})\mathbf{v}+3\tau'\Delta^{(1)}_0\mathbf{v}-\tau'\Delta^{(1)}_2\mathbf{v}\right]_m\delta_{l1}$$
$$+i(-i)^{-l}(-1)^{-m}(2l+1)\sum_{l'}\sum_{m'=-1}^{1}(2l'+1)\begin{pmatrix} l' & 1 & l\\ 0 & 0 & 0\end{pmatrix}\begin{pmatrix} l' & 1 & l\\ 0 & m' & -m\end{pmatrix}$$
$$\times\left[\ldots\Delta^{(1)}_{l'}\nabla\Phi^{(1)}+2(\Phi^{(1)}+\Phi^{(1)})\nabla\Delta^{(1)}_{l'}+3\tau'\Delta^{(1)}_{l'}\mathbf{v}+\ldots\tau'\Delta^{(1)}_2\mathbf{v}\right]_{m'}$$
$$+14\tau'(-i)^{-l}(-1)^{-m}(2l+1)\sum_{m',m''=-1}^{1}\begin{pmatrix} 1 & 1 & l\\ 0 & 0 & 0\end{pmatrix}\begin{pmatrix} 1 & 1 & l\\ m' & m'' & -m\end{pmatrix}$$
$$\times\frac{4\pi}{3}\int\frac{d^3k_1}{(2\pi)^3}v^{(1)}_0(\mathbf{k}_1)v^{(1)}_0(\mathbf{k}_2)Y^*_{1m'}(\hat{\mathbf{k}}_1)Y^*_{1m''}(\hat{\mathbf{k}}_2)$$
$$-2i(-i)^{-l}\sqrt{\frac{2l+1}{4\pi}}\sum_{m',m''=-1}^{1}\sum_L(2L+1)\int d^2\hat{n}Y_{1m'}(\hat{n})Y_{1m''}(\hat{n})Y^*_{lm}(\hat{n})\frac{\partial P_L(\hat{n}\cdot\hat{\mathbf{k}}_2)}{\partial(\hat{n}\cdot\hat{\mathbf{k}}_2)}$$
$$\times\left(\frac{4\pi}{3}\right)^2\int\frac{d^3k_1}{(2\pi)^3}k_1(\Phi^{(1)}+\Phi^{(1)})(\mathbf{k}_1)\Delta^{(1)}_L(\mathbf{k}_2)Y^*_{1m'}(\hat{\mathbf{k}}_1)Y^*_{1m''}(\hat{\mathbf{k}}_2).$$

These terms only

Calculating $S_{\lambda_1\lambda_2\lambda_3}(k_1,k_2,k_3)$ for products of first-order

These are non-zero only four cases

$$S_{000}=4i\tau'v_0(k_1)\Delta_1(k_2)+8\Psi'(k_1)\Delta_0(k_2),$$
$$S_{110}=\frac{4}{\sqrt{3}}\{-5\tau'v_0(k_1)v_0(k_2)+2k_1(\Psi+\Phi)(k_1)\tilde{\Delta}(k_2)\},$$
$$S_{101}=2i\sqrt{3}\{\tau'v_0(k_1)(4\delta_e+4\Phi+2\Delta_0-\Delta_2)(k_2)$$
$$+4k_1\Phi(k_1)(\Delta_0-\Psi)(k_2)+k_1\Delta_0(k_1)(\Psi+\Phi)(k_2)\},$$
$$S_{112}=2\sqrt{\frac{10}{3}}\{7\tau'v_0(k_1)v_0(k_2)-k_1(\Psi+\Phi)(k_1)\tilde{\Delta}(k_2)\}.$$

S does not depend on k_3. This property enable us to integrate the analytic formula of the bispectrum over k_3

$$\tilde{B}_{l_1l_2l_3}=\frac{2}{\pi}\sum_{\mathrm{all}\,l'\lambda}i^{l_3-l'_3+R}I_{l'_1l'_2l'_3}I_{l_1l'_1\lambda_1}I_{l_2l'_2\lambda_2}I_{l_3l'_3\lambda_3}\begin{Bmatrix} l_1 & l_2 & l_3\\ l'_1 & l'_2 & l'_3\\ \lambda_1 & \lambda_2 & \lambda_3\end{Bmatrix}\sqrt{\frac{4\pi}{\prod_i(2\lambda_i+1)}}$$
$$\times\int dre^{-\tau}\prod_{i=1}^{2}\int dk_ik_i^2P_\zeta(k_i)j_{l'_i}(rk_i)g_{l_i}(k_i)S_{\lambda_1\lambda_2\lambda_3}(k_1,k_2)+perm.$$

・χ^2 minimization

Minimize: $$\chi^2\equiv\sum_{2\le l_1\le l_2\le l_3}\frac{\left(B^{obs}_{l_1l_2l_3}-\sum_i A_iB^{(i)}_{l_1l_2l_3}\right)^2}{\sigma^2_{l_1l_2l_3}}$$ i=2nd, local

$$\sigma_{l_1l_2l_3}\equiv\langle B^2_{l_1l_2l_3}\rangle-\langle B_{l_1l_2l_3}\rangle^2\approx C_{l_1}C_{l_2}C_{l_3}\Delta_{l_1l_2l_3}$$

We only consider ideal cosmic-variance.

Fisher matrix: $$F_{ij}\equiv\sum_{2\le l_1\le l_2\le l_3}\frac{B^{(i)}_{l_1l_2l_3}B^{(j)}_{l_1l_2l_3}}{\sigma^2_{l_1l_2l_3}}$$

The Fisher matrix are Sumed up to $l_3=l_{max}$

○Results

・Shapes

2nd-order Boltsmann eq. $\quad\frac{l_1l_2}{(2\pi)^2}\times\frac{B_{l_1l_2l_3}}{I_{l_1l_2l_3}}\quad l_1\le l_2\le l_3$

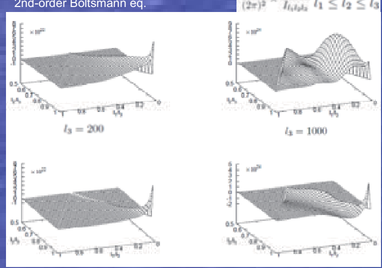

Signal-to-noise ratio

$$\left(\frac{S}{N}\right)_i=\frac{1}{\sqrt{F^{-1}_{ii}}}$$

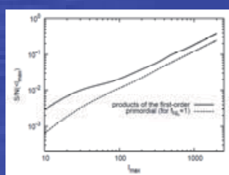

S/N=0.38 (lmax=2000)

Cross-correlation coefficient

$$r_{ij}\equiv\frac{F_{ij}}{\sqrt{F_{ii}F_{jj}}}$$

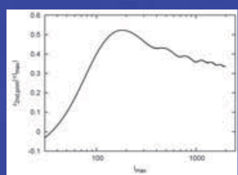

$r_{2nd,local}$=0.5 (lmax～200)

・contamination

Minimize the following function: $$\sum_{2\le l_1\le l_2\le l_3}\frac{\left(f_{NL}B^{prim}_{l_1l_2l_3}-B^{2nd}_{l_1l_2l_3}\right)^2}{\sigma^2_{l_1l_2l_3}}$$

We define f_{NL}: $$f^{con}_{NL}=\frac{1}{N}\sum_{2\le l_1\le l_2\le l_3}\frac{B^{2nd}_{l_1l_2l_3}B^{prim}_{l_1l_2l_3}}{\sigma^2_{l_1l_2l_3}}\qquad N=\sum_{2\le l_1\le l_2\le l_3}\frac{B^{prim\,2}_{l_1l_2l_3}}{\sigma^2_{l_1l_2l_3}},$$

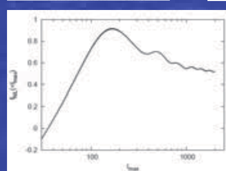

fNL=0.9 (lmax=200)

○Summary

・We obtain the general formula of the CMB angular averaged bispectrum.
・The bispectrum has maximum signal in the squeezed triangles, similar to the local-type primordial bispectrum.
・However, detailed calculations show that their shapes are sufficiently different
・We conclude that the product of the first-order terms may be safely ignored in analysis of the future CMB experiments.

GENERAL PROPERTIES OF NON-RADIAL PULSATIONS (NRP): EFFECTS OF ROTATION

APRILIA

ASTRONOMY, D3, TOHOKU UNIVERSITY

INTRODUCTION

A star's pulsation is NRP if the oscillation is in such a way as to deviate from its spherical shape. NRP is characterized by *n* (number of nodes of eigenfunctions between the center and surface of star), ℓ (number of surface nodal lines), and *m* (number of such lines that pass through the star's rotation axis), which correspond to the spherical harmonics $Y_\ell^m(\theta,\varphi)$. In the observer's co-rotating frame, waves with $m < 0$, propagating in the same direction to star's rotation, are called *prograde* modes; those with $m > 0$, traveling in the opposite direction to rotation, are called *retrograde* modes.

Here we analyze the NRP of a $4M_\odot$ star to see the effects of rotation to the stability of gravity modes (*g*-modes) at the zero-age main sequence evolution stage. The rotation effects are in the form of the Coriolis force, as the first effect of rotation, and the Centrifugal force (hence the rotational equilibrium deformation) as the second effects of rotation. The $4M_\odot$ itself is an SPB (Slowly Pulsating B-type star) which shows NRP of high-order (*n*) *g*-modes.

CALCULATION METHOD

By employing a series expansion in terms of the $Y_\ell^m(\theta,\varphi)$. Modes with $\ell = |m|+2(j-1)$ are defined as even modes, while $\ell = |m|+2j-1$ are odd modes with $j = 1,2,\ldots$

$$\xi_a = a\sum_{\ell\ge|m|} S_\ell(a)Y_\ell^m(\theta,\varphi)e^{i\sigma t}$$

$$\xi_\theta = a\sum_{\ell\ge|m|}\left[H_\ell(a)\frac{\partial}{\partial\theta}Y_\ell^m(\theta,\varphi)+T_{\ell'}(a)\frac{1}{\sin\theta}\frac{\partial}{\partial\varphi}Y_{\ell'}^m(\theta,\varphi)\right]e^{i\sigma t}$$

$$\xi_\varphi = a\sum_{\ell\ge|m|}\left[H_\ell(a)\frac{1}{\sin\theta}\frac{\partial}{\partial\varphi}Y_\ell^m(\theta,\varphi)-T_{\ell'}(a)\frac{\partial}{\partial\theta}Y_{\ell'}^m(\theta,\varphi)\right]e^{i\sigma t}$$

RESULTS & CONCLUSIONS

Slow Rotation

The complex eigenfrequency ω is approximated by

$$\omega = \omega_0 + mC_1\Omega + C_2\Omega^2$$

where ω_0 is eigenfrequency of mode at $\Omega = 0$. Modes with $\omega_I < 0$ are unstable. For $\Omega > 0$, if $C_{1l} > 0$, the retrograde modes are stabilized and prograde modes are destabilized by rotation; if $C_{2l} > 0$, both retrograde and prograde modes are stabilized by rotation.

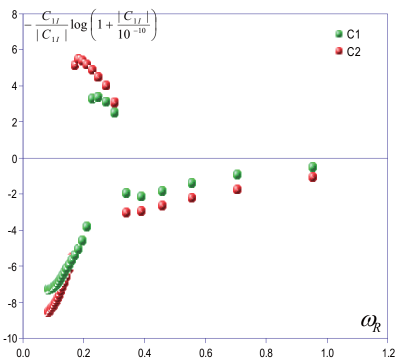

The first and second order effects of rotation work both for destabilizing and stabilizing the oscillation modes, but only a few modes can change their stabilities as a result of the second order effects.

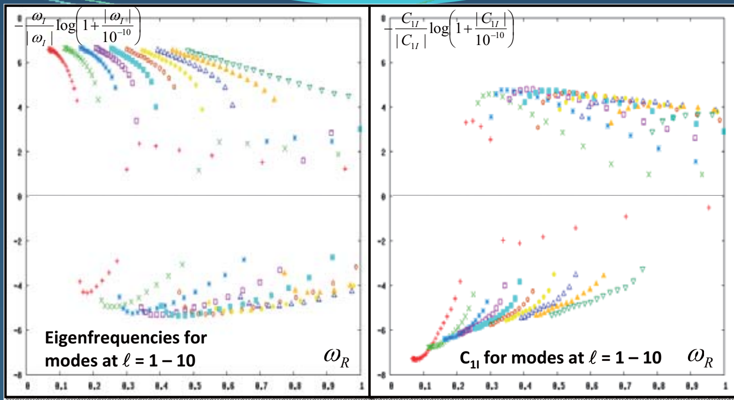

If without rotation, most of the high-order *g*-modes are stable modes, while the unstable modes are in the certain range of ω of the low-order *g*-modes.

When rotation is included, C_{1l} of the high-order *g*-modes are negative, mean that the retrograde modes are destabilized and prograde modes are stabilized by rotation. Unstable modes are only found at $\ell < 10$.

Rapid Rotation

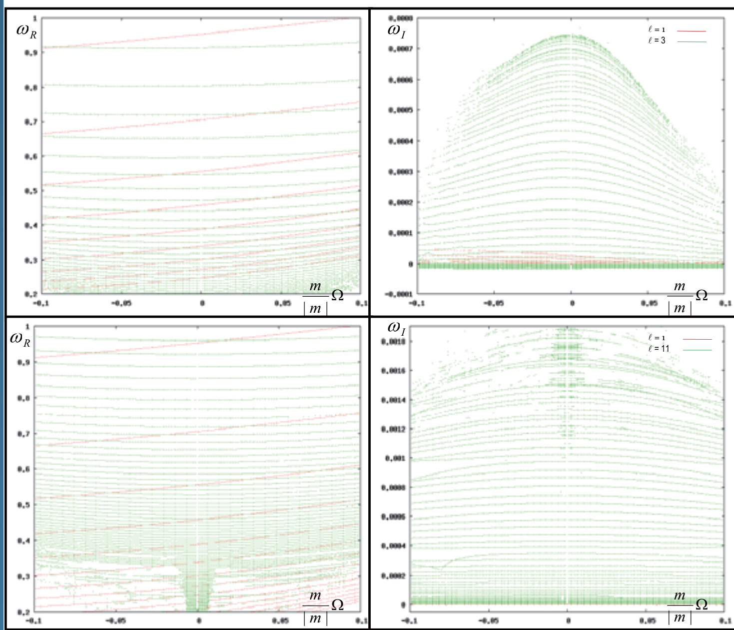

As Ω increases, many avoided crossings occur between the modes as can be seen in the behavior of ω_R. At the crossings, the mode properties are exchanged between the modes, as is shown by the behavior of ω_I. Only modes with not so different ℓ–values can cross (e.g. $\ell = 1$ & $\ell = 3$) because the different of their ω_Is are not very large.

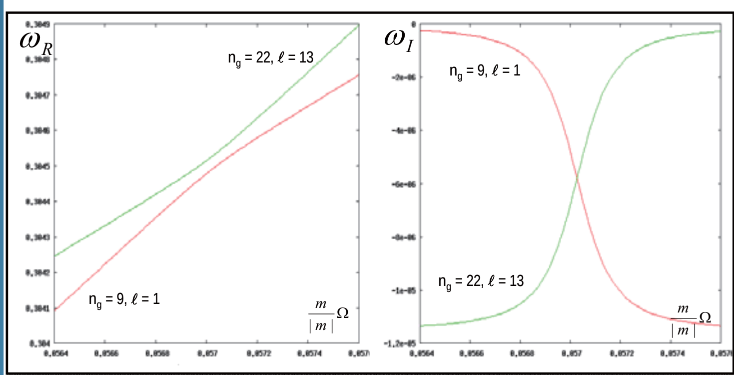

Example of avoided crossing: $n_g = 9$ $\ell = 1$ & $n_g = 22$ $\ell = 3$

A Study on Mathematical Fuzzy Logic

Ahmad Termimi Bin Ab Ghani

1. Preliminaries

Fuzzy logic is understood a logic with *comparative notion of truth*, the standard set of truth values is $[0,1]$. A *t-norm* is a binary operation $*$ in $[0,1]$ which is commutative, associative, non-decreasing and satisfying $0 * x = 0$ and $1 * x = x$ for each x. Each continuous *t*-norm $*$ determines uniquely its *reduum* $\Rightarrow$ satisfying, $\forall x, y, z$, the condition

$$z \leq x \Rightarrow y \text{ iff } x * z \leq y \qquad (*)$$

Three most important continuous *t*-norms are

name	$x+y$	$x \Rightarrow y$ for $x > y$	$\neg x \Rightarrow 0$
Ł	$\max(0, x+y-1)$	$1-x+y$	$1-x$
G	$\min(x,y)$	y	$\begin{cases} 1 \text{ for } x = 0 \\ 0 \text{ for } x > 0 \end{cases}$
Π	$x \cdot y$	y/x	

2. Basic Fuzzy Logic and three stronger systems

The following formulas are *axioms* of the logic BL

(A1) $(\varphi \to \psi) \to \big((\psi \to \chi) \to (\varphi \to \chi)\big)$

(A2) $(\varphi \& \psi) \to \varphi$

(A3) $(\varphi \& \psi) \to (\psi \& \varphi)$

(A4) $\big(\varphi \& (\varphi \to \psi)\big) \to \big(\psi \& (\psi \to \varphi)\big)$

(A5a) $\big(\varphi \to (\psi \to \chi)\big) \to \big((\varphi \& \psi) \to \chi\big)$

(A5b) $\big((\varphi \& \psi) \to \chi\big) \to \big(\varphi \to (\psi \to \chi)\big)$

(A6) $\big((\varphi \to \psi) \to \chi\big) \to \Big(\big((\psi \to \varphi) \to \chi\big) \to \chi\Big)$

(A7) $\overline{0} \to \varphi$

Łukasiewicz logic Ł is BL plus the axiom of double negation $\neg\neg\varphi \to \varphi$; Gödel logic G is BL plus the axiom of idempotence of conjunction $\varphi \to (\varphi \& \varphi)$; Product logic Π, originally introduced in [1], is defined in [2] as the extension of BL by axiom $\neg\neg\varphi \to \big((\varphi \to (\varphi \& \psi)\big) \to (\psi \& \neg\neg\psi))$.

General algebras of truth functions for BL are called *BL-algebras*. A BL-algebras is a structure $\mathbf{L} = (L, \cap, \cup, *, \Rightarrow, 0, 1)$ with several properties. The axioms A1-A7 are $\mathbf{L}$-tautologies for any BL-algebra $\mathbf{L}$. If $*$ is a continuous *t*-norm and $\Rightarrow$ its residuum then $([0,1], \min, \max, *, \Rightarrow, 0, 1)$ is a particular linearly ordered BL-algebra $[0,1]_*$ given by $*$ (called *t*-algebras or standard BL-algebras). The standard MV-algebra (G-algebra, Π-algebra) is just $[0,1]_*$ where $*$ is Ł (G, Π) *t*-norm. Let now $\mathcal{C}$ stand for BL, Ł, G, Π, let $\mathcal{C}$-algebras be BL, MV, G and Π-algebras respectively.

General completeness theorem. For each formula φ, following are equivalent: (i) φ is provable in $\mathcal{C}$, (ii) for each $\mathcal{C}$-algebra $\mathbf{L}$, φ is an $\mathbf{L}$-tautology, (iii) for each linearly ordered $\mathcal{C}$-algebra $\mathbf{L}$, φ is an $\mathbf{L}$-tautology

3. Computational complexity

Follows are survey on fuzzy propositional calculi. We consider four sets of formulas as:

$SAT_1^{\mathcal{C}} = \{\varphi | \text{for some } \mathbf{L}\text{-evaluation } e, e_{\mathcal{C}}(\varphi) = 1\}$
$SAT_{pos}^{\mathcal{C}} = \{\varphi | \text{for some } \mathbf{L}\text{-evaluation } e, e_{\mathcal{C}}(\varphi) > 1\}$
$TAUT_1^{\mathcal{C}} = \{\varphi | \text{for each } \mathbf{L}\text{-evaluation } e, e_{\mathcal{C}}(\varphi) = 1\}$
$TAUT_{pos}^{\mathcal{C}} = \{\varphi | \text{for each } \mathbf{L}\text{-evaluation } e, e_{\mathcal{C}}(\varphi) > 1\}$

Summarizing, we have the following:

(1) $SAT_1^G = SAT_{pos}^G = SAT_1^{\Pi} = SAT_{pos}^{\Pi} = SAT_1^{Bool}$ is NP-complete.

(2) $TAUT_{pos}^G = TAUT_{pos}^{\Pi} = TAUT^{Bool}$ is co-NP-complete.

(3) $TAUT_1^G, TAUT_1^{\Pi}, TAUT_1^{Bool}$ are pairwise distinct and all co-NP-complete.

(4) $SAT_{pos}^{Ł} \supset SAT_1^{Ł} \supset SAT^{Bool}$, all NP-complete.

(5) $TAUT_1^{Ł} \subset TAUT_{pos}^{Ł} \subset TAUT^{Bool}$, are co-NP-complete.

3. Predicate Fuzzy Logic and three stronger systems

A *standard interpretation* of the language is a structure $\mathbf{M} = (M, (r_P)_P, (m_c)_c)$ where each $m_c \in M$ and for each n-ary predicate P, $r_P: M^n \to [0,1]$. An $\mathbf{L}$-interpretation over BL is a structure as above but r_P is an $\mathbf{L}$-fuzzy relation, i.e. $r_P: M^n \to L$. The *truth value* $\|\varphi\|_{\mathbf{M},v}^{\mathbf{L}}$ of a formula φ, is given by BL-algebra $\mathbf{L}$, an $\mathbf{L}$-interpretation $\mathbf{M}$ and an evaluation v assigning to each variable x an element $v(x) \in M$.

$\|P(u_1, \dots, u_n)\|_{\mathbf{M},v}^{\mathbf{L}} = r_P\big(v(u_1), \dots, v(u_n)\big)$,
$\|\varphi \to \psi\|_{\mathbf{M},v}^{\mathbf{L}} = \|\varphi\|_{\mathbf{M},v}^{\mathbf{L}} \Rightarrow \|\psi\|_{\mathbf{M},v}^{\mathbf{L}}$, similarly &,$*$,
$\|(\forall x)\varphi\|_{\mathbf{M},v}^{\mathbf{L}} = \inf\{\|\varphi\|_{M,v'}^{L} | v' \equiv_x v\}$, similarly $\exists$,sup

where $v' \equiv_x v$ means that $v'(y) = v(y)$ for all variables y except possibly x. The $\mathbf{L}$-interpretation $\mathbf{M}$ is *safe* if $\|\varphi\|_{\mathbf{M},v}^{\mathbf{L}}$ is defined for all φ and v. Let $\mathcal{C}\forall$ be BL$\forall$, Ł$\forall$, $G\forall$, $\Pi\forall$.

General completeness theorem. For each theory T and formula φ, $T \vdash_{\mathcal{C}\forall} \varphi$ iff for each linearly ordered $\mathcal{C}$-algebra $\mathbf{L}$ and each $\mathbf{L}$-model $\mathbf{M}$ of T, φ is $\mathbf{L}$-true in $\mathbf{M}$. In particular, $\mathcal{C}\forall \vdash \varphi$ iff for each $\mathcal{C}$-algebra $\mathbf{L}$, φ is an $\mathbf{L}$-tautology.

4. Arithmetical complexity

We interested in arithmetical complexity of sets of predicate tautologies and sets of satisfiable formulas.

$TAUT^{\mathcal{C}} = \{\varphi | \text{for all standard } \mathcal{C} \text{ algebras } \mathbf{L} \text{ and } \mathbf{L}\text{-safe } \mathbf{M}, \|\varphi\|_{\mathbf{M}}^{\mathbf{L}} = 1\}$
$genTAUT^{\mathcal{C}} = \{\varphi | \text{for all } \mathcal{C} \text{ algebras } \mathbf{L} \text{ and } \mathbf{L}\text{-safe } \mathbf{M}, \|\varphi\|_{\mathbf{M}}^{\mathbf{L}} = 1\}$
$SAT^{\mathcal{C}} = \{\varphi | \text{for some standard } \mathcal{C} \text{ algebras } \mathbf{L} \text{ and } \mathbf{L}\text{-safe } \mathbf{M}, \|\varphi\|_{\mathbf{M}}^{\mathbf{L}} = 1\}$
$genSAT^{\mathcal{C}} = \{\varphi | \text{for some } \mathcal{C} \text{ algebras } \mathbf{L} \text{ and } \mathbf{L}\text{-safe } \mathbf{M}, \|\varphi\|_{\mathbf{M}}^{\mathbf{L}} = 1\}$

The results are summarized in the following table.

	Provable = gen.TAUT	stand. TAUT	gen. SAT = consistent	stand. SAT
BL$\forall$	Σ_1-compl.	Π_2-hard	Π_1-compl.	Not Arithm.
Ł$\forall$	Σ_1-compl.	Π_2-compl.	Π_1-compl.	Π_1-compl.
$G\forall$	Σ_1-compl.	Σ_1-compl.	Π_1-compl.	Π_1-compl.
$\Pi\forall$	Σ_1-compl.	Π_2-hard	Π_1-compl.	Not Arithm.

Since by completeness theorem general tautologies coincide with provable formulas, $genTAUT^{\mathcal{C}}$ is evidently Σ_1; Σ_1-completeness is proved in [3]. Similarly, general satisfiability coincide with consistence; thus $genSAT^{\mathcal{C}}$ is Π_1-complete. $TAUT^{Ł\forall}$ being Π_2-complete is a classical result of Ragaz. The fact that $SAT^{\Pi\forall}$ is not arithmetical is proved in [3]. We found there are open problems concerning the arithmetical complexity on monadic logic [4].

Reference

[1] Hájek, P.; Godo, L.; Esteva, F., *A complete many-valued logic with product conjunction*, Arch. Math. Logic, 35 (1996), 191-208.
[2] Hájek, P., *Metamathematics of fuzzy logic*. Kluwer 1998.
[3] Hájek, P., *Fuzzy logic and arithmetical hierarchy III*, Studia logica, 68 (2001), 129-142.
[4] Hájek, P., *Monadic fuzzy predicate logic*, Studia logica, 71 (2002), 165-175.

Some space-time integrability estimates of the solution for heat equations in two dimension

Norisuke Ioku

Mathematical institute, Tohoku University, Japan

sa6m02@math.tohoku.ac.jp

Heat equation in 2-dimension

$$I = (0,T),\ \ \Omega \subset \mathrm{R}^2 : \text{bounded domain}$$

$$(\mathrm{H}) \quad \begin{cases} \partial_t u - \Delta u = f, & \text{in } \ I \times \Omega, \\ u = 0, & \text{on } I \times \partial\Omega, \\ u(0) = u_0, & \text{on } \{0\} \times \Omega. \end{cases}$$

Lorentz-Zygmund space

$$f \in L^p \log L^q(\Omega) \iff \int_{B_R} \left\{ \left(\log \frac{R}{|x|} \right)^q f^\sharp(x) \right\}^p dx < \infty$$

$f^\sharp$ is a symmetric-decreasing rearrangement of f. $|B_R| = |\Omega|$.

Remark $(q > 1,\ p > 0)$

$$L^q(\Omega) \subset L^1 \log L^p(\Omega) \subset L^1(\Omega)$$

Figure of $f^\sharp$

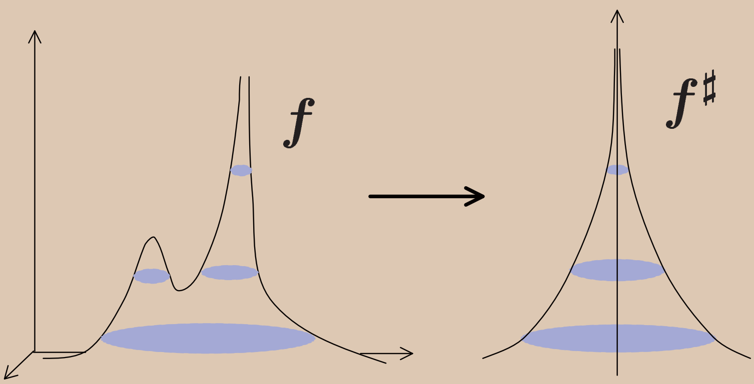

Known Results

Maximal regularity

Let $1 < p, q < \infty$. $\forall f \in L^q(I; L^p(\Omega))$, $\exists u \in W^{1,q}(I; L^p(\Omega)) \cap L^q(I; W^{2,p}(\Omega))$ s.t.

$$\|\partial_t u\|_{L^q(I;L^p)} + \|\Delta u\|_{L^q(I;L^p)} \le C\|f\|_{L^q(I;L^p)}$$

Harada-Nagai-Senba-Suzuki

Let $f \in L^\infty(I; L^1(\Omega))$, u : weak solution. Then $0 < \forall\alpha < 4\pi$, $\exists C > 0$ s.t.

$$\sup_{0<t<T} \int_\Omega \exp\left(\frac{\alpha |u(t,x)|}{\|f\|} \right) dx \le C|\Omega|.$$

PROBLEM

How about the regularity of a weak solution u for $f \in L^q(I; L\log L^p(\Omega))$?

Main Theorem

Definition (Orlicz space)

$$\exp L^p(\Omega) := \left\{ u \in L^1_{\mathrm{loc}};\ \|u\|_{\exp L^p(\Omega)} < \infty \right\},$$

where $\|u\|_{\exp L^p(\Omega)}$ is a Luxemburg norm.

Theorem1

Let $f \in L^q\left(I; L^1\log L^p\right)$, $u_0 \in L^q\log L^{p-1}$ $(0 < p \le 1, 1 < q < \infty) \Longrightarrow \exists u$ sol. s.t.

$$\sup_{0<t<T} \|u\|_{L^q\log L^{p-1}} + \|u\|_{L^q(I,\exp L^{\frac{1}{1-p}})} \le C\left(\|f\|_{L^q(I,L^1\log L^p)} + \|u_0\|_{L^q\log L^{p-1}} \right).$$

Theorem2

Let $f \in L^1\left(I; L^1\log L^p\right)$, $u_0 \in L^1\log L^p$ $(0 < p \le 1) \Longrightarrow \exists u$ sol. s.t.

$$\sup_{0<t<T} \|u\|_{L^1\log L^p} + \|u\|_{L^1(I,\exp L^{\frac{1}{1-p}})} \le C\left(\|f\|_{L^1(I,L^1\log L^p)} + \|u_0\|_{L^1\log L^p} \right).$$

Remark

Theorem 1,2 can not be obtained by a simple application of the estimate of the maximal regularity.

Lemma

Let $p \ge 1$, $u \in \exp L^p(\Omega)$. Then

$$\|u\|_{\exp L^p(\Omega)} \simeq \sup_{0<r<R} \frac{u^\sharp(r)}{\left(\log \frac{R}{r} + 1\right)^{1/p}}.$$

Proof of Theorem 1 (Outline)

- Step1 Use the differential inequality of $u^\sharp$

$$\partial_t u^{\sharp\sharp} - 2\frac{\partial_r u^\sharp}{r} \le f^{\sharp\sharp},$$

where $u^{\sharp\sharp}(r) := \frac{2}{r^2}\int_{B_r} u^\sharp(x)dx$.

- Step2 Test by $r\left(\log \frac{eR}{r}\right)^{(p-1)q} u^{\sharp\sharp q-1}$.

Well-posedness for Navier-Stokes equations in modulation spaces with negative derivative indices

Tsukasa Iwabuchi (Tohoku University)

Abstract. The Cauchy problems for Navier-Stokes equations are studied in modulation spaces $M^s_{q,\sigma}(\mathbb{R}^n)$. Our aim is to reveal the conditions of s, q and σ of $M^s_{q,\sigma}(\mathbb{R}^n)$ for the existence of local and global solutions for initial data in $M^s_{q,\sigma}(\mathbb{R}^n)$.

1 Modulation spaces $M^s_{q,\sigma}(\mathbb{R}^n)$

In this section, we define Modulation spaces $M^s_{q,\sigma}(\mathbb{R}^n)$ and introduce their properties.

Definition (Modulation spaces). $\{\varphi_k\}_{k\in\mathbb{Z}^n}$: partition of unity with $\operatorname{supp}\varphi_k \subset \{\ \xi \in \mathbb{R}^n \ \mid\ |\xi - k| \le \sqrt{n}\ \}$. For example, in the case of $\mathbb{R}^2$,

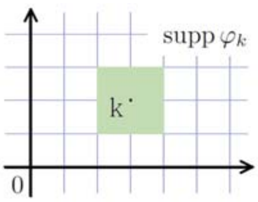

For $s \in \mathbb{R}, 1 \le q, \sigma \le \infty$,

$$M^s_{q,\sigma}(\mathbb{R}^n) := \left\{ f \in \mathcal{S}'(\mathbb{R}^n) \ \middle|\ \left(\sum_{k\in\mathbb{Z}^n} (1+|k|)^{s\sigma} \|\mathcal{F}^{-1}\varphi_k \mathcal{F} f\|^{\sigma}_{L^q(\mathbb{R}^n)} \right)^{\frac{1}{\sigma}} < \infty \right\}.$$

Proposition.[Feichtinger (1983), Toft (2004), Wang, Hudzik (2007)]

(i) $M^s_{q,\sigma}(\mathbb{R}^n) \hookrightarrow M^{s_0}_{q_0,\sigma_0}(\mathbb{R}^n)$ if $s \ge s_0,\ q \le q_0,\ \sigma \le \sigma_0$.

(ii) $M^0_{q,\min\{q,q'\}}(\mathbb{R}^n) \hookrightarrow L^q(\mathbb{R}^n) \hookrightarrow M^0_{q,\max\{q,q'\}}(\mathbb{R}^n)$ if $\dfrac{1}{q} + \dfrac{1}{q'} = 1$.

Remark. In Besov spaces $B^s_{q,\sigma}(\mathbb{R}^n)$, we use dyadic decomposition instead of square decomposition. Then, we have

$$B^s_{q,\sigma}(\mathbb{R}^n) \not\hookrightarrow B^s_{q_0,\sigma}(\mathbb{R}^n) \quad \text{if } 1 \le q < q_0 \le \infty.$$

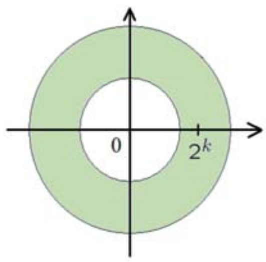

2 Results

$$\text{(NS)} \quad \begin{cases} \partial_t u - \Delta u + u\cdot\nabla u + \nabla p = 0 & \text{for} \quad (t,x) \in (0,\infty)\times\mathbb{R}^n, \\ \operatorname{div} u = 0 & \text{for} \quad (t,x) \in (0,\infty)\times\mathbb{R}^n, \\ u(0,x) = u_0(x) & \text{for} \quad x \in \mathbb{R}^n. \end{cases}$$

Known Results. Let $n \le q < \infty$.

	Local solutions	Global solutions
T. Kato (1984)	$u_0 \in L^n(\mathbb{R}^n)$	small $u_0 \in L^n(\mathbb{R}^n)$
F. Planchon (1998)		small $u_0 \in \dot{B}^{-1+\frac{n}{q}}_{q,\infty}(\mathbb{R}^n)$
H. Koch, D. Tataru (2001)	$u_0 \in vmo^{-1}$	small $u_0 \in BMO^{-1}$
B. Wang, L. Zhao, B. Guo (2006)	$u_0 \in M^0_{2,1}(\mathbb{R}^n)$	
I. (2008)	$u_0 \in M^0_{\infty,\frac{n}{n-1}}(\mathbb{R}^n)$	small $u_0 \in M^0_{n,\frac{n}{n-1}}(\mathbb{R}^n)$

$$PM^s_{q,\sigma}(\mathbb{R}^n) := \{\ f \in [M^s_{q,\sigma}(\mathbb{R}^n)]^n \ \mid\ \operatorname{div} f = 0 \text{ in } \mathcal{S}'(\mathbb{R}^n)\ \}.$$

Main Theorem. Let n, s, q and σ satisfy

$$n \ge 2, \quad s \ge -1 + \frac{n(\sigma-1)}{\sigma}, \quad 1 \le q \le \infty.$$

Then, for any $u_0 \in PM^s_{q,\sigma}(\mathbb{R}^n)$ there exists $T > 0$ such that (NS) has a unique solution u in some subspace of $\left[C([0,T], M^s_{q,\sigma}(\mathbb{R}^n))\right]^n$.

If $q \le n$ and u_0 is sufficiently small, the solution exists globally in time.

Remark. (i) If $s = 0$, then we have $\sigma \le n/(n-1)$. Therefore, this Theorem is an extension of our previous result.

(ii) Since $s \ge -1 + n(\sigma-1)/\sigma$, we have $s \ge -1$. If $s < -1$, (NS) is ill-posedness in $M^s_{2,\sigma}(\mathbb{R}^n)$ $(1 \le \sigma < \infty)$. Therefore, the derivative index $s = -1$ is optimal to obtain well-posedness. The way of the proof is applying the argument of I. Bejenaru, T. Tao (2006). They studied the nonlinear Schrödinger equation $i\partial_t u + \Delta u = u^2$ in one space dimension, and we apply their argument to the Navier-Stokes equation.

(iii) If $s = -1$, our initial data are included in the result by Koch and Tataru (2001). In fact, we have the following continuous embeddings

$$M^{-1}_{q,1}(\mathbb{R}^n) \hookrightarrow vmo^{-1} \quad \text{if } 1 \le q \le \infty,$$
$$M^{-1}_{q,1}(\mathbb{R}^n) \hookrightarrow BMO^{-1} \quad \text{if } 1 \le q \le n.$$

The other cases are not clear in general by $M^s_{q,\sigma}(\mathbb{R}^n) \not\hookrightarrow M^{-1}_{q,1}(\mathbb{R}^n)$ in the case of $1 \le q \le \infty$ and $s = -1 + n(\sigma-1)/\sigma > -1$.

3 Proposition to prove theorems

We introduce the proposition to prove our theorem in the case of $-1 \le s \le 0$. The way of the proof is applying Banach's fixed point theorem with the following propositions.

Let $s, \widetilde{s} \in \mathbb{R}$, $1 \le q, r, \sigma, \nu \le \infty$, $e^{t\Delta} := \mathcal{F}^{-1} e^{-t|\xi|^2} \mathcal{F}$, we have the following estimates.

(i) $\|e^{t\Delta}u\|_{M^s_{q,\sigma}} \le C\,(1+t)^{-\frac{n}{2}(\frac{1}{r}-\frac{1}{q})} \|u\|_{M^s_{r,\sigma}}$ if $q \ge r$.

(ii) $\|e^{t\Delta}u\|_{M^s_{q,\sigma}} \le C \left(1 + t^{-\frac{s-\widetilde{s}}{2}}\right) \|u\|_{M^{\widetilde{s}}_{q,\sigma}}$ if $s \ge \widetilde{s}$.

(iii) $\|e^{t\Delta}u\|_{M^s_{q,\sigma}} \le C \left(1 + t^{-\frac{n}{2}(\frac{1}{\sigma}-\frac{1}{\nu})}\right) \|u\|_{M^s_{q,\nu}}$ if $\sigma \le \nu$.

(iv) [Toft (2004)] If $\dfrac{1}{q} = \dfrac{1}{q_1} + \dfrac{1}{q_2}$ and $\dfrac{1}{\sigma} = \dfrac{1}{\sigma_1} + \dfrac{1}{\sigma_2} - 1$,
$\|uv\|_{M^0_{q,\sigma}} \le C \|u\|_{M^0_{q_1,\sigma_1}} \|v\|_{M^0_{q_2,\sigma_2}}$.

(v) $\|e^{t\Delta}u\|_{L^2(0,T;M^0_{q,1})} \le C \left(1 + T^{\frac{1}{2}}\right) \|u\|_{M^{-1}_{q,1}}$.

(vi) $\left\| \displaystyle\int_0^t \nabla e^{t\Delta} f(\tau) d\tau \right\|_{L^2(0,T;M^0_{q,1})} \le C \left(1 + T^{\frac{1}{2}}\right) \|f\|_{L^1(0,T;M^0_{q,1})}$.

Remark. (1) We use the estimates (ii), (iii) and (iv) to obtain local solutions of our theorem in the case $-1 < s \le 0$, and the case $s = -1$ can be treated with (iv), (v) and (vi). (i) is used for the proof of the existence of global solutions.

(2) Similar estimates to (i) and (ii) are known in Sobolev spaces.

$$\|e^{t\Delta}u\|_{H^{s,q}} \le Ct^{-\frac{n}{2}(\frac{1}{r}-\frac{1}{q})}\left(1 + t^{-\frac{s-\widetilde{s}}{2}}\right)\|u\|_{H^{\widetilde{s},r}} \quad \text{if } s > \widetilde{s},\ q \ge r.$$

The soul conjecture for Riemannian orbifolds

Naoki Oishi (Mathematical Institute Tohoku University)

1 Introduction

In 1994 , Perelman solved the Cheeger-Gromoll soul conjecture:

Theorem 1. M^n : non-compact, complete Riemannian manifold with $K(M^n) \geq 0$, $\exists p \in M^n$ s.t. $K(p) >0$.
$\Rightarrow$ The soul S of M^n is one point set. Consequently M^n is diffeomorphic to $\mathbb{R}^n$.

Here the soul S of M^n is a totally geodesic submanifold of M^n , which is constructed by some inductive way. M^n is diffeomorphic to a normal bundle of S.

One of the ideas of proving the theorem is to construct a flat rectangle on S and extend the rectangle along geodesics until it contains p.

By the way, Perelman constructed a soul on an Alexandrov space. But he couldn't generalize the theorem to the Alexandrov space. We show an analogous result to the theorem for Riemannian orbifolds with nonegative curvature, which belong to Alexandrov spaces.

2 Riemannian orbifolds

- M : complete Riemannian manifold.

$\Gamma \subset$ Isom(M) , $\Gamma \curvearrowright M$: discontinuously.
$\pi : M \ni x \mapsto [x]_\Gamma \in M/\Gamma$.
$\tilde{d}([x]_\Gamma, [y]_\Gamma) := d(\pi^{-1}([x]_\Gamma), \pi^{-1}([y]_\Gamma))$.
$\Rightarrow (M/\Gamma, \tilde{d})$: metric space.

Definition . $O := (M/\Gamma, \tilde{d})$: (good) Riemannian orbifold.

Definition . $p \in O$ is said to be a positively curved point if $K(\tilde{p}) > 0$ holds for $\forall \tilde{p} \in \pi^{-1}(p)$.

- $\tilde{a} \in M$, $\Gamma_{\tilde{a}} := \{g \in \Gamma |\, g\tilde{a} = \tilde{a}\}$.

$\Gamma_{\tilde{x}} \simeq \Gamma_{\tilde{y}}$ holds for $\forall x \in O, \forall \tilde{x}, \tilde{y} \in \pi^{-1}(x)$.

Definition . $\Gamma_x := \Gamma_{\tilde{x}}$. $x \in O$ is called a singular point if $\Gamma_x \neq \{e\}$.

- $x \in O$, γ : geodesic in O with $\gamma(0) = x$.

$c(x) :=\sup\{c > 0|$ any γ with $L(\gamma) < c$ can extend to a geodesic $\overline{\gamma}$ with $L(\overline{\gamma}) = c$ and $\overline{\gamma}(0) = x\}$.

Definition . $E(A) := \inf\{c(x) \,|\, x \in A\}$ for $A \subset O$.

Remark. $E(A)$ may not be positive. For example, let O be a cone. In this case, the origin o is a singular point, and any geodisic γ can't pass through o ; see Figure.

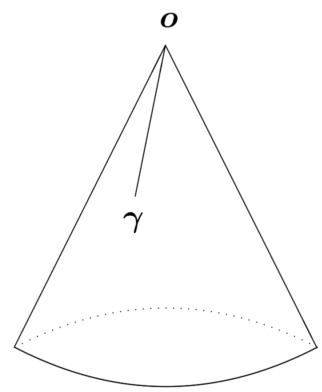

Figure

Theorem 2. O : non-compact, complete Riemannian orbifold with $curv(O) \geq 0$, $\exists p \in O$: positively curved point.
Moreover, we assume the followings with respect to the soul S in O :
(1) $\forall x, y \in S$, $\Gamma_x \simeq \Gamma_y$.
(2) $d(p, S) \leq E(S)$.
$\Rightarrow S$: one point set.

Remark. (1) implies $E(S) > 0$. Therefore by (2), we can apply the Perelman's method on S.

A new approach to the existence of harmonic maps

OMORI Toshiaki

(Mathematical institute, Tohoku University, Sendai, Japan)

sa6m07@math.tohoku.ac.jp

$\mathrm{sect}^N \leq 0 \Rightarrow \mathrm{ExpHarm}(M, N)$: compact

Main Theorem

[redacted]

Corollary

[redacted]

What is exponentially harmonic maps ?

Harmonic maps

$$E(u) := \frac{1}{2}\int_M |du|^2 d\mu_g$$

$$\Delta_g u + A(u)(\nabla u, \nabla u) = 0$$

ε-exponentially harmonic maps $(\varepsilon > 0)$

$$\mathbb{E}_\varepsilon(u) := \int_M e^{\varepsilon|\nabla u|^2} d\mu_g$$

$$\Delta_g u + \varepsilon\langle \nabla|\nabla u|^2, \nabla u\rangle + A(u)(\nabla u, \nabla u) = 0$$

Remark

$\nexists\, u \in \mathrm{Harm}(\mathbb{T}^2, \mathbb{S}^2)$ with $\deg(u) = \pm 1$

On the other hand

Fact [Duc & Naito]

$\forall\, \mathscr{H} \in [M, N]$

$\exists\, u_\varepsilon \in C^\infty(M, N)$: $\mathbb{E}_\varepsilon$-minimizer in $\mathscr{H}$

Proof of Main Theorem

[redacted]

Stability of the interface of a Hele-Shaw flow with two injection points

Michiaki ONODERA (Mathematics, DC3, Tohoku University)
sa5m08@math.tohoku.ac.jp

The 2nd GCOE International Symposium "Weaving Science Web beyond Particle-Matter Hierarchy"
February 18–19, 2010

1 Hele-Shaw flows with free boundaries

Hele-Shaw flows are fluid flows in an experimental device which consists of two closely-placed parallel plates. Since the gap between two plates is sufficiently narrow, one can regard them as two-dimensional flows. We consider a Hele-Shaw flow produced by the injection of fluid from two points. Let the fluid initially occupy a bounded domain $\Omega(t_0) \subset \mathbb{C}$ at the initial time $t = t_0$, and assume that $\pm i \in \Omega(t_0)$. From each point $\pm i$, additional fluid is injected at the respective rate α_1, $\alpha_2 > 0$ per unit time. The fluid domain at time $t > t_0$ is denoted by $\Omega(t)$ and its boundary by $\partial\Omega(t)$. We are interested in the behavior of the interface of the Hele-Shaw flow as time tends to infinity. In particular, we consider the stability of the interface under disturbance.

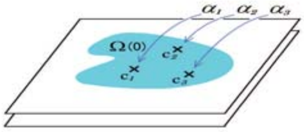

One of the significant features of the Hele-Shaw flow is that the flow is characterized as a two-dimensional potential flow with the potential being its pressure p. Let $p = p(z,t)$ be the pressure of the fluid at position $z \in \mathbb{C}$ and time $t > 0$. Then, p is assumed to satisfy the following equation and boundary conditions:

$$\begin{cases} (1) \quad -\Delta p = \alpha_1\delta_i + \alpha_2\delta_{-i} & \text{in } \Omega(t) \\ (2) \quad p = 0 & \text{on } \partial\Omega(t) \\ (3) \quad -\partial_n p = v_n & \text{on } \partial\Omega(t) \end{cases}$$

From (1) and (2), for each time $t > t_0$, the function p can be represented by

$$p(z,t) = \alpha_1 G_{i,\Omega(t)}(z) + \alpha_2 G_{-i,\Omega(t)}(z) \quad \text{for } z \in \Omega(t),$$

where $G_{\pm i,\Omega(t)}$ are the Green's functions of $\Omega(t)$ with pole at $\pm i$, respectively. We call a family $\{\Omega(t)\}_{t>t_0}$ of domains a solution of the Hele-Shaw problem if it satisfies (1)–(3) with the function p defined above.

2 Explicit solutions

By means of a complex analytic method, we are able to construct an explicit solution $\{\Omega_0(t)\}_{t>t_0}$ of the equation (3). The domain $\Omega_0(t)$ is represented as the image of the unit disk D through a conformal mapping φ_t, i.e., $\Omega_0(t) = \varphi_t(D)$. The mapping φ_t is given by

$$\varphi_t(w) = \varphi(w,t) = \frac{R^4 - 1}{R} \cdot \frac{w - i\eta}{w^2 + R^2} + i\eta R,$$

where $R = R(t)$ and $\eta = \eta(t)$ are smooth functions of t and they have the following asymptotic forms:

$$R(t) = \sqrt{\frac{\alpha_1 + \alpha_2}{\pi}} \cdot t^{1/2} + O(t^{-1/2}), \quad \eta(t) = \frac{\alpha_2 - \alpha_1}{\sqrt{\pi(\alpha_1 + \alpha_2)}} \cdot t^{1/2} + O(t^{-1/2}),$$

as $t \to \infty$.

3 Derivation of an evolution equation

Our objective is the stability of the solution $\{\Omega_0(t)\}$ of the equation (3) under disturbance of the initial domain $\Omega_0(t_0)$. We investigate the behavior of a solution starting from a domain $\Omega(t_0)$ which is sufficiently close to $\Omega_0(t_0)$ for a large positive number t_0. In this section we derive an evolution equation from the free boundary problem (3).

For a continuous function $r = r(\xi)$ on the unit circle $\mathbb{S}^1$, we define

$$D_r := \{w \in \mathbb{C} \setminus \{0\} \mid |w| < 1 + r(w/|w|)\} \cup \{0\}.$$

Let us assume that a family $\{\Omega(t)\}_{t \ge t_0}$ of domains satisfies the equation (3), and that each domain $\Omega(t)$ is represented by $\Omega(t) = \varphi_t(D_{r(\cdot,t)})$ for some time-dependent smooth function $r = r(\xi,t)$, $\xi \in \mathbb{S}^1$, $t \ge t_0$. Then, after some computations we see that the function r satisfies the following equation:

$$\partial_t r(\xi,t) = -\frac{\left\langle {}^t\nabla G(w_r(\xi),t)\,,\, n_{\partial D_r}(w_r(\xi))\right\rangle + \left\langle {}^t\nabla H_{r(\cdot,t),t}(w_r(\xi))\,,\, n_{\partial D_r}(w_r(\xi))\right\rangle}{\det D_w\varphi(w_r(\xi),t) \cdot \left\langle \xi\,,\, n_{\partial D_r}(w_r(\xi))\right\rangle} - \frac{\left\langle \partial_t\varphi(w_r(\xi),t)\,,\, (D_w\varphi(w_r(\xi),t)) n_{\partial D_r}(w_r(\xi))\right\rangle}{\det D_w\varphi(w_r(\xi),t) \cdot \left\langle \xi\,,\, n_{\partial D_r}(w_r(\xi))\right\rangle}, \tag{4}$$

where $w_r(\xi) := (1 + r(\xi,t))\xi$, and $\langle\cdot,\cdot\rangle$ denotes the usual inner product in $\mathbb{R}^2$, and $n_{\partial D_r}(w)$ is the unit outward normal vector to ∂D_r at point w. The function $G = G(w,t)$ is defined by

$$G(w,t) := \alpha_1 G_{\varphi_t^{-1}(i),D}(w) + \alpha_2 G_{\varphi_t^{-1}(-i),D}(w),$$

and $H_{r,t} = H_{r,t}(w)$ is a unique solution to the Dirichlet problem

$$\begin{cases} \Delta H_{r,t}(w) = 0 & \text{for } w \in D_r, \\ H_{r,t}(w) = -G(w,t) & \text{for } w \in \partial D_r. \end{cases}$$

Note that $r \equiv 0$ corresponds to the family $\{\Omega_0(t)\}_{t>t_0}$, and hence $r \equiv 0$ is a solution to the equation (4).

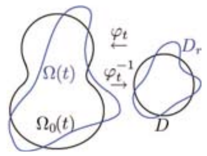

4 Main result

To state our main result, we recall some function spaces. The Hölder space $C^{k,\gamma}(\mathbb{S}^1)$ is a Banach space consisting of those functions r that are k-times continuously differentiable with their k-th order derivatives $r^{(k)}$ satisfying

$$|r^{(k)}(\xi_1) - r^{(k)}(\xi_2)| \le C|\xi_1 - \xi_2|^\gamma$$

for some constant C independent of ξ_1, $\xi_2 \in \mathbb{S}^1$. Then, the little Hölder space $h^{k,\gamma}(\mathbb{S}^1)$ is defined to be the closure of the subspace $C^\infty(\mathbb{S}^1)$ of infinitely many differentiable functions, in the topology of $C^{k,\gamma}(\mathbb{S}^1)$.

Theorem. *Suppose t_0 is sufficiently large. For $\varepsilon > 0$, there are $\delta, M > 0$ s.t. if $\|r_0\|_{h^{2,\gamma}(\mathbb{S}^1)} < \delta$, then there exists a unique solution $r \in C([t_0,\infty); h^{2,\gamma}(\mathbb{S}^1)) \cap C^1([t_0,\infty); h^{1,\gamma}(\mathbb{S}^1))$ satisfying*

$$\|r(t)\|_{h^{2,\gamma}(\mathbb{S}^1)} + t\|r'(t)\|_{h^{1,\gamma}(\mathbb{S}^1)} \le Mt^{-1+\varepsilon}\|r_0\|_{h^{2,\gamma}(\mathbb{S}^1)}.$$

Therefore, the solution $\{\Omega_0(t)\}_{t>t_0}$ is stable under disturbance, and the disturbance decays with algebraic order as time goes to infinity.

5 Outline of the proof

We treat the equation (4) as an evolution equation on $h^{1,\gamma}(\mathbb{S}^1)$ as follows:

$$\begin{cases} r' = \mathcal{F}(r,t), \quad t \ge t_0, \\ r(t_0) = r_0 \in h^{2,\gamma}(\mathbb{S}^1), \end{cases}$$

where $\mathcal{F} : h^{2,\gamma}(\mathbb{S}^1) \times [t_0,\infty) \to h^{1,\gamma}(\mathbb{S}^1)$, and $\mathcal{F}(0,t) = 0$.

$\boxed{\text{Lemma 1.}}$ $t \cdot D_r\mathcal{F}(r,t) \to \mathcal{A}$ in $\mathcal{L}(h^{2,\gamma}(\mathbb{S}^1), h^{1,\gamma}(\mathbb{S}^1))$ as $t \to \infty$ and $r \to 0$.

$\boxed{\text{Lemma 2.}}$ $\mathcal{A}$: sectorial in $h^{1,\gamma}(\mathbb{S}^1)$, and $\sup\{\mathrm{Re}\lambda \mid \lambda \in \sigma(\mathcal{A})\} = -1$.
('97 Escher & Simonett, '09 Vondenhoff)

Set $\tau := \log(t/t_0)$ and $\tilde{r}(\tau) := r(t)$, then

$$\tilde{r}'(\tau) = t \cdot r'(t) = t \cdot \mathcal{F}(r,t) = \mathcal{A}\tilde{r} + \mathcal{G}(\tilde{r},\tau), \tag{5}$$

where $\mathcal{G}(0,\tau) = 0$, $D_{\tilde{r}}\mathcal{G}(\tilde{r},\tau) \to 0$ as $t \to \infty$ and $\tilde{r} \to 0$.

$\boxed{\text{Lemma 3.}}$ (Linearized stability for asymptotically autonomous equations)
$\|r_0\|_{h^{2,\gamma}(\mathbb{S}^1)} < \delta \Rightarrow \exists\tilde{r}$: solution of (5) satisfying

$$\|\tilde{r}(\tau)\|_{h^{2,\gamma}(\mathbb{S}^1)} + \|\tilde{r}'(\tau)\|_{h^{1,\gamma}(\mathbb{S}^1)} \le M'e^{(-1+\varepsilon)\tau}\|r_0\|_{h^{2,\gamma}(\mathbb{S}^1)}.$$

• Maximal regularity property of $h^{k,\gamma}(\mathbb{S}^1)$ ('79 Da Prato & Grisvard)
$\tilde{r}_j \in C([0,\infty); h^{2,\gamma}(\mathbb{S}^1)) \Rightarrow \mathcal{G}(\tilde{r}_j,\tau) \in C([0,\infty); h^{1,\gamma}(\mathbb{S}^1))$
$\Rightarrow \tilde{r}_{j+1} \in C([0,\infty); h^{2,\gamma}(\mathbb{S}^1))$
(The case where $\mathcal{G} = \mathcal{G}(\tilde{r})$ and $D_{\tilde{r}}\mathcal{G}(0) = 0$ is already known.)

Turning back to the original time variable t, we see that

$$\|r(t)\|_{h^{2,\gamma}(\mathbb{S}^1)} + t\|r'(t)\|_{h^{1,\gamma}(\mathbb{S}^1)} \le Mt^{-1+\varepsilon}\|r_0\|_{h^{2,\gamma}(\mathbb{S}^1)}.$$

The isomorphism between motivic cohomology and K-groups for equi-characteristic regular local rings.

Yuki Kato `sa4d01@math.tohoku.ac.jp`

Mathematical Institute, Tohoku University, Aoba, Sendai, JAPAN, 980-8578.

Sendai, Feb. 18 - Feb. 19, 2010

1 Notations.

- $R :=$ a regular local ring of equi-characteristic.
- $\mathrm{CH}^r(X,n) =$ the higher Chow groups for arbitrary integral scheme X.
- $K_n(X) =$ the algebraic K-groups for arbitraly scheme X.
- $\mathcal{Z}_{eq}(X/S,r) := \mathbb{Z}\,[Z \subset X \mid X \to S : \text{equi-dimensional of dimension } r]$ ($S :=$ a geometrically unibranch scheme, $X :=$ a scheme of finite type over S).
- $K^{\mathcal{Q},T}(X)$:=the K-theory spectrum of the scheme $X \times_S T$ with family of supports consisting of all closed subschemes quasi-finite over X

Question 1.1.

$$K_n(X)_{\mathbb{Q}} \overset{??}{=} \bigoplus_{r \geq 0} \mathrm{CH}^r(X,n)_{\mathbb{Q}}.$$

Theorem 1.2. *Let R be an equi-characteristic regular local ring. Then we have an isomorphism*

$$\mathrm{cl} : K_n(R)_{\mathbb{Q}} \to \bigoplus_{r \geq 0} \mathrm{CH}^r(R,n)_{\mathbb{Q}}$$

for any $n \geq 0$, where cl *is the cycle-class map.* □

According to Voevodsky–Suslin–Friedlander [4], we can define the higher Chow group by another approach, and this coincides with Bloch's [1] for an arbitrary quasi-projective variety over a field.

2 Friedlander–Suslin–Voevodsky's motivic complex $\mathbb{Q}_{X/S}(r)[\bullet]$.

We always assume that a scheme S is noetherian, reduced and separated of finite dimensional. Write $\square^n = \mathbb{A}^n_S$. The cubical structure of $\square^n$ is defined by the faces which are intersections of some of the Cartier divisor $\{t_i = 0\}$ or $\{t_i = 1\}$.

Definition 2.1.

$$\mathbb{Z}_{X/S}(r)[n] = \mathcal{Z}_{eq}(X \times_S \square^n_S \times_S \mathbb{A}^r / X \times_S \square^n_S, 0) / \sum_{i=1}^{n} \pi_i^*(\mathcal{Z}_{eq}(X \times_S \square^{n-1}_S \times_S \mathbb{A}^r / X \times_S \square^{n-1}_S, 0)),$$

and write $\mathbb{Q}_{X/S}(r)[n] = \mathbb{Z}_{X/S}(r)[n] \otimes \mathbb{Q}$. We obtain and a cubical complex $\mathbb{Q}_{X/S}(r)[\bullet]$ and define the motivic cohomology

$$\mathrm{CH}^r_t(X,n)_{\mathbb{Q}} = \mathbf{H}^{-n}_t(X, \mathbb{Q}_{X/S}(r)[\bullet]),$$

where t is a topology as follows; qfh, ét, Nis or Zar.

3 The proof of the main theorem.

3.1 The construction of the cycle-class map "cl″

Write $\mathbb{Z}^{\mathcal{Q},T}(X) = \mathcal{Z}_{eq}(X \times_S T/X, 0)$. Then the canonical map

$$\mathrm{cl} : K^{\mathcal{Q},T}(X) \to \pi_0(K^{\mathcal{Q},T}(X)) \to \mathbb{Z}^{\mathcal{Q},T}(X)$$

is given by taking the cycles $[\mathrm{Supp}\mathcal{F}] = \sum_W \mathrm{length}(\mathcal{F}_W)[W]$ of the coherent sheaves $\mathcal{F}$, where $W \subset \mathrm{Supp}\mathcal{F}$ runs over all irreducible components.

Lemma 3.1. *Let S be a regular noetherian scheme, T a smooth scheme of finite type over S and $f : Y \to X$ be a morphism of smooth schemes over S. Then the diagram*

$$\begin{tikzcd} K^{\mathcal{Q},T}(X) \arrow[r, "\mathrm{cl}"] \arrow[d, "f^*"] & \mathbb{Z}^{\mathcal{Q},T}(Y) \arrow[d, "f^*"] \\ K^{\mathcal{Q},T}(X) \arrow[r, "\mathrm{cl}"] & \mathbb{Z}^{\mathcal{Q},T}(Y) \end{tikzcd}$$

is commutative. □

The main theorem is proved by the following lemmas:

Lemma 3.2. *$(T_\alpha, f_{\alpha\beta})$ a directed inverse system of smooth schemes over S, X_0 a scheme of finite type over S. Assume $T = \varprojlim T_\alpha$ is also regular and noetherian. Then we have the isomorphism:*

$$\varinjlim \mathcal{Z}_{eq}(X_\alpha/T_\alpha, 0) \otimes \mathbb{Q} \to \mathcal{Z}_{eq}(X/T,0) \otimes \mathbb{Q},$$

where we write $X_\alpha = X_0 \times_S T_\alpha$ and $X = X_0 \times_S T$. □

Lemma 3.3. *Let k be a field, X be a smooth scheme and F be a homotopy invariant sheaf of $\mathbb{Q}$-vector space on $(\mathrm{Sm}/X)_{\mathrm{Zar}}$. Then we have an isomorphisms*

$$H^n_{\acute{e}t}(X,F) = H^n_{\mathrm{qfh}}(X,F) = H^n_{Nis}(X,F) = H^n_{\mathrm{Zar}}(X,F).$$

□

References

[1] S. Bloch, *Algebraic cycles and higher K-theory*, Adv. in Math. **61** (1986), no. 3, 267–304.

[2] Eric M. Friedlander and A. Suslin, *The spectral sequence relating algebraic K-theory to motivic cohomology*, Ann. Sci. École Norm. Sup. (4) **35** (2002), no. 6, 773–875 (English, with English and French summaries).

[3] Y. Kato, *The isomorphism between motivic cohomology and K-groups for equi-characteristic regular local rings.*, preprint.

[4] V. Voevodsky, A. Suslin, and Eric M. Friedlander, *Cycles, transfers, and motivic homology theories*, Annals of Mathematics Studies, vol. 143, Princeton University Press, Princeton, NJ, 2000.

Bifurcations in semilinear elliptic equations on thin domains

Toru Kan

Mathematical Institute, Tohoku University

(E-mail: `sa7m08@math.tohoku.ac.jp`)

1 Thin Domain and Limit Equation

Thin domain

$$\begin{cases} \Delta u + f(u,\lambda) = 0 & \text{in } Q_\varepsilon, \\ \dfrac{\partial u}{\partial \nu_\varepsilon} = 0 & \text{on } \partial Q_\varepsilon. \end{cases}$$

$\lambda \in \mathbb{R}$: bifurcation parameter

$f(0,\lambda) \equiv 0$

$Q_\varepsilon := \{(x,y) \in \mathbb{R}^2; 0 < y < \varepsilon g(x),\ 0 < x < 1\}$

($\varepsilon > 0$: small parameter, $g \in C^2([0,1]),\ g > 0$)

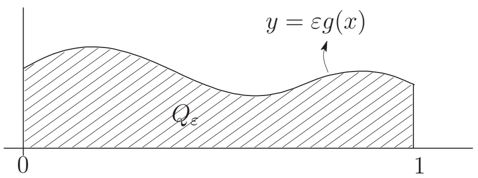

Change of variables $Q := (0,1) \times (0,1) \ni (x,y) \mapsto (x, \varepsilon g(x) y) \in Q_\varepsilon$

$$\longrightarrow \quad (\mathrm{P})_\varepsilon \begin{cases} L_\varepsilon u + f(u,\lambda) = 0 & \text{in } Q, \\ \dfrac{\partial u}{\partial \nu_{B_\varepsilon}} = B_\varepsilon u \cdot \nu = 0 & \text{on } \partial Q. \end{cases}$$

$$L_\varepsilon := \frac{1}{g}\mathrm{div} B_\varepsilon, \quad B_\varepsilon := \begin{pmatrix} g\dfrac{\partial}{\partial x} - g_x y \dfrac{\partial}{\partial y} \\ -g_x y \dfrac{\partial}{\partial x} + \dfrac{1}{g}\left\{\dfrac{1}{\varepsilon^2} + (g_x y)^2\right\}\dfrac{\partial}{\partial y} \end{pmatrix}.$$

Limit equation at $\varepsilon = 0$

The limit equation of $(\mathrm{P})_\varepsilon$ at $\varepsilon = 0$ is given by

$$(\mathrm{P})_0 \begin{cases} \dfrac{1}{g(x)}(g(x)v_x)_x + f(v,\lambda) = 0 & \text{in } (0,1), \\ v_x(0) = v_x(1) = 0. \end{cases}$$

2 Problem

How can the bifurcation diagram of $(\mathrm{P})_\varepsilon$ be approximated by that of the limit equation $(\mathrm{P})_0$? Do solution branches of $(\mathrm{P})_\varepsilon$ persist near those of $(\mathrm{P})_0$ including bifurcation points?

More precisely, we consider the following three situations:

1. Bifurcation from the trivial branch
2. Regular branch of solutions
3. Saddle-node bifurcation

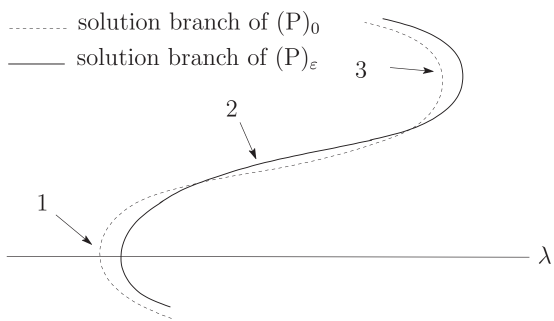

3 Definition

Norm on $H^1(Q)$

For $u \in H^1(Q)$, we define

$$\|u\| := \left(\|u\|^2_{H^1(Q)} + \frac{1}{\varepsilon^2}\left\|\frac{\partial u}{\partial y}\right\|^2_{L^2(Q)}\right)^{\frac{1}{2}}.$$

4 Main Results

Theorem 1 (Bifurcations from the trivial branch)

Suppose that $(0,\lambda_0)$ is a simple bifurcation point of $(\mathrm{P})_0$, i.e.,

$v = 0$ is degenerate soilution of $(\mathrm{P})_0$ at $\lambda = \lambda_0$,

$f_{u\lambda}(0,\lambda_0) \neq 0$

$\Rightarrow \exists \varepsilon_0 > 0, \exists C > 0$ s.t. $0 < \forall \varepsilon \leq \varepsilon_0$, $\exists! \lambda_0^\varepsilon \in \mathbb{R}$ s.t.

λ_0^ε is a simple bifurcation point of $(\mathrm{P})_\varepsilon$,

$|\lambda_0^\varepsilon - \lambda_0| \leq C\varepsilon$.

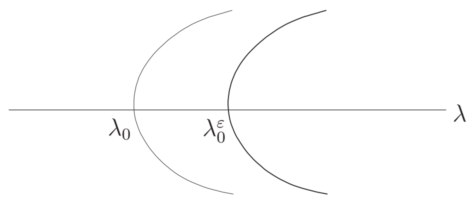

Theorem 2 (Regular solution branches)

$I \subset \mathbb{R}$: bounded closed interval,

$\{(v(\lambda),\lambda); \lambda \in I\}$: regular solution branch of $(\mathrm{P})_0$

$\Rightarrow \exists \varepsilon_0 > 0, \exists C > 0$ s.t. $0 < \forall \varepsilon \leq \varepsilon_0$, $\exists! \{(u^\varepsilon(\lambda),\lambda); \lambda \in I\}$ s.t.

$\{(u^\varepsilon(\lambda),\lambda); \lambda \in I\}$ is a regular solution branch of $(\mathrm{P})_\varepsilon$,

$\sup_{\lambda \in I}\|u^\varepsilon(\lambda) - v(\lambda)\| \leq C\varepsilon$.

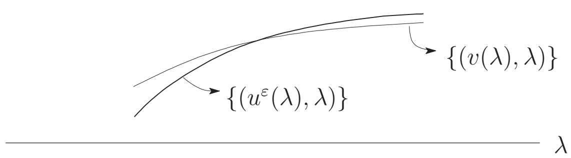

Theorem 3 (saddle-node bifurcations)

(v_0,λ_0) : turning point of $(\mathrm{P})_0$

$\Rightarrow \exists \varepsilon_0 > 0, \exists C > 0$ s.t. $0 < \forall \varepsilon \leq \varepsilon_0$, $\exists! (u_0^\varepsilon, \lambda_0^\varepsilon)$ s.t.

$(u_0^\varepsilon, \lambda_0^\varepsilon)$ is a turning point of $(\mathrm{P})_\varepsilon$,

$\|u_0^\varepsilon - v_0\| + |\lambda_0^\varepsilon - \lambda_0| \leq C\varepsilon$.

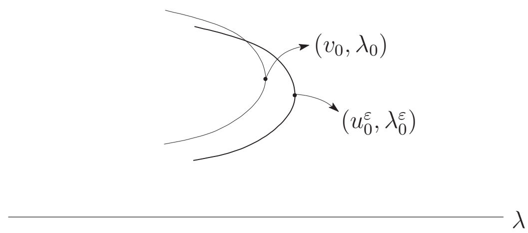

On the curvature of the pseudo-volume form defining the Carathéodory measure hyperbolicity

Shin Kikuta
Mathematical Insititute, Tohoku university
email : sa6m15@math.tohoku.ac.jp

Theorem [Schwarz' lemma].

$$f : \text{holomorphic on } \Delta := \{z \in \mathbb{C}\,;\, |z| < 1\},\ |f| < 1,\ f(0) = 0 \Longrightarrow |f'(0)| \leq 1$$

This theorem can be interpreted as follows.

$$|f| < 1 \quad \Longrightarrow \quad f : \text{holomorphic map between } \Delta$$

$$|f'(0)| \leq 1,\ f(0) = 0 \quad \Longrightarrow \quad \frac{4}{(1-|f(0)|^2)^2}|f'(0)|^2 dxdy \leq \frac{4}{(1-|0|^2)^2} dxdy$$

But

$$\text{Möbius transformation on } \Delta \Longrightarrow \begin{cases} \cdot \text{ Any } z \in \Delta \text{ can be mapped to } 0 \\ \cdot \text{ Poincaré volume element } v_1 := \dfrac{4}{(1-|z|^2)^2} dxdy \\ \quad \text{with constant curvature } K_{v_1} = -1 \text{ is invariant} \end{cases}$$

Therefore it follows that

$$f^* v_1 := \frac{4}{(1-|f(z)|^2)^2}|f'(z)|^2 dxdy \leq \frac{4}{(1-|z|^2)^2} dxdy \quad \text{for } f : \text{holomorphic map between } \Delta$$

We consider $|f'(z)|^2 dxdy$ as a change of variables by f.

Geometric interpretation of Schwarz' lemma

Any holomorphic map between Δ decreases volumes measured by v_1

With requiring this volume decreasing property of holomorphic mappings,

$$v_1 \text{ on } \Delta \overset{\text{generalization}}{- - - - \longrightarrow} \text{what on a higher dimensional complex manifold } X\ ?$$

Definition-Theorem [a gerenalization of (Δ, v_1)].

$v_X^C := \sup\{f^* v_1^{(n)}\,;\, f \in \mathrm{Hol}(X, \mathbb{B}^n)\}$: **Carathéodory pseudo-volume form**

("pseudo" : it may take 0 at some point

$v_1^{(n)}$: Poincaré volume element which generalizes v_1 on Δ to $\mathbb{B}^n := \{z \in \mathbb{C}^n\,;\, |z| < 1\}$)

$\Longrightarrow$ All holomorphic maps decrease volumes measured with respect to the Carathéodory pseudo-volume form v_X^C

Main theorem [curvature of v_X^C].

$$K_{v_X^C}(\ := \text{a curvature of the Carathéodory pseudo-volume form } v_X^C) \leq -1$$

Gödel's Incompleteness Theorem, Recursively Axiomatizable Theories and Medvedev Degrees of Unsolvability

Takayuki Kihara

Mathematical Institute, Tohoku University

Gödel's Incompleteness Theorem (1931)

Fix a set $\mathcal{L}$ of symbols, say $\&, \forall, =, \in, \dots$, and assume that an $\mathcal{L}$-theory T agrees with the following **3** conditions:

- T is consistent.
- T is capable of expressing elementary arithmetic.
- It is knowable what axioms of T are. (that is, T is recursively axiomatizable.)

Then, T must be incomplete, even for sentences generated from just $\mathcal{L}$!

Goal

- Our purpose is to classify every possible recursively axiomatizable theories whether or not studied in the history of mankind.
- To simplify this problem, we focus on the spaces T^* of ultrafilters of Lindenbaum algebras of recursively axiomatizable theories T with the Zariski topology.
- T^* is homeomorphic to some Π^0_1 class in the Cantor space.

"The conclusion (*of Gödel's Incompleteness Theorem*) is unescapable that even for such a fixed, well defined body of mathematical propositions, *mathematical thinking is, and must remain, essentially creative*".

–Emil L. Post (1944), Recursively Enumerable Sets of Positive Integers and their Decision Problems.

Definition

A consistent recursively axiomatizable theory T is creative if there is a computable function F such that both affirmation and negation of $F(S)$ are unprovable in S for every consistent recursively axiomatizable extension S of T.

Example

- Peano arithmetic (**PA**) is creative via $F(S) = Con(S)$, where $Con(S)$ is a sentence expressing that "S is consistent".
- Zelmero-Fraenkel set theory (**ZFC**), *a foundational axiomatic system for mathematics*, is also creative.

Theorem of Pour-El and Kripke (1967)

- There are deduction-preserving recursive isomorphisms between every creative theories.
- **PA** is isomorphic to **ZFC** via a deduction-preserving computable procedure!

Definition

- Y is Medvedev reducible to X ($Y \leq_M X$) if there is a computable map $F : X \to Y$.
- The Medvedev degree of X ($\deg_M(X)$) is the equivalent class of X under $\equiv_M$.

Intuition

- We might think of a set X as a solution set of some problem.
- If X has a computable element then we think X as a computably solvable problem.
- We might regard the empty set as a problem without solution.
- $Y \leq_M X$ (via F) represents that X is more difficult problem than Y. (We have a solution $F(x)$ to Y whenever we know a solution x to X.)

Observation

- The empty set $\emptyset$ is the most difficult problem. ($\emptyset$ has the greatest Medvedev degree ∞.)
- A computably solvable problem is a easiest problem. (Such a problem has the least Medvedev degree **0**.)

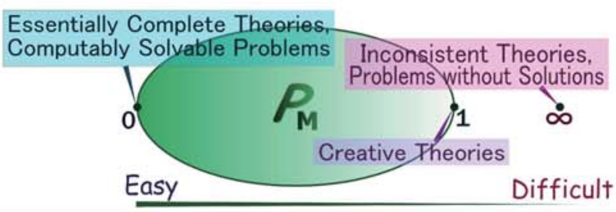

Definition

- The Cantor space $2^{\mathbb{N}}$ is the countably infinite topological product of the discrete space $\{0, 1\}$.
- A Π^0_1 class is a computably generated closed set in the Cantor space.

Theorem (Folklore)

- In the Cantor space, there exists a nonempty Π^0_1 class P such that $Q \leq_M P$ for every nonempty Π^0_1 class Q.
- Thus, the lattice structure
$$\mathcal{P}_M = ((\text{nonempty } \Pi^0_1 \text{ classes})/\equiv_M, \leq_M)$$
has the greatest element **1** and the least element **0**.

Observation

Let T be a recursively axiomatizable theory.

- T is *essentially incomplete* $\iff$ $0 < \deg_M(T^*) \leq 1$.
- T is *creative* $\iff$ $\deg_M(T^*) = 1$.
- T is *inconsistent* $\iff$ $\deg_M(T^*) = \infty$.
- $\deg_M(T_0^*) = \deg_M(T_1^*) = 1$ $\implies$ T_0^* is computably homeomorphic to T_1^*.

Definition

- A Σ^0_1 set is a computably generated open set in the discrete space $\mathbb{N}$ of all positive integers.
- y is Turing reducible to x if there is a computable map F such that $F(x) = y$.

- As explained along the way, Medvedev degrees of Π^0_1 classes are enormously beneficial to understand meta-mathematics and eventually human intelligence.
- Our theorem clarifies the structure of Π^0_1 Medvedev degrees, and it suggests that some hard problems on Σ^0_1 Turing degrees are solvable if we replace the word "Σ^0_1 Turing" with "Π^0_1 Medvedev".

Longstanding Open Question (1960-)

Is the $\forall\exists$-theory of the Σ^0_1 Turing degrees decidable?

Theorem of Cole and Kihara [2]

The $\forall\exists$-theory of the Π^0_1 Medvedev degrees is decidable!

Longstanding Open Question (1940-)

Find a "concrete" intermediate Σ^0_1 Turing degree!

Theorem of Cenzer-Kihara-Weber-Wu [1]

The greatest *tree-immune-free* Medvedev degree exists, and it is an intermediate Π^0_1 Medvedev degree!

[1] D. Cenzer, T. Kihara, R. Weber, and G. Wu, Immunity and non-cupping for closed sets, *Tbilisi Mathematical Journal* **2** (2009), pp. 77–94.
[2] J. A. Cole, and T. Kihara, The $\forall\exists$-theory of the effectively closed Medvedev degrees is decidable, *Archive for Mathematical Logic* **49** (2010), pp. 1–16.
[3] T. Kihara, Medvedev and Muchnik degrees of Π^0_1 classes with incomplete c.e. filters, submitted.

Hypergeometric Series over a p-adic field

Kensaku Kinjo

Mathematical Institute, Tohoku University, Sendai, Japan

p-adic fields

p : odd prime.

$\forall x \in Q\backslash\{0\}, \exists! n_x \in Z, \exists\, a,b \in Z\backslash pZ$, s.t. $x = p^{n_x}a/b$.

Let $|x|_p := p^{-n_x}$ ($|0| := 0$). Then $|\cdot|_p$ defines a distance on Q.

Q_p : completion of Q with respect to $|\cdot|_p$.

$Z_p := \{x \in Q_p; |x|_p \leq 1\}$.

Monsky-Washnitzer Cohomology

F_p : finite field with $\sharp F_p = p$.

$E_\mu : y^2 = x(x-1)(x-\mu)$ $(\mu \in F_p\backslash\{0,1\})$

(affine ordinary elliptic curve over F_p).

$\mathrm{Frob}_p \curvearrowright F_p[x,y]/(y^2 - x(x-1)(x-\mu))$.

Then Frob_p lifts on

$$R := Z_p\langle x,y\rangle^\dagger/(y^2 - x(x-1)(x-\tilde{\mu})),$$

where $\tilde{\mu} \in Z_p$ is the Teichmüller lift of μ.

Overconvergent Power Series

$$Z_p\langle x,y\rangle^\dagger := \left\{ \sum_{i,j\geq 0} a_{i,j}x^iy^j \;\middle|\; \begin{array}{l} a_{i,j} \in Z_p, \\ \rho^{i+j}|a_{i,j}| \to 0\ (\exists \rho > 1) \end{array} \right\}$$

$D^1(R)$: differential module of R over Z_p.

$\mathrm{H}^1(E_\mu) := \mathrm{Coker}[d_1 : R\otimes Q_p \to D^1(R)\otimes Q_p]$

(Monsky-Washnitzer cohomology for E_μ)

Property

- $\mathrm{H}^1(E_\mu)$ is a 2 dimensional Q_p vector space.
- Frob_p induces a mapping : $\mathrm{H}^1(E_\mu) \to \mathrm{H}^1(E_\mu)$.

a_1, a_2 : eigenvalues of Frob_p on $\mathrm{H}^1(E_\mu)$.

$$\begin{cases} a_1 + a_2 = p - \sharp E(F_p), \\ a_1 \cdot a_2 = p, \\ a_1 \text{ or } a_2 \in Z_p^\times. \end{cases}$$

The eigenvalue in $Z_p^\times$ is called the unit root of $\mathrm{H}^1(E_\mu)$.

Family of Elliptic Curves

$$m = (p-1)/2,\ H(\lambda) := \lambda(\lambda-1)\sum_{i=1}^m \binom{m}{i}^2 \lambda^i,$$

$$B := Z_p\langle \lambda, H(\lambda)^{-1}\rangle := \left\{ \sum_{i,j\geq 0} a_{i,j}\lambda^i H(\lambda)^{-j} \;\middle|\; a_{i,j} \in Z_p, |a_{i,j}|_p \to 0 \right\},$$

$A := B\langle x,y\rangle^\dagger/(y^2 - x(x-1)(x-\lambda))$.

$D^1(A/B)$: differential module of A over B.

$\mathrm{H}^1 := \mathrm{Coker}[d : A\otimes Q_p \to D^1(A/B)\otimes Q_p]$.

NOTE

Let $\mu \in F_p$ is ordinary ($:\Leftrightarrow E_\mu$ is ordinary), and $\tilde{\mu}$ Teichmüller lift of $\mu \in F_p$. Then under $B \ni \lambda \mapsto \tilde{\mu} \in Q_p$, we see

$$\mathrm{H}^1 \otimes_B Q_p \simeq \mathrm{H}^1(E_\mu).$$

$D^1(A/Z_p)$: differential module of A over Z_p.

$\exists P, Q \in B[x]$ s.t.

$$x(x-1)(x-\lambda)P(x) + \frac{3x^2 - 2(1+\lambda)x + \lambda}{2}Q(x) = 1.$$

Property

Let $\tau := yP(x)dx + Q(x)dy$.

- $D^1(A/Z_p) = Ad\lambda \oplus A\tau$.
- $D^1(A/B) = A(dx/y) \simeq D^1(A/Z_p)/Ad\lambda$.
- $D^2(A/Z_p) := D^1(A/Z_p)\wedge D^1(A/Z_p) = Ad\lambda\wedge\tau$.

Gauss-Manin Connection

$\forall a \in A, \exists! L(a) \in A$ s.t. $d(a\tau) = L(a)d\lambda\wedge\tau$. Therefore we obtain the mapping

$$D^1(A/B) \ni a\frac{dx}{y} \mapsto L(a)\frac{dx}{y} \in D^1(A/B),$$

and this induces $\nabla : \mathrm{H}^1 \to \mathrm{H}^1$ satisfying

- $\nabla(m_1 + m_2) = \nabla(m_1) + \nabla(m_2)$ $(m_1, m_2 \in \mathrm{H}^1)$,
- $\nabla(bm) = b'\cdot m + b\nabla(m)$ $(b \in B\otimes Q_p, m \in \mathrm{H}^1)$.

∇ is called Gauss-Manin connection.

Frobenius on H^1

$\phi : B \to B$: Z_p alg. hom. with $\phi(\lambda) = \lambda^p$.

$\Longrightarrow \exists\phi$-linear ring hom. $F : A \to A$ s.t. $F(z) \equiv z^p (\mod pA)$.

This induces a ϕ-linear mapping : $\mathrm{H}^1 \to \mathrm{H}^1$, which is also denoted by F.

Proposition

Let ω be the image of dx/y in H^1.

- $\{\omega, \nabla(\omega)\}$ is a basis for H^1 as $B\otimes Q_p$ modules.
- $4\lambda(1-\lambda)\nabla^2(\omega) + 4(1-2\lambda)\nabla(\omega) - \omega = 0$.
- $\eta \in \ker\nabla \Leftrightarrow \eta = \lambda(1-\lambda)f'\omega - \lambda(1-\lambda)f\nabla(\omega)$ where $f \in B$ satisfying $4\lambda(1-\lambda)f'' + 4(1-2\lambda)f' - f = 0$.
- F is stable on $\ker\nabla$.
- F is also stable on $B\omega + B\nabla(\omega)$. Moreover, $\exists u \neq 0 \in B\omega + B\nabla(\omega)$ s.t. Bu is the unique direct summand of $B\omega + B\nabla(\omega)$ satisfying $F(Bu) = Bu$.

Let $\mu \in F_p$ be an ordinary and $\tilde{\mu}$ Teichmüller lift of μ. Then under $\lambda \mapsto \tilde{\mu}$, we obtain the following commutative diagram :

$$\begin{array}{ccccccc} \mathrm{H}^1 & \xrightarrow{F} & \mathrm{H}^1 & \qquad & u & \mapsto & \xi(\lambda)u \\ \downarrow & & \downarrow & & \downarrow & & \downarrow \\ \mathrm{H}^1(E_\mu) & \xrightarrow[\mathrm{Frob}]{} & \mathrm{H}^1(E_\mu), & & v & \mapsto & \mathrm{Frob}_p(v) = \xi(\tilde{\mu})v, \end{array}$$

where v is the image of u in $\mathrm{H}^1(E_\mu)$. Therefore we see $\xi(\tilde{\mu})$ is the unit root of $\mathrm{H}^1(E_\mu)$.

Theorem[Dwork]

- $\xi(\lambda)$: holom. on $\{\lambda \in Q_p \mid |\lambda|_p \leq 1, |H(\lambda)|_p = |\lambda(\lambda-1)|_p\}$.
- $\xi(\lambda) = (-1)^m\mathcal{F}(\lambda)/\mathcal{F}(\lambda^p)$ on $\{\lambda \in Q_p\ ; |\lambda|_p < 1\}$, where

$$\mathcal{F}(x) := \sum_{n\geq 0}\binom{(2n-1)/2}{n}^2 x^n$$

is the hypergeometric series.

On Hasse principle of purely transcendental extension field in one variable

Makoto Sakagaito

2010/2/18

Classical result

k: global field(i.e. number field or algebraic function field in one variable over finite field).

$\mathfrak{p}$: prime of k including the archimedean ones if k is number field.

$\hat{k_{\mathfrak{p}}}$: completion of k at $\mathfrak{p}$.

Hasse principle

local-global map

$$\mathrm{Br}(k) \to \prod_{\mathfrak{p}} \mathrm{Br}(\hat{k_{\mathfrak{p}}})$$

is injective. Here, $\mathfrak{p}$ runs through all primes of k.

Special case

For $a, b \in \mathbb{Z}$, q: prime number

There exist $x, y \in \mathbb{Q}$ s.t. $ax^2 + by^2 = q$

$\Leftrightarrow$ There exist $x_p, y_p \in \mathbb{Q}_p$ s.t. $ax_p^2 + by_p^2 = q$

Here, p runs through all prime numbers and ∞, $\mathbb{Q}_\infty = \mathbb{R}$.

Application

There exist $x, y \in \mathbb{Q}$ s.t. $q = x^2 + 26y^2$

$$\Updownarrow$$

$$\begin{cases} q \equiv 1 \bmod 8 \ \text{ and } \ q \equiv \text{one of } \ 1,3,4,9,10,12 \bmod 13 \\ \text{or} \\ q \equiv 3 \bmod 8 \ \text{ and } \ q \equiv \text{one of } \ 1,3,4,9,10,12 \bmod 13 \end{cases}$$

Study

Related to this classical result, I studied the question of whether the Hasse principle holds in the case where the field $K(X)$ is a purely transcendental extension in one variable of any field K.

I ascertained the result that the local-global map of $K(X)$ restricted to

$$\mathrm{Br}(K(X))' = \mathrm{Ker}(\mathrm{Br}(K(X)) \stackrel{\mathrm{res}}{\to} \prod_{\mathfrak{p} \in \mathrm{Spec}(K[X])} \mathrm{Br}(K(X)_{\bar{\mathfrak{p}}})$$

is injective.

Here, $K(X)_{\bar{\mathfrak{p}}}$ is the maximal unramified extension field at $\mathfrak{p} \in \mathrm{Spec(K[X])}$.

Remarks

In the case where m is a natural number prime to the characteristic of K,

$$\mathrm{Br}(K(X))_m = \mathrm{Ker}(\mathrm{Br}(K(X)) \stackrel{\times m}{\to} \mathrm{Br}(K(X))) \subset \mathrm{Br}(K(X))'.$$

In the case where K is a perfect field,

$$\mathrm{Br}(K(X))' = \mathrm{Br}(K(X)).$$

References

[1] K.Kato, N.Kurokawa, T.Saito : Number theory.1 Fermat's dream

Large time behavior of solutions for system of nonlinear damped wave equations

Hiroshi Takeda (Tohoku University)

Feb. 18-19th, 2010

Abstract: We consider the Cauchy problem for a system of semilinear damped wave equations with small initial data. We derive the asymptotic profile of the nonlinear system corresponding to the results for the nonlinear single equation and we obtain the sufficient condition of the growth order on the nonlinear term to ensure the existence of the solution with the optimal decay. Our proof is based on the analysis for the fundamental solution of the linear damped wave equation.

1 Nonlinear damped wave system

$m \geq 2$, $u : \mathbb{R}_+ \times \mathbb{R}^n \to \mathbb{R}^m$; unknown vector-valued function,
$F : \mathbb{R}^m \to \mathbb{R}^m$; $F_j(u) \sim \prod_{k=1}^m |u_k|^{p_{j,k}}$.

$$\text{(DW)} \quad \begin{cases} \partial_t^2 u - \Delta u + \partial_t u = F(u), & t > 0, \quad x \in \mathbb{R}^n, \\ u(0,x) = a(x), \ \partial_t u(0,x) = b(x), & x \in \mathbb{R}^n. \end{cases}$$

2 Problem

• When does the initial value problem (DW) have a global solution ?
Find the critical condition for the nonlinear term to ensure the existence of time in global solutions!

3 Known Results

Sun-Wang (2007) $m = 2$, $p_{1,1} = p_{2,2} = 0$, $p_{1,2}, p_{2,1} > 1$

$\dfrac{\max\{p_{1,2}, p_{2,1}\} + 1}{p_{1,2}p_{2,1} - 1} \geq \dfrac{n}{2}$	$\dfrac{\max\{p_{1,2}, p_{2,1}\} + 1}{p_{1,2}p_{2,1} - 1} < \dfrac{n}{2}$
finite time blow-up $(n \geq 1)$	small data global existence $(n = 1, 3)$

4 Notation and assumptions

$$P = \begin{pmatrix} p_{1,1} & \cdots & p_{1,m} \\ \vdots & & \vdots \\ p_{m,1} & \cdots & p_{m,m} \end{pmatrix}, \alpha = (P - I)^{-1} \begin{pmatrix} 1 \\ \vdots \\ 1 \end{pmatrix} = \begin{pmatrix} \alpha_1 \\ \vdots \\ \alpha_m \end{pmatrix}.$$

- $p_{j,k} \in [1, \infty) \cup \{0\}$, $\sum_{k=1}^m p_{j,k} > 1$, $j, k = 1, \cdots, m$,
- $\exists (P - I)^{-1}$,
- $(a, b) \in \{W^{1,1}(\mathbb{R}^n) \cap W^{1,\infty}(\mathbb{R}^n) \times L^1(\mathbb{R}^n) \cap L^\infty(\mathbb{R}^n)\}^m$.

5 Results

Theorem. 1. (existence of the global solution) $n = 1, 2, 3$.

$$0 < \alpha_j < \frac{n}{2}, \quad j = 1, \cdots, m, \quad (a, b) : \text{small}$$

$\Longrightarrow \exists !\ u(t)$: global solution of (DW) in

$$\{C([0, \infty); L^1(\mathbb{R}^n) \cap L^\infty(\mathbb{R}^n))\}^m.$$

$$F_j(u) = |u_l|^{p_j} : j - l \ \textit{cyclic}, \ P = \begin{pmatrix} 0 & \ldots & 0 & p_1 \\ p_2 & \ldots & 0 & 0 \\ \vdots & \ddots & \vdots & \vdots \\ 0 & \ldots & p_m & 0 \end{pmatrix}.$$

Theorem. 2. (nonexistence of global solutions) $n \geq 1$,

$$\max_{1 \leq j \leq m} \alpha_j \geq \frac{n}{2},$$
$$\int_{\mathbb{R}^n} a_j(x)dx > 0, \quad \int_{\mathbb{R}^n} b_j(x)dx > 0, \qquad j = 1, \cdots, m$$

$\Longrightarrow u(t)$: blow-up i.e. $\exists T < \infty$ s.t.
$\limsup_{t \nearrow T} \|u(t)\|_{L^1(\mathbb{R}^n) \cap L^\infty(\mathbb{R}^n)} = \infty$.

Theorem. 3. (asymptotic profile) $n = 1, 2, 3$,

$$\min_{1 \leq j \leq m} \sum_{k=1}^m p_{j,k} > 1 + \frac{2}{n}, \quad (a, b) : \text{small}$$

$\Longrightarrow \exists !\ u(t)$: global solution of (DW),

$$G_t(x) := \left(\frac{1}{4\pi t}\right)^{\frac{n}{2}} e^{-\frac{|x|^2}{4t}} \quad \text{(Heat kernel)},$$
$$\|u(t) - MG_t\|_{L^p(\mathbb{R}^n)} = o(t^{-\frac{n}{2}(1 - \frac{1}{p})}), \quad \text{as} \quad t \to \infty,$$

where $M = (M_1, \cdots, M_m)$,

$$M_j = \int_{\mathbb{R}^n} a_j(y) + b_j(y)dy + \int_0^\infty \int_{\mathbb{R}^n} F_j(u(s, y))dy\, ds.$$

6 Remarks on the theorems

For the $j - l$ cyclic case, we see the relationship between the Theorem 1, 2 and 3.

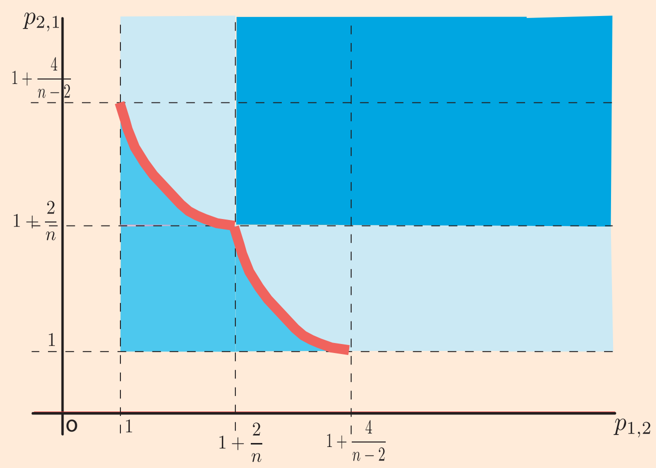

Non-abelian generalization of Iwasawa theory

Kazuaki Ta ima
athematical nstitue Tohoku niversity D1

1 Classical Iwasawa Theory

Let p be a prime number. $\mathbb{Z}_p$**-extension** of a number field k is a Galois e tension k_∞/k with Galois group Γ Gal k_∞/k $\sim \mathbb{Z}_p$ the additive group of p-adic integers. Such a $\mathbb{Z}_p$-e tension can be regard as a tower of fields

$$k \quad k_0 \subset k_1 \subset \cdots \subset k_n \subset \cdots \subset k_\infty \quad \bigcup_{n\geq 0} k_n$$

with Gal k_n/k $\sim \mathbb{Z}/p^n\mathbb{Z}$ where the fields k_n are uni ue sube tensions of k_∞/k with k_n k p^n.

Let k ζ_{p^∞} be the e tension of k obtained by adjoining all the primitive roots of unity of p-power order. hen there e ist precisely one $\mathbb{Z}_p$-e tension of k inside k ζ_{p^∞} . his e tension is called **the cyclotomic** $\mathbb{Z}_p$**-extension** of k.

Let A_n denote the p-primary part of the ideal class group of k_n. y class field theory A_n is isomorphic to the Galois group of the ma imal abelian unramified p-e tension L_n of k_n and these groups have finite order. hen X_∞ $\varprojlim A_n$ is isomorphic to the Galois group of the ma imal unramified abelian p-e tension L_∞ of k_∞. ence we know that Λ $\mathbb{Z}_p$ Γ acts naturally on X_∞. In 1 Iwasawa was studied the structure of X_∞ as Λ-module and he proved following beutiful theorem

heorem 1.1 I asa a 1959). *There exist non-negative integers* μ k_∞/k , λ k_∞/k *and an integer* ν k_∞/k *such that*

$$\sharp A_n \quad p^{\mu(k_\infty/k)p^n+\lambda(k_\infty/k)n+\nu(k_\infty/k)}$$

for all sufficiently large integer $n \geq$.

he integers μ and λ are the invariant of the structure of X_∞ and sometimes also ν are called **the i a-sa a invariants**. specially λ $\mathrm{rank}_{\mathbb{Z}_p} X_\infty$ holds. For the cyclotomic e tension the iwasawa invariants are denoted by μ_p k , λ_p k and ν_p k .

Calculate the i asa a invariants It is no known that general way to calculate the iwasawa invariants. ut following result gives a simple sufficient condition such that all the iwasawa invariants vanish

heorem 1.2 I asa a 1956). *Supose that* p *does not divide the class number* h k *of* k *and* p *is non-split in* $k/\mathbb{Q}$. *Then we have* μ_p k λ_p k ν_p k .

For e ample we see that μ_p $\mathbb{Q}$ λ_p $\mathbb{Q}$ ν_p $\mathbb{Q}$ for any prime p.

2 Non-abelian Iwasawa Theory

For a $\mathbb{Z}_p$-e tension k_∞/k we consider the Galois group of the ma imal unramified **not nessesary abelian** p-e tension $\widetilde{L}_\infty$ resp. $\widetilde{L}_n$ of k_∞ resp. k_n . ut $\widetilde{G}_\infty$ Gal $\widetilde{L}_\infty/k_\infty$, $\widetilde{G}_n$ Gal $\widetilde{L}_n/k_n$.

Our main purpose is to study the group structure of $\widetilde{G}_\infty$ by using "i asa a thoretical methods". ut it is very hard to describe this structure in direct so we shall consider a filtration of $\widetilde{G}_\infty$

$$\widetilde{G}_\infty \quad C_1\ \widetilde{G}_\infty\ \supset C_2\ \widetilde{G}_\infty\ \supset \cdots \supset C_i\ \widetilde{G}_\infty\ \supset \cdots$$

ore precisely we adopt the lower central se uence as the filtration that is C_{i+1} $\widetilde{G}_\infty$ C_i $\widetilde{G}_\infty$, $\widetilde{G}_\infty$ $i \geq 1$ the commutator group of C_i $\widetilde{G}_\infty$ and $\widetilde{G}_\infty$. hen we define **the *i*-th i asa a module** by $X_\infty^{(i)}$ C_i $\widetilde{G}_\infty$ $/C_{i+1}$ $\widetilde{G}_\infty$. e also define $X_n^{(i)}$ as similary.

Let $L_\infty^{(i)}$ resp. $L_n^{(i)}$ be the fi ed field of $\widetilde{L}_\infty$ resp. $\widetilde{L}_n$ by C_{i+1} $\widetilde{G}_\infty$ resp. C_{i+1} $\widetilde{G}_n$. y definition we have $X_\infty^{(i)}$ Gal $L_\infty^{(i)}/L_\infty^{(i-1)}$, $X_n^{(i)}$ Gal $L_n^{(i)}/L_n^{(i-1)}$ especially $X_\infty^{(1)} \sim X_\infty$ and $X_n^{(1)} \sim A_n$ are the usual iwasawa modules. Furtheremore we know that $L_\infty^{(i)}$ is the central p-class field of $L_\infty^{(i-1)}/k_\infty$ namely $L_\infty^{(i)}$ is the ma imal unramified p-e tention of $L_\infty^{(i-1)}$ such that $L_\infty^{(i)}/k_\infty$ is Galois and $X_\infty^{(i)}$ Gal $L_\infty^{(i)}/L_\infty^{(i-1)}$ is conteined in the center of Gal $L_\infty^{(i)}/k_\infty$. his is a reason why we adopt the lower central se uence as a filtration of $\widetilde{G}_\infty$ and this fact plays important role. In fact we know that $X_n^{(i)}$ is finite and $X_\infty^{(i)}$ has the natural Λ-module structure by the virtue of the fact. Furthremore if μ k_∞/k we can prove $X_\infty^{(i)}$ is a finitely generated torsion Λ-module so we define **the *i*-th λ-invariant** by $\lambda^{(i)}$ k_∞/k $\mathrm{rank}_{\mathbb{Z}_p} X_\infty^{(i)}$.

he following theorem which is an analogy of heorem 1.1 is proved by O aki

heorem 2.1 O aki 2007). *Suppose* μ k_∞/k . *Then there exist an integer* $\nu^{(i)}$ k_∞/k *for all* $i \geq 1$ *such that*

$$\sharp X_n^{(i)} \quad p^{\lambda^{(i)}(k_\infty/k)n+\nu^{(i)}(k_\infty/k)}$$

for all sufficiently large integer $n \geq$.

From heorem 2.1 we can regard the i-th iwasawa module $X_\infty^{(i)}$ as sufficiently good objects to study the structure of $\widetilde{G}_\infty$ by using iwasawa theoretical methods .

References

1 .O aki *Non-abelian Iwasawa theory of $\mathbb{Z}_p$-extensions* ournal fur die reine und angewandte athematik 2 2 –

The quadratic subextension of the class field of a real quadratic field

Toshihide DOI

sa6m22@math.tohoku.ac.jp

Mathematical Institute, Tohoku University, Japan

The 2nd GCOE internaitonal symposium in Sendai Feb. 18 – 19, 2010.

1 INTRODUCTION

Let F be an arbitrary algebraic number field and H_F be the maximal unramified (including ∞) abelian extension of F. From the global class field theory, the extension H_F/F is finite and its galois group $G = \mathrm{Gal}(H_F/F)$ is isomorphic to the ordinary ideal class group of F. The field H_F is called the Hilbert class field of F. (For F, Cl_F and h_F denote the ordinary ideal class group of F and its order that is called the class number of F, respectively.)

In general, it is difficult to derive H_F from F. But, if F is quadratic field, there are several way to obtain the H_F. Among these ways, there is a way for real quadratic fields with even class number. The purpose of this poster is to introduce that way with examples of $\mathbb{Q}(\sqrt{85})$.

2 h_F AND FUNDAMENTAL UNIT OF F

Let F be a real quadratic field $\mathbb{Q}(\sqrt{m})$ where m is a square-free positive rational integer, D be the discriminant of F, and ε be the fundamental unit of F.

2.1 DEFINITIONS and TERMS

Deffinition 1
If $a, b, c \in \mathbb{Q}$ satisfy $D = b^2 - 4ac$ and $(a, b, c) = 1$, then the roots θ, θ' of

$$ax^2 + bx + c = 0$$

are called a quadratic irrational number in D (denote by QI in D). Moreover, if θ satisfies

$$\theta > 1,\ 0 > \theta' > -1,$$

then θ is called a reduced quadratic irrational number in D (denote by RQI in D).

Set the relation "$\sim$" on $\mathbb{R}$ as follows; For $\theta, \theta_0 \in \mathbb{R}$, if $\theta \sim \theta_0$ then there exist $a, b, c, d \in \mathbb{Z}$ such that

$$\theta = \frac{a\theta_0 + b}{c\theta_0 + d} \text{ and } \det\begin{pmatrix} a & b \\ c & d \end{pmatrix} = \pm 1.$$

"$\sim$" satisfies equivalence condition, transitive, symmetric, reflexive. If

$$\theta_n = a + \frac{1}{\theta_{n+1}} = \frac{a\theta_{n+1} + 1}{1 \cdot \theta_{n+1} + 0},$$

then $\theta_n \sim \theta_{n+1}$ since $\det\begin{pmatrix} a & 1 \\ 1 & 0 \end{pmatrix} = -1$. So each end-term θ_n of the expanding to (all numerator equal 1) continued fraction of $\theta \in \mathbb{R}$ satisfies $\theta \sim \theta_n$.

2.2 FACTS and THEOREMS

Fact1: If θ is QI in D and $\theta \sim \theta_0$, then θ_0 is also QI in D and appear in the expanding to continued fraction of θ as an end-term.

Fact2: All QIs are expanded to cyclic continued fraction. Moreover, all end-term of cyclic part of continued fraction of a QI are RQI.

Theorem 1
The number of RQI in D is finite. More precisely, the necessary and sufficient condition of that $ax^2 + bx + c = 0, a, b, c \in \mathbb{Z}$ has a root of RQI in D is below;

$$b < 0,\ |b| < \sqrt{D},$$
$$a > 0,\ c < 0,$$
$$|ac| = \frac{\sqrt{D} + |b|}{2} \cdot \frac{\sqrt{D} - |b|}{2},$$
$$\frac{\sqrt{D} + |b|}{2} > a,\ |c| > \frac{\sqrt{D} - |b|}{2},$$
$$(a, b, c) = 1.$$

Theorem 2
Let $F = \mathbb{Q}(\sqrt{m}), m > 0$, square-free, and D be the discriminant of F, and set h be the number of classes of $\{\text{All QI in } D\}/\sim$. Then

$$h = h_F.$$

Theorem 3
F, D as above. Let θ be RQI in D and ε be the fundamental unit of F and

$$\theta = k_0 + \cfrac{1}{k_1 + \cdots \cfrac{1}{k_{n-1} + \cfrac{1}{\theta}}} = \frac{p_n\theta + p_{n-1}}{q_n\theta + q_{n-1}}$$

be the first section of cycles of the expanding to continued fraction. Then

$$\varepsilon = q_n\theta + q_{n-1}.$$

Now we can calculate h_F and ε by using above facts & theorems.

Example
If $F = \mathbb{Q}(\sqrt{85})$, then $D = 85$. From theorem 1,

b	$\lvert ac\rvert$	range of $a, \lvert c\rvert$	a	c	θ
-9	1	$[1, 9]$	1	-1	$\frac{9+\sqrt{85}}{2} = \theta_1$
-7	9	$[3, 8]$	3	-3	$\frac{7+\sqrt{85}}{6} = \theta_2$
-5	15	$[3, 7]$	3	-5	$\frac{5+\sqrt{85}}{6} = \theta_3$
"	"	"	5	-3	$\frac{5+\sqrt{85}}{10} = \theta_4$

The expanding to continued fraction of θ_2 tells us $\theta_2 \sim \theta_3 \sim \theta_4$ so $h_F = 2$. And since $\theta_1 = 9 + \frac{1}{\theta_1} = \frac{9\theta_1 + 1}{\theta_1}$, we get $\varepsilon = \theta_1$.

3 HILBERT CLASS FIELD OF F WITH $h_F = 2$

To determinate the Hilbert class field H_F of a real quadratic field F with $h_F = 2$, we use following theorems.

Theorem 4
For an algebraic extention K/F, $\mathcal{D}(K/F), \mathcal{D}(\alpha, K/F)$ denote the relative different of K/F and the relative different of K/F for $\alpha \in K$, respectively. Let $f_\alpha(x)$ be the minimal polynomial of $\alpha \in K$ over F. Then, for all $\alpha \in K$,

$$\mathcal{D}(K/F) \mid \mathcal{D}(\alpha, K/F) \text{ and } \mathcal{D}(\alpha, K/F) = (f_\alpha{}'(\alpha)).$$

Theorem 5
Let $K, F, \mathcal{D}(K/F)$ same as avobe and $\mathfrak{p}$ be a prime of F. Then

$$\mathfrak{p} \text{ ramifies in } K/F \Longleftrightarrow \mathfrak{p} \mid \mathcal{D}(K/F).$$

From above theorems, we only have to find $\alpha_1, \alpha_2, \ldots$ such that

$$\bigcap_{i=1} (f_{\alpha_i}{}'(\alpha_i)) = 1$$

to say that K/F is unramified extension.

Example
Let $F = \mathbb{Q}(\sqrt{85})$ and $K_1 = F(\sqrt{\varepsilon}), K_2 = F(\sqrt{5}), K_3 = F(\sqrt{5\varepsilon})$. Where $\varepsilon = \frac{9+\sqrt{85}}{2} = \theta_1$. We prove that K_2/F is uanramified extension in following. Let $\alpha_1 = \sqrt{5}$ and $\alpha_2 = \frac{1+\sqrt{17}}{2}$. Then

$$f_{\alpha_1} = x^2 - 5,\ f_{\alpha_2} = x^2 - x - 4$$
$$\text{and hence } \mathcal{D}(\alpha_1, K_2/F) = (2\sqrt{5}),\ \mathcal{D}(\alpha_2, K_2/F) = (\sqrt{17}).$$

Consequently, we obtain

$$\mathcal{D}(K_2/F) \mid \mathcal{D}(\alpha_1, K_2/F) \cap \mathcal{D}(\alpha_2, K_2/F) = (1),$$

so that K_2/F is unramified extension.

The pattern formation of head regeneration model of Hydra

Madoka Nakayama (Tohoku University)

Abstract: Hydra is a small animal living in fresh water, which is best known for its ability of regeneration. When a hydra is cut into two pieces, two hydras will regenerate. There has been several mathematical models proposed to describe this experiment. A classical model proposed by Gierer and Meinhardt in 1972, is based on the idea of diffusion- driven instability between two chemicals called activator and inhibitor. Recently, Anna Marciniak proposed new regeneration models from a more biologically refined viewpoint. Her models consist of free and bound receptors, ligands and an enzyme, and a head is formed at place of higher bound receptor concentration.

1 What is Hydra?

- freshwater coelenterate
- best known for its ability to regenerate.

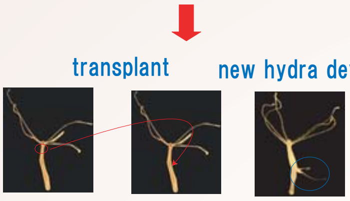

2 Idea of the model

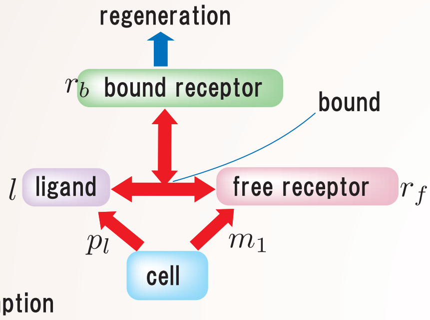

Assumption

Density of bound receptor is the highest at a head.

3 Marciniak-Czochra model(2006)

At first we consider the following problem for

$$\frac{\partial r_f}{\partial t} = -\mu_f r_f - b r_f l + d r_b + m_1, \tag{1}$$

$$\frac{\partial r_b}{\partial t} = -\mu_b r_b + b r_f l - d r_b, \tag{2}$$

$$\frac{\partial l}{\partial t} = \frac{1}{\gamma}\frac{\partial^2 l}{\partial x^2} - \mu_l l - b r_f l + d r_b + p_l, \tag{3}$$

$$\frac{\partial pl}{\partial t} = -\delta_l \frac{p_l}{1+p_l^2} + \frac{m_2 l r_b}{(1+\sigma_l p_l^2 - \beta_l p_l)(1+\alpha_l r_b)} \tag{4}$$

$r_f \geq 0$:density of free receptors,
$r_b \geq 0$:density of bound receptors,
$l \geq 0$:density of bound ligands,
$p_l \geq 0$:production term of ligands,
$\mu_f, \mu_b, \mu_l, m_1, m_2, b, d, \sigma_l, \beta_l, \delta_l$:positive constants.

4 Stationary problem

To consider stationary problem, we put

$$\frac{\partial r_f}{\partial t} = \frac{\partial r_b}{\partial t} = \frac{\partial l}{\partial t} = \frac{\partial pl}{\partial t} = 0,$$

and reduce (1) to the following two component system:

$$\begin{cases} \dfrac{1}{\gamma}\dfrac{d^2 u}{dx^2} + f(u,v) = 0, \\ g(u,v) = 0 \\ \dfrac{du}{dx} = \dfrac{dv}{dx} = 0, (x = 0, 1) \end{cases}$$

where $u = l, v = p_l$ and let $\mu_b \mu_f + d\mu_f = M$,

$$f(u,v) = v - \mu_l u - \frac{m_1 \mu_b b u}{M + \mu_b b u},$$

$$g(u,v) = -\delta_l \frac{v}{1+v^2} + \frac{m_1 m_2 b u^2}{(M + \mu_b b u + \alpha_l m_1 b u)(1 + \sigma_l v^2 - \beta_l v)}.$$

To draw nullclines, we consider $f(u,v) = 0, g(u,v) = 0$.

$$f(u,v) = 0 \Leftrightarrow v = \mu_l u - \frac{m_1 \mu_b b u}{M + \mu_b b u},$$

$$g(u,v) = 0 \Leftrightarrow \delta_l \frac{v}{1+v^2}(1 + \sigma_l v^2 - \beta_l v) = \frac{m_1 m_2 b u^2}{M + u(\mu_b b + \sigma_l m_1 b)} =: \Psi(u)$$

Lemma
Let $A = \dfrac{\psi(u)}{\delta_l}$. Assume that
(i) $9\sigma_l - 1 > 0$ and $\sqrt{3\sigma_l} < \dfrac{\beta_l}{9\sigma_l - 1}$, $\sqrt{3\sigma_l} < A < \dfrac{\beta_l}{9\sigma_l - 1}$, or
(ii) $9\sigma_l - 1 > 0$ and $\dfrac{\beta_l}{9\sigma_l - 1} < \sqrt{3\sigma_l}$, $\dfrac{\beta_l}{9\sigma_l - 1} < A < \sqrt{3\sigma_l}$.
In addition, if A satisfies
$-(A+\beta_l) - \sqrt{(A+\beta_l)^2 - 3\sigma_l} < \dfrac{3\sigma_l\{\beta_l + A(1-9\sigma_l)\}}{2(3\sigma_l - A^2)} < -(A+\beta_l) + \sqrt{(A+\beta_l)^2 - 3\sigma_l}$,
then $g(u,v) = 0$ and $f(u,v) = 0$ intersect at three points (u_-, v_-),(u_m, v_m), (u_+, v_+).

From the Lemma, we obtain the relationship of parameters for which the system (1)-(4) has three stationaly solutions.
Let $(u_- < u_m < u_+)$

$$\begin{cases} v = h_0(u)\,(u_0 < u < u_+,\ v_0 < v < v_+) \\ v = h_m(u)\,(u_0 < u < u_+,\ v_+ < v < v_-) \\ v = h_1(u)\,(u_0 < u < u_+,\ v_- < v < v_1) \end{cases} \tag{5}$$

In particular, we focus on the curve $v = h_j(u) (j = 0, 1)$.

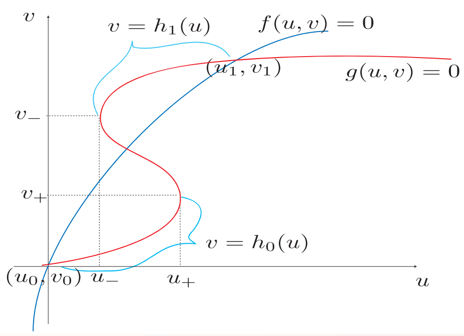

We substitute $v = h_j(u)\,(j = 0, 1)$ in $f(u,v)$, then we have the following systems.

$$\begin{cases} \dfrac{1}{\gamma}\dfrac{d^2 u}{dx^2} + f(u, h_j(u)) = 0, \\ \dfrac{du}{dx} = \dfrac{dv}{dx} = 0 \quad (x = 0, 1). \end{cases} \tag{6}$$

From the lemma, we obtain the following theorem.

Theorem
There exists a monotone increasing solution of (6) which is C^1 in [0,1].

Outline of the proof
We consider the following initial value problems

$$\begin{cases} \dfrac{1}{\gamma}\dfrac{d^2 \hat{u}}{dx^2} + f_0(\hat{u}, h_0(\hat{u})) = 0, \\ \dfrac{d\hat{u}}{dx}(0) = 0, \\ \hat{u}(0) = k \quad (u_0 < k < u_+), \end{cases} \tag{7}$$

$$\begin{cases} \dfrac{1}{\gamma}\dfrac{d^2 \bar{u}}{dx^2} + f_0(\bar{u}, h_0(\bar{u})) = 0, \\ \dfrac{d\bar{u}}{dx}(0) = 0, \\ \bar{u}(0) = p \quad (u_+ < p < u_1). \end{cases} \tag{8}$$

We show $\hat{u}$ is monotone increasing, and $\bar{u}$ is monotone decreasing . Combining these facts, we can choose k and p so that the graphs of $\hat{u}$ and $\bar{u}$ are tangent to each other at $u = \beta$, where β is an arbitrarily fixed constant in $[u_0, u_+] \cap [u_-, 1]$.

The computational methods of the canonical height on elliptic curves

Tadahisa Nara (Mathematical Institute, Tohoku University)

Elliptic curves and the canonical height

$\mathbb{Q}$: set of rational numbers

The elliptic curve E over $\mathbb{Q}$ is defined as a curve of the form of $y^2 = x^3+Ax+B, (A, B \in \mathbb{Q})$ having some conditions. And then we think of the point (∞, ∞) as is on E and denote it O. In number theory one of interests about elliptic curves is studying rational points, that is a solution in $\mathbb{Q}$ of the equation above. Mordell-Weil theorem is one of basic guidelines for this problem, which states that all the ratoinal points on an elliptic curve form an finitely generated abelian group. This means that you can know all the rational points if you find specific points of finite number on the curve.

The height of a point is numerical size of the points for certain arithmetic. The canonical height is one of heights which is defined on elliptic curves.

Definition 0.1 *The naive heght on $E(\mathbb{Q})$ denoted by h is function defined by*

$$h : E(\mathbb{Q}) \to \mathbb{R},\ P = (a/c, *) \mapsto \log \max\{|a|, |c|\}.$$

The canonical height on $E(\mathbb{Q})$ denoted by $\hat{h}$ is function defined by

$$\hat{h} : E(\mathbb{Q}) \to \mathbb{R},\ P \mapsto \lim_{n\to\infty} \frac{1}{4^n} h([2^n]P),$$

where $[2^n]P$ means 2^n times addition of P about its group operation.

The features of the canonical height are as follows.

- $\hat{h}([m]P) = m^2\hat{h}(P)$
- $\hat{h}(P+Q) + \hat{h}(P-Q) = 2\hat{h}(P) + 2\hat{h}(Q)$

Computation of the canonical height

The definition above, which is usually used, is brief but not suitable for practical computaion. Neron and Tate showed that there is local height function λ_p such that $\hat{h}(P) = \sum_{p:prime,\infty} \lambda_p(P)$. So the canonical height is decomposed into something local. Those factors of the decomposition are not difficult to compute. For example for all prime p that do not divide $4A^3+27B^2$ nor c (the denominator of the x-coordinate of P) $\lambda_p(P) = 0$, so this is a finite sum indeed. For other primes we can determine algebraically $\lambda_p(P)$ using the results of reduction type of elliptic curves. And about the case of $p = \infty$ following theorem is useful.

Theorem 0.2 *(Tate) Suppose that there is an $\epsilon > 0$ so that every point P in $E(\mathbb{Q})$ satisfies $|x(P)| > \epsilon$. Then for all $P(\neq O) \in E(\mathbb{Q})$, $\lambda_\infty(P) = \log|x(P)| + \frac{1}{4}\sum_{n=0}^{\infty} 4^{-n} \log|z([2]^n P)|$, where $x(P)$=x-coordinate of P and $z(P) = 1 - 2A/x(P)^2 - 8B/x(P)^3 + A^2/x(P)^4$.*

Using modified versions of above theorem, we see following.

Theorem 0.3 *Let α and β be coprime odd integers with $\alpha \geq 1.232\beta > 3$ and $E/\mathbb{Q} : y^2 = x^3 + \alpha^6 + \beta^6$ be a elliptic curve. Suppose every order of the prime divisors of $\alpha^6 + \beta^6$ is odd and $P_1 + P_2 \notin 2E(\mathbb{Q})$, where $P_1 = (-\alpha^2, \beta^3), P_2 = (-\beta^2, \alpha^3)$. Then there is a basis of $E(\mathbb{Q})$ including P_1 and P_2, in particular if the* rank $E(\mathbb{Q}) = 2$, *$\{P_1,\ P_2\}$ is basis of the free part of $E(\mathbb{Q})$.*

Spatial branching process in random environment

NISHIMORI Yasuhito
(Mathematical Institute Tohoku University)

Introduction

An outline of these notes is as follows. After defining the Galton-Watson process, we introduce the branching Brownian motion among Poisson obstacles. In the following section, we present some result on exponential growth. Our main purpose is to compare the growth order of Galton-Watson process with strictly dyadic branching Brownian motion among Poisson obstacles.

1 Galton-Watson process

We consider Galton-Watson process $\{G_n\}_{n=0}^{\infty}$ with offspring distribution $\{p_k\}_{k=0}^{\infty}$ satisfying $m = \sum_{k=1}^{\infty} kp_k > 1$ and $p_k \neq 1$ for any $k \in \mathbf{N} \cup \{0\}$.

Theorem 1 (H.Kesten, B.P.Stigum, 1966)
Let $W = \lim_{n\to\infty} m^{-n} G_n$. Then

$$\sum_{k=2}^{\infty} p_k k \log k < \infty \ \Rightarrow\ E[W] = 1 \quad . \tag{1}$$

Theorem 1 says the growth rate of $\{G_n\}$.

2 Branching Brownian motion and Poisson obstacles

Firstly, we call $(\{\hat{Z}_t\}_{t\geq 0}, P_x)$ strictly dyadic branching Brownian motion on $\mathbf{R}^d$ with branching rate $\beta(x)$, if for any $g \in C_b^+$, $u(x,t) = E_x[e^{-\langle g, \hat{Z}_t\rangle}]$ solves

$$\begin{cases} \dfrac{\partial u}{\partial t} = \dfrac{1}{2}\triangle u + \beta(u^2 - u) \ \ on \ \ \mathbf{R}^d \times (0,\infty) \\ \lim\limits_{t\downarrow 0} u(\cdot,t) = e^{-g(\cdot)} \ \ on \ \ \mathbf{R}^d \times (0,\infty) \\ 0 \leq u \leq 1, \end{cases}$$

where $\langle g, \hat{Z}_t\rangle = \int_{\mathbf{R}^d} g(x)\hat{Z}_t(dx)$. $(\{\hat{Z}_t\}_{t\geq 0}, P_x)$ is following that one particle starts at $x \in \mathbf{R}^d$, performing an Brownian motion on $\mathbf{R}^d$. Her life time distributions is exponential with parameter $\beta(x)$. Just as it dies, one particle splits into two one and descendants perform same as their parent.

Secondly, we set random environment by $(\omega, \mathbf{P})$ which is a Poisson point process in $\mathbf{R}^d$ with intensity measure $\nu(dx) = \nu dx$ where $\nu > 0$ and dx is the Lebesgue measure. For $a > 0$, let K_ω denote a random set given by a-neighborhood of each configuration ω:

$$K_\omega \overset{\text{def}}{=} \bigcup_{x\in supp(\omega)} \bar{B}(x,a)$$

And for fixed $0 < \beta_1 < \beta_2$, we define the strictly dyadic branching Brownian motion $(\{Z_t\}_{t\geq 0}, P^\omega)$ with branching rate $\beta(x)$:

$$\beta(x) = \beta_1 \cdot \chi_{K_\omega}(x) + \beta_2 \cdot \chi_{K_\omega^c}(x)$$

Here χ is indicator function. Then, as long as a particle in K_ω, the splitting rate is less than in K_ω^c. Thus we may consider the random field K_ω as obstacles. So K_ω is said to Poisson obstacles and branching Brownian motion $(\{Z_t\}_{t\geq 0}, P^\omega)$ generated by above $\beta(x)$ is strictly dyadic branching Brownian motion among Poisson obstacles(DBBP).

3 Some results

Our main purpose is to compare the growth rate Galton-Watson process with DBBP. According to the latter, the following result shows growth order of it. We denote $|Z_t| = \langle 1, Z_t\rangle$.

Theorem 2 (J. Engländer [2])
On a set of full $\mathbf{P}$ measure

$$\lim_{t\to\infty} \exp\Big[-t\Big\{\beta_2 - c(d,\nu)(\log t)^{-\frac{2}{d}}\Big\}\Big] E^\omega[|Z_t|] = 1 \tag{2}$$

as $t \to \infty$, where ω_d is the volume of the d-dimensional unit ball, λ_d is the principal Dirichlet eigenvalue of $-\frac{1}{2}\triangle$ on it, and $c(d,\nu) = \lambda_d(\frac{d}{\nu\omega_d})^{-\frac{2}{d}}$.

Outline of the proof of theorem 2

We set $T_t f(x) = E_x[f(Y_t)]$ where $\{Y_t\}_{t\geq 0}$ is $\frac{1}{2}\triangle + \beta$-diffusion, and $\{T_t\}_{t\geq 0}$ is the semigroup of it. Then

$$E[|Z_t|] = (T_t 1)(x)$$

by *The first moment formula*. Hence *the Feynman-Kac formula* implies

$$(T_t 1)(x) = \mathbb{E}_x\Big[\exp\Big\{\int_0^t \beta(W_s)ds\Big\}\Big],$$

where $(\{W_t\}_{t\geq 0}, \mathbb{P}_x)$ is d-dimensional Brownian motion. Thus,

$$\begin{aligned} E^\omega[|Z_t|] &= \mathbb{E}_x\Big[\exp\Big\{\int_0^t \beta_2 - (\beta_2 - \beta_1)\cdot\chi_{K_\omega}(W_s)ds\Big\}\Big] \\ &= e^{\beta_2 t}\exp\Big[-c(d,\nu)t(\log t)^{-\frac{2}{d}}(1+o(1))\Big] \end{aligned} \tag{3}$$

as $t \to \infty$. To obtain the second equality of (3), we use a theorem of the large time behavior of Brownian motion among Poisson obstacles (cf.[1]).

Theorem 2 tells us that the growth order of $E^\omega[|Z_t|]$ is determined by the effect of each particles hitting K_ω.

References

[1] M. Donsker, S. R. S. Varadhan : Asymptotics for the Wiener sausage, Comm. Pure. Appl. Math., **28**, 1975.

[2] J. Engländer : Quenched law of large numbers for branching Brownian motion in random medium, Ann. Inst. H. Poincaré Probab. Statist., 2007.

On a periodic decomposition of meromorphic functions

Takanao Negishi (Tohoku University)

★ Introduction

For an arbitrary $c \in \mathbb{C}$, we denote by Δ_c the difference operator about c , i.e. $\Delta_c f = f(z+c) - f(z)$, where $f \in \mathfrak{M}(\mathbb{C})$ (the set of meromorphic functions on $\mathbb{C}$) . Then , we consider the difference equation $\Delta_{c_1}\Delta_{c_2}\cdots\Delta_{c_n} f = 0 \cdots$ **(1)** $(c_1, c_2, \cdots, c_n \in \mathbb{C})$. We easily see that functions which is a sum of periodic functions $P_{c_1} + P_{c_2} + \cdots + P_{c_n}$ where each P_{c_k} is a c_k-periodic meromorphic function satisfy **(1)** . On the contrary , can all functions satisfying **(1)** be always represented as such a sum of periodic functions ?

We consider this periodic decomposition problem of meromorphic functions . By applying the method we used in 1-dimensional case , we try to investigate the 2-dimensional case .

★ Historical Background

Problem: If a function $f : \mathbb{R} \longrightarrow \mathbb{R}$ satisfies the difference equation $\Delta_{c_1}\Delta_{c_2}\cdots\Delta_{c_n} f = 0 \cdots$ **(2)** for some $c_1, c_2, \cdots, c_n \in \mathbb{R}$, then can f be written in the form of $f = P_{c_1} + P_{c_2} + \cdots + P_{c_n}$ $(P_{c_k} : \mathbb{R} \longrightarrow \mathbb{R};\ c_k\text{-periodic} ,\ 1 \le k \le n) \cdots$ **(3)** ?

Such periodic decomposition problem has already been studied in real analysis so far . However in complex analysis , it has not been considered . It started with some unpublished work of I.Z.Rusza and continued among others .

To study this problem , we have two ways . First we restrict functions to some class . A class $\mathcal{F}$ of real functions is said to have the decomposition property (DP) , if for every $f \in \mathcal{F}$ and $c_1, \cdots, c_n \in \mathbb{R}$, **(2)** implies that f has a decomposition as **(3)** with $P_{c_k} \in \mathcal{F}$ $(1 \le k \le n)$.

● Examples of the classes having the DP

- $\boldsymbol{B}(\mathbb{R}) = \{\text{bounded functions}\}$
- $\boldsymbol{BC}(\mathbb{R}) = \{\text{bounded continuous functions}\}$
- $\boldsymbol{BM}(\mathbb{R}) = \{\text{bounded measurable functions}\}$
- $\boldsymbol{B}(\mathbb{Z} \to \mathbb{Z}) = \{\text{bounded } \mathbb{Z} \longrightarrow \mathbb{Z} \text{ functions}\}$

(In case of $\boldsymbol{B}(\mathbb{Z} \to \mathbb{Z})$, periods c_ks are all integers)

However the class $\boldsymbol{C}(\mathbb{R}) = \{\text{continuous functions}\}$ and $\mathbb{R}^{\mathbb{R}} = \{\text{all real functions}\}$ do not have .

The second idea is to complement **(2)** with other conditions , so that these will be sufficient and necessary for the existence of periodic decompositions . I.Z.Ruzsa showed that if $\frac{c}{d} \notin \mathbb{Q}$, $f(x) = x$ can be split into a c-periodic function and a d-periodic function . And he showed more generally , if $\frac{c_i}{c_j} \notin \mathbb{Q}$ for $i \neq j$, then **(2)** implies the decomposition in the form of **(3)** .

★ The Results on the 1 − dimensional case

Before Investigating the general form **(1)** , it is basically important to study the easier equation $\Delta_c\Delta_d f = 0 \cdots$ **(4)** .

Concerning **(4)** , we can show the following theorem :

Theorem 1. Let $\mathfrak{E}(\mathbb{C})$ be the set of entire functions on $\mathbb{C}$ and $\mathfrak{M}(\mathbb{C})$ be the set of meromorphic functions on $\mathbb{C}$. The function f satisfying the difference equation $\Delta_c\Delta_d f = 0$ can be decomposed as follows ,

[A] if c and d are linearly independent over $\mathbb{R}$, i.e. $\frac{c}{d} \notin \mathbb{R}$,
  $(a)$when $f \in \mathfrak{E}(\mathbb{C})$, then $f = Cz + P_c + P_d$ $\quad (C : const, P_c, P_d \in \mathfrak{E}(\mathbb{C}))$
  $(b)$when $f \in \mathfrak{M}(\mathbb{C})$, then $f = P_c + P_d$ $\quad (P_c, P_d \in \mathfrak{M}(\mathbb{C}))$

[B] if $\frac{c}{d} = \frac{c'}{d'} \in \mathbb{Q}$ ($\frac{c'}{d'}$ is an irreducible fraction , $c = \mu c', d = \mu d'$),
  $(a)$when $f \in \mathfrak{E}(\mathbb{C})$, then $f = P_c + P_d + P_\mu z$ $\quad (P_c, P_d, P_\mu \in \mathfrak{E}(\mathbb{C})$, $P_\mu : \mu - periodic)$
  $(b)$when $f \in \mathfrak{M}(\mathbb{C})$, then $f = P_c + P_d + P_\mu z$ $\quad (P_c, P_d, P_\mu \in \mathfrak{M}(\mathbb{C})$,$P_\mu : \mu - periodic)$

[C] if $\frac{c}{d} \in \mathbb{R}\backslash\mathbb{Q}$,
  $(a)$when $f \in \mathfrak{E}(\mathbb{C})$, then $f = Cz + P_c + P_d + \sum_{n=1}^{\infty}({Q_c}^n + {Q_d}^n)$
  $(C : const, P_c, P_d, {Q_c}^n, {Q_d}^n \in \mathfrak{E}(\mathbb{C}), {Q_c}^n : c - periodic,$ ${Q_d}^n : d - periodic)$

The method of proof is based on the Fourier expansion of entire periodic functions and the Mittag-Leffler theorem . Applying the above theorem again and again , we can gain the following theorem :

Theorem 2. Let $c_1, c_2, \cdots, c_n \in \mathbb{C}$ be pairwise linearly independent over $\mathbb{R}$.

[A] $\forall f \in \mathfrak{E}(\mathbb{C})$ s.t. $\Delta_{c_1}\Delta_{c_2}\cdots\Delta_{c_n} f = 0$ can be decomposed in the form of
$$f = a_1 z + a_2 z^2 + \cdots + a_{n-1} z^{n-1} + P_{c_1} + P_{c_2} + \cdots + P_{c_n}$$
$$(a_j \in \mathbb{C}, P_{c_j} \in \mathfrak{E}(\mathbb{C}) : c_j - periodic, 1 \le j \le n)$$

[B] $\forall f \in \mathfrak{M}(\mathbb{C})$ s.t. $\Delta_{c_1}\Delta_{c_2}\cdots\Delta_{c_n} f = 0$ can be decomposed in the form of
$$f = P_{c_1} + P_{c_2} + \cdots + P_{c_n}$$
$$(P_{c_j} \in \mathfrak{M}(\mathbb{C}) : c_j - periodic, 1 \le j \le n) \cdots \textbf{(5)}$$

Corollary 1. Let $c_1, c_2, \cdots, c_n \in \mathbb{C}$ be pairwise linearly independent over $\mathbb{R}$. Then , an arbitrary $(n-1)$-degree polynomial can be decomposed in the form of **(5)** .

Next we try to consider the 2-dimensional case , that is the decomposition problem of meromorphic functions on $\mathbb{C}^2$.

Then we apply the ways that we used in 1-dimensional case . So , here we state left or right solution of $\Delta_1 f = h$ $(h \in \mathfrak{M}(\mathbb{C}))$. We denote the set of $h(z)$'s poles whose real parts are positive by $\{s_n\}$ and non-positive by $\{t_n\}$. By Mittag-Leffler theorem , we can decompose h into two meromorphic functions h_1, h_2 $(h = h_1 + h_2)$ where the polar set of h_1 is $\{s_n\}$ and that of h_2 is $\{t_n\}$. $\Delta_1 f_1 = h_1$ has a solution that has a form of $f_1 = \sum_{n=1}^{\infty}(h(z-n) - p_n) + E_1$ $(p_n : polynomial$, $E_1 \in \mathfrak{E}(\mathbb{C}))$. We call a solution of this type "right solution" . And $\Delta_1 f_2 = h_2$ has a solution that has a form of $f_2 = -\sum_{n=0}^{\infty}(h(z+n) - q_n) + E_2$ $(q_n : polynomial$, $E_2 \in \mathfrak{E}(\mathbb{C}))$. We call a solution of this type "left solution" . Then $f = f_1 + f_2$ is a solution of $\Delta_1 f = h$.

★ The 2 − dimensional case

In case of entire functions on $\mathbb{C}^2$, we can show following theorem :

Theorem 3. [A] Let $e_1 = {}^t(1, 0)$, $\alpha = ae_1$ $(a \notin \mathbb{R})$. Then a function $f(z, w) \in \mathfrak{E}(\mathbb{C}^2)$ satisfying $\Delta_{e_1}\Delta_\alpha f = 0$ has a representation as
$$f = Cz + P_{e_1} + P_\alpha \ (C : const ,\ P_{e_1}, P_\alpha \in \mathfrak{E}(\mathbb{C}^2))$$
[B] Let $e_2 = {}^t(0, 2)$. Then a function $f(z, w) \in \mathfrak{E}(\mathbb{C}^2)$ satisfying $\Delta_{e_1}\Delta_{e_2} f = 0$ has a representation as
$$f = P_{e_1} + P_{e_2} \ (P_{e_1}, P_{e_2} \in \mathfrak{E}(\mathbb{C}^2))$$

Because the poles of meromorphic functions are not isolated , the meromorphic case is not easy . Furthermore , we have some phenomena which do not arise in 1-dimensional case . For example , even the most basic type of difference equation $\Delta_c f = h$ may not have a solution in $\mathfrak{M}(\mathbb{C}^2)$.

(Ex. $\Delta_{e_1} f = \frac{1}{zw-1}$)

When we consider $\Delta_{e_1} f(z, w) = h(z, w)$, we regard the variable w as a parameter , that is we think the functions $f(z; w)$ and $h(z; w)$ in z varies as the w chenges . Then the polar distribution also depends on the value of w .

Now we restrict the value of w by removing some points from w-plane . First we remove the points $w = a$ s.t. $h(z, a) \equiv 0$ or ∞ . Next we remove the points at which some poles of $h(z; w)$ generate to ∞ . Finally , we remove the points $w = a$ s.t. $I(x, a) := \inf_{y \in \mathbb{R}} |A(x + yi, a)| = 0$ for $\forall x \in \mathbb{R}$ where $h(z, w) = \frac{B(z,w)}{A(z,w)}$ $(A, B \in \mathfrak{E}(\mathbb{C}^2)$) .

We denote the removal set by $R = R(h; e_1)$. When $w = w_0 \in \mathbb{C}\backslash R$ has a neighborhood $U \subset \mathbb{C}\backslash R$ such that for $\forall y \in \mathbb{R}$ we can find $\exists M \in \mathbb{R}$, $\delta > 0$ s.t. $h(z, w)$ is holomorphic in $\{z \in \mathbb{C} \mid \Re z < M , |\Im z - y| < \delta\} \times U$, then we call the set of all such points right-solvable domain $(\mathcal{S}_R(h; e_1))$. And if h is is holomorphic in $\{z \in \mathbb{C} \mid \Re z > M , |\Im z - y| < \delta\} \times U$, then we call the set of all such points left-solvable domain $(\mathcal{S}_L(h; e_1))$.

If $w_0 \in \mathcal{S}_R(h; e_1)$, we can find a right solution of $\Delta_{e_1} f = h$ on $\mathbb{C} \times U$ where U is a neighborhood of w_0 . If $w_0 \in \mathcal{S}_L(h; e_1)$, we can find a left solution of $\Delta_{e_1} f = h$ on $\mathbb{C} \times U . If w_0 \in \mathbb{C}\backslash R$, then we can decompose h as $h = h_1 + h_2$ where $w_0 \in \mathcal{S}_R(h_1; e_1)$, $w_0 \in \mathcal{S}_L(h_2; e_1)$. Therefore we can gain some local solutions of $\Delta_{e_1} f = h$. right or left solution can be extended to the right or left solvable domain .

In regard to $\Delta_{e_1}\Delta_{e_2} f = 0$, I have not completed the study . However , under some assumptions , a function satisfying $\Delta_{e_1}\Delta_{e_2} f = 0$ has a periodic decomposition . For example , if $\exists w_0, w_0 + 1 \in \mathcal{S}_R(f; e_1)$, then f has a periodic decomposition .

Difficulties of Solving Problems

Kojiro Higuchi

- Computability Theory:

– *Computability theory* is the study of algorithm, computability and uncomputability.

- A study of difficulties of solving problems:

– What are *problems*? How are difficulties of solving problems *defined*?
– What is the *distribution* of difficulties of solving problems like?

- My study is to clarify the distribution of difficulties of solving Π^0_1 Mass Problems:

– Difficulties are defined by the concept of *Algorithms*.

Mass Problems:=

"Sets of functions on natural numbers".
But we consider mass problems and their elements as follows:
Mass Problems =
"Sets of solutions to corresponding problems",
Elements =
"Solutions to the corresponding problem".

Examples:

1. Make a complete table of prime numbers,
2, 3, 5, 7, 11, 13, 17, 19, 23, 29, 31, 37, $\cdots$.
2. Calculate π by decimal expansion,
3.141592653589793238462643383279$\cdots$.
3. Construct a transcendental number except for e and π,
0.153625035358421993710300427342$\cdots$.
4. Find an uncomputable function.
5. Find an infinite random sequence,
01101000101110110001011011101100$\cdots$.
6. Extend Mathematics (ZFC) to some complete consistent theory.

Degrees:=

"Difficulties of solving mass problems".
P is not more difficult than Q (P≤Q) =
"Some algorithm gives a solution to P by any solution to Q".

The Distribution of Degrees:

1. There are infinitely many degrees.
2. There are P and Q such that P$\not\leq$Q and P$\not\geq$Q.
3. The top degree and the bottom degree exist.

–A problem without solutions is of the top degree.
–A problem with a computable solution is of the bottom degree.

Algorithms:=

Programs written by "Computer Language + an Instruction *Oracle*".

For a solution p and a number x, the calculation of Φ(p; x) is as follows:
1. Calculate step by step along the algorithm Φ,
2. Put p(y) into z if "z:=Oracle(y)" appears,
3. Let Φ(p; x) = Output, if this calculation halts.

For a solution p, Φ(p)↑ =
"Φ never halts on the input p without number x".

Π^0_1 Mass Problems:=

"Sets of p's satisfying Φ(p)↑ for an algorithm Φ".

Examples:

1. Make a complete table of prime numbers,
2, 3, 5, 7, 11, 13, 17, 19, 23, 29, 31, 37, $\cdots$.
2. Calculate π by decimal expansion,
3.141592653589793238462643383279$\cdots$.
5. Find an infinite random sequence,
01101000101110110001011011101100$\cdots$.
6. Extend Mathematics (ZFC) to some complete consistent theory.

The Distribution of Degrees:

1. There are infinitely many degrees.
2. There are P and Q such that P$\not\leq$Q and P$\not\geq$Q.
3. The top degree and the bottom degree exist.

–The example 6 is of the top degree.
–A problem with a computable solution is of the bottom degree.

A Problem on Π^0_1 Mass Problems:

Does there exist P and Q such that P<Q and no problem R such that P<R<Q?

Undecidability and weak theory of concatenation

Yoshihiro HORIHATA
Mathematical Institute, D2
E-mail: sa6m31@math.tohoku.ac.jp

Background of the theory of concatenation

* In 2005's, A. Grzegorczyk defined the new theory of concatenation denoted by TC, and he proved that TC is undecidable theory([1]).
* In 2008's, A. Grzegorczyk and K. Zdanowski proved that the theory TC is essentially undecidable. And they left the open question whether the weak arithmetic Q is interpretable in TC.
* For the above question, in 2009's, V. Švejdar, A. Visser and M. Ganea independently gave a positive answer.

Main results

* We defined the new theory of concatenation WTC and proved that this system is properly weaker than TC.
* We proved the theory WTC is Σ_1-complete, that is, for any Σ_1 sentence φ, if φ is true in the standard model of WTC, then is provable in WTC.
* We proved that WTC interprets R. This implise that WTC is essentially undecidable. About the converse of this, we conjecture that R interprets WTC.

1. Robinson's weak arithmetic Q

The arithmetic Q is PA$-$(Induction) whose axioms are followings:

(Q1) $\forall x \forall y (S(x) = S(y) \to x = y)$.

(Q2) $\forall x (S(x) \neq 0)$.

(Q3) $\forall x (x \neq 0 \to \exists y (x = S(y)))$.

(Q4) $\forall x (x + 0 = x)$.

(Q5) $\forall x \forall y (x + S(y) = S(x + y))$.

(Q6) $\forall x (x \cdot 0 = 0)$.

(Q7) $\forall x \forall y (x \cdot S(y) = x \cdot y + x)$.

2. Robinson's very weak arithmetic R

Robinson's arithmetic R has the following axioms: for each standard number m, n,

(R1) $\bar{m} + \bar{n} = \overline{m+n}$.

(R2) $\bar{m} \cdot \bar{n} = \overline{m \cdot n}$.

(R3) $\bar{m} \neq \bar{n}$ (if $m \neq n$) .

(R4) $\forall x (x \leq \bar{n} \to x = \bar{0} \vee \cdots \vee x = \bar{n})$.

(R5) $\forall x (x \leq \bar{n} \vee \bar{n} \leq x)$.

3. Our new theory WTC

Oer theory has the following axioms: for each $x, y, z, u, v \in \{a, b, c\}^*$,

(W1) $x ^\frown \varepsilon = \varepsilon ^\frown x = x$.

(W2) $x ^\frown (y ^\frown z) = (x ^\frown y) ^\frown z$.

(W3) $x ^\frown y = u ^\frown v \to \exists w ((x ^\frown w = u \wedge y = w ^\frown v) \vee (x = u ^\frown w \wedge w ^\frown y = v))$.

(W4) $\alpha \neq \varepsilon \wedge x ^\frown y = \alpha \to x = \varepsilon \vee y = \varepsilon$.

(W5) $\beta \neq \varepsilon \wedge x ^\frown y = \beta \to x = \varepsilon \vee y = \varepsilon$.

(W6) $\gamma \neq \varepsilon \wedge x ^\frown y = \gamma \to x = \varepsilon \vee y = \varepsilon$.

(W7) $\alpha \neq \beta \wedge \beta \neq \gamma \wedge \gamma \neq \alpha$.

(W8) $\forall x (x \sqsubseteq u \to \bigvee_{v \sqsubseteq u} x = v)$.

4. Our conjecture

Q	$\trianglerighteq \trianglelefteq$	TC
$\triangledown$		$\triangledown$
R	$^{??}\trianglerighteq \trianglelefteq$	WTC

References

[1] A. Grzegorczyk. Undecidability without arithmetization. *Studia Logica*, Vol. 79, No. 1, pp. 163–230, 2005.

Davies' Conjecture for Pseudo-Schrödinger Operators and Its Applications to Penalization Problem

Masakuni MATSUURA*†
Mathematical Institute, Tohoku University

February 18, 2010‡

1 Abstract

We call $(-\Delta)^{\alpha/2}+V(x)$ $(0<\alpha\le 2, V\in C_0^\infty(\mathbb{R}^d))$ a "pseudo-Schrödinger operator" and we consider asymptotic behavior of heat kernels of stochastic processes associated with pseudo-Schrödinger operators. It is well known that Pinchover has solved Davies' conjecture for second-order elliptic operators. (See, Theorem 1.2, [Pin1] or Theorem 1.1, [Pin2]). We derive the result of Davies' conjecture for pseudo-Schrödinger operators from Pinchover's results as follows.

Conjecture 1. *Let $k_t(x,y)$ and $\varphi(x)$ be the heat kernel and the ground state associated with pseudo-Schrödinger operator. Then, if H_α is sub-critical or null-critical, then for every $x,y\in\mathbb{R}^d$,*

$$\lim_{t\to\infty} k_t(x,y)=0.$$

If H_α is positive-critical, then for every $x,y\in\mathbb{R}^d$,

$$\lim_{t\to\infty}\frac{k_t(x,y)}{k_t(0,0)}=\varphi(x)\varphi(y).$$

Though we can easily prove subcritical cases, we have not completed the proof of critical cases yet.

2 Preliminaries

The following stories are well known.

Let $H_\alpha=(-\Delta)^{\frac{\alpha}{2}}+V(x)$ be a pseudo-Schrödinger operator. Then, there is a (C_0)-semigroup $(T_t)_{t\ge 0}$ on $C_\infty(\mathbb{R}^d)$, which is generated by H_α. Riesz's representation theorem implies the existence of the heat kernel $k_t(x,dy)$ such that

$$T_t v(x)=\int_{\mathbb{R}^d} k_t(x,dy)v(y) \tag{1}$$

for all $v\in C_0^\infty(\mathbb{R}^d)$, every $x,y\in\mathbb{R}^d$, and every $t\ge 0$. Then, the heat kernel $k_t(x,dy)$ is the minimal fundamental solution of the initial problem with pseudo-Schödinger operator.

For all $v\in C_0^\infty(\mathbb{R}^d)$ and every $x\in\mathbb{R}^d$, $T_t v$ can be represented as

$$T_t v(x)=\mathbb{E}_x\left[e^{\int_0^t V(X_s)ds}v(X_t)\right]. \tag{2}$$

Here, X_t is the symmetric α-stable process. Further, the range of principal eigenvalues λ_0 of H_α is non-negative.

3 Motivation

We would like to solve Davies' conjecture for pseudo-Schrödinger operators in order to solve penalization. Let us suppose the following assumption.

Assumption 2. *If H_α is positive critical, then*

$$\lim_{t\to\infty}\frac{k_t(x,y)}{k_t(0,0)}=\varphi(x)\varphi(y). \tag{3}$$

for every $x,y\in\mathbb{R}^d$.

Then, there is a limit distribution $\mathbb{P}_0^\varphi$ such that

$$\lim_{t\to\infty}\frac{\mathbb{E}_0\left[e^{\int_0^t V(X_u)du}\Sigma\right]}{\mathbb{E}_0\left[e^{\int_0^t V(X_u)du}\right]}=\mathbb{E}_0^\varphi[\Sigma] \tag{4}$$

for all $\Sigma\in\mathscr{F}_s$.

Indeed, if we define

$$\mathbb{P}_0^\varphi:=\frac{\varphi(X_s)}{\varphi(X_0)}e^{\lambda_0 s+\int_0^s V(X_u)du}\mathbb{P}_0,$$

then as $t\to\infty$,

$$\begin{aligned}
&\frac{\mathbb{E}_0\left[e^{\int_0^t V(X_u)du}\Sigma\right]}{\mathbb{E}_0\left[e^{\int_0^t V(X_u)du}\right]}\\
=\;&\frac{\mathbb{E}_0\left[\mathbb{E}_0\left[e^{\int_0^s V(X_u)du}e^{\int_s^t V(X_u)du}\Sigma\,\middle|\,\mathscr{F}_s\right]\right]}{\mathbb{E}_0\left[e^{\int_0^t V(X_u)du}\right]}\\
=\;&\frac{\mathbb{E}_0\left[e^{\int_0^s V(X_u)du}\Sigma\,\mathbb{E}_0\left[e^{\int_0^{t-s} V(X_u)du}\circ\theta_s\,\middle|\,\mathscr{F}_s\right]\right]}{\mathbb{E}_0\left[e^{\int_0^t V(X_u)du}\right]}\\
=\;&\frac{\mathbb{E}_0\left[e^{\int_0^s V(X_u)du}\Sigma\,\mathbb{E}_{X_s}\left[e^{\int_0^{t-s} V(X_u)du}\right]\right]}{\mathbb{E}_0\left[e^{\int_0^t V(X_u)du}\right]}\\
=\;&\frac{\mathbb{E}_0\left[e^{\int_0^s V(X_u)du}\Sigma\,\mathbb{E}_{X_s}\left[e^{\int_0^{t-s} V(X_u)du}\Big/k_t(0,0)\right]\right]}{\mathbb{E}_0\left[e^{\int_0^t V(X_u)du}\Big/k_t(0,0)\right]}\\
\to\;&\frac{\mathbb{E}_0\left[e^{\lambda_0 s+\int_0^s V(X_u)du}\Sigma\varphi(X_s)\int\varphi(y)dy\right]}{\mathbb{E}_0[\varphi(0)\int\varphi(y)dy]}\\
=\;&\mathbb{E}_0^\varphi[\Sigma].
\end{aligned}$$

Here, we have used

$$\frac{k_{t-s}(X_s,y)}{k_t(0,0)}\to\varphi(X_s)\varphi(y)\ \mathbb{P}_0\text{-a.s.}$$

as $t\to\infty$ in the last computation.

We call such a problem "Feynman-Kac penalization".

References

[ABJ] Anker, J.P., Bougerol, P., and Jeulin, T., *The infinite Brownian loop on a symmetric space,* Rev. Mat. Iberoamericana **18**, pp. 41 – 97, 2002.

[Dav1] Davies, E.B., *Non-Gaussian aspects of heat kernel behavior,* J. London Math. Soc. (2) **55**, pp. 105 – 125, 1997.

[Dav2] Davies, E.B., *Heat Kernel and Spectral Theory,* Cambridge Univ. Press, Cambridge, 1989.

[Jac1] Jacob, N., *Pseudo-differential operators and Markov processes, Volume I,* Imperial College Press, 2001.

[Jac2] Jacob, N., *Pseudo-differential operators and Markov processes, Volume III,* Imperial College Press, 2005.

[Pin1] Pinchover, Y., *Large Time Behavior of the Heat Kernel and the Behavior of the Green Function near Criticality for Nonsymmetric Elliptic Operators,* Journal of Functional Analysis **104**, pp. 54 – 70, 1992.

[Pin2] Pinchover, Y., *On Davies' conjecture and strong ratio limit properties for the heat kernel,* Advanced Studies in Pure Mathematics XX, pp. 1 – 13, 2005.

*Mail : `sa9d10@math.tohoku.ac.jp`
†Web : `http://www.math.tohoku.ac.jp/~sa9d10/`
‡Poster session, Global COE symposium "Weaving Science Web beyond Particle-Matter Hierarchy".

Torsion points of abelian varieties with values in infinite extension fields

Yuken Miyasaka

Mathematical Institute, Tohoku University

(E-mail : sa7m27@math.tohoku.ac.jp)

We consider a problem "**the torsion part $A(L)_{\mathrm{tor}}$ of an abelian variety A over a number field or p-adic field K wih values in some infinite extension L of K is finite or infinite ?**". On the other hand, the periodic points of an arithmetic dynamical system have some relationship with the torsion points of abelian varieties, and there also is a problem related to the finiteness. We compare the side of the variety with that of the dynamics in this problem.

Side of Variety

K : number field, A/K : abelian variety, L/K : extension
$A(L)$: set of K-rational points of A with values in L.
$A(L)_{\mathrm{tor}} := \{P \in A(L) : nP = 0 \text{ for } \exists n \in \mathbb{Z}\}$

Well-Kown Fact

L/K : finite extension $\Rightarrow \#A(L)_{\mathrm{tor}} < \infty$

- It is true even if we replace K with a p-adic field.

Uniformly Bounded

Thm. (Mazur-Morel)

$A = E$: elliptic curve over number field K
L/K : finite extension $^{\exists}C = C(d)$: constant
s.t. $\#E(L)_{\mathrm{tor}} < C$.

- Mazur proved it when $K = \mathbb{Q}$, and Morel proved in the general case. Their proof of this theorem is very difficult !
- It is an open problem in the case of abelian varieties.

Problem

A : abelian variety over number field or p-adic field K
If L is an infinite extension field of K,
$A(L)_{\mathrm{tor}}$ is finite or infinite?

Global and Local Results

In the global case, there are many results for this problem. We pick up the following Ribet's result.

Thm. (Ribet)

K : number field, $L := K(\mu_\infty) \Rightarrow \#A(L)_{\mathrm{tor}} < \infty$

Ribet proved this theorem by reducing it to the following local result which is proved by Imai and Serre.

Thm. (Imai-Serre)

K : p-adic field, $L := K(\mu_{p^\infty})$
A : abelian variety with ordinary reduction
$\Rightarrow \#A(L)_{\mathrm{tor}} < \infty$

Recently, This local result is refined to more large field L by Ozeki.

Manin- Mumford Conjecture

Finally we note that for curves with a higher genus, it is known the following Manin- Mumford conjecture, proved by Raynaud.

Thm. (Raynaud)

K : alg. closed field of char. 0, C/K : curve of genus > 1
J : Jacobi variety of C $\Rightarrow C \cap J(K)_{\mathrm{tor}} < \infty$

Side of Dynamics

K : number field, $f(X) \in K(X)$, L/K : extension
$P \in \mathbb{P}^1(L)$ is periodic, if $f^{(n)}(P) = f \circ \cdots \circ f(P) = P$.
$\Pi_f(L) := \{P \in \mathbb{P}^1(L) : f^{(m)}(P) \text{ is periodic } ^{\exists}m \in \mathbb{Z}\}$

Thm. (Nothcott)

L/K : finite extension $\Rightarrow \Pi_f(L)$: finite

- There are not results for a p-adic field.

Uniformly Bounded (dynamical version)

Conj. (Morton-Silverman)

L : finite extension of number field K, $f(X) \in K(X)$
Then $^{\exists}C$: constant depending only on L and $\deg(f)$
s.t. $\#\Pi_f(L) < C$.

- This conjecture includes the Mazur-Morel's theorem stated the side of variety, thus it is considered that it is difficult to prove it. it is not known even when $f(X) = X^2 + c$.

Problem (dynamical version)

$f(X)$: rational function over number field or p-adic field
If L is an infinite extension field of K,
$\Pi_f(L)_{\mathrm{tor}}$ is finite or infinite?

Lattés Map

The Lattés map f_E is one of the most important rational maps in the study of this problem. It is obtained by the projection of the multiplication by m map on an elliptic curve E such as the following:

$$\begin{array}{ccc} E(K) & \xrightarrow{[m]} & E(K) \\ {\scriptstyle \text{proj.}}\downarrow & & \downarrow{\scriptstyle \text{proj.}} \\ \mathbb{P}^1(K) & \xrightarrow{f_E} & \mathbb{P}^1(K) \end{array}$$

The Lattes map has the property $\#\Pi_{f_E}(L) \leq \#E(L)_{\mathrm{tor}}$ for an extension L of K. Therefore the results in the side of the variety give some examples of the finiteness problem in the side of the dynamics.

Dynamical Manin- Mumford Conjecture

Finally, we state the dynamical system version of the Munin-Mumford conjecture. This conjecture is also an open problem.

Conj. (Zhang)

K : alg. closed field of char. 0, ϕ : morphism on $\mathbb{P}^N(K)$
X : variety in $\mathbb{P}^N$
$\Pi_\phi(K) \cap X \subset X$: dense $\Leftrightarrow X$: pre-periodic variety

Maximum principle for a biological model related to the motion of amoebae

Harunori Monobe (Tohoku University)

February , 2010

1 Model of amoebae motion

Tamiki Umeda (Kobe University) proposed a biological model of amoebae considering the motion and the chemical reaction in the body. We modify Umeda's model from a mathematical viewpoint, and analyze the following model:

$$
\text{(P)}\begin{cases} u_t = \Delta u + k_1 w(t) - k_2 u & x \in \Omega(t),\ t > 0, \\ u = 1 + A\kappa + BV & x \in \partial\Omega(t),\ t > 0, \\ V = -\nabla u \cdot \mathbf{n} + g(u)w(t) & x \in \partial\Omega(t),\ t > 0, \\ u = \phi & x \in \Omega(0), \end{cases}
$$

where

$\Omega(t)$: domain of $\mathbf{R}^2$, $\partial\Omega(t)$: boundary of $\Omega(t)$,
$\kappa = \kappa(x,t)$: curvature of $\partial\Omega(t)$,
$V = V(x,t)$: normal velocity of $\partial\Omega(t)$,
$\mathbf{n} = \mathbf{n}(x,t)$: outward normal vector to $\partial\Omega(t)$,
$g(\cdot)$: smooth function, $w(t) = C_0 - \int_{\Omega(t)} u\,dx$
k_1, k_2, A, B, C_0 : positive constant, $\phi(x)$: initial data.

In (P), $u(x,t)$ is an unknown function depending on space and time, and the function represents a F-actin which assumes the role of bones and muscles in the body of amoebae. $w(t)$ represents a G-actin which is produced by F-actin. This model is mainly constructed by the law of conservation of mass and the relationship between G-actin, F-actin and the normal velocity of the boundary $\partial\Omega(t)$:

$$
u_t + \mathrm{div}(u\boldsymbol{v}) = k_1 w(t) - k_2 u, \qquad V = \boldsymbol{v} \cdot \mathbf{n} + g(u)w(t).
$$

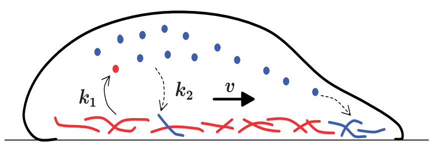

Figure 1: Chemical reaction and Motion of amoebae

2 Motivation

In Umeda's model, chemotactic substance gives amoebae a positive effect [Figure 2]. Therefore, the function g which represents the activity of a chemical reaction is positive. However, there are some chemotactic substance which also give amoebae a negative effect [Figure 3]. Now we consider the situation that there are such a substance around amoebae, and we try taking g as a negative function. Then we expect amoebae to become smaller. However, it is natural for amoebae not to become smaller than a certain size. We predict the sign of the function g on the basis of asymptotic behavior in some special conditions.

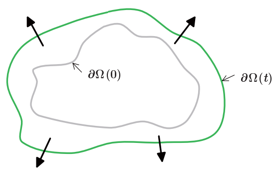

Figure 2: Case of positive effect

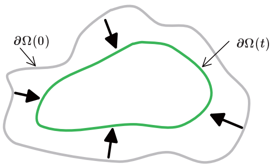

Figure 3: Case of negative effect

3 Main Result

Let $|x| = r$, $v(r,t) = u(x,t)$ in (P), then (P) becomes

$$
\text{(RP)}\begin{cases} \dfrac{\partial v}{\partial t} = v_{rr} + v_r/r + k_1 w(t) - k_2 v & r \in (0, s(t)),\ t > 0, \\ v = 1 + A/s(t) + B\dot{s}(t) & r = s(t),\ t > 0, \\ \dot{s}(t) = -v_r + g(v)w(t) & r = s(t),\ t > 0, \\ v_r = 0 & r = 0,\ t > 0, \\ v(r,0) = \phi & r \in (0, s(t)), \end{cases}
$$

where $s(t)$ is an unknown function depending only on time, and the function represents the radius of the circular domain which is the body of amoebae.

Definition 1. *A pair $(v, s(t))$ is said to be a solution of* (RP) *if there exists $T > 0$ such that*

$$
(v,\ s(t)) \in C^{2+\alpha,\ (2+\alpha)/2}\left(\bigcup_{0 \le t \le T} [0, s(t)] \times \{t\}\right) \times C^{(3+\alpha)/2}([0,T])
$$

satisfies (RP) *for some $\alpha \in (0,1)$.*

Assumption 1. *We assume that the initial data satisfy the following condition:*

$$
s(0) \in \left(0, \frac{-A + \sqrt{A^2 + 4C_0/\pi}}{2}\right), \quad \max_{r \in [0, s(0)]} \phi = \phi(s(0), 0),
$$
$$
\phi(r, 0) > 0, \quad C_0 - 2\pi \int_0^{s(0)} r\phi\,dr > 0.
$$

Then we have the following results:

Lemma 1. *Let $(v, s(t))$ be a solution of* (RP) *and the initial data satisfies* Assumption 1. *Moreover, $g(v)$ is depend only on time and satisfies*

$$
0 > g > -\frac{1}{BC_0}.
$$

Then $v > 0$, $w(t) > 0$, $\dot{s}(t) < 0$ for all $t \in [0,T]$.

Theorem 1. *Suppose that the initial data satisfy the same assumption as in* Lemma 1 *and*

$$
\frac{k_1 C_0}{k_2} < \phi(s(0), 0).
$$

Then

$$
\max_{Q_T} v = \max_{0 \le t \le T} v(s(t), t).
$$

Moreover, if $T = \infty$, then $s(t) \to 0$, $\max_{r \in [0, s(t)]} v \to \infty$ as $t \to \infty$.

Remark 1. *From* Lemma 1 *and* Theorem 1, *if g is negative at any time, we may construct an extinction solution. Therefore, if the model (P) have validity from a biological viewpoint, we expect the sign of g to be non-negative when amoebae is smaller than a certain size.*

References

H. Monobe, Existence of solutions for a mathematical model related to the motion of an amoeba (preprint).

Asymptotic Behavior of Solutions to the Drift-Diffusion Equation in the Whole Space

Masakazu YAMAMOTO (sa5m27@math.tohoku.ac.jp)
Mathematical Institute, Graduate School of Science, D3

February 18, 2010

Abstract

We consider the asymptotic behavior of the solution to the Cauchy problem for the Nernst–Planck type drift-diffusion equation arising from the plasma dynamics model. For our problem, it is already proved that the time global existence and decay of the solution. We also show an asymptotic expansion of the solution as $t \to \infty$.

1 Introduction

We study the following Cauchy problem for the drift-diffusion equation.

$$(1)\qquad \begin{cases} \partial_t u - \Delta u + \nabla\cdot(u\nabla\psi) = 0, & t>0,\ x\in\mathbb{R}^3,\\ -\Delta\psi = -u, & t>0,\ x\in\mathbb{R}^3,\\ u(0,x) = u_0(x)\ge 0, & x\in\mathbb{R}^3.\end{cases}$$

The drift-diffusion equation is the model of a plasma dynamics. The unknown functions $u = u(t,x)$ and $\psi = \psi(t,x)$ denote the density of charges and the potential of statistic electric field, respectively.

The well-posedness and the global existence of solution are already proved([5]). The mass conservation and L^p-decay estimate for the solution to (1) with large initial data were derived. Moreover, the effect from the non-linear part decays faster than the top term from the linear part([4]). Namely, the estimate $\|u(t) - MG(1+t)\|_p = o(t^{-\gamma})$ $(t\to\infty)$ holds for $1\le p\le\infty$, $\gamma = \frac{3}{2}(1-\frac{1}{p})$, where $G(t,x) := (4\pi t)^{-3/2}e^{-|x|^2/(4t)}$ and $M := \int_{\mathbb{R}^3} u_0(y)dy$.

2 Main Result

Now, our main concern here is the second asymptotic expansion of the solution. For $u_0 \in L^1_2(\mathbb{R}^3)\cap L^\infty(\mathbb{R}^3)$, where $L^1_2 := \{f\in L^1 \mid |x|^2 f\in L^1\}$, we introduce the following functions:

$$\begin{aligned} V_0(t,x) :=& G(t,x)\int_{\mathbb{R}^3} u_0(y)dy, \quad V_1(t,x) := \nabla G(t,x)\cdot\int_{\mathbb{R}^3} y u_0(y)dy,\\ J(t,x) :=& \int_0^t \nabla e^{(t-s)\Delta}\cdot(V_0\nabla(-\Delta)^{-1}V_0)(s)ds,\\ K(t,x) :=& -\frac{1}{3}\log(1+t)\Delta G(t,x)\int_{\mathbb{R}^3} y\cdot(V_0\nabla(-\Delta)^{-1}J\\ &+ J\nabla(-\Delta)^{-1}V_0)(1,y)dy.\end{aligned}$$

Then the following estimate holds.

Theorem 1 ([9]) *Let $u_0\in L^1_2(\mathbb{R}^3)\cap L^\infty(\mathbb{R}^3)$ and $u_0\ge 0$. Then for $1\le p\le\infty$, $\gamma = \frac{3}{2}(1-\frac{1}{p})$, the following estimate holds*

$$(2)\quad \|u(t) - V_0(t) - V_1(t) - J(t) - K(t)\|_p = O\left(t^{-\gamma-1}\right) \quad \text{as} \quad t\to\infty.$$

Moreover, the functions J and K satisfy $J, K\not\equiv 0$.

We should denote that the functions V_0, V_1, J and K satisfy the following equalities for any $\lambda > 0$:

$$(3)\qquad \begin{aligned} &\lambda^3 V_0(\lambda^2 t, \lambda x) = V_0(t,x),\\ &\lambda^4 V_1(\lambda^2 t,\lambda x) = V_1(t,x), \quad \lambda^4 J(\lambda^2 t,\lambda x) = J(t,x).\end{aligned}$$

Theorem 1 states that the asymptotic expansion of the solution to (1) contains logarithmic term at the rate $t^{-\frac{3}{2}(1-\frac{1}{p})-1}$.

There are very much related model called the Navier–Stokes equation and the Keller–Segel equations. They appears in a model for the incompressible fluid flow and the chemotaxis respectively. For the Navier–Stokes equations, an asymptotic behavior of the solution was considered ([1, 2]). In the case of the Keller–Segel equation, it was shown that there exists a special term likes $J(t)$ in an asymptotic expansion of the solution ([3, 6]). Moreover, in the even-dimensional cases, the asymptotic expansion of the solutions contains a logarithmic term at the rate $t^{-\frac{n}{2}(1-\frac{1}{p})-\frac{n+1}{2}}$ ([8]).

3 Outline of the Proof

In order to prove Theorem 1, we see the first asymptotic expansion estimate for the solution.

Proposition 2 (cf.[7]) *Under the same assumption as in Theorem 1, the following estimate holds for $1\le p\le\infty$ and $\gamma := \frac{3}{2}(1-\frac{1}{p})$;*

$$\|u(t) - V_0(1+t) - V_1(1+t) - J(1+t)\|_p \le C(1+t)^{-\gamma-1}\log(2+t).$$

To have an estimate for $\nabla\psi$, we prepare the following Sobolev type estimate.

Lemma 3 (Hardy–Littlewood–Sobolev's inequality) *Let $f\in L^p(\mathbb{R}^3)$ for $1<p<3$. Then $\nabla(-\Delta)^{-1}f\in L^{p_*}(\mathbb{R}^3)$ and $\|\nabla(-\Delta)^{-1}f\|_{p_*}\le C\|f\|_p$ for $3/2<p_*<\infty$ with $\frac{1}{p_*} = \frac{1}{p}-\frac{1}{3}$.*

The Cauchy problem (1) is equivalent to the following integral equation:

$$(4)\qquad u(t) = e^{t\Delta}u_0 + \int_0^t \nabla e^{(t-s)\Delta}\cdot\left(u\nabla(-\Delta)^{-1}u\right)(s)ds, \quad t>0,\ x\in\mathbb{R}^3,$$

where $\{e^{t\Delta}\}_{t\ge 0}$ is the heat semigroup. A combination of Proposition 2 and Lemma 3 immediately gives

$$u\nabla(-\Delta)^{-1}u \sim V_0\nabla(-\Delta)^{-1}V_0 + V_0\nabla(V_1+J) + (V_1+J)\nabla(-\Delta)^{-1}V_0.$$

Then the nonlinear part on the right hand side of (4) converges to

$$(5)\qquad \begin{aligned} &\int_0^t \nabla e^{(t-s)\Delta}\cdot\left(u\nabla(-\Delta)^{-1}u\right)(s)ds\\ &\sim \int_0^t \nabla e^{(t-s)\Delta}\cdot(V_0\nabla(-\Delta)^{-1}V_0\\ &\qquad + V_0\nabla(V_1+J) + (V_1+J)\nabla(-\Delta)^{-1}V_0)(1+s)ds\\ &\sim \sum_{|\beta|=1}\nabla^\beta\nabla G(t,x)\cdot\int_0^t\int_{\mathbb{R}^3}(-y)^\beta(V_0\nabla(-\Delta)^{-1}V_0\\ &\qquad + V_0\nabla(V_1+J) + (V_1+J)\nabla(-\Delta)^{-1}V_0)(1+s)ds,\end{aligned}$$

where we use the Taylor expansion. The right hand side of (5) contains a logarighmic term K. Indeed, by the scaling arguments (3), we have

$$\begin{aligned} &\sum_{|\beta|=1}\nabla^\beta\nabla G(t,x)\int_0^t\int_{\mathbb{R}^3}(-y)^\beta(V_0\nabla(-\Delta)^{-1}J + J\nabla(-\Delta)^{-1}V_0)(1+s,y)dyds\\ &= \sum_{|\beta|=1}\nabla^\beta\nabla G(t,x)\int_0^t(1+s)^{-1}\int_{\mathbb{R}^3}(-(1+s)^{-1/2}y)^\beta\big(V_0\nabla(-\Delta)^{-1}J\\ &\qquad + J\nabla(-\Delta)^{-1}V_0\big)(1,(1+s)^{-1/2}y)(1+s)^{-3/2}dyds\\ &= -\log(1+t)\sum_{j=1}^3\partial_j^2 G(t,x)\int_{\mathbb{R}^3}\eta_j(V_0\partial_j(-\Delta)^{-1}J + J\partial_j(-\Delta)^{-1}V_0)(1,\eta)d\eta\end{aligned}$$

where we put $(1+s)^{-1/2}y = \eta$ and use the relation $\int_{\mathbb{R}^3}\eta_j(V_0\partial_k(-\Delta)^{-1}J + J\partial_k(-\Delta)^{-1}V_0)(1,\eta)d\eta = 0$ $(j\ne k)$ in the second equality. This term gives the desired function K since the following relation holds:

$$\begin{aligned} &\int_{\mathbb{R}^3}\eta_j(V_0\partial_j(-\Delta)^{-1}J + J\partial_j(-\Delta)^{-1}V_0)(1,\eta)d\eta\\ =&\frac{1}{3}\int_{\mathbb{R}^3}\eta\cdot(V_0\nabla(-\Delta)^{-1}J + J\nabla(-\Delta)^{-1}V_0)(1,\eta)d\eta \quad (j=1,2,3).\end{aligned}$$

Applying Perseval's equality, we can confirm that $\int_{\mathbb{R}^3}\eta\cdot(V_0\nabla(-\Delta)^{-1}J + J\nabla(-\Delta)^{-1}V_0)(1,\eta)d\eta \ne 0$.

References

[1] Carpio, A., *SIAM J., Math. Anal.* **27** (1996), 449–475.
[2] Fujigaki, Y., Miyakawa, T., *SIAM J. Math. Anal.* **33** (2001), 523–544.
[3] Kato, M., *Differential Integral Equations* **22** (2009), 35–51.
[4] Kawashima, S., Kobayashi, R., *Funkcial. Ekvac.* **51** (2008), 371–394.
[5] Kurokiba, M., Ogawa, T., *J. Math. Anal. Appl.* **342** (2008), 1052–1067.
[6] Nagai, T., Yamada, T., *J. Math. Anal. Appl.* **336** (2007), 704-726.
[7] Ogawa, T., Yamamoto, M., *Math. Models Methods Appl. Sci.* **19** (2009), 939–967.
[8] Yamada, T., *Hiroshima Math. J.* **39** (2009), 363–420.
[9] Yamamoto, M., *RIMS Kôkyûroku Bessatsu* **B15** (2009), 189–208.

A study of the idea of systematic knowledge: On the relation between nature and spirit in the organizational view of nature

Fukuko ABE **(Philosophy, Tohoku University)**

Abstract

In the studies of the humanities and science which have become increasingly technical, sophisticated and interdisciplinary, the idea of the assimilation of literature and science attracted growing academic interest in recent years. This idea naturally requires not aggregate but systematic knowledge accompanied by a philosophy that addresses the question of what it is that we conceive as knowledge. It was the German philosophy as it evolved during the 18-19th century, which, based on works on systematic or speculative knowledge, attempted to establish an organizational view of nature becoming known under the notion of natural philosophy. Here, nature and spirit, which were traditionally conceived as divided notions within the mechanical view on nature, were now viewed in a new light as something unified through life. Although modern natural philosophy contains a large number of difficult questions with regard to its present-day validity, this study investigates, based on the currents of the organizational view on nature in contemporary philosophy, the relation between nature and spirit in this particular theoretical notion as well as the systematic knowledge itself which attempts to apprehend such an organizational whole.

1. Transition of the philosophical view on nature

(1) The teleological view on nature (e.g. Aristotle)

- Nature
  = The essence of things which have a source of movement in themselves
- Unidentifiable materials are identified through their form.
- Formal ("eidos") ⇨ "Telos" of the self-making contained in nature.
- Everything from the individual to the world as a whole has a necessary purpose.
- An ordered cosmos held by "unmoved movers (*kinoun akinēton*) = God".
- "Not only is immaterial being or absolute mind logically prior to nature, but the differentiation of mind into minds is prior to nature also."

(Collingwood[1960],p.90)

(2) The mechanistic view on nature (e.g. Renaissance, Modern science)

- Descartes
  Substance = God, spirit, matter
  Spirit = *res cogitans* Matter = *res extensa*
  Nature as matter ⇨ causality as mechanism of transmission of movements (mechanical causality)
- Order based on the Christian world view

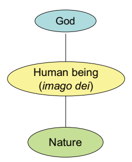

- Principle of causality in the mechanistic view on nature
  ⇨ The concept of "*causa finalis*" and "*causa formalis*" is not valid. Only "*causa efficiens*" is valid.

(3) The organizational view on nature (e.g. Romanticism, German Idealism)

- Opposition to the mechanistic view on nature
  Nature isn't mechanical but living.
- Nature as subject in the work of Schelling
  While nature produces itself, it is produced from

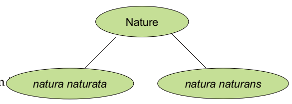

2. Epistemology as the basis of each view on nature

(1) The teleological view on nature
natural knowledge on the schema "*hylē*" – "*eidos*"
"eideische = qualitative Naturerkenntnis"(cf. Hirschberger [1953], p.33)

(2) The mechanistic view on nature
natural knowledge on the dualism of subject and object
"mechanistische = quantitative Naturerkenntnis"(cf. ibid.)

(3) The organizational view on nature
systematic and holistic knowledge of nature and spirit as life
To grasp the whole not as an aggregation but a system.

3. The relation between nature and spirit in the organizational view on nature
(part. on Schelling and Hegel)

Schelling's natural Philosophy

- **The concept of "living nature"**
  "So long as I myself am *identical* with Nature, I understand what a living nature is as well as I understand my own life; I apprehend how this universal life of Nature reveals itself in manifold forms, in progressive developments, in gradual approximations to freedom. As soon, however, as I separate myself, and with me everything ideal, from Nature, nothing remains to me but a dead object, and I cease to comprehend how a *life outside* me can be possible. "
  (*Ideas for a philosophy of nature as introduction to the study of this science (1797)*,p.36)

⇨ Nature and spirit ("I") are ideally identical as something living.

- **The concept of Organization**
  "Every organic product carries the reason of its existence in *itself*, for it is cause and effect of itself. No single part could arise except in this whole, and this whole itself consists only in the *interaction* of the parts. […] The organism, however, is not mere appearance, but is *itself* object, and indeed an object subsisting through itself, in itself whole and indivisible, and because in it the form is inseparable from the matter, the *origin* of an organism, as such, can no more be explained mechanically than the origin of matter itself." (ibid, p. 31)

Hegel

- **"Spirit is higher than nature."**
  " if […] that infinite expansion and this infinite withdrawal into itself, are completely one […], spirit is higher than nature. For if nature is absolute self-intuition and the actuality of the infinitely differentiated meditation and development [Entfaltung], then spirit, which is the intuition of itself as itself – or absolute cognition – is, in the withdrawal of the universe into itself, both the scattered totality of this multiplicity which it [i.e. spirit] encompasses, and the absolute ideality of this same multiplicity, in which it nullifies this separateness and reflects it into itself as the unmediated point of unity of the infinite concept."
  (*On the Scientific Ways of Treating Natural Law (1802/03)*, p.158)

⇨ Hegel also understands nature as something living and subjective, especially the living process ("Lebensprozeß").
Unlike on Schelling, spirit is not identical with Nature on Hegel.
Hegel thinks that nature itself and conceptualization of nature "completely are one".

- **"Impotence of nature (Ohnmacht der Natur)"**

"It is not only that in nature the play of forms has unbounded and unbridled contingency, but that each shape by itself is devoid of its Notion. Life is the highest to which nature drives in its determinate being, but as merely natural Idea, life is submerged in the irrationality of externality, and the living individual is bound with another individuality in every moment of its existence, while spiritual manifestation contains the moment of a free and universal relation of spirit to itself."

(*The Philosophy of Nature*, § 248 Remark)

"The *impotence* of nature is to be attributed to its only being able to maintain the determinations of the Notion in an abstract manner, and to its exposing the foundation of the particular to determination from without."

(ibid., § 250)

⇨ Hegel's theory of "the impotence of nature" is a radical form of the idealistic view on nature.

Indeed Hegel also considers nature as an organic life, but it is classified or opposed to nature and spirit according to the degree of the realization of the idea of freedom.
Hegel's view on nature does not represent a return to the mechanistic view which implies a human supremacy over nature. But he also attempts to prove the possibility that the spirit forms itself freely and voluntarily in the necessity and autonomy accident of nature is emphasized.

4. Spirit and nature on Whitehead

Whitehead's "Process Philosophy" or "Philosophy of organism"

- Whitehead: An exponent of the organizational view on nature in the 20th century
- "We are merely endeavoring to exhibit the type of relations which hold between the entities which we in fact perceive as in nature."(*The Concept of Nature*) ⇨ Getting ride of the relation between subject and object, and metaphysical arguments
- The first category of Existence
  "Actual Entities (also termed Actual Occasions), or Final Realities, or Rēs Verae." (*Process and Reality*, p.22)
- The reformed subjectivist principle
  Whitehead does not suppose the" immovable mover", an absolute spirit, or subjective substance on the basis of the organism, but he considers the world in its solidarity through actual entities and occasions.

Conclusion

- Because the modern organizational view of nature (part. Schelling) takes its origin from the humanism of romanticism (elevation from the finite to the infinite), identity between nature and spirit is described from the element of intellectual intuition, and it is not finally problematic how is a correspondence between the constructed (experienced) and true nature.
  ☞ However it is also said that this point of view is a source of today's environmental ethics which criticizes anthropocentrism.
- It is the most important point on the organizational view on nature that nature and spirit only statically unite, but that both reciprocally and organically relate and creatively evolve. Therefore this view doesn't fall into anthropocentrism like in the mechanistic view even if spirit oft might have the initiative in observations, speculation and so on. The idea of Systematic knowledge is also a cosmology of nature and spirit.

References

- Georg Wilhelm Friedrich Hegel, *Gesammelte Werke*, in Verbindung mit der Deutschen Forschungsgemeinschaft, Hamburg 1968 ff.
- *Schellings Werke*, Nach der Originalausgabe in neuer Anordnung herausgegeben von Manfred Schröter, München 1927ff.
- G.W.F. Hegel, *Political Writings*, edited by Laurence Dickey and H. B. Nisbet, tranlated by H. B. Nisbet, Cambridge University Press, 1999.
- *Hegel's Philosophy of nature*, edited and translated by M. J. Petry, Allen & Unwin, London 1970.
- F. W. J. Schelling, *Ideas for a philosophy of nature as introduction to the study of this science (1797)*, translated by Errol E. Harris and Peter Health, with an introduction by Robert Stern, Cambridge University Press, 1988.
- A. N. Whitehead, *The Concept of Nature*, Cambridge University Press, 1964.
- A. N. Whitehead, *Process and Reality: An Essay in Cosmology*, Corrected Edition, Edited by Griffin David Ray and Sherburne Donald W., The Free Press, New York 1978.
- R. G. Collingwood, *The Idea of Nature*, Oxford University Press, London, Oxford, New york 1960.
- Johannes Hirschberger, *Geschichte der Philosophie I Altertum*, Freiburg 1965.

Medical technology and surrogate decision-making

Haruka HIKASA (Philosophy D3, Tohoku University)

1. Introduction

With regard to medical technology it is bioethics which emphasizes the principle of respecting the autonomy of the individual. Yet, in the case of doubtfully autonomous or non-autonomous patients the principle of bioethics may not be granted or even be absent. In this presentation, I wish to discuss the framework of standards for surrogate decision-making in order to make decisions on behalf of individuals incompetent to seek decisions on their own.

2. Incompetent patients and standards for surrogate decision-making

In the case of some patients only insufficient autonomy is granted or may even be absent.

Ex. persistent vegetative state patients, dementia patients

→ formerly competent patients

newborns suffering a serious illness

→ never competent patients

Two types of standards for surrogate decision-making in Bioethics

[a] The Pure Autonomy Standard

(←The Substituted Judgment Standard)

[b] The Best Interests Standard

3. The pure autonomy standard and its problems

This standard requires the surrogate decision-maker to formulate a decision for formerly autonomous, now incompetent patients based on the patient's prior autonomous preferences (precedent autonomy).

→ ・The decision might be made based on values held by the patient that are little relevant to it

・The precedent autonomous preferences might conflict with the interests of the patient

・The preferences or choices of the reasonable (competent) people could be different from the preferences or values of the incompetent people

4. The best interests standard and its limits

This standard requires the surrogate decision-maker to determine the option that result in the highest net benefit for incompetent patient by evaluating burdens and benefits of the available options.

→ ・The decisions might fail to reflect the patient's subjective benefits, because surrogate decision-makers evaluate benefits and burdens, more or less, dependently on objective judgment (QOL chosen by a reasonable person)

・Whether the burdens should be limited to physical pain and suffering

5. Towards a new method of surrogate decision-making

1) In evaluating the result of medical interventions for incompetent patients, surrogate decision-makers must attempt to ascertain the patient's *present* point of view

→ cognitive science and neuroscience might be useful for interpretations of this present point of view

2) Surrogate decision-makers take the patient's present benefits (preferences, experiential interests) and the precedent autonomy (formerly preferences, values, perspectives) into consideration in order to make decisions on behalf of formerly competent patients.

→ the need to distinguish the patient from the person who he/she used to be, while at the same time regarding the patient as a person who continues to live a human life

3) With regard to 1) and 2), not only the physical but also the mental (spiritual) pain and suffering of the incompetent patient should be included in the assessments.

4) Surrogate decision-makers assume that some medical interventions will be extreme terror on patients who are unable to understand the reasons for these burdens (ex. invasive or immobilizing treatments)

5) Protecting and promoting the abilities which still held by incompetent patients. These abilities must be regarded as important.

References

Beauchamp, Tom L., and Childress, James F. 2001: *Principles of Biomedical Ethics*. 5th ed., New York, Oxford University Press. Dresser, Rebecca and Whitehouse, Peter J. 1994: "The incompetent patient on the slippery slope", *Hastings Center Report*, Vol.24, No.4, pp.6-12. Dresser, Rebecca. 1995: "Dworkin on Dementia. Elegant Theory, Questionable Policy", in:*Hastings Center Report*, Vol.25, No.6, pp.32-38. Dworkin, Ronald. 1994: *Life's Dominion*, New York. Jonsen, Albert R. and Siegler, Mark and Winslade, William J. 2002: *CLINICAL ETHICS:A Practical Approach to Ethical Decisions in Clinical Medicine*. 5th ed. , McGraw-Hill Medical Publishing.

Hume's empiricism and the experimental method of reasoning

SUGAWARA Hiromichi (Philosophy, D1)
Graduate School of Arts and Letters, Tohoku University

Introduction

Hume intended to introduce the experimental* method of reasoning into moral subject, a method of which Isaac Newton successfully provides a secure foundation in the natural philosophy. As is commonly known, Hume confines, in his works, our speculations to our *perceptions*, namely in empiricistical terms of *impressions*, and the copy of them, that is *ideas*. Therefore his claims place emphasis on the importance of phenomenal resources given to us by experiences. According to him, if we engage in the study of real nature and the operations of the external world beyond experiences, we would encounter serious difficulties. Yet, it seems that hume has not necessarily the faithfulness in his own statements with regard to the empiricistic doctrine. It is here, that I argue, that we can reconsider Hume's empiricism.

Ⅰ Two empiricisms in moral sciences

Hume's empiricism is interpreted in various way. D.Garrett finely divides the characters of Hume's empiricism into five kinds: such as methodological, conceptual, nomological, explanatory, and reductive empiricism (Garrett: 29-38). I take out two empiricisms from them that correlate with the following arguments.

1. Methodological empiricism

Hume writes in his *Treatise* that 'the only solid foundation we can give to this science itself must be laid on experience and observation' (THN: xvi). Garrett construes Hume's attitude that 'observation should be the main determinant of theory, and that, in case of apparent conflict, theory should generally be revised to accommodate the interpreted observations, …' (Garrett: 30). That is to say, the theory of *science of man* has acceptability of revision in response to observations.

2. Conceptual empiricism

According to Garrett, it is 'the view that the semantic content of thought is always fully derived from things or features of things as they have been encountered in sensory or reflective experience' (Garrett: 33). Hume considers his *Copy Principle* as that 'all our simple ideas in their first appearance are derive'd from simple impressions, which are correspondent to them, and which they exactly represent' (THN: 9).

Ⅱ Newton's four rules of scientific reasoning

Newton originally thoughts that 'the basic problem of philosophy seems to be to discover the forces of nature from the phenomena of motions and then to demonstrate the other phenomena from these forces' (MP: 382). What he seeks out is not the ultimate nature of forces of nature, but the forces of nature insofar as nature revealed by experiment and observations. After demonstrating the mathematical principles of the laws and conditions of certain motions, and powers or force in *Philosophiae Naturalis Principia Mathematica*, he first gives rules for the study of natural philosophy to demonstrate the frame of '*the System of the World*' (MP: 794-796).

Rule 1:

No more causes of natural things should be admitted than are both true and sufficient to explain their phenomena.

⇒ We could call it a principle of simplicity. Newton's commentary on the first rule above is that '…more causes are in vain when fewer suffice. For nature is simple and does not indulge in the luxury of superfluous causes'. Hume says in his *Treatise* that 'we must endeavour to render all our principles as universal as possible, by tracing up our experiments to the utmost, and explaining all effects from the simplest and fewest causes, …'(THN: 5). (We may associate this understanding with the principle of *Ockham's razor*.)

Rule 2:

Therefore, the causes assigned to natural effects of the same kind must be, so far as possible, the same.

⇒ This rule clearly influences Hume's fourth rule in '*Rules by which to judge of causes and effects*': 'The same cause always produces the same effect…' (THN: 116). In *An Enquiry concerning the Principles of Morals*, Hume refers to this rule as 'Newton's chief rule of philosophizing' (EPM: 98).

Rule 3:

Those qualities of body that cannot be intended and remitted and that belong to all bodies on which experiments can be made should be taken as qualities of all bodies universally.

⇒ This rule was added in the second edition of MP. We could call it a principle of universality. The content of this rule seem to be conveyed as Hume's positive attitude toward inductive reasonings supported by his *association of ideas*, rather than negative one that falls into skepticism.

Rule 4:

In experimental philosophy, propositions gathered from phenomena by induction should be considered either exactly or very nearly true notwithstanding any contrary hypotheses, until yet other phenomena make such propositions either more exact or liable exceptions.

⇒ This rule was added in the third edition of MP. Newton's commentary on the last rule above is that 'This rule should be followed so that arguments based on induction may not be nullified by hypotheses'. Newton's insight here is that we should give a certain authority to the method of induction, which makes provisional propositions possible. Hume argues the same many times. Newton appears to accept a priori principles in rules 1, 2, and 3. But, as E.A.Burtt said, Newton restricts them by fourth rule within narrower limits (Burtt: 194).

Ⅲ Assumptions of Hume's Arguments

There are several notable arguments in the work of Hume which seem not to be genuinely based on his empiricism, and which are concerned with the existence of body, and the existence of power or force. These arguments, I think, underlie the empiricistical arguments as an assumption or belief. That is to say, they are tacit understandings for Hume. Therefore they need to be received in his studies without verification. And it seems that Hume uses the term 'necessity connection' as *determination of the mind*, and the term 'power' or 'force' as unknown quality of objects.

1. Arguments concerning the existence of body

(1) I need not observe, that a full knowledge of the object is not requisite, but only of those qualities of it, which we believe to exist (THN: 116).

(2) …'tis in vain to ask, whether there be body or not? That is a point, which we must take for granted in all our reasonings (THN: 125).

2. Arguments concerning the existence of powers or forces

(3) The operations of nature are independent of our thought and reasoning, I allow it; … (THN: 113).

(4) The scene of the universe are continually shifting, and one object follows another in an uninterrupted succession; but the power or force, which actuates the whole machine, is entirely concealed from us, and never discovers itself in any of the sensible qualities of body (EHU: 136).

These descriptions are neither grounded on a priori knowledge or principle of the external world, nor are they grounded on his empiricism that would have been influenced by Newton, in that Hume does not properly employs the experimental method of reasoning. They are rather our ordinary belief or assumption, on which we speak and behave in daily life, and with which scientific investigations begin. These thoughts maintain the view of naïve causal realism proposed by G.Strawson that though we cannot perceive the necessary connection between objects, it nevertheless really exists (Strawson: 31-48). And this interpretation is partly due to the view of contextualism suggested by M.Williams that claims relativity between ordinary or scientific statement and skeptical statement. (Williams: 22-31).

Conclusion

・Hume's empiricism is based on ordinary assumptions or beliefs, but they needs not to be verified, because they make all the reasoning possible.

・Hume's experimental method of reasoning is influenced by Newton's fourth rule, in that they acknowledge the authority of the provisional character of induction, in the same manner, as a conductive principle in moral sciences.

・Though Hume believes in the existence of the external objects or real powers, he has to adopt agnosticism concerning them in his empiricism. Because his aim of *science of man* is to provide a secure and solid foundation for moral sciences.

Footnote
* At that time, the term 'experiment' had two meanings: As an 'experiment' in natural science, and as an 'empirical fact'. Hume mainly employed the concept based on its second meaning.

References
THN: Hume, D. [1739-40], *A Treatise of Human Nature*, edited by D. F. Norton and M. J. Norton: Oxford University Press, 2000.
EHU: Hume, D. [1748], *An Enquiry concerning Human Understanding*, edited by T. L. Beauchamp: Oxford University Press, 1999.
EPM: Hume, D. [1751], *An Enquiry concerning the Principles of Morals*, edited by T. L. Beauchamp: Oxford University Press, 1998.
Burtt, E.A. [1925], *The Metaphysical Foundations of Modern Physical Science; A Historical and Critical Essay*: BiblioLife, 2009; 邦訳『近代科学の形而上学的基礎』: 平凡社、1988年.
Garrett, D. [1997], *Cognition and Commitment in Hume's Philosophy*; Oxford University Press.
MP: Newton, I. [1687-1726], *The Principia, Mathematical Principles of Natural Philosophy,* A New Translation by I. Bernard Cohen and Anne Whitman: University of California Press, 1999.
Strawson, G. [2000], "Objects and Power" in *The New Hume Debate*, edited by R.Read and K.A.Richman: Routledge.
Williams, M. [1996], *Unnatural Doubts,; Epistemological Realism and the Basis of Scepticism*: Princeton University Press.

Epistemic Deference and Transmission of Knowledge

NIHEI Mariko (D3, Philosophy Faculty of Arts and Letters, Tohoku University)

Introduction

Suppose the following case …

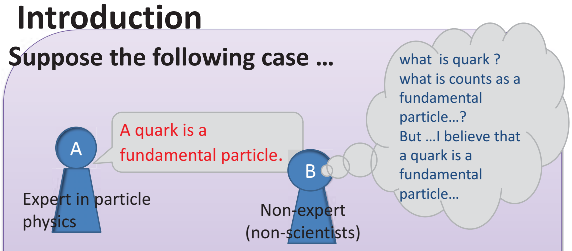

Does B Know that a quark is a fundamental particle?

We believe in countless expert claims without being able to confirm their truth and in many cases we lack the necessary competence to do so. It is difficult to acquire all relevant evidence concerning particular situations by ourselves because we do not go through extensive specialized training.

Strange as it may seem to the non-philosopher, mainstream epistemologists have paid little attention to the phenomenon of epistemic dependence or intellectual division of labor. The aim of my research is to advance a new epistemological theory to explain this phenomenon and to provide a vivid description of the social-public character of knowledge. For this aim, in this presentation, I focus on the following three works in order to show how the traditional epistemology does not keep in step with the situation of 'epistemic dependence' which is to be a commonplace affair in our time.

1.)I present the conception of 'epistemic dependence' suggested by John Hardwig.

2.) According to Hardwig, if we receive 'epistemic dependence' then we must face the dilemmatic choice between two epistemological models . I will point out that both options are incomplete.

3.) I clarify that Hardwig falls into this dilemma because he has not perfectly freed himself from the old epistemological obsession and that if we would abandon this obsession the dilemma could be eliminated.

1.) Hardwig's insistence on epistemic dependence

In Hardwig [1985]:

• According to traditional epistemology, one can only have rational reasons for believing p, if he has evidence for p; and evidence is anything that establishes the truth of *p*.

•But, in our culture, the more is known that is relevant to the truth of one's beliefs the nor anyone is able to know by himself.

•Therefore, we can never avoid some **epistemic dependence** on experts.

➡ **Non-expert B can acquire *knowledge* of some proposition *p* from expert A**, even though

(a) B has not performed the inquiry capable of providing the evidence for *p,*

(b) B is not competent to perform that inquiry,

(c) B is not competent to assess the merits of the evidence provided by A,

(d) B cannot understand what *p* means.

•We must say that B's belief is rationally justified and B knows *p* if we do not want to receive that a very large percentage of beliefs in this complex culture are irrational.

•According to Hardwig, to accept this conception of epistemic dependence is to deviate from the traditional epistemological view. Instead of the old view, he suggests two options: *the epistemic deference model* and *the epistemic community model.*

*This naming is not by Hardwig but by my own.

2-1.) The epistemic deference model

In this model, the individual knower needs not to posses direct evidence for knowledge ,but the knower can only be an Individuals.

- B knows *p*, if, B epistemologically defers to A.
- Non-expert B must obey expert A's opinion to acquire rationally warranted beliefs about *p*.
- By yielding to A, B is justified to belie *p*.

* This model is compatible with reliabilism.

?

Is deference not an all-or-nothing affair but a matter of degree?
Authoritarianism…?
Infinite regress or begging the question about "who is expert? "
Helpless against difference of opinions between competing experts.

*Brewer[2006] suggests a procedure in order to check the reliance about expert's testimony.

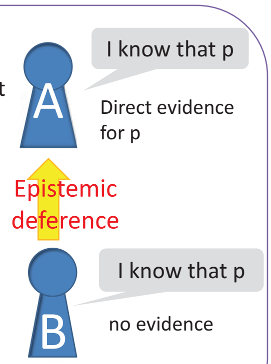

2-2.)The epistemic community model

Knowledge and its evidence are common property of the community

• In this model the primary knower is not individual A or B but community of A and B.

• *p* is known not by any person but by the community. Thus, members of group cannot say that 'I know that *p*', but only 'We know that *p*'.

•By belonging to the epistemic community, each member's belief is justified believing *p*.

This model retains the intuition that the knower must possess evidence within himself, but permits a 'community' or 'group' to count as knowers.

* This model represents a kind of naïve communitarian epistemology. See Welbourne[1981] and Kush[2002]

?

• Hardwig does not define what the criterion for an epistemic community is.

•Granting that *p* is common knowledge of communities, this is not to mean expert A and non-expertB have the same information about *p*.

• When something is transmitted as knowledge, A and B are already standing in a normative context. (Ex. teacher-student, doctor-patient, that is, the context of 'epistemic deference'?)

3.) Tentative conclusion: Drawing the moral from Hardwig's story

Should we make a decision in favor of either one? Perhaps not. Surely, Hardwig points out the narrow conception of evidence in old individualistic epistemology and presents the new direction towards a socialistic epistemology. Yet he remains too conservative because he endures the old notion of 'knowledge'. He seems to treat knowledge as something non-temporal and to suppose that knowledge itself is invariable through the transmission from one person to another. In other words, supposing that p could be known, that is that p is knowledge, then for all positive knowers (whether individuals or not) who know p posses p while those who do not know p do not posses p. However when we abandon this assumption we need not to faces the dilemma between an all-out deference to experts and a posit community as one whole epistemic subject. (Like Kusch[2002], we can define knowledge as a kind of entitlement and commitment among persons concerning testimony.)Obviously, there is some epistemic deference in our culture. But I think that 'deference' is constructed in dynamic processes of transmission of testimony among members of a community. Therefore, I argue that 'knowledge' represents not something fixed-timelessness but something historical-variable, just like deference.

Bibliography

Brewer [2006]: "Scientific expert testimony and Intellectual due process", in Selinger &Crease(eds.) *The philosophy of Expertise*, Columbia U.P.

Hardwig [1985]: "Epistemic dependence", in *The Journal of Philosophy*, Vol.82. No.7. pp.335-349.

Kusch [2002]: *Knowledge by Agreement*, Oxford U.P.

Welborne [1981]: "The community of knowledge", in *The Philosophical Quarterly*, Vol.31. No.125. pp.302-314.

The Finiteness of Human Beings and the Role of Technology

SUZUKI Ryozo (Tohoku University : Philosophy D3)

1. Introduction

This study explores the meanings of technics for human beings with regards to “reliability” or “durability” that technology creates.

2. Human Beings As “Life”

In the first place, organisms fight and eat each other. “Life” (in German: *Leben*) produces the tissues of itself and survives after these die. Human beings live in the same fashion.

→We fight for survival, kill other lives, and produce children who live over the death of their parents. In this process, we cannot help feeling the finiteness of ourselves.

Thus T. Hobbs and G. W. F. Hegel argued that human beings want to overcome this natural process(ex: excessive emotions like fear). For this purpose, we need to find a way for continuous control of nature. Such techniques include politics and science technology (politics and science are fundamentally related to each other in this point).

3. Magic as primitive technology

Parents maintain themselves by producing their children, and the family exists longer than their individual members. According to Hegel, this durability gives human beings a **most primitive and elemental intuition of “eternity”**. (Therefore we tend to favor whatever is stable and continue to exist longer than we do.)

→Thus, magic as the primitive technology took a role of protecting people against the fierceness of nature—and this force was God for them. He was a king who could handle the magic. He provided his people with “durability” of their family.

4. Modern state of affairs

In modern times, in “the twilight of the faith in God” (M. Horkheimer), the power of magic ceases to exist. But is it only the magic that extinguished?

The kingship extinguished as did the conventional family. (Hegel foresaw this fact in the early 18th century.)—“Falling down of all the value” (F. Nietzsche). As J. Habermas argues, that “securalization” and “demagicalization (in German: Entzauberung)” are the back of rationalization and only the abstract political power remains without old-fashioned kings.

5. What kind of technology is the greatest concern today?-And its reason

From the point of practical significance, technology encompasses a deep relation with the hope for ***durability*** (speaking metaphysicaly, “eternity”!) －in short, ***the continuance of family, the stability of everyday life*** － against life’s changeability or ambiguity. (“*Life against death*”－ Norman. O. Brown)

→For that reason, one of the deepest interests in science technology at present concentrates on reproductive technologies. And in this sense, as A. Gehlen has pointed out, the reason for why human beings come to depend on petrochemistry becomes obvious. Because this technology is more *stable* than other natural things.

6. “The eternal irony”

On the other hand, economical changes in modern times demand from us “the quickness to adapt, ability to correctly react to stimuli and specialized skill” (Horkheimer). But we know that the family represents something that we cannot substitute artificially. In this sense, Hegel calls the characteristics of the family “the eternal irony”, as long as it is opposed to human work, because **the community and society where the rationality has a meaning depend on members of the family**.

If we cannot go back to ‘good old times’, then we should reconsider the meaning of technology into which human beings lay their hopes, over and over again.

* References

Hegel. *Phänomenologie des Geistes* : in Werke in zwanzig Bänden, Bd. 3, Frankfurt am Main, 1973.

M. Horkheimer, *Traditionelle und kritische Theorie und andere Aufsätze* (Japanische Edition), 1974.

A. Gehlen, *Anthropologische Forschung*, Reinbek bei Hambrug, 1961.

N. O. Brown, *Life against death*, Wesleyan University Press, 1959.

J. Harbermas, *Technik und Wissenschaft als*〉*Ideologie*〈, Frankfurt am Main, 1968.

What is ethically problematic in Biogenetics?

Takuma OBARA (Philosophy, D3, Tohoku Univ.)

１. 序

本発表では、今日の遺伝子工学系科学の発展にともなって起こりうる倫理的な問題を明確化することを試みている。初めに、その種の科学が今後もたらすであろう事態について言及し、次に、それに対してなされる一般的な倫理的反論について言及する。最後に、そうした反論によって実は覆い隠されてしまっている問題、我々が真に考察せねばならない問題を提示する。

２. 遺伝子工学的発展がもたらす事態と一般的倫理的反論

遺伝子工学にみられるような科学的進展の主な帰結は、一言で言って、「人間性」の終焉である。ひとたびその構造の規則性が遺伝子レベルで知られてしまえば、人間的有機体は操作可能な対象と化す。もはや神秘的なところは何もなく、すべては物理法則に従って計算可能、予測可能な物的存在とみなされる。もちろんこうした考えはそれほど新しいものではないが、しかし遺伝子という（これまでのところ）我々のもっとも基礎的な構成単位のレベルでそうであるという点で、深刻である。それは遺伝子工学が我々の尊厳の感覚や自律といった「人間本性」に影響を及ぼすことを意味している。我々がどれほど自由にどれほど自律的に行動した（と思っている）としても、それはあらかじめ遺伝子にプログラムされていた行動にすぎない、というわけだ。

この場合、人格としてのその人のアイデンティティーの核心が破壊される、という反論が考えられる。それは同時に教育概念の破壊でもある。というのも、我々は、人は教養形成を通じて道徳的アイデンティティーを発達させる、と考えているからだ。しかし、自然科学系の究極の帰結にしたがえば、どれだけ教育し訓練して道徳的人格を形成しようと、人は遺伝子に即して行動するとみなされる。教育の観念は無意味化する。その結果、たとえば、いわゆる更生的訓練（懲役）ではなく、生化学的遺伝子工学的な手段で犯罪を撲滅するような社会になるだろう。犯罪者には、過剰な攻撃衝動を抑える薬物の服用が強制され、あるいは、彼の人格から攻撃性そのものを取り除くような遺伝子操作が施されるだろう。彼は文字通り人格を矯正されるわけである。

３. 旧来の倫理への固執は倫理的ではない

しかしだからといって、根本的な人間性を守るために遺伝子操作のような技術を制限しなければならないという態度をとるのは誤っている。それは、知っているにもかかわらずあたかも知らないふりをするという、物神的な分裂態度である。すなわち、「科学が主張していることを私は十分によく知っているが、にもかかわらず、人間性（という見かけ）を保持するために、私はそれを無視し、あたかも自分がそれを知らないかのように振る舞う」という態度である。こうした態度は真の問題、つまり、自由や自律、尊厳といった人間本性が新たな科学的条件によってどう変化するのか、という真の問題に直面することを妨げてしまう。

かつてデカルトはこうした旧来の倫理観（に固執する態度）を「一時的倫理」と呼んだ。なぜ「一時的」かと言えば、今や新たな人間観の地平が開かれているからである。新たな地平へ乗り出すことはこれまでの土台を失うことであり、支えなしに自立することである。それは一つの危機である。それを回避するためにも、これまでの慣習やならわしに今一度そしてこれを最期に身を浸す必要がある。しかし、それはあくまで新たな地盤を築くためであって、旧来の土台を守るためではない。一度知ってしまった以上、もはや純真無垢な無知へ帰ることはできない。今やこの新たな現実のもとにとどまり、回避したり隠蔽したりすることなく、それを引き受けなければならない。これまでの倫理に固執すること、それは実際には倫理的態度ではない。新たな地平で新たな倫理を構築しようとすること、これこそが真に倫理的な態度なのである。

４. 遺伝子工学系科学の発展において、何が真に倫理的な問題であるのか？

先に挙げた「矯正」の例を考えてみよう。仮に罪を犯したある人間が、懲役としての数年の更生訓練の代わりに、衝動を抑制する薬品を常用することを条件にすぐさま社会復帰したとしよう。おそらく人々は容易には彼を受け入れられないだろう。しかもそれは更生訓練を経て社会復帰した人より以上にである。なぜか。それは、彼が自律的ではなく他律的に衝動を抑えていると人は考えるからである。言い換えれば、薬物は「外的」操作とみなされ、その人固有の特性とは認められえない。人は人間の内面性に価値を置き、それゆえ、人間の内面を形成するものとしての教育や訓練を評価してきたのである。したがって、彼は本質的には（薬なしには）未だ攻撃的人間とみなされる。

この話をもう一歩進めてみよう。今述べたような衝動を抑える薬ならばまだ容易に外的と判断することができる。では、そうではなくてたしかに更生訓練によって自律的に衝動を抑えられるようになったが、実はその訓練において苦闘に耐えることを可能する薬を使っていたとしたらどうか。外的操作は確かに認められるが、当人が苦しい経験をしたこともまた確かである。さらには、上でも述べたように、彼の人格そのものを矯正したとしたらどうか。要するに、どこまでが個人に属するもので、どこからが外的操作の範囲になるのか。人間における内的なものと外的なものの境界のこうした曖昧化が、遺伝子工学のような科学の発展によってもたらされる事態である。こうした条件に立って、そもそも人間性とはいったい何なのかを考察すること、それが真に哲学的な問いであろう。こうした問題こそが真に倫理的な問題として考察され、解答されなければならない問題なのである。

1. Introduction

In this presentation, I will try to precise the ethical problems that may be posed with particular scientific breakthroughs such as success in decoding the human genome. First, I will elaborate on what such scientific advances can bring about. Second, I am going to mention general, ethical oppositions against it. Finally, I will propose problems that this opposition unconsciously hides, and that we should really consider.

2. Situations that progress in biogenetics can bring about and general, ethical oppositions against them

The main consequence of the scientific breakthroughs in biogenetics is the end of "humanity". Once we know the rules of its construction at the level of the genome, human organisms are transformed into objects amenable to manipulation. Human beings are not mysterious and they are regarded as material objects which act by the laws of physics. Of course, this idea is not new, but it is serious in the sense that it is true at the level of genomes which are our most basic components. This means that our behavior is only a result of the program of genomes even if (we believe) we act freely or autonomically.

Against this, opposition has been expressing arguing that the very heart of one's identity as a person could be destructed in such cases. Moreover, the concept of education could also be destructed given the fact that we think that we develop our moral identity through education. However, according to ultimate consequences which natural sciences has, human beings act by the rules of genomes no matter how they educate themselves and form their moral identity. The notion of education may be rendered meaningless. As a result, for example, there would be a society that has intention to fight crime through direct biochemical or biogenetic intervention instead of imprisonment at hard labor. The criminals would be compelled to take medications against excessive aggression or be administered to biogenetic manipulations to remove their aggression itself from their personalities. Literally, they would be reformed.

3. Persisting in old ethics is not ethical

However, it is false to assert that technology such as biogenetic manipulations should be restricted for preserving the fundamental humanity. It is a fetishistic splitting attitude: you ignore it while you know it. That is to say, "I know very well what science claims, but, nonetheless, in order to retain [the appearance of] humanity, I choose to ignore it and act as if I don't know it". This attitude prevents us from confronting the true question: 'How do these new scientific conditions transform and reinvent the very human nature such as freedom, autonomy, and dignity?'

Descartes called (the persistence of) the old ethics the "provisional ethic". The reason why it is called "provisional" is that a new horizon is opening now. To take a step toward a new field is to lose our previous foundation and to stand on our own legs without any support. It represents a crisis. In order to evade it, it is necessary to put ourselves into our previous custom or convention again and for the last time. However, it is not to protect the old foundation but to construct the new one. Once we know it, there is no return to innocent ignorance. We have to tarry in the new reality and accept it rather than to evade or conceal it. Persisting old ethics is in fact not ethical attitude. It is attempting to constitute new ethics on the new field that is truly ethical attitude.

4. What is ethically problematic in biogenetic breakthroughs?

Let us consider the above mentioned example of "reformation". What would happen if a criminal immediately returned to his society on condition that he takes medications against his own aggression, instead of receiving a sentence of imprisonment? Certainly, people would consider it to be difficult to accept him much more than a person that receives a sentence of imprisonment. Why? That is because people would think he can control his own aggression not autonomically but heteronomously. In other words, medications are thought to be "external" manipulation, not his proper personality. We have valued the human's interior or inherence and thus estimated education or training as forming it. In short, he would still be regarded as a dangerous person essentially (without medicine).

Finally, let us go one more step further in this example. It is easy to judge drugs that we have just mentioned as external. Now, what would happen if he came to be able to autonomically control his own compulsion through intensified training, whereas he had taken medicine to enable him to endure struggle or agony during the training? Moreover, as I have mentioned above, what would happen if his personality itself was reformed? In a word, can we draw a line of division between the internal and the external within an individual? It is this blurring of the borderline that scientific advances such as biogenetics may bring about. It seems to be an authentic question of philosophy to consider what humanity is under that condition at all. This is the very problem that should be reflected and responded as being the truly ethical one.

The Ontological Genesis of the Theoretical Attitude

Tetsurou YAMASHITA (Tohoku University)

If we conceive scientific activities radically, that is in terms of the ontological structure of the human being, we may understand that science is not the primary way of our being but a modification of practical activities in everydayness. In this presentation I will sketch the process of the ontological genesis of the theoretical attitude. In doing so, I am dependent heavily on *Martin Heidegger*'s ontological insights regarding the human being.

Ⅰ. The Structure of the Understanding of Being

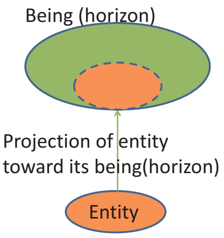

Human beings exist, understanding being of beings (entities). Understanding has the structure in which we project beings toward their being (horizon).

Ⅱ. The Way in which We are Concerned with Beings

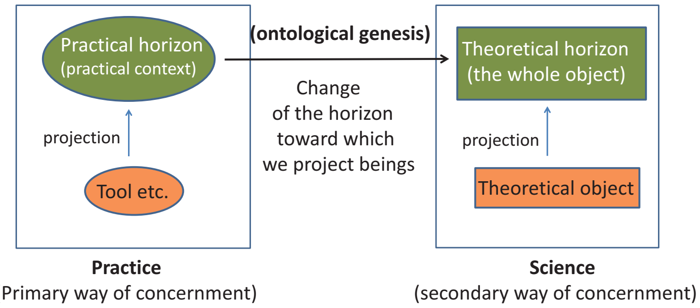

Ⅲ. Practical Attitude

Availableness and Discovery of the Available Beings

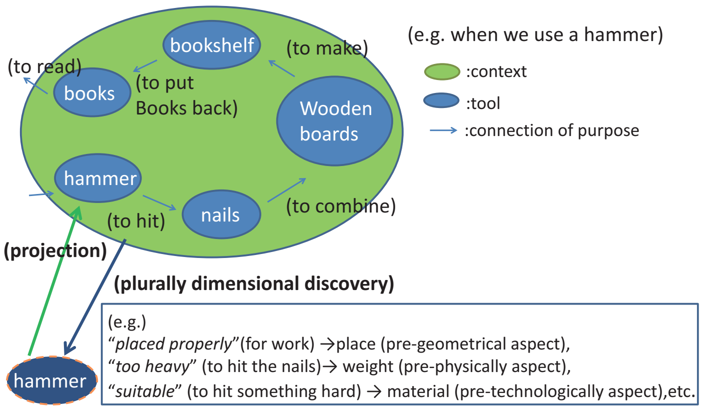

Tools occupy their own proper places, related with other specific tools in each practical context (a connection of purposes). I call this way of being in which tools exist (extremely) context-dependently, "*availableness*" (readiness-to-hand).

In practices, we can discover unthematically various properties of the available beings in terms of our purpose in each context. The discovered properties are pluralistic according to their context.

Those properties can, however, be discovered only in a definite practical context; that is, the available beings don't beforehand have properties without practical context, such as physical weight or spatial position etc. The properties of the available beings are regulated and structured according to their context. They don't have the same degree of clarity; which aspect should be centered or put on the periphery, or which property in the centered aspect should come to the fore, and so on, are all determined according to practical attitude. Thus, in practices **"subject" is extremely involved in practical context**; subject should behave and take the viewpoint as the context demands.

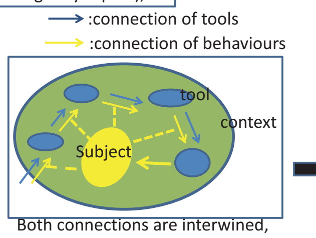

Both connections are interwined, foming the connection of purposes. Subject is involved in it, behaving along it on the one hand and functioning as the end of it on the other.

Ⅳ. Change into Theoretical Attitude

1. Change of Understanding of Being

Theoretical attitude is formed through the change from availableness into "*forwardness-to-hand*", the way of being in which beings exist constantly, independent of subject in practical context. Forwardness-to-hand is formed through the release of subject from the involvement in practical context.

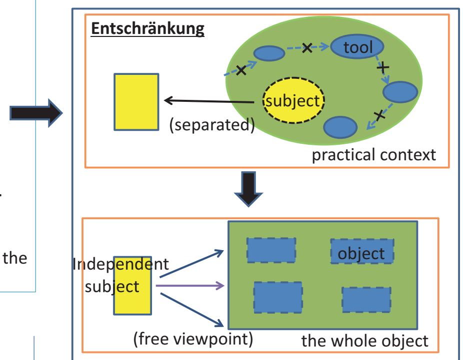

This change into f*orwardness-to-hand* contains "*moving-boundaries-away*" ("*Entschränkung*" in German). This operation removes the boundaries between the proper places of available beings, and changes various places(environmental) into uniform positions (spatial). Through this change, beings lose their practical context (or availableness) and appear as the wholeness of independent objects. Subject is independent of objects; thus he/she can take an optional viewpoint voluntarily.

2. Formation of Theoretical Attitude

"Moving-boundaries-away" invalidates practical context; thus, all the viewpoint (aspects) which have already been built in this context are released, without being regulated according to practical context. From these viewpoints each, we can divide the wholeness of objects into the various fields of sciences (space, matter, life, history and so on). Theoretical attitude is formed through this operation.

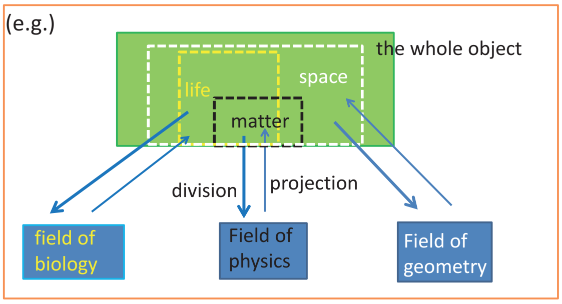

Each field of science is understood from a single viewpoint (monistically). Because subject is free from involvement in practical context, subject can take an optional viewpoint and discover optional properties which have already been understood, but not clearly. By fixing a viewpoint, we can articulate the field more clearly and minutely than we can expect in everyday practices.

For example, mathematical physics finds its field by discovering in advance the consistently existing beings(matter) and then noticing previously their constituent moments specifiable quantitatively (ex. motion, force, position, time).This operation is called *the mathematical projection of nature*. Discovery of facts, organization of concepts, regulation of methods including experiments, decision of the form of arguments, and so on, are all possible under the light of this projection.

Conclusion and Suggestion

Because of its projection toward a specific viewpoint, theoretical attitude can discribe (a part of) nature in such clarity and preciseness that practical attitude cannot. However, we cannot constitute the genuine wholeness of nature by combining these right but partial pictures of nature. Theoretical pictures of nature are only results of the division of a specific viewpoint. Nature as it is, the source from which we can derive various viewpoints, always exceed theoretical discovery in abundance. The substance of nature is the possibility that we can derive various theory from it. So science cannot access being of nature in this sense. This is by no means a fault of science, but the price for its clarity and preciseness. From this standpoint, it is necessary to consider the validity of the conception of scientific comprehensive picture of nature, and to clarify ontological significance of scientific trurh, that is, significance of non-ontological truth of science.

Tohoku University Scienceweb GCOE

"Weaving Science Web beyond Particle-matter Hierarchy"

The 2nd GCOE International Symposium

Risk, uncertainty and the precautionary principle: How to deal with scientific uncertainty?

FUJIO Yasuhiko

Graduate School of Arts and Letters, Tohoku University

Introduction

Risk deriving from the development of science and technology

We are in need of risk analysis and management in order to coexist with risks, whose approaches are based on the theory of probability or statistics.

Scientific uncertainty and risk management

We must assess the occurrence of undesirable events probabilistically or statistically.

There are some realms of science in which we cannot use such approaches because of a lack of sufficient knowledge with regard to complex phenomena (ex. global warming).

Precautionary principle: an approach to risks

The **precautionary principle**(**PP**) requires that we should adopt approaches such as regulating or banning the use of chemical substances or new technology in order to protect the human health and the environment despite the lack of sufficient scientific certainty.

PP is thought of as the principle which is to be applied in the issues of risk, under scientific uncertainty, concerning the severe and irresistible harm to the human health and the environment.

I wish to examine the notion of scientific uncertainty with regard to complex phenomena, and PP as a reasonable principle for decision making confronted with such uncertainty.

Uncertainty in risk management

Emergence and development of the concept of risk

We cannot obtain complete knowledge about future events; we can only anticipate future events probabilistically or statistically.

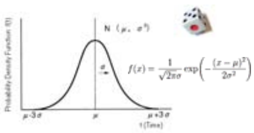

The magnitude of risk is calculated as the product of probability of the occurrence of undesirable events and severity of damage which they might pose.

The magnitude of risk

= (Probability of the occurrence of events) × (Severity of damage)

Accordingly, we must make decisions concerning issues of risk under uncertainty of the occurrence of undesirable damage in the future.

Problematic of risk management

Such procedures as RCBA(risk-cost-benefit analysis)embody uncertainties; models used in RCBA are not always perfectly sophisticated models of real events.

In principle, we never entirely know what happened, happens and will happen in the real world, which makes us more modest about our actions that might pose harm to the human health or the environment.

Example of failed risk management: BSE in UK

The government did not acknowledge the infection with BSE to humans at first.

The Southwood Committee's Report recognized the slim possibility of humane infection with BSE.

However, the government paid no attention to it, but overestimated the safety. Afterwards the government acknowledged the infection with BSE and the failure of risk management.

Negligence or underestimation of uncertainty of scientific knowledge or evaluation of risk might lead to the failure of risk management.

The limits of our knowledge and science

As science is the process for exploring veiled realms, in cutting-edge research the scientific knowledge is incessantly renewed by new scientific discoveries.

There are, however, some cases where we cannot elucidate the causal mechanism of complex phenomena at the present time due to the complexity of phenomena(ex. global warming)

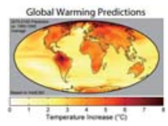

Thus, scientific uncertainty is due to the plasticity or limits of our knowledge.

Attitudes towards uncertainty in science

In regulating or prohibiting a certain product or procedure, it seems to be necessary to prove the causal relationship between products and the possible harmful effect.

As we know, since scientific knowledge might be renewed, we must not have too much confidence in science.

Therefore, we, especially policy-makers, must keep in mind that science has limitations.

Precautionary principle

The origin of the conception of PP

The cholera epidemic in London in 1854: John Snow, the founder of epidemiology, recommended removing the handle of the water pump in order to stop the cholera epidemic. (At that time, it was not proved that cholera was transmitted by polluted water.)

This case may suggest that the conception of PP was known and applied earlier before PP has emerged in the 1970s.

The emergence of PP

PP has been adopted in the legislation for protection of human health and the environment. The most prominent and frequently cited version of PP is probably the 1992 *Rio Declaration*:

> **"In order to protect the environment, the precautionary approach shall be widely applied by States according to their capabilities. Where there are threats of serious or irreversible damage, lack of full scientific certainty shall not be used as a reason for postponing cost-effective measures to prevent environmental degradation."**

One of the most remarkable characteristics of PP is that even if there exist no full scientific evidences it is possible and legitimate to regulate or prohibit products or procedures which might pose serious and irreversible damage to human health or the environment.

Criticism against PP

Opponents of PP characterize the defect of PP as:

1) The definition of PP is too vague to serve as a regulatory standard,

2) PP forces decision-makers to pay unreasonable attention to extremely unlikely scenarios,

3) PP would lead to more risk-taking or another risk,

4) PP is a value judgment, not a scientific one,

5) PP does not take science seriously and marginalizes the role of science in decision-making.

Objections against criticism of PP

Proponents of PP argue against each criticism:

1') Vagueness of PP does not necessarily imply uselessness in practice; PP may be given more precise formulations through elaboration and practice,

2') PP is not willing to prohibit all actions which may pose harm; all actions may have unforeseen, more or less, harmful consequences, so it is impossible and unreasonable to ban all actions,

3') The way of framing of the decision problem to which PP is applied might cause more risks; PP itself does not pose more risk,

4') All decision rules including PP are value-based,

5') PP is not based on science, but does not contradict science.

Outlook for PP

Development of PP for better policy-making

In the *Communication from the Commission on the Precautionary Principle*(2000) the Commission of the European Communities noted that measures based on the PP:

・based on an examination of potential costs and benefits of action or lack of action,

・subject to review, in the light of new scientific data,

・capable of assigning responsibility for producing the scientific evidence necessary for a more comprehensive risk assessment.

The foundation of PP in philosophy and ethics

Philosophy might be able to argue 'uncertainty' in risk management in the light of philosophy of probability or statistics.

> **"Our current moral theories are not suitable to deal with issues of risk."(Hanson,2007)**

We should, therefore, explicate the ethical implication of PP.

Conclusions

- **We are forced to deal with risk under uncertainty, for we can only recognize the occurrence of undesirable events in the future probabilistically or statistically.**
- **We must perform risk management on the ground that there might be scientific uncertainty.**
- **PP does not disregard the role of science, but acknowledges the limitations of science and the confidence in science.**
- **We should elucidate the ethical implication of PP and make PP more available in processes of policy-making so that moral theories can address issues of risk.**

Reference

- 大竹千代子、東賢一『予防原則　人と環境の保護のための基本理念』合同出版、2005年
- Commission of the European Communities, *Communication from the Commission on the Precautionary Principle,* http://ec.europa.eu/environment/docum/20001_en.htm, 2000.
- Hansson, S.O., "Risk and ethics: three approaches", In *Risk: Philosophical Perspectives*, ed. Lewens, T., Routledge,2007.
- Jensen, K. K., "The Moral Foundation of the Precautionary Principle", *Journal of Agricultural and Environmental Ethics*, 15(1), 2002, p.39-55.
- Sandin, P., "Common-sense precaution and varieties of precautionary principle", In *Risk: Philosophical Perspectives*, ed. Lewens, T., Routledge,2007.
- Sandin, P. et al., "Five charges against the precautionary principle", *Journal of Risk Research*,5(4),2002,p.287-99.
- Sunstein, C., *Laws of Fear: Beyond the Precautionary Principle*, Cambridge University Press, 2005.

The mechanism of suppressed dynamical friction in a constant density core of dwarf galaxies

Inoue Shigeki (Tohoku Univ.)

Abstract : **Dynamical friction problem is a long-standing dilemma. In dwarf galaxies, dynamical friction on their globular clusters (GCs) is too strong to keep their orbital motions. Nonetheless, GCs do exist even in current dwarfs. However, a solution have been proposed. If dwarf galaxies have a cored dark matter halo which has a constant density region in its center, the dynamical friction is significantly weakened. But, the mechanism of the suppressed dynamical friction has not been clarified yet.**

By means of N-body simulation, I find that the mechanism of the suppressed dynamical friction is the effect of orbital resonance between the GC and the halo.

Miller et al. (1998)

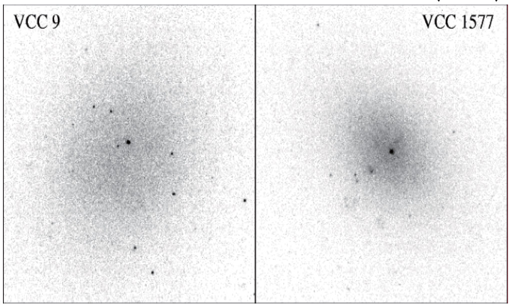

dwarf galaxeis and their GCs

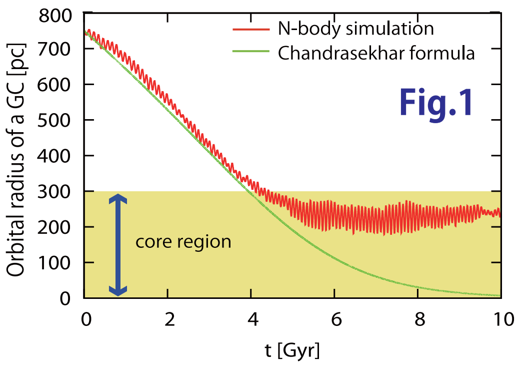

A favorable answer to "the cusp-core problem" : In Fig.1, I show a result of my simulation. As mentioned above, the GC can survive from the strong dynamical friction in the cored structure. This result impllies that the cored halo is a favorable dark matter structure for dwarf galaxies on the point of the existence of the GCs in dwarfs.

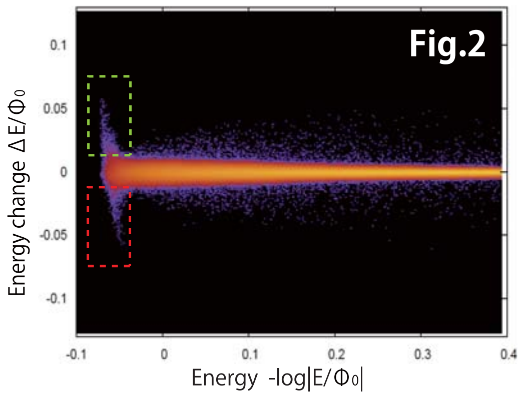

The mechanism of the suppressed dynamical friction : I examine orbital energies and changes of the energies of halo particles (E-ΔE diagram, Fig.2). I find that the energies of some particles largely increase or decrease (the green & red squares on Fig.2) and these particles have prograde rotations with the GC. These particles resonate with the GC and have very complex orbits. In Fig.3, I show a example of the orbits in the rotating coodinate of the GC.

I extract such resonant particles and calculate energy transfers from the resnant particles to the GC. I find that the resonant particles inject energy to the GC (Fig.4).

This result means that the dynamical friction on the GC is canceled out by the resonant particles in the core structure.